Acknowledgements

I would like to express my gratitude to my advisors, Prof. Paulo Cruz and Prof. Maurizio Piazza for their guidance and support. Thank you for your teaching, experience and friendship.

For the interesting discussions we had, I would like to thank Prof. Humberto Varum and my friend Luís Neves.

There are many important contributors that have made possible to achieve this work. I am grateful to Ana Santos, Matos and Marco for their support during the experimental work performed at the Laboratory of Structures of University of Minho. I am also grateful to all the staff of the Structural Testing Laboratory of the University of Trento for their help during the tests there performed: Marco Molinari, Luca Corradini, Tiziano Dalla Torre, Stefano Girardi, Alfredo Pojer and Martin. For his tremendous support during the numerical analysis, I would like to thank Bruno Egídio. I am also indebted with my brother-in-law José Manuel for his help during the field load tests. For supplying some trusses examples included in Appendix A, I would like to thank Tiago Dias, Ricardo Braz and Carlos Cunha. I would like also to thank José Pequeno for the draftings.

To my colleagues at University of Trento, for the unforgettable time I spent in "casetta rosa", namely, Ali, Lensir, Roberto, Mauro, Nicola, Martin, Leqia, Lorenzo, Marco, Charles and Mariapaola. I would like to thank also my colleagues at the University of Minho for their support and friendship.

The financial support of the Portuguese Science Foundation (FCT) through grant SFRH/BD/18515/2004 and of University of Minho is gratefully acknowledged. The thesis is part of a research program supported by FCT (contract reference POCI/ECM/56552/2004). The work carried out in Trento, where I spent 10 months, has been supported with a partial financial contribution of the Italian Earthquake Engineering Laboratory Network (RELUIS), within the research program carried out for the Italian Agency for Emergency Management. I am also grateful to the support of Adico Industry (field tests) and Casais S. A. (connection specimens preparation and supply).

I would like to thank all my family who have always encouraged and inspired me, despite having no real interest in my research subject.

Finally, I would like to dedicate this thesis to Marisa and Maria João for keeping me connected to the real world. Thank you for being always there when I need you and let me "disappear" when it was necessary.

Abstract

Connections are the key element in the behaviour of traditional timber trusses. The overall behaviour and stresses distribution are function of connections strength and stiffness, in particular under non-symmetric loads and extreme events. In these situations, the connections are loaded well beyond their pseudo-elastic limit.

Normally, traditional timber connections are assumed as hinges or rigid. However, even without any strengthening device, they have a significant rotational stiffness and may be better classified as semi-rigid and friction-based.

It is the misunderstanding of the connections behaviour that normally leads to the replacement of old timber structures, instead of their retrofitting to satisfy safety.

In order to better predict and understand the behaviour of timber structures, analytical models of connections are crucial. Semi-rigid models, using nonlinear laws and hysteretic rules, intend to represent the behaviour of timber structures with a comparable level of detail for all the structural components.

In this thesis, structural analysis of some full-scale timber trusses is presented. After a primary survey an extensive experimental program, using full-scale connections investigating the monotonic and cyclic behaviours of traditional timber connections, identifying, and evaluating suitable strengthening techniques with metal devices was performed. Based on the test results a numerical analysis over unstrengthened connections was carried out aiming to extend the parameters evaluated through tests. Then, semi-rigid models for the analysis of traditional timber connections are presented. Synthetic laws are calibrated and the tests performed are modelled. Full-scale timber trusses examples were loaded under symmetric and non-symmetric cyclic loads and the test results were compared to the numerical analysis using the semi-rigid models proposed. Two dismantled Italian King-post truss examples were tested and strengthened in laboratory facilities and one Portuguese Queen-post truss example was tested in field conditions.

Resumo

As ligações desempenham um papel crucial no comportamento de asnas tradicionais de madeira. O comportamento global duma estrutura desse tipo e a distribuição dos esforços internos pelos vários elementos dependem da resistência e da rigidez das ligações, em particular, quando sujeitas a acções assimétricas e acidentais. Nestas condições, as ligações são, frequentemente, submetidas a tensões que ultrapassam o limite elástico, com a consequente introdução de fenómenos não-lineares.

O desconhecimento do comportamento das ligações conduz, frequentemente, à substituição de asnas antigas de madeira, impedindo que se promova o seu reforço, restituindo os necessários níveis de segurança.

O comportamento das ligações não costuma ser considerado pela generalidade dos projectistas, assumindo-se, normalmente, que estas se comportam como articulações perfeitas ou ligações rígidas. No entanto, mesmo na ausência de qualquer elemento de reforço, verifica-se que estas apresentam rigidez rotacional pelo que, em geral, devem ser classificadas como semi-rígidas. Assim, na análise de asnas de madeira devem ser adoptados modelos que simulem o comportamento real das ligações, considerando leis não-lineares e regras de comportamento histerético.

Na presente investigação realizou-se um vasto conjunto de ensaios das ligações mais comuns em asnas de madeira, cujas características se obteve de um exaustivo levantamento de tipologias existentes em Portugal. Essas ligações foram submetidas a carregamentos monotónicos e cíclicos. Nesses ensaios foram considerados diferentes tipos de reforços metálicos. Os resultados obtidos experimentalmente foram reproduzidos com modelos de análise não-linear, baseados no método dos elementos finitos. A partir destes, foram desenvolvidos modelos numéricos simplificados adequados à simulação, expedita, do comportamento semi-rígido das ligações em asnas de madeira.

A eficácia dos modelos numéricos propostos foi claramente comprovada com os resultados obtidos num conjunto de ensaios em laboratório e *in-situ* de asnas à escala real, submetidas a carregamentos cíclicos, simétricos e assimétricos.

Sommario

I collegamenti sono un elemento chiave nel comportamento delle capriate lignee tradizionali. Il comportamento globale e la distribuzione degli sforzi sono funzione della resistenza e rigidezza dei collegamenti, in particolare nel caso di carichi non simmetrici ed eventi estremi. In queste situazioni, i collegamenti sono caricati ben oltre il loro limite pseudo-elastico, introducendo elementi di non linearità nel comportamento strutturale globale.

Questa complessità, in genere, non è considerata nel progetto, dove i collegamenti lignei tradizionali sono assunti come cerniere o come rigidi. Comunque, anche senza nessun intervento di rinforzo, essi presentano una rigidezza rotazionale significativa e potrebbero essere meglio classificati come semi-rigidi e basati sull'attrito. E' la mancata comprensione del comportamento dei collegamenti che di solito porta alla sostituzione delle vecchie strutture di legno, invece del loro recupero al fine di assicurarne la sicurezza, in conseguenza della sottostima della resistenza delle strutture.

Al fine di comprendere e valutare meglio il comportamento delle strutture lignee, sono essenziali dei modelli analitici per i collegamenti. Grazie a modelli semi-rigidi, considerando leggi non lineari e comportamento isteretico, si intende rappresentare il comportamento delle strutture lignee con un livello simile di dettaglio per tutti i componenti strutturali. In questa tesi è presentata l'analisi strutturale di alcune capriate lignee di dimensioni reali. Dopo un'indagine preliminare, è stato eseguito un vasto programma sperimentale, utilizzando collegamenti in scala reale, per investigare il comportamento monotono e ciclico dei collegamenti lignei tradizionali, individuando e valutando le tecniche di rinforzo mediante elementi metallici più adatte. A partire dai risultati sperimentali, è stata eseguita un'analisi numerica sui collegamenti privi di rinforzi.

Sono quindi stati presentati modelli semi-rigidi per l'analisi di collegamenti lignei tradizionali. Sono stati calibrati modelli semplificati e si sono modellate le prove eseguite. Sono state analizzate capriate lignee in scala reale sotto carichi ciclici simmetrici e non simmetrici e i risultati delle prove sono stati messi a confronto con le analisi numeriche effettuate utilizzando i modelli semi-rigidi proposti.

Glossary

α	Skew angle
β	Slope of the bigger notch surface
δ	Reduction factor
ΔF	Increment of load
Δw	Increment of deformation
ϕ_u^+, ϕ_u^-	Maximum rotation at first loading
ϕ_y^+, ϕ_y^-	Rotation values corresponding to the yielding
γ	Slope
μ	Coefficient of friction
ν	Poissons ratio
σ_c	Axial compression stress
τ	Shear force

b	Width of the timber element
d	Distance corresponding to the rear compress surface of the notch
d_e^+	Positive apparent elastic limit displacement
d_e^-	Negative apparent elastic limit displacement
$f_{\mathrm{c,90}}$	Compression strength perpendicular to the grain
f_{m}	Bending strength
f_{v}	Shear resistance
$f_{\mathrm{v,d}}$	Design value of the shear resistance
h	Heigth of the rafter
k_e^+, k_e^-	Elastic stiffness
k_p^+, k_p^-	Post-elastic stiffness
k_r	Average residual stiffness
k_u^+, k_u^-	Secant stiffness at complete unloading
k_0^+, k_0^-	Initial tangent stiffness
M_y^+, M_y^-	Moment values corresponding to the yielding
M_u^+, M_u^-	Maximum moment at first loading
q	Behaviour factor
t_v	Notch depth

A_g	Ratio of the sum of the minimal diameters of all the knots
A_{rafter}	Nominal notch area
E	Youngs modulus
E_{b}	Elastic modulus in bending according to Silvatest®
$E_{\mathrm{c},0}$	Modulus elasticity in compression parallel to the grain
$E_{\mathrm{c},90}$	Modulus of elasticity in compression perpendicular to the grain
$E_{\mathrm{m,l}}$	Local value of the modulus of elasticity in bending
$E_{\mathrm{m,g}}$	Global value of the modulus of elasticity in bending
E_0	Elastic modulus in the direction along the fiber
E_{90}	Elastic modulus in the ortogonal to the fiber direction
F	Force
F_{b}	Bending strength according to Silvatest®
$F_{\mathrm{c},0}$	Compression strength parallel to the grain
$F_{\mathrm{c},0,\mathrm{max}}$	Maximum load of the compression parallel to the grain tests
$F_{\mathrm{c},90,\mathrm{max}}$	Maximum load of the compression perpendicular to the grain tests
F_{max}	Maximum force value
F_1	Force perpendicular to the smaller notch surface
F_2	Force perpendicular to the bigger notch surface
G	Shear modulus
L	Longitudinal direction of the tree trunk
R	Radial direction of the tree trunk
R	Load force
T	Transversal direction of the tree trunk
V_{app}	Apparent volume of wood
V_{eq}	Equivalent viscous damping ratio

CoV	Coefficient of variance
DCH	Ductility class high
DCL	Ductility class low
DCM	Ductility class medium
DCs	Ductility classes
DG	Dial gauges
FEM	Finite element method
H	Horizontal force corresponding to N
LVDT's	Linear voltage differential transducer
MEF	Método dos elementos finitos
MoE	Modulus of elasticity in bending
$M-\phi$	Moment-rotation
N	Axial compression force on the rafter
NDT	Non-destructive tests
RM	Resistance measure
V	Vertical force corresponding to N

Contents

Acknowledgements **iii**

Abstract **v**

Resumo **vii**

Sommario **ix**

Glossary **xi**

Contents **xiii**

List of Figures **xvii**

List of Tables **xxiii**

1 Introduction **1**
1.1 General 1
1.2 Objectives 2
1.3 Outline of the thesis 2

2 Traditional Portuguese timber trusses **5**
2.1 Historic evolution of timber truss system 5
2.1.1 Ancient times 5
2.1.2 After 19th century 8
2.2 Traditional Portuguese timber trusses 8
2.2.1 King-post truss 9
2.2.2 Howe truss 11
2.2.3 Connections in timber trusses 12
2.2.4 On site assessment 13
2.3 Structural behaviour and design 15
2.3.1 Truss static behaviour 16
2.3.2 Traditional connections 17
2.3.2.1 Strength 19
2.3.2.2 Stiffness 22
2.3.2.3 Ductility 23

2.3.3 Degradation and strengthening 24
2.4 Conclusions 25

3 Experimental analysis of traditional timber connections 27
3.1 Introduction 27
3.2 Wood characterization 29
3.2.1 Bending 29
3.2.2 Compression perpendicular to the grain 31
3.2.3 Compression parallel to the grain 31
3.2.4 Discussion of the tests results 33
3.2.5 test setup and instrumentation 34
3.3 Cyclic test procedure 35
3.4 Strengthening techniques studied 36
3.5 Analysis and discussion of the tests results 37
3.5.1 Efficiency evaluation of the strengthening techniques . . 42
3.5.1.1 Stirrup 44
3.5.1.2 Bolt 46
3.5.1.3 Binding strip 50
3.5.1.4 Tension ties 54
3.5.1.5 Strengthening conclusions and comparisons . . 56
3.6 Conclusions 61

4 Numerical modelling of traditional timber connections 63
4.1 Numerical modelling 63
4.1.1 Material model 63
4.1.2 Geometric constraints, mesh and loading 65
4.2 Numerical *versus* experimental results 66
4.3 Sensitivity study 69
4.3.1 Friction coefficient 69
4.3.2 Compression level on the rafter 71
4.3.3 Skew angle 72
4.3.4 Notch depth 73
4.3.5 Angle of the notch 76
4.3.6 Height of the rafter 76
4.4 Effects of the wood specie 77
4.5 Conclusions 79

5 Semi-rigid modelling of traditional timber connections 81
5.1 Introduction 81
5.2 Models behaviour of semi-rigid traditional timber connections . 82
5.3 Numerical modelling 82
5.3.1 Definition of the model parameters 82
5.3.2 Assessment and discussion of the model parameters . . 84
5.3.3 Synthetic characterization 86
5.3.3.1 Monotonic tests 86
5.3.3.2 Cyclic tests 93

5.3.4 Effectiveness of the physical models 95
5.4 Application to the full-scale tests results 97
5.4.1 FEM model 98
5.4.2 unstrengthened connections 99
5.4.3 strengthened connections 99
5.5 Conclusions 99

6 Laboratory tests on full-scale timber trusses 101
6.1 Introduction 101
6.2 Trusses evaluated 102
6.3 Non-destructive evaluation of the trusses 102
6.3.1 Geometric assessment 102
6.3.2 Moisture content 103
6.3.3 Density evaluation 103
6.3.4 Visual grading 104
6.3.5 Non-destructive tests 106
6.3.5.1 Hardness test 106
6.3.5.2 Pilodyn® 107
6.3.5.3 Resistograph® 107
6.3.5.4 Sylvatest® 109
6.3.5.5 Mechanical evaluation of the modulus of elasticity in bending 111
6.3.6 Analysis and discussion of NDE 112
6.4 Load-carrying tests 113
6.4.1 Test setup, instrumentation and procedure 114
6.4.2 Evaluation of the trusses behaviour 115
6.4.3 Strengthening 119
6.4.4 Efficiency evaluation of the strengthening 121
6.4.5 Strengthening influence 123
6.4.6 Numerical analysis 127
6.4.6.1 Material model 127
6.4.6.2 Geometric and mechanical models 127
6.4.6.3 Loads 127
6.4.6.4 Semi-rigid modelling of connections 127
6.4.6.5 Numerical versus experimental results 128
6.4.7 Conclusions 131

7 Field load tests on full-scale timber trusses 133
7.1 Abstract 133
7.2 Introduction 133
7.3 Preliminary tests 134
7.4 Adico queen-post truss 135
7.5 Test setup, instrumentation and procedure 137
7.6 Analysis of the test results 140
7.7 Numerical Analysis 144
7.8 Numerical *versus* tests results 144

7.8.1 Symmetric tests 144
7.8.2 Asymmetric tests 145
7.9 Conclusions 148

8 Conclusions and Recommendations **151**
8.1 Conclusions 151
8.2 Recommendations 154

Bibliography **157**

A Examples of Portuguese traditional timber trusses **163**

B Full-scale connections tests results **169**
B.1 Unstrengthened connections 169
B.2 Strengthened connections 170

C ABAQUS/Standard input file **177**

D Parameters of the $M - \phi$ experimental curves **183**

List of Figures

2.1 Timber truss of the St. Catherine church in Mount Sinai (Tampone, 1996). 6
2.2 Different timber truss configurations following (Serlio, 1584). . . . 7
2.3 Representation of the timber roof of Westminster Hall (Tampone, 1996). 7
2.4 Most common timber trusses configuration in Portugal (Costa, 1955). 9
2.5 King-post truss. 10
2.6 Possible basic static behaviours of the king-post truss. 10
2.7 Italian king-post truss with double rafters. 11
2.8 Howe truss with Princess posts (Princess-post truss). 12
2.9 Most frequent step joints in traditional timber roofs structures. . . 12
2.10 Examples of step joints of timber trusses presenting tenon and mortise (Appleton, 2003). 13
2.11 Examples of different notches geometries for single step joints of rafter-tie beam connections. 14
2.12 Examples of connections strengthened with metal elements. 14
2.13 Faulty design examples. 15
2.14 Different misconceived connections between the tie beam and the king post. 15
2.15 Main resistant mechanism in a traditional timber connection. . . . 18
2.16 Force mechanisms in a single step frontal joint (tie beam-rafter) disregarding friction forces and geometric imperfections and under compression of the rafter. 19
2.17 Force decomposition in a single step frontal joint. 20
2.18 Force mechanism in a single posterior step joint. 21
2.19 Force mechanism in a double step joint. 22

3.1 Load mid-span deformation curves obtained in the bending tests. . 30
3.2 Force-deformation curves of the compression perpendicular to the grain tests. 31
3.3 Force-deformation curves of the compression parallel to the grain tests. 32
3.4 Testing apparatus and instrumentation layout. 34
3.5 Connections geometry (mm). 35

3.6 Traditional strengtheneing techniques evaluated. 36
3.7 Force-displacement curves of unstrengthened connections with 30° skew angle for monotonic loading in positive direction and different rafter compression stress. 38
3.8 Slip mechanism observed when decreasing the skew angle (negative direction). 38
3.9 Force-displacement curves of unstrengthened connections with 30° skew angle for monotonic loading in negative direction and different rafter compression stress. 39
3.10 Force-displacement curves of unstrengthened connections with 30° skew angle for monotonic tests under different rafter compression stress. 40
3.11 Force-displacement curves of unstrengthened connections with 60° skew angle for monotonic tests under different rafter compression stress. 41
3.12 Force-displacement curves of unstrengthened connections with 30° and 60° skew angle for monotonic tests under different rafter compression stress. 42
3.13 Force-displacement curves of unstrengthened connections with 30° and 60° skew angle under ciclic loading for different rafter compression stress. 43
3.14 Damages observed in the connections with a skew angle of 30° in the cyclic tests for 2.5 MPa compression stress. 44
3.15 Force-displacement curves of stirrup strengthened connections with 30° and 60° skew angles under monotonic loading. 45
3.16 Final position of the strengthened connections under monotonic loading (30° skew angle). 46
3.17 Force-displacement loops for stirrup strengthened connections with 30° and 60° skew angle under cyclic loading. 47
3.18 Force-displacement curves of bolt strengthened connections with 30° and 60° skew angles under monotonic loading. 47
3.19 Damages observed in the 30° skew angle strengthened connections with bolt under monotonic loading in the positive direction. 49
3.20 Damages observed in the 30° skew angle strengthened connections with bolt under monotonic loading in the negative direction. . . . 49
3.21 Force-displacement loops for bolt strengthened connections with 30° and 60° skew angle under cyclic loading. 50
3.22 Force-displacement curves for 30° skew angle strengthened connections with binding strip under monotonic loading. 51
3.23 Damage observed in the 30° skew angle strengthened connections with binding strip under monotonic loading in positive direction. . 52
3.24 Force-displacement loops for 30° skew angle strengthened connections with binding strip under cyclic loading. 53
3.25 Damages observed in the 30° skew angle strengthened connections with binding strip under cyclic loading. 54

3.26 Force-displacement curves of tension ties strengthened connections with 30° and 60° skew angles under monotonic loading. 54
3.27 Damages observed in the 60° skew angle strengthened connections with tension ties under monotonic loading. 55
3.28 Force-displacement loops for tension ties strengthened connections with 30° and 60° skew angle under cyclic loading. 56
3.29 Force-displacement curves for unstrengthened and strengthened connections with 30° skew angle under monotonic loading. 57
3.30 Force-displacement curves for unstrengthened and strengthened connections with 60° skew angle under monotonic loading. 58
3.31 Force-displacement loops for unstrengthened and strengthened connections with 30° skew angle under cyclic loading. 59
3.32 Force-displacement loops for unstrengthened and strengthened connections with 60° skew angle under cyclic loading. 60
3.33 Out-of-plane movements detected in the 60° skew angle connections strengthened with binding strip. 61

4.1 $\sigma - \epsilon$ law for compression ortogonal to the grain assumed in the model. 65
4.2 Boundary conditions and material axes adopted. 66
4.3 Finite element mesh adopted and definition of the contact surfaces. 67
4.4 Comparison between experimental and numerical force-displacement curves (30° skew angle). 68
4.5 Comparison between experimental and numerical force-displacement curves (60° skew angle). 69
4.6 Front notch geometric deviation effect in the force-displacement numerical curve for 60° skew angle under positive rotation. 70
4.7 Front notch geometric deviation effect in the resistant mechanism for 60° skew angle under positive rotation. 70
4.8 Friction coefficient effects on the numerical force-displacement curves under negative rotation (30° skew angle). 71
4.9 Friction coefficient effects on the numerical force-displacement curves under negative rotation (60° skew angle). 71
4.10 Effect of the rafter's compression level on the numerical force-displacement curves (30° skew angle). 72
4.11 Effect of the rafter's compression level on the numerical force-displacement curves (60° skew angle). 72
4.12 Geometry of the 45° skew angle connection (mm). 73
4.13 Effect of the skew angle on the numerical force-displacement curves. 74
4.14 Effect of the notch depth on the numerical force-displacement curves (30° skew angle). 75
4.15 Effect of the notch depth on the numerical force-displacement curves (60° skew angle). 75
4.16 Effect of the notch angle on the numerical force-displacement curves under negative rotation (30° skew angle). 76
4.17 Effect of the notch angle on the numerical force-displacement curves under negative rotation (60° skew angle). 76

4.18 Effect of the rafter height's on the numerical force-displacement curves (30° skew angle). 77
4.19 Effect of the rafter height's on the numerical force-displacement curves (60° skew angle). 78
4.20 Material properties effects on the numerical force-displacement curves (60° skew angle). 80

5.1 Model parameters of the experimental $M - \phi$ first loading curve (positive rotation). 83
5.2 Yielding and ultimate moments dependency reported by tests results on unstrengthened connections. 84
5.3 Comparison of the $M - \phi$ bilinear curves fitted to tests results on unstrengthened connections. 85
5.4 Synthetic model of the resisting mechanism at elastic proportionality limit (Candelpergher, 1999). 88
5.5 Relative negative rotation of elements at ultimate state under 2.5 MPa axial compression of the rafter. 90
5.6 Ultimate equilibrium for negative rotation. 91
5.7 Relative positive rotation of elements at ultimate state. 93
5.8 Ultimate equilibrium for positive rotation. 93
5.9 Non linear rotational spring element proposed by Parisi and Piazza (1998). 94
5.10 C_1 and C_2 dependency from l_v value. 96
5.11 Effectiveness of the M_y^- prediction. 96
5.12 M_u^- dependency. 97
5.13 M_u^+ dependency. 98
5.14 FEM model adopted to modelled the cyclic tests. 98

6.1 Scheme of the two king-post trusses evaluated with the rule adopted for numbering the timber elements. 102
6.2 Comparison between the geometric properties of the cross-sections: a) supposing rectangular and b) with detailed measurements (dimensions in millimeters). 103
6.3 Correlation between depth penetration obtained with Pilodyn® and density 108
6.4 Correlation between MoE given by non-destructive methods and MoE found through the direct mechanical evaluation according EN408(2003).113
6.5 Load procedure applied in the load-carrying tests. 114
6.6 Instrumentation layout. 115
6.7 Asymmetric behaviour of $Truss$ 1 under symmetric loading condition (S-U-S). 116
6.8 Behaviour of the connection between the king post and the tie beam under symmetric loading conditions. 116
6.9 Horizontal displacement recorded in the support under symmetric loading. 117

6.10 Asymmetric behaviour emphasised under non-symmetric loading of *Truss* 1 during S-U-Dx test. 117
6.11 Distortion of the tie beam under non-symmetric loading of *Truss* 1 during S-U-Sx test. 118
6.12 Bending of the steel rod inserted in the tie connection. 118
6.13 Out-of-plane movement observed in the *Truss* 1 (unstrengthened) under ULS at the end of 1st cycle. 119
6.14 Strengthening of *Truss* 1. 120
6.15 Strengthening of *Truss* 2. Screws and binding strip applied in the beyond part of the step in the rafter/tie beam connection. 121
6.16 Failure damages of *Truss* 1. 122
6.17 Shear failure of the tie beam-rafter connection for *Truss* 2. 123
6.18 Double step connections between the rafters and the tie beam of *Truss* 2. 123
6.19 Moment-rotation response of the left rafter-tie beam connection of *Truss* 2 under unstrenghthened and strengthened conditions. . . . 124
6.20 Moment-rotation response of the left rafter-tie beam connection of *Truss* 1 under unstrenghthened and strengthened conditions. . . . 125

7.1 Adico princess-post truss. 134
7.2 Luanda princess-post truss configuration and connection detail. . . 135
7.3 Truss geometry (mm). 136
7.4 Emergence holes over the surface of sapwood. 136
7.5 Map of the decay extension in the truss. 137
7.6 Calculation of the cross-section reduction based in a Resistograph test profile. 137
7.7 Instrumentation of the tests. Eight LVDTs and six DGs. 138
7.8 Displacement recorded by LVDTs 1, 2 and 3 during 3F-C test. . . 140
7.9 Behaviour of the king post-tie beam connection during 3F-C test. . 141
7.10 Behaviour of the connections between the queen posts and the tie beams during 3F-C and 5F-S tests. Negative values are recorded when the two elements are approaching. 141
7.11 Behaviour of the left rafter-tie beam connection during 3F-C test. 142
7.12 Displacement recorded by LVDTs 1, 2 and 3 during 3F-N test. . . 142
7.13 Comparison between rotations calculated based on values recorded by LVDTs 4 and 6 during 3F-C and 5F-S tests. 143
7.14 Comparison between the displacements recorded by LVDTs 1, 2 and 3 during 3F-C and 5F-C tests. 143
7.15 Bending moment on the truss in the 3F-C test. 145
7.16 Rotational stiffness of connections influence in the model results in comparison with test results under symmetric loading. 148
7.17 Rotational stiffness of connections influence in the model results in comparison with test results under non-symmetric loading. 149

A.1 City hall, Pátio do Salema (Évora). 163
A.2 University of Évora, Verney College (Évora). 163

A.3 Galp garage, main truss (Guimarães). 164
A.4 Galp garage, secondary truss (Guimarães). 164
A.5 Rodrigues de Freitas High school, building A (Porto). 164
A.6 Rodrigues de Freitas High school, building B (Porto). 164
A.7 Rodrigues de Freitas High school, building C (Porto). 165
A.8 Rodrigues de Freitas High school, building D (Porto). 165
A.9 St. Domingos building (Porto). 165
A.10 Sá de Miranda High school, main building (Braga). 165
A.11 Sá de Miranda High school, secondary building (Braga). 166
A.12 Sá de Miranda High school, gymnasium (Braga). 166
A.13 Jacques Delors rail-station (Mirandela). 166
A.14 Adico Industries (Avanca). 166
A.15 Refer warehouse (Ovar). 167
A.16 Refer warehouse (Régua). 167
A.17 Teixeira sawmill (S. João da Madeira). 167

B.1 Force-displacement curves of unstrengthened connections with 30º skew angle for monotonic loading in positive direction under 1.4MPa rafter compression stress. 169
B.2 Force-displacement curves of unstrengthened connections with 30º skew angle for monotonic loading in negative direction under 1.4MPa rafter compression stress. 170
B.3 Force-displacement curves of unstrengthened connections with 30º skew angle for monotonic loading in positive direction under 2.5MPa rafter compression stress. 171
B.4 Force-displacement curves of unstrengthened connections with 30º skew angle for monotonic loading in negative direction under 2.5MPa rafter compression stress. 172
B.5 Force-displacement curves of unstrengthened connections with 60º skew angle for monotonic loading in positive direction under 1.4MPa rafter compression stress. 173
B.6 Force-displacement curves of unstrengthened connections with 60º skew angle for monotonic loading in negative direction under 1.4MPa rafter compression stress. 173
B.7 Force-displacement curves of unstrengthened connections with 60º skew angle for monotonic loading in positive direction under 2.5MPa rafter compression stress. 174
B.8 Force-displacement curves of unstrengthened connections with 60º skew angle for monotonic loading in negative direction under 2.5MPa rafter compression stress. 175
B.9 Force-displacement loops of 30º skew angle strengthened connections with tension ties under cyclic loading. 175
B.10 Force-displacement loops of 60º skew angle strengthened connections with tension ties under cyclic loading. 176

List of Tables

3.1 Tests performed on traditional timber connections. 28
3.2 Bending tests results. 30
3.3 Compression perpendicular to the grain tests results. 32
3.4 Compression parallel to the grain tests results. 33
3.5 Comparison between the mechanical properties for *Pinus Pinaster*, Ait. quality class E obtained in the test results and reported by LNEC (1997). 34
3.6 Effect of the rafter compression levels in the response of unstrengthened connection with 30º skew angle under monotonic loading. . . 40
3.7 Effect of the rafter compression levels in the response of unstrengthened connection with 60º skew angle under monotonic loading. . . 41
3.8 Effect of the rafter compression stress in the response of unstrengthened connection under monotonic loading. 44
3.9 Monotonic tests results of strengthened connections with stirrups. 45
3.10 Cyclic tests results of strengthened connections with stirrups. . . . 48
3.11 Monotonic tests results of strengthened connection with bolts. . . 48
3.12 Cyclic tests results of strengthened connection with bolts. 50
3.13 Monotonic tests results of strengthened connection with binding strip. 52
3.14 Cyclic tests results of strengthened connection with binding strip. 53
3.15 Monotonic tests results of strengthened connection with tension ties. 55
3.16 Cyclic tests results of strengthened connection with tension ties. . 57
3.17 Cyclic tests results of 30º skew angle connections. 59
3.18 Cyclic tests results of 60º skew angle connections. 61

4.1 Material properties adopted in the numerical model. 65
4.2 Material properties adopted in the numerical model. 79

5.1 Parameters of the $M-\phi$ experimental curves obtained for negative rotation. 86
5.2 Parameters of the $M-\phi$ experimental curves obtained for positive rotation. 87
5.3 Coefficients C_1 and C_2. 89
5.4 Coefficients C_3 and C_4. 92

5.5 Effectiveness of the FEM results. Error in (%) of the FEM prediction in comparison with the test result. 96

6.1 Moisture content values measured in each element of both trusses. 104
6.2 Density values for each element of the two trusses studied. 105
6.3 Results of the visual strength grading according to UNI 11035 (2003).106
6.4 Elastic modulus estimated by means of the Turrini-Piazza hardness test. 107
6.5 Depth penetration mean values measured with the Pilodyn®. . . . 108
6.6 Sylvatest® results for the element Rafter 22. 110
6.7 Sylvatest® results using the direct method. 111
6.8 Elastic modulus obtained by means of four-point bending tests. . . 112
6.9 Load-carying tests performed. 115
6.10 Maximum displacement recorded by the instrumentation setup during the load-carrying tests on *Truss 2*. 126
6.11 Maximum displacement recorded by the instrumentation setup during the load-carrying tests on *Truss 2*. 130
6.12 Nlinks stiffness values used on numeric analysis of the load-carrying tests on *Truss 2*. 132

7.1 Summary of the tests performed. 139
7.2 Comparison between numerical values (Num.) and tests results (Exp.). Error express in (%). 146
7.3 Axial stiffness values (kN/m) used in the numerical model. 146
7.4 Axial stiffness values (kN/m) used in the numerical model of 3F-N test. 147

B.1 Tests results of unstrengthened connections with 30° skew angle for monotonic loading in positive direction under 1.4MPa rafter compression stress. 170
B.2 Tests results of unstrengthened connections with 30° skew angle for monotonic loading in negative direction under 1.4MPa rafter compression stress. 171
B.3 Tests results of unstrengthened connections with 30° skew angle for monotonic loading in positive direction under 2.5MPa rafter compression stress. 171
B.4 Tests results of unstrengthened connections with 30° skew angle for monotonic loading in negative direction under 2.5MPa rafter compression stress. 172
B.5 Tests results of unstrengthened connections with 60° skew angle for monotonic loading in positive direction under 1.4MPa rafter compression stress. 172
B.6 Tests results of unstrengthened connections with 60° skew angle for monotonic loading in negative direction under 1.4MPa rafter compression stress. 174

B.7 Tests results of unstrengthened connections with 60° skew angle for monotonic loading in positive direction under 2.5MPa rafter compression stress. 174
B.8 Tests results of unstrengthened connections with 60° skew angle for monotonic loading in negative direction under 2.5MPa rafter compression stress. 175
B.9 Cyclic tests results of 30° skew angle strengthened connections with tension ties. 176

D.1 Parameters of the $M - \phi$ experimental curves obtained on unstrengthened connections under negative rotation. 184
D.2 Parameters of the $M - \phi$ experimental curves obtained on strengthened connections under negative rotation. 185
D.3 Parameters of the $M - \phi$ experimental curves obtained on unstrengthened connections under positive rotation. 186
D.4 Parameters of the $M - \phi$ experimental curves obtained on strengthened connections under positive rotation. 187

Chapter 1

Introduction

1.1 General

Traditional building construction in Portugal (from the 18^{th} to early 20^{th} century) adopted timber roof and floor structures and, in some cases, also timber reinforced masonry walls. A significant number of these buildings is still in use, despite some major modifications. Even when the use of concrete became generalised, timber structures kept an important use in roof construction. The common Portuguese timber roof structures are composed of trusses, width different geometries, depending on the Architecture of the building, its use and, in most cases, the span of the roof. Traditionally, Portuguese timber roofs are formed by trusses with an average free span of 6 m, mostly following a king-post configuration. For higher spans, auxiliary posts and struts are introduced to receive the extra purlins, following the Howe truss, also called Queen-post truss if two posts are added and Princess-post truss in the case of four auxiliary posts. Step joints, in some cases presenting tenon and mortise, single (one notch) or double (two notchs), make the connections between truss members. Forces are directly transferred by compression and/or friction. To improve the contact between the connected members, joints are usually strengthened with metal elements. These metal elements significantly increase the resistance of the joints to out-of-plane loads as well as reversal actions. Usually, stirrups, binding strip and bolts are used to strength traditional timber connections. The most frequently used wood species are: Maritime Pine (*Pinus pinaster*, Ait.), Eucalyptus (*Eucalyptus globulus*, Labill.) and Chestnut (*Castanea sativa*, Mill.). As consequence of the abandoned that they suffered, a significant part of the know-how about the design and construction of timber trusses disappeared. Examples presenting faulty design decisions (model, connections, details, etc.) became popular. Nowadays, traditional timber trusses are analyzed assuming common models like hinges or rigid for their connections. However, their behaviour is semi-rigid, presenting a significant moment-resisting capacity friction based. In particular under non-symmetric loading conditions like wind, snow or earthquake the role of the connections is crucial because, normally, in

these situations, the connections are loaded well beyond their pseudo-elastic limit. In fact, it is the lack of realistic, but practical, models for the connections that normally leads to the replacement of old timber structures, instead of their retrofitting to satisfy safety. Moreover, the misunderstanding of the overall behaviour of the truss can result in unacceptable stress distribution in the members because of inappropriate joints strengthening (in terms of stiffness and/or strength). In order to better predict and understand the behaviour of timber structures, analytical models of connections are crucial. The restoration or the design of new timber structures needs the correct load transfer that can only be determined in an analysis when the real behaviour of the connections is know. The semi-rigid modelling of timber connections, using nonlinear moment-rotation laws and hysteretic rules, intends to represent the behaviour of timber structures with a comparable level of detail for all the structural components. In particular, with these models, the seismic design acknowledges and exploits the dissipation capabilities of their hysteresis behaviour. A research program aimed of investigating the monotonic and cyclic behaviours of traditional timber connections, identifying, and evaluating suitable strengthening techniques with metal devices was proposed. University of Minho (Portugal), University of Trento (Italy) and the Timber Structures Division of National Laboratory for Civil Engineering (Portugal) collaborate in a research program in which this thesis fits.

1.2 Objectives

The main goals of the thesis work can be summarized in:

- Assessment of the structural behaviour of traditional timber trusses and connections;
- Evaluation of traditional timber connections behaviour and assess the influence of different strengthening tehcniques with metal devices;
- Semi-rigid modelling of traditional timber connections;
- Full-scale tests on traditional timber trusses;
- Efficiency studies of the semi-rigid models.

1.3 Outline of the thesis

Following a brief historic resume of the timber truss evolution as a structural system, the results of a preliminary survey intending to describe must common geometries, materials and on site pathologies is presented in Chapter 2. The overall structural behaviour of traditional Portuguese timber trusses is analysed and special attention is paid to structural connections and construction errors effects. Degradation process and strengthening techniques are reported.

In Chapter 3 a series of monotonic and cyclic tests on unstrengthened specimens were performed in order to characterize the original behaviour of connections representative of traditional timber trusses. Subsequently, connections strengthened with metal devices were tested under monotonic and cyclic loading. Tests on assembled connections were preceded by accurate material characterization, in terms of the mechanical properties of the timber elements used for all full-scale models.

Chapter 4 focuses in the main parameters affecting the mechanical behaviour of the unstrenghthened traditional timber connections experimentally analyzed. For that, a numerical analysis using FEM was performed. Parametric studies followed the calibration process of the model.

Chapter 5 comprises the semi-rigid modelling of traditional timber connections. The tests results on full-scale connections were reproduce in a numerical analysis considering semi-rigid models. Synthetic Moment - Rotation laws, defined based in the monotonic tests results, were introduced in the SAP2000 (2007) commercial software. Using this software and the synthetic laws, cyclic tests of unstrengthened and strengthened connections were reproduced.

In Chapter 6, an accurate geometric and mechanical evaluation of the timber elements of two timber king-post trusses, based in grading results with data gathered from non-destructive tests (NDT), including mechanical evaluation of the modulus of elasticity in bending (MoE), followed by full-scale tests were performed. The trusses were reassembled in laboratory and submitted to a series of symmetric and non-symmetric tests, according to the Limit States. Strengthening techniques evaluated in precedents research steps were used in a second phase of the carrying tests.

The last step of this thesis is the analysis of field load tests on traditional timber trusses, which is done in Chapter 7. The main goal of the tests was to evaluate the overall behaviour of the timber truss under symmetric and non-symmetric loading. Moreover, the influence of the location of point loads application, without and with eccentricity relatively to joints, was assessed. The carrying tests were preceded by a visual and non-destructive inspection aiming to collect geometric data and to assess the decay level. The field tests results of a queen-post truss are presented and analyzed. A numerical model was developed to reproduce the test results.

Chapter 8 summarizes all the important concluding remarks derived during the thesis, and also future work in the structural analysis of traditional timber trusses is proposed.

Chapter 2

Traditional Portuguese timber trusses

2.1 Historic evolution of timber truss system

In this item, historic evolution of the timber truss system is briefly described. For a more deep analysis the reading of Tampone (1996) and Barbisan and Laner (2000) is suggest.

2.1.1 Ancient times

Truss represents the most traditional timber structure with an extraordinary importance in the construction progress. The use of these sturctures is old as man kind. In fact, the first timber trusses were used by primitive men as protection against the atmospheric agents, and since then, its presence in Architecture is permanent. Altrough the low robustness of those structures hindered that few examples survived, there are proofs that in Ancient Greece (4^{th} century BC) a well defined technique of construction of inclined timber roofs existed. However, these roofs structure did not use trusses but were formed by simply supported rafters. The timber truss structural configuration is based on the Roman techniques of the 4^{th} century, developed when Christian churches were cover by king-post trusses. It is believed that the most ancient example of timber trusses, built by architect Stephen of Aila in the 6th century, is located at the St. Catherine church in Mount Sinai. These timber trusses are formed by two rafters and one king post connected to a tie beam, all with the same cross-section and with two struts of minor section, Figure 2.1.

This structural example, innovative for its time, represents unfortunately one isolate example. In fact, for centuries different configurations were used as can be concluded from the observations of different manuals of Architecture. For example, in 14^{th} century timber trusses were constructed with precise techniques but without a clear idea of the structural scheme to use. In the beginning of the Renaissance, 1427-1433, Mariano di Jacopo designs diverse timber trusses, in particular: two with the king post stiffly connected

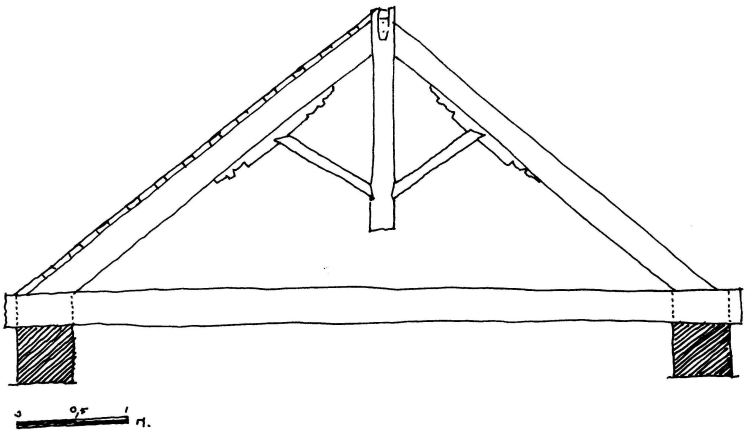


Figure 2.1: Timber truss of the St. Catherine church in Mount Sinai (Tampone, 1996).

to the tie beam reinforced at mid-span; one without tie beam and, another one without king post and with the tie beam made of steel. Moreover, the solution of connecting the tie beam to the king post has not precise date. For instance, in 1539 Giovan Battista Da Sangallo draws one truss with three posts and two rafters where the tie beam is not connected to the posts while Andrea Palladio in 1570, presents diverse trusses with the tie beam connected to the king post. However, for the first time, in "The Four Books on Architecture" by Andrea Palladio published in 1570, Palladio (1945), the configuration of the truss became defined by the static system that better fits (safety) the roof Architecture. In 1584, Serlio (1584) in his "Seven books of Architecture" presents a large range of possible structural schemes for timber trusses. However, the selection of the best solution and the design of the different elements is left to the carpenter experience. In Figure 2.2 some trusses proposed by Serlio (1584) are show. In these examples, the suggestion to increase the number of posts for bigger spans, resulting in a significant decrease of the bending stress in the tie beam is clear.

The evolution of the truss configuration differs significantly from region to region. While in Mediterranean regions a type of truss with slight pitch is consolidate, in Central and North Europe a more complex and Gothic geometry have been developed. For example, in Westminster Hall (London) in 1394, in order to give greater strength to the framing, a large arched piece of timber is carried across the hall, rising from the bottom of the wall piece to the centre of the collar beam. The latter is also supported by curved braces rising from the end of the hammerbeam. Those elements are the portions remaining of the tie beam when this is cut through in order to give greater height in the centre.

In Northern Europe, timber roofs structures with a three-dimensional structural behaviour are common, in particular in roofs with significant pitches. In

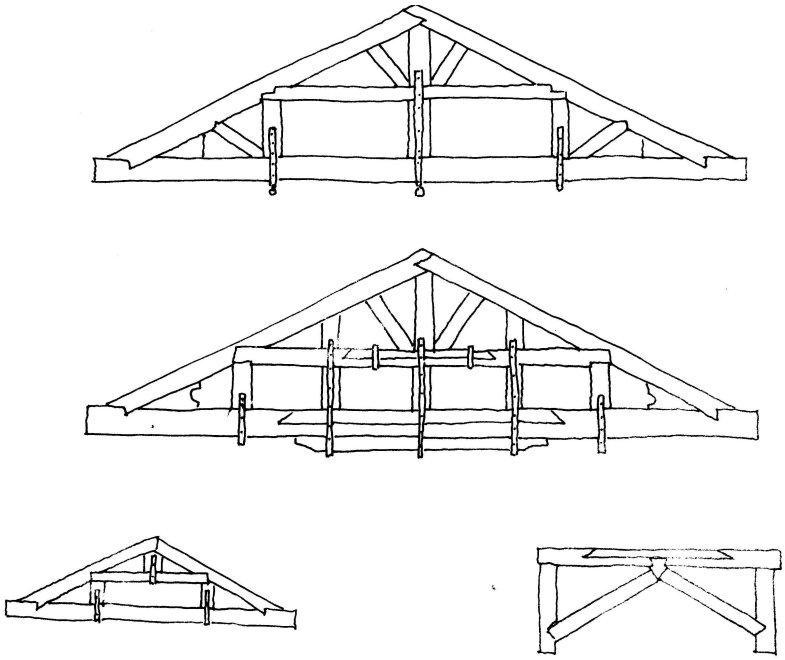


Figure 2.2: Different timber truss configurations following (Serlio, 1584).

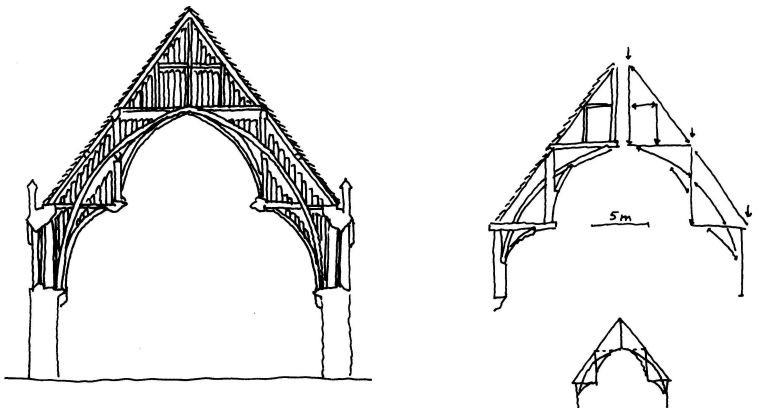


Figure 2.3: Representation of the timber roof of Westminster Hall (Tampone, 1996).

fact, in this case, lateral wind loads are higher and bracing elements in all three directions are of greater importance. This type of solution is also present in Mediterranean regions, in particular in structuraly demanding roofs. In Centre and Northern Europe, the timber truss is part of the structure, having habitable lofts, and tie beam has the additional function of supporting the pavement. In some cases, as the medieval stave churches (northwester Europe), timber trusses are integrate in a post and beam construction related to timber framing. The wall frames are filled with vertical planks and, for lateral bracing, additional wooden brackets are inserted between the rafters, resulting in a very rigid construction.

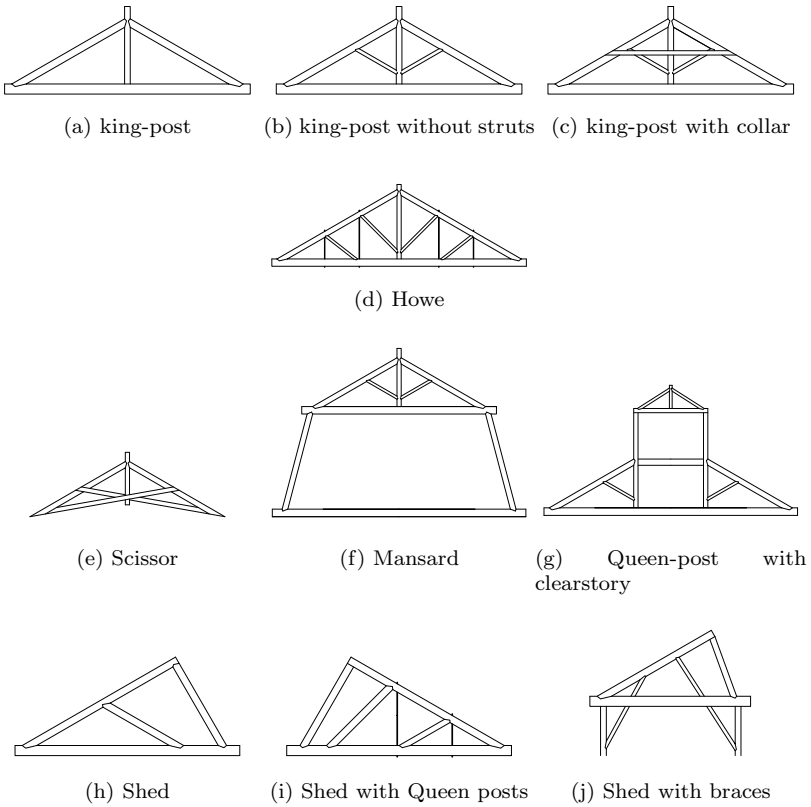
2.1.2 After 19th century

Until the 19th century, timber trusses were designed as simple supported beams or as reticular structures. In these structures, elements, in particular the tie beam, are subjected to considerable bending. Only after this period, structures were designed so that axial forces (compression or tension) were the main stresses. This was achieves using the three-hinged static scheme, detaching the tie beam from the post. After this, construction manuals are based on more consistent knowledge on the structural behaviour of timber trusses and of wood as material. In this context, the field of application of timber trusses is significantly reduced, as more noble structures are built in iron, and later in steel and concrete. Therefore, designers turn their attention towards light trusses, more or less complex variations of the king-post truss. The range of possible configurations in which it is practical to assemble different timber elements to form a truss is vast. Obviously, the selection depends of many factors: span, loads, roof inclination, etc. Nevertheless, the disposition of the different timber elements, normally follow the rule that the shorter elements should work in compression and the longer in tension, thus preventing problems of buckling.

2.2 Traditional Portuguese timber trusses

Following Costa (1955), the most common timber trusses configurations in Portuguese construction are: (a) King-post, (b) King-post without struts, (c) King-post with a collar, (d) Howe, (e) Scissors, (f) Mansard, (g) Queen-post with a clearstory, (h), (i), and (j) Shed trusses, see Figure 2.4.

However, the tipical Portuguese timber roof structures use king-post trusses for spans until 7-8 meters and for higher spans, seldonly over 13-14 meters, the Howe truss is employed. Due to their importance, not only in the Portuguese Architecture, but in all Mediterranean regions, those two truss typologies will be described with more detail.



(a) king-post (b) king-post without struts (c) king-post with collar

(d) Howe

(e) Scissor (f) Mansard (g) Queen-post with clearstory

(h) Shed (i) Shed with Queen posts (j) Shed with braces

Figure 2.4: Most common timber trusses configuration in Portugal (Costa, 1955).

2.2.1 King-post truss

King-post truss is certainly the most wide spread timber truss configuration. They represent the simple timber truss geometry that has been used in monumental constructions, like churches and monasteries, and in rural Architecture. This truss is characterized for having a horizontal member (tie beam), two principal rafters connected to the tie beam inclined to form the roof, a vertical member at the middle (king post) and two inclined struts, connecting the king post to each principal rafter, Figure 2.5.

However, some variations of this geometry are known, for small spans or when the purpose of the truss is to support one point load, the struts can be removed (see Figure 2.4b); sometimes the tie beam is removed and replaced by a collar located in an upper level (see Figure 2.4c). King-post trusses are the most basic structural configuration of inclined timber roofs and can have three different static behaviours: three-hinged arch, simply supported beam

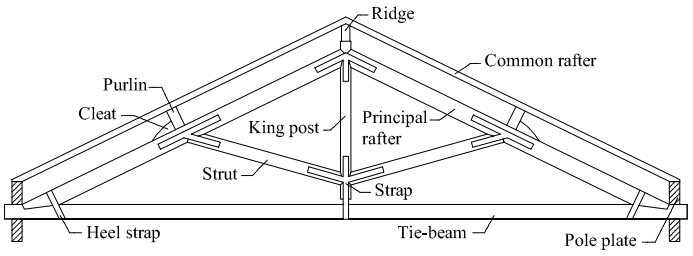


Figure 2.5: King-post truss.

and reticular beam, see Figure 2.6.



(a) Three-hinged arch



(b) Simply suport beam



(c) Reticular beam

Figure 2.6: Possible basic static behaviours of the king-post truss.

It is the connection between the king post and the tie beam that determines the overall static behaviour of the truss:

- Three-hinged arch (Figure 2.6a) - in theory the best behaviour, only possible when the tie beam is detached or connected without the introduction of bending stiffness. Therefore the tie beam is essentially tensioned, and bending is associated majorly with self-weight;
- Simply supported beam (Figure 2.6b) - cannot be considered a real truss. The loads applied will be directly transmitted through the king post to the tie beam, which behaves as a simply support beam with a three point bending diagram;
- Reticular beam (Figure 2.6c) - to the isostatic triangle, composed by the struts and the tie beam, the king post connected to the tie beam with

different possible joints is added. Therefore, the tie beam becomes a element subjected to tension and bending, in which the bending stress can be important.

Below the purlins, two oblique elements, called struts, leaving from the base of the king post, support the rafter. Consequently the rafters bending provided by the purlins point loads, is minimized. Moreover, now, the king post is submitted to tension provided by the vertical component of the compression force acting on the struts. In Portugal, in opposition to others Mediterranean countries, trusses are made by rafters incapable to resist to bending moments. In fact, traditional Portuguese timber trusses are characterizes by slender elements, which should only subjected to axial stresses. In Italy, for example, timber trusses have more robust cross-sections, since significant bending moments in the rafters are common. In some cases, double rafters are employed to increase the resistance of the structure, Figure 2.7.

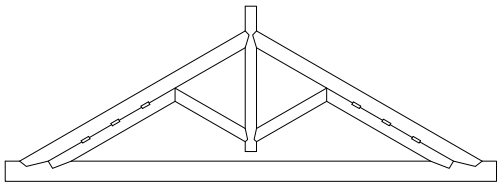


Figure 2.7: Italian king-post truss with double rafters.

In Portugal, when more purlins are needed to support the covering structure, posts are added to the king-post truss originating a more complex truss geometry (Howe truss).

2.2.2 Howe truss

Howe truss results from the addition of posts to the king-post truss configuration. For spans over 7-8 meters, king-post configuration no longer is acceptable. In fact, more purlins are required and, as already pointed out, the rafters are not prepared to suffer significant bending stresses. As consequence more struts supporting the rafters are included, resulting in trusses as that show in Figure 2.8. To balance the vertical component of the compression force acting in the struts, a post, connecting the tie beam to the rafters is needed. Suspending the tie beam from the post reduces bending moments and self-weight bending deformation. The first post is the king, the second and third are called queens and the forth and fifth are the princess posts. It is common to call the Howe truss by the name of the posts, see Figure 2.8.

Howe truss allows longer spans by simply adding few elements to the king-post configuration, keeping slender elements. Usually the spans do not exceed 13 meters and the Howe truss more common is the so-called Princess-post truss.

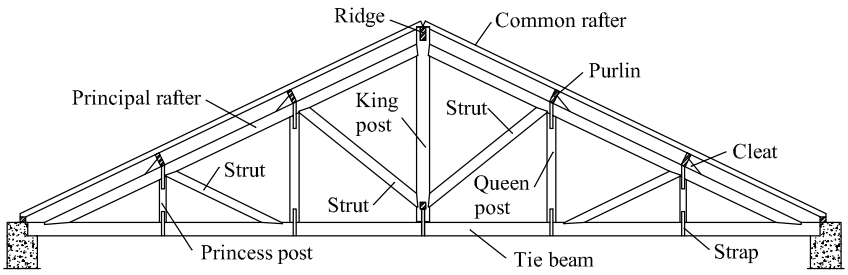
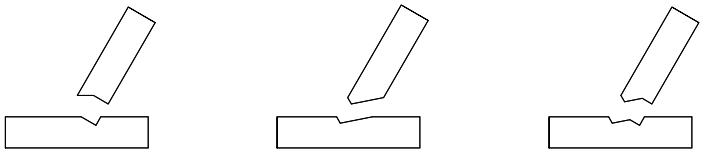


Figure 2.8: Howe truss with Princess posts (Princess-post truss).

2.2.3 Connections in timber trusses

During the timber roofs structure gold period, between the 13^{th} and 19^{th} centuries, joints between members were made by notches or, in a general term, woodworking joints aiming to prepare the connections between two or more elements. In 20^{th} century, the necessity to fullfield industrial criteria (large production scale, prefabrication, standard quality, etc.) and the wide spread of metallic elements such as nails, screws, bolts and straps, the need for carpenter art declined. As a consequence, less carpentry work was needed and metallic elements became essential to correct and improve the contact between the connected members. In any case, the conception and execution of joints has always been the most complex task for the designer. In fact, most frequent pathologies or failures of timber roofs structures are caused by inefficient joints, wrongly designed and/or wrongly executed.

Usually, joints between roof structural members are made by notches, called single step in the case of one notch and, when it has more than one notch, it is a double step joint, etc. (Figure 2.9).



(a) Single step frontal (b) Single step posterior (c) Double step

Figure 2.9: Most frequent step joints in traditional timber roofs structures.

Stresses are directly transfered by compression and/or friction between the surfaces in contact. In some cases, in particular in the oldest examples, notched joints present tenon and mortise (Figure 2.10). Those elements were used to ensure the perfect contact between the connected elements and to prevent the

out-plane instability

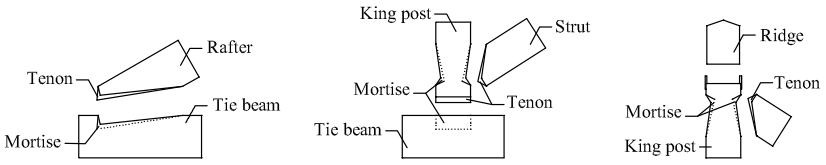


Figure 2.10: Examples of step joints of timber trusses presenting tenon and mortise (Appleton, 2003).

In the more recent examples, as a cause-effect of the reduction of available carpenters, joints are usually strengthened with metal elements. The use of those elements, not only counteracts out-of-plane actions, but also ensure the adequate contact between connected elements. In addition, the strengthening through metal elements provides an important improvement in the timber truss structural behaviour under seismic actions by ensuring safety under reversal loads.

The most relevant connections to the timber roof structural behaviour are those of the tie beam to rafters and posts. However, the most stresses connection is the tie beam-rafter. Stresses can be so high, that in some cases, in these connections the notched should have double steps. In addition, in terms of durability, they represent one of the most vulnerable points of a timber roof structure.

2.2.4 On site assessment

Several timber roofs structures were surveyed in order to collected common values and ranges of geometry, connections solutions, wood species and load parameters. A considerable number of buildings were visited from which more than thirty timber truss were assess. In Appendix A the most representative examples are reported. The survey confirmed the importance of king-post and Howe trusses configurations in Portuguese timber roofs construction. The span defines the truss configuration used. Therefore, king-post trusses are the most popular due to the common small value of span, bellow 7 meters, altrough, even for higher span values, this configuration is, wrongly, employed. For spans over 10 meters, the Howe truss is the most common configuration used, in particular, in the form of Princess-truss. The distance between the axes trusses is normally in the range of 3 to 4 meters, with a common value of 3,5 m. The trusses are composed by slender timber elements, 7-10 cm of width by 10-12 cm height for posts and struts and, 18-25 cm in the case of rafters and tie beams. The wood species more frequent are: Maritime Pine (*Pinus pinaster*, Ait.), Eucalyptus (*Eucalyptus globulus*, Labill.) and Chestnut (*Castanea sativa*, Mill.). The use of Chestnut is most common in monumental buildings related to ecclesiastical orders, like monasteries and churches. In recent years, the use of Eucalyptus

increased significantly, due to its low cost, fast growth and high availability. The Maritime Pine, as the most spread species in Portugal, was always present in Portuguese construction. Single or double steps, presenting in some cases tenon and mortise, make the joints between truss members. The range values for the geometry characteristics of the steps have significant variation. For example, the rafter-tie beam connection is commonly made using a single step however, the notch geometry is not precise (see Figure 2.11).



(a) (b)

Figure 2.11: Examples of different notches geometries for single step joints of rafter-tie beam connections.

Connections are usually strengthened with metal elements. While nails are extensive to all connections, binding strip and straps are common in the connections with the tie beam and stirrups are frequent in rafter-tie beam and king post-rafters connections.



(a) Chicken-foot strap (b) Binding stip



(c) Nailed stirrup (d) Bolted stirrup

Figure 2.12: Examples of connections strengthened with metal elements.

Improper maintenance of the structure and faulty design or construction are the main causes of safety reduction of Portuguese timber trusses. Problems

associated with moisture contents, especially near the supports, are usually present. The faulty design is frequently consequence of a wrong selection of the truss configuration for the roof span (see Figure 2.13a) and due to excentricities in the purlins. In fact, altrough, a strong emphasis is traditionally placed on the need to limit bending moments in the truss elements, excentricities in the purlins are common (see Figure 2.13b).



(a) Wrong truss configuration for the span value



(b) Wrong positioning of the purlins with eccentricity relatively to truss joints

Figure 2.13: Faulty design examples.

Despite being less significant, eccentricities of the supports to the tie beam-rafter connection are common. When important eccentricity exists it is normal to introduce braces. A major source of uncertainty in the global structural behaviour of traditional trusses, in particular in the case of the king post configuration, is related to the connection between the king post and the tie beam. Altrough traditional construction manuals suggest the disconnection between the post and the tie beam, in practice, examples of misconceived connections are not uncommon (see Figure 2.14).



(a) Tie beam not suspended



(b) King post nailed to the tie beam



(c) Direct contact between king post and tie beam

Figure 2.14: Different misconceived connections between the tie beam and the king post.

2.3 Structural behaviour and design

For a correct design, of any element or structure, it is essential to understand is structural behaviour. Designers must be aware of the material properties

and must feel comfortable in the interpretation of the structural system performance. The misunderstanding of the global behaviour of traditional timber trusses can result in unacceptable stress distribution in the members as result of inappropriate joints strengthening (in terms of stiffness and/or strength).

In this work, attention will be focused on the interpretation and analysis of the structural behaviour of traditional timber trusses. Works of Bodig and Jayne (1982), Dinwoodie (1989) and Giordano (1999) about the wood material properties are suggested. The design of traditional timber trusses is a common topic in timber structures manuals (e.g. Alvarez et al. (1996), Pfeil and Pfeil (2003) and Piazza et al. (2005)). Usually, attention is focused on the overall static behaviour of trusses and on the joints design. The truss timber elements are designed following the Eurocode 5 (2004) and some verification rules for the connections, derived from the possible failure modes, are given because traditional carpentry joints are not directly analized in Eurocode 5. In the definition of the static model, loads are assumed as point loads applied in the nodes and the joints are modelled as perfect hinges, despite their semi-rigid behaviour even when not strengthened. Timber roof structures need a more concise knowledge of the real behaviour to determine internal loads and to control the load transfer. For seismic loading for instance, semi-rigidity and ductility are crucial for structural safety and analysis. The refurbishment of large historical roof structures requires the correct load transfer that can only be determined in an analysis when the real behaviour of the connections is known.

2.3.1 Truss static behaviour

Traditional Portuguese trusses are subjected, essentially, to normal stresses associated with axial forces and bending moments induced by the self-weight and asymmetric loads (as the ones produced by snow and earthquakes). The elements with higher stresses are the rafters. The tie beam and struts have only significant normal stress and the posts only shows tension stresses. In a plane structure, like traditional timber trusses, submitted to concentrated loads on the joints, without bending of the members, stress distribution in the structure results directly from its geometry. However, this behaviour can be easily modified if the static model is changed. Assessment of constructed timber trusses shows various differences on their structural model. In fact, despite construction recommendations, intuitively developed over centuries by carpenters, it is common to find examples where they were not taken into account. After an evaluation of the variations in the truss behaviour that can be achieve as result of the model assumed in the design (Branco et al., 2006), it is suggested:

- The application of concentrated loads out of the joints, for example originated by a wrong positioning of the purlins, can compromise the structural global safety;

- The eccentricity of the supports, relatively to the tie beam-rafter connection must be minimizing. It is recommended that the reaction force pass by the intersection point of the tie beam and rafter axis;
- The tie beam must be suspended to the posts. Iron strap shall be used, nailing it only in the post, suspending the tie beam with a connection without bending stiffness and preventing out-of-plane deformations;
- When the tie beam-post connection is rigid, the natural frequencies and modal shapes of the truss are clearly modified;
- For non-symmetric loads, *e.g.,* snow, earthquakes and wind, the influence of the joint stiffness became relevant;
- The performance of the tie beam-rafter connection is crucial, not only in consequence of the high level of stresses concentrated there but also because they represent zones where biological deterioration is more frequent;
- The supports must be able to resist horizontal movements. Friction forces are insufficient to resist do horizontal movements caused by earthquakes.

Altrough the importance of these observations and recommendations, the key for an adequate structural behaviour is the selection of the adequate truss configuration. Indeed, traditional Portuguese timber trusses were think to behave as plane structure submitted to point loads on the joints causing essentially axial stresses in the members. When the number of posts is less than the total of purlins, the structural safety is severely reduced. In this case rafters are subjected to bending moments despite be slender. As a practical rule, the truss configuration must have a number of posts equal to total of purlins used to support the covering structure.

2.3.2 Traditional connections

For a better understanding of the mechanical behaviour of traditional timber connections is essential to point out the resistant mechanisms of wood under compression. The wood compression strength differs with the stress direction relatively to the fibres orientation. Parallel to fibres, the maximum resistance is achieved and the failure mode can be compared with the buckling instability of cellulose. In the normal direction of fibres orientation, the resistance is minim and the failure mode is associated with the instability of cellulose under radial compression. For compression at an angle to the fibres intermediates resistance values are obtained, which can be quantified following Hankinson formula and adopted by various standards. Some standards propose different expressions, tanking into account the reduction of resistance caused by the possibility of crushing of the fibres in consequence of the difference between the strength of earlywood and latewood. For instance, SIA 265 (2003) suggests reducing in

20% the resistance of compression parallel to the grain. However, such difference between those two methods became off small account for compression at an angle range of 30º to 60º to the grain, which represents the most realistic values. In addition, some standards take into account the increase in resistance to compression perpendicular to grain resulting from the enlargement of the ratio between the surface loaded and it total. The design of traditional timber connections comprehends essentially the verification of the compression transmitted between the contact surfaces of the connected elements. Behind this simple definition, it is important to point out that the contact surface, through which the forces are transmitted, is normally smaller than the cross-section of the element and is not orthogonal to the grain direction of any connected element. In the schematic drawing of Figure 2.15, reporting a connection between the tie beam and the rafter, which can be assumed as the general example, the main resistant mechanism are presented.

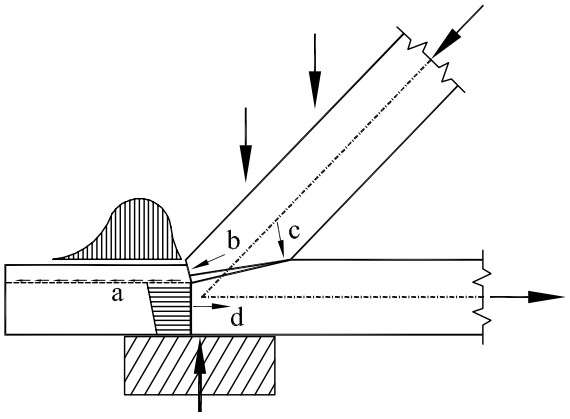


Figure 2.15: Main resistant mechanism in a traditional timber connection.

In the design of traditional timber connections, it is essential to understand the force equilibrium in the joint and, therefore, to identify all critical zones verifying for each one its resistance capacity. Analysing the forces mechanism that occurs inside the joint it is important to draw attention to:

- Existence of not negligible tension perpendicular to the grain often followed by significant shear stresses;
- Concentration of stresses caused by the particular shape of the notches of each connected element;
- Possibility that cracks begin in the step edges;
- Eccentricity in force transmission.

2.3.2.1 Strength

In the single step frontal, the slope of the notch must minimize the angle between the stresses and the grain direction for both connected elements, increasing therefore the crushing resistance of the joint. Base on simple geometric considerations, it is possible to demonstrate that the ideal configuration of the step is the one reported in Figure 2.16, where the angle of the notch is half of the angle $\pi - \alpha$. According to (Götz et al., 1993), (DIN 1052, 2004) and (C.T.E., 2006), the depth of the notch (t_v) should not exceed $h/4$ for skew angles $\alpha \leq 50^{o}$ and $h/6$ for skew angles $\alpha > 60^{o}$, being possible a linear interpolation between those values.

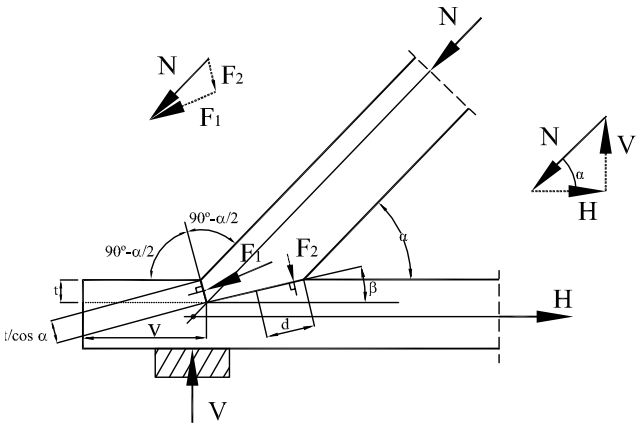


Figure 2.16: Force mechanisms in a single step frontal joint (tie beam-rafter) disregarding friction forces and geometric imperfections and under compression of the rafter.

In general, friction forces and geometric imperfections are not considerer in the resistance of these joints. Based on this assumption, the axial force is easily decomposed in F_1 and F_2 forces perpendicular to the two surfaces of the notch, see Figure 2.17, which can be quantified as:

$$F_1 = N \cdot \cos\frac{\alpha}{2} - N \cdot \sin\frac{\alpha}{2} \cdot \tan\left(\frac{\alpha}{2} - \beta\right) < N \cdot \cos\frac{\alpha}{2} \tag{2.1}$$

$$F_2 = \frac{N \cdot \sin\frac{\alpha}{2}}{\cos\left(\frac{\alpha}{2} - \beta\right)} \tag{2.2}$$

The single step frontal design comprehends the verification of the compression at an angle to the grain direction in the notch and the shear resistance in the frontal part of the notch.
Shear surface in front of the notch:

$$\tau = \frac{N \cdot \cos\alpha}{b \cdot v} \leq f_v \tag{2.3}$$

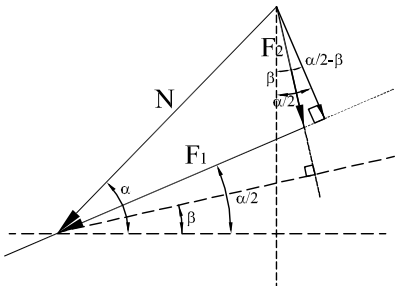


Figure 2.17: Force decomposition in a single step frontal joint.

Frontal surface under compression:

$$\sigma_c = \frac{N \cdot \cos^2\left(\frac{\alpha}{2}\right)}{b \cdot t} \leq f_{c,\frac{\alpha}{2}} \tag{2.4}$$

Rear surface under compression:

$$\sigma_c = \frac{F_2}{b \cdot d} \leq f_{c,90-\beta} \tag{2.5}$$

where almost all variables were presented in the previous schemes, b is the width of the timber element and d is the distance corresponding to the rear compress surface of the notch.

This last verification, often forgot, can be important in consequence of the possible concentration of high stresses in a limited length. In a more realistic design, in particular in historic constructions, it is possible to assume the d value as result of the following empiric rule suggested by Parisi and Piazza (2000):

$$d \equiv (1/5 - 1/3) \cdot t / \sin\beta \tag{2.6}$$

It is important to draw attention to the fact that the hypothesis of absence of friction forces assumed is quite far from reality and their presence increase the stresses in the shear surface (see Figure 2.15). The safety verification of the shear stresses in front of the notch must be done with caution. In consequence of the fragile nature of the shear rupture, for instance, some earthquake resisting standards (e.g. Ordinanza 3431 (2005)) adopted a higher partial factor for material properties equal to 1.3 in the quantification of $f_{v,d}$.

In the single posterior step, the geometry of the notch should increase the shear resistance of the joints by increasing the shear surface in front of the notch (see Figure 2.18). However, as result of practical reasons (easiest execution), it is common to cut the notch perpendicular to the longitudinal direction of the carved member. In this case, for the reasons already exposed resistance to compression of the joint decreases. This step joint configuration require some geometric rules, as example the necessity to consider a gap (1 or 2 mm) between the two connect members to ensure that only the notch transfer the loads and tension perpendicular to the grain are avoided.

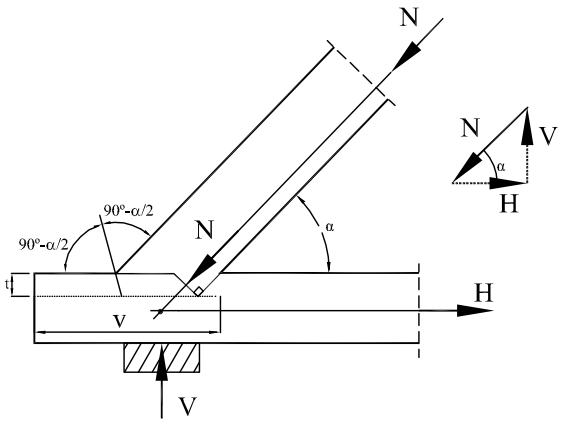


Figure 2.18: Force mechanism in a single posterior step joint.

For the design of the single posterior step, supposing the rafter under compression, it is normal to use the follow expressions: Shear surface in front of the step:

$$\tau = \frac{N \cdot \cos\alpha}{b \cdot v} \leq f_v \tag{2.7}$$

Compress surface of the notch (of the tie beam):

$$\tau = \frac{N \cdot \cos\alpha}{b \cdot t} \leq f_{c,\alpha} \tag{2.8}$$

In alternative of those joint geometries, single step joints (frontal and posterior), it is common to use the double step joint, which geometry results from the sum of those two different single steps joints (see Figure 2.19).

Double step joint has the advantage of increase the resistance surface to shear stresses and to reduce the compression stresses in the steps, resulting in a better performance of the joints. This advantage is only possible if the rear step is deeper than the frontal, condition not always verified. The execution of a double step joints force to have a precision, to ensure that all surfaces will be in contact, that in nowadays is not easy to reach without CAD-CAM systems. For instance, following CNR-DT 206 (2006) it is necessary to guarantee that the manufacture tolerances verify:

$$t_1 \leq \begin{cases} 0.8 \cdot t_2 \\ t_2 - 10mm \end{cases} \tag{2.9}$$

Whichever the skew angle of the connections, for a double step joint, Götz et al. (1993) and C.T.E. (2006) recommend:

$$\begin{cases} t_1 \leq h/6 \\ t_2 \leq h/4 \end{cases} \tag{2.10}$$

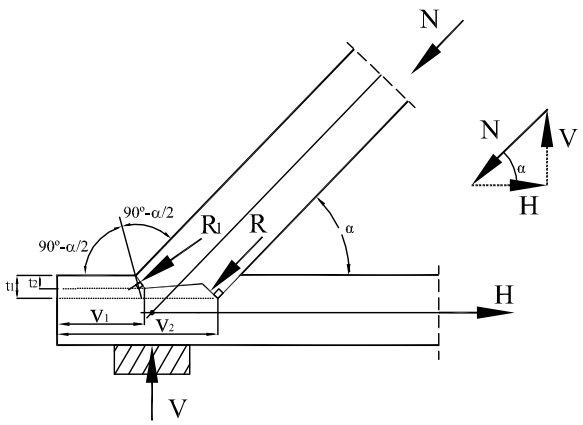


Figure 2.19: Force mechanism in a double step joint.

2.3.2.2 Stiffness

The traditional timber joints, even without any strengthening device, usually have a significant moment-resisting capacity. Therefore, they cannot be represented by common constraint models, like perfect hinges, but should be considered semi-rigid and friction based. Test results on full-scale connections, Candelpergher (1999), Palma and Cruz (2007) and Branco et al. (2006), shows that this capacity is function of the compression level in the rafter, the width of the rafter, the friction angle, the skew angle and the notch depth. Rotational capacity is positively related to the first three parameters. Eurocode 5 (2004) propose expressions for the stiffness of dowel type timber joint, function of the fastener diameter and density of wood, however, do not give any information about the stiffness of carpentry joints. The common design method of traditional timber connections looking out only to the strength characteristics can be explained by several reasons (Larsen and Jensen, 2000):

- The structural design may be very complicated, especially if non-linearity is considered;
- The load-displacement behaviour for traditional fasteners is not known with sufficient accuracy;
- fasteners exhibit an unpredictable initial (low load level) slip response;
- Lack of realistic semi-rigid models for the connections;
- The deformation capacity is insufficient because of premature brittle failure in tension perpendicular to the grain or shear parallel to the grain.

Trusses are highly statically indeterminate, therefore the real behaviour of joints have an important influence on the force distribution. All the same, the

axial forces in the members and the forces in the joints are normally calculated assuming pinned joints in all nodes (joints). The effect of errors on the design of the timber members is small, but the consequences of ignoring the moments in the joints may be quite serious. Many joints are stiff and brittle when loaded by moment because of the load component perpendicular to the grain. Therefore, in some cases, the joints are assumed infinitely stiff. These errors are on the safe side for the joints but often results in an uneconomic design. In the particular example of traditional timber connections, in a numeric analysis assuming the semi-rigid behaviour of the joints, maximum differences of 20% were obtain between the stresses comparing to the experimental results, while assuming the joints pinned or rigid increase the difference until 40% (Uzielli, 2004).

2.3.2.3 Ductility

The ductility of a structure (or structural component or material) is its ability to sustain large deformation without any substantial reduction in seismic resistance. Timber is generally considered to be a good structural material for construction in seismic areas due its light weight and reasonable strength in tension and in compression. The good seismic performance of wood is reflected by its strength/mass range similar to structural steel $[35-55]$. However, *a*) timber elements do not present large deformational ductility; *b*) response of timber elements up to failure is approximately linear elastic; *c*) collapse is sudden, mostly associated with defects inherent to the natural origin of timber. For timber structures, Eurocode 8 (2004) distinguishes between dissipative and low-dissipative structural behaviour. However, in view of the limited ability of timber to behabe nonlinearly, energy dissipation should be mostly in connections and timber elements should respond linearly. Some, little, nonlinear behaviour can be expected in compression perpendicular to the grain but, tension perpendicular to grain is markedly brittle. Distinction between dissipative and low-dissipative structures depends mostly on connections nature. Semi-rigid and rigid connections are associated with this distinction, respectively. Dissipation of energy in connections has two main sources: *a*) cyclic yielding of metallic (normaly steel) dowel type fasteners of the connections (nails, staples, screws, dowels or bolts) and *b*) crushing of the wood fibres bearing against the dowel. The first mechanism results in large hysterectic cycles while the second causes thin hysterectic loops with significant degradation, due to the cavity being formed in front of the dowel. Eurocode 8 (2004) propose a classification of timber structures in Ductility Class Medium (DCM) and Ductility Class High (DCH) for dissipative structures and Ductility Class Low (DCL) in the case of non-dissipative structures. The choice of the Ductility Classes (DCs) is left to the designer but National Authorities may limit the use of the various DCs. Ductility classification depends mostly on the structural type/redundancy and from the nature of structural connections. The properties of dissipatives zones, structural connections, must be determine by testing following EN 12512 (2001). As general requirements, dissipative zones shall

be able to deform plastically for at least three fully reversed cycles at a static ductility ratio of 4 for DCM structures and at a static ductility ratio of 6 for DCH structures, without more than a 20% reduction of their resistance. The use of carpentry joints in seismic zones is allowed only if, suitable capacity of energy dissipation without fragile failures is presented. Nevertheless, Eurocode 8 (2004) does not propose clear values of behaviour factor (carpentry joints with force transfer by contact are not mentioned in table 8.1). Without any more information, a behaviour factor ($q = 1.5$) correspond to a careful position. Results carpentry joints in EN 12512 (2001) loading conditions should allow a more realistic evaluation of behaviour factor and another ductility classification.

2.3.3 Degradation and strengthening

Nowadays, a considerable number of timber roofs require structural intervention in consequence of natural degradation of the material (aging), improper maintenance of the structure, faulty design or construction, lack of reasonable care in handling of the wood or accidental actions. A correct assessment of the degradation extension and their effects in the overall structural behaviour is urgent. Only after that, accurate restoration actions, which can varied from simple works in the covering structures to large substitution of structural members with joints and elements strengthening, is possible.

The most common degradation processes in timber roofs structures can be divided in three families. The first, of biological origin, results in a reduction of the resistant cross-section of the elements caused by wood-degrading organism. This type of degradation is more frequent near the supports because of the presence of high level of moisture, normally related with bad construction details incapables to keep exterior wood dry and accelerate runoff. Second degradation process is related with structural requirements, in particular, with insufficient load-bearing capacity of structural members, normally translate in significant deformations and, with deficient bracing systems. Changes in the nature of the use of the construction, resulting in different service loads, scarce cross-section of the structural elements to resist the stress level applied, insufficient elements in the bracing system, inadequate design or construction of the connections and the presence of natural wood defects are the main causes of this type of anomalies. Finally, bad structural systems can be responsible for stresses, in an element or in various, that can compromise the local and overall safety of the structure. The most frequent examples of this faulty design of timber roofs are: wrong positioning of the purlins; tie beam-rafter connections eccentricity relatively to supports; and incorrect connection between the tie beam and posts, in particular, with the king post. The application of concentrated loads out of the joints, originated by a wrong positioning of the purlins, can compromise the structural global safety. Indeed, it is demonstrated by Branco et al. (2006) that, the consideration of an eccentricity of 20 cm, a value smaller than the ones reported in the preliminary survey undertaken, is enough to compromise the rafters safety of typical Portuguese king-post truss. The tie beam must

be suspended to the posts. Iron strap shall be used, nailing it only in the post, suspending the tie beam with a connection without bending-stiffness and preventing out-of-plane deformations. Frequently, restoration works requires the strengthening of timber structures. In the case of timber roofs structures, this strengthening normally involved connections between the truss structural elements. Joints strengthening can be done in different forms: from simple replacement or addition of fasteners, to the use of metal plates, glued composites or even full injection with fluid adhesives. Each solution has unique consequences in terms of the joint final strength, stiffness and ductility. Although being widely used, the number of studies on the mechanical performance of existing traditional carpentry joints and possible strengthening techniques is not worldwide. With few exceptions, see e.g. King et al. (1996), Bulleit et al. (1999), Seo et al. (1999) and Parisi and Piazza (2000), timber joints research has been oriented towards new engineering configurations.

2.4 Conclusions

In the design of new structures or assessment of existing ones, it is common to model trusses considering each member with perfect hinges at both ends. However, these joints offer a significant moment resistance and may be better classified as semi-rigid connections. This capability is especially important under non-symmetric loads as those induced by snow, wind and especially earthquakes. In restoration works, the lack of practical but realistic models for the joints generally leads to very conservative retrofits and upgrades in order to satisfy the safety and serviceability requirements present in recent Codes and Recommendations. Moreover, the misunderstanding of the global behaviour of traditional timber trusses can result in unacceptable stress distribution in the members because of inappropriate joints strengthening (in terms of stiffness and/or strength). The restoration or the design of new timber roof structures needs the correct load transfer that can only be determined in an analysis when the real behaviour of the connections is know. This is the topic of the present thesis.

Chapter 3

Experimental analysis of traditional timber connections

3.1 Introduction

The experimental research was carried out at the Laboratory of Structures of the University of Minho (Portugal), and includes monotonic and cyclic tests of full-scale traditional timber connections. A series of monotonic and cyclic tests on unstrengthened specimens were performed in order study the primary behaviour characteristics of the connection, as well as its sensitivity to a few parameters. Subsequently, connections strengthened with basic metal devices were tested under monotonic and cyclic loading. The purpose of these tests was to uncover any advantages and deficiencies in the behaviour of the joint and of the device itself, as well as to determine a need for different types of strengthening. Tests on assembled connections were preceded by accurate material characterization, determining the mechanical properties of the timber elements used for all full-scale models. Table 3.1 summarises the more important tests on traditional timber connections performed in this experimental analysis. Because of their frequency in the preliminary survey undertaken, two skew angle of the connections were adopted: 30º and 60º. Two compression levels of the rafter were adopted, 1.4 MPa and 2.5 MPa, in accordance with the Service and Ultimate Limit States, respectively, defined for common Portuguese timber roof structures (see Branco et al. (2005b)). For all type of connection evaluated, nine tests were performed: 6 monotonic, 3 in each loading direction (positive and negative) and 3 others under cyclic loading. Strengthened connections were studied only under a compression level in the rafter of 1.4 MPa corresponding to the Service Limit State conditions. The analysis of the behaviour of traditional strengthening techniques, using metal elements, in service conditions is one objective of this work. Four strengthening techniques were initially selected but, during the experimental campaign one of them was abandoned.

In addition, others tests were carried out, mostly resulting of attempts to

Table 3.1: Tests performed on traditional timber connections.

Specimen	Loading Method	Type of connection	Compression stress (MPa)	Skew angle
$U3-1.4-1,2,3$ $U3-1.4-4,5,6$ $U3-1.4-7,8,9$	Monot. + Monot. − Cyclic	Unstrengthened	1.4	30^o
$U3-2.5-1,2,3$ $U3-2.5-4,5,6$ $U3-2.5-7,8,9$	Monot. + Monot. − Cyclic	Unstrengthened	2.5	
$S3-1,2,3$ $S3-4,5,6$ $S3-7,8,9$	Monot. + Monot. − Cyclic	Stirrup	1.4	
$B3-1,2,3$ $B3-4,5,6$ $B3-7,8,9$	Monot. + Monot. − Cyclic	Bolt		
$BS3-1,2,3$ $BS3-4,5,6$ $BS3-7,8,9$	Monot. + Monot. − Cyclic	Rigid binding strip		
$TT3-1,2,3$ $TT3-4,5,6$ $TT3-7,8,9$	Monot. + Monot. − Cyclic	Binding strip		
$U6-1.4-1,2,3$ $U6-1.4-4,5,6$ $U6-1.4-7,8,9$	Monot. + Monot. − Cyclic	Unstrengthened	1.4	60^o
$U6-2.5-1,2,3$ $U6-2.5-4,5,6$ $U6-2.5-7,8,9$	Monot. + Monot. − Cyclic	Unstrengthened	2.5	
$S6-1,2,3$ $S6-4,5,6$ $S6-7,8,9$	Monot. + Monot. − Cyclic	Stirrup	1.4	
$B3-1,2,3$ $B3-4,5,6$ $B3-7,8,9$	Monot. + Monot. − Cyclic	Bolt		
$TT6-1,2,3$ $TT6-4,5,6$ $TT6-7,8,9$	Monot. + Monot. − Cyclic	Binding strip		

NOTE: Based on the test results obtained for 30^o skew angle connections, it was decided not to extended the binding strip (BSi) to the 60^o skew angle case.

analyse others materials (carbon fibre reinforced polymers) or different ways of using some of the strengthening techniques studied (in particular, stirrups nailed, bolts with a smaller diameter and two slender bolts instead of one with 12 mm of diameter). More details about those tests and their results can be obtained in Branco et al. (2008b) and Branco et al. (2005a), respectively.

3.2 Wood characterization

A mechanical characterization of the Maritime pine timber (*Pinus pinaster* Ait.) used in the connections was performed. In the carpentry where the joints were fabricated, all wood elements used were classified as belonging to quality class E as result of a visual strength grading according the Portuguese National Standard NP 4305 (1995). At the laboratory characterization tests were performed following EN 408 (2003) on samples collected during the fabrication of the connections. Characterization tests are divided in two steps: the first, when connections with a skew angle of 30º were prepared and the second, later, when the 60º skew angle connections were set. In those two different moments, the local and global modulus of elasticity in bending and the bending strength were estimated and, in the latest, compression perpendicular and parallel to the grain strength and modulus of elasticity were determinate. For all tests, the failure time was register and the moisture content of each specimen was measure with an electronic thermo hygrometer for wood.

3.2.1 Bending

Bending strength was evaluated through four-point bending tests of beams with a cross section of 80×100 mm^2 and 1.90 m length using a test arrangement following EN 408 (2003). A displacement control procedure (0.14 mm/s) with an 100 kN actuator were used. In each test, apart the registration of the deformations measured at the centre of a central gauge length of 5 times the depth of the section, the deformations at mid-span at the centre of the tension side edge were measured. Based on these results local ($E_{\mathrm{m,l}}$) and global ($E_{\mathrm{m,g}}$) values of the modulus of elasticity in bending were possible to assess. Incrementing the load, the bending strength (f_{m}) was also measured. The bending tests results found are presented in Table 3.2.

As expected, the local value for the modulus of elasticity ($E_{\mathrm{m,l}}$) are higher than the global value ($E_{\mathrm{m,g}}$) in all cases, as no shear deformation is taken into account in the first case contrarily to the second. The results achieved in both set of bending tests are quite homogeneous, in particular, in terms of the local and global modulus of elasticity. By contrast, more heterogeneity is observed on the bending strength results. In particular, beams B4 and B6 failed at much lowerstress levels than all other specimens. In conclusion, it can be point out that the values obtained for modulus of elasticity in bending are quite consistent, since lower CoV are reported, and the bending strength, as more dependent of eventual defects of the wood, are quite heterogeneous where the minimum value obtained represents only 64% of the mean value (Figure 3.1).

Table 3.2: Bending tests results.

Beam	Skew angle	W (%)	F_{max} (kN)	Time (s)	$E_{m,l}$ (MPa)	$E_{m,g}$ (MPa)	f_m (MPa)
B1	30°	24.3	24.32	415	10249	9902	54.71
B2		29.8	19.76	380	9835	9658	44.45
B3		23.8	19.60	374	12730	11207	44.10
B4		22.3	11.99	207	8894	8666	26.98
				Mean	10427	9858	42.56
				CoV	0.16	0.11	0.27
B5	60°	19.6	31.01	420	12021	11221	69.77
B6		16.6	12.16	152	8552	8144	27.36
B7		18.7	27.46	420	8808	9184	61.79
B8		21.4	34.85	351	13468	13384	78.42
B9		18.9	20.61	235	10390	9754	46.38
B10		20.3	21.57	226	11560	10768	48.52
				Mean	10800	10409	55.37
				CoV	0.18	0.18	0.33
				Mean	10651	101889	42.56
				CoV	0.16	0.15	0.27

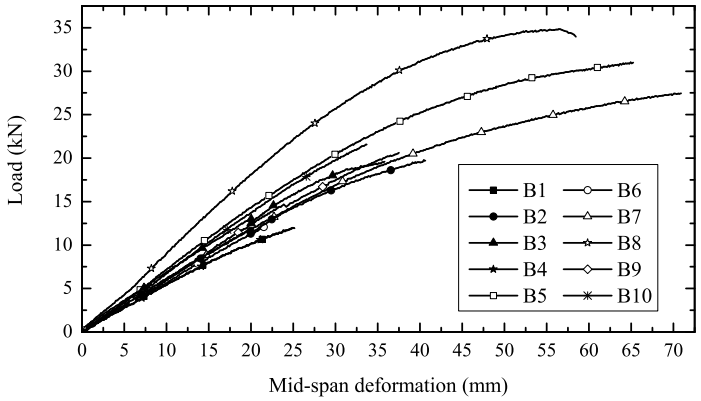


Figure 3.1: Load mid-span deformation curves obtained in the bending tests.

3.2.2 Compression perpendicular to the grain

Specimens of $45 \times 70 \times 90$ mm^3 were used in accordance with EN 408 (2003) recommendations to assess the resistance to compression perpendicular to the grain. For these tests, conducted under displacement control and using a load cell of 200 kN, a movement rate of 0.005 mm/s was adjusted based on preliminary tests, with the objective to reach the maximum load within (300 ± 120) seconds. Using this rate movement, only one test result (C90-2) does not fulfil the EN 408 (2003) requirements. Five LVDT's (Linear Voltage Differential Transducer) were used for measuring the deformations, four placed in each side of the test piece with a gauge length of 54 mm (0.6 the piece height) and another one measuring the loading head of the test machine. The load-deformation curve was plot using the deformation average value given by the LVDT's placed in the two larger sides (70x90 mm^2 surfaces) (see Figure 3.2).

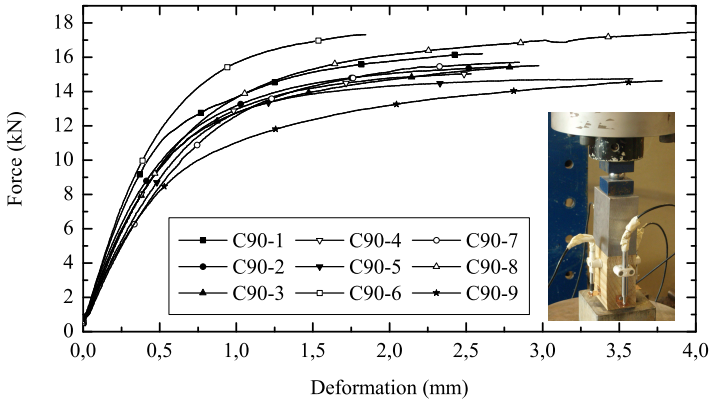


Figure 3.2: Force-deformation curves of the compression perpendicular to the grain tests.

Using the methodology suggested by EN 408 (2003) for the determination of the maximum load ($F_{c,90,max}$), the results of the compression perpendicular to the grain tests are reported in Table 3.3. The test result of specimen C90-2 was not considered because the time of failure is out of the allowable range.

The tests results obtained for the compression strength perpendicular to the grain ($f_{c,90}$) are very consistent (CoV=0.06) but lower than expected. Despite presenting larger variability, the modulus of elasticity perpendicular to the grain ($E_{c,90}$) also exhibit good homogeneity.

3.2.3 Compression parallel to the grain

Specimens of $80 \times 100 \times 480$ mm^3 were used in the compression parallel to the grain tests conducted in accordance with the recommendations presented by EN 408 (2003). The tests were performed under displacement control with a

Table 3.3: Compression perpendicular to the grain tests results.

Specimen	W (%)	Time (s)	$F_{c,90,max}$ (kN)	$F_{c,90}$ (MPa)	$E_{c,90}$ (MPa)
C90-1	16.3	278	14.23	4.52	469
C90-2*	18.2	117	11.96	3.80	339
C90-3	14.9	332	15.83	5.03	356
C90-4	16.5	259	14.24	4.52	312
C90-5	14.8	218	15.75	5.00	482
C90-6	16.8	200	13.45	4.27	307
C90-7	16.6	222	13.64	4.33	383
C90-8	15.4	280	14.10	4.48	381
C90-9	15.2	234	14.12	4.48	386
			Mean	4.58	385
			CoV	0.06	0.17

$*$ test disregarded according to EN 408 (2003)

movement rate of 0.01 mm/s using a load cell of 500 kN. Displacements were measured using five LVDT's: four measuring the deformation on each side of the test piece, with a gauge length of 320 mm, and another one placed on the loading head of the test machine. The rate of movement of the loading-head was estimated based on preliminary tests aiming to reach the maximum force ($F_{c,0,max}$) within (300 ± 120) seconds. The deformation was assumed as the mean value of the measurements of the four LVDT's placed in each side. Figure 3.3 shows the force-deformation curves of the compression parallel to the grain tests carried out.

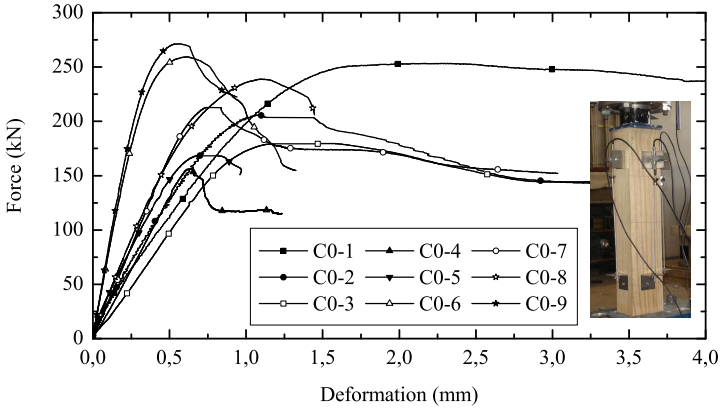


Figure 3.3: Force-deformation curves of the compression parallel to the grain tests.

Based on the deformation measured in the elastic range it was possible to quantified the modulus elasticity ($E_{c,0}$) and with the maximum force value ($F_{c,0,max}$) to quantify the compression strength parallel to the grain ($F_{c,0}$). Table 3.4 shows the compression parallel to the grain tests results obtained.

Table 3.4: Compression parallel to the grain tests results.

Specimen	W (%)	Time (s)	$F_{c,0,max}$ (kN)	$F_{c,0}$ (MPa)	$E_{c,0}$ (MPa)
C0-1	16.3	420	253.34	31.67	9125
C0-2	28.2	408	208.95	26.12	9589
C0-3	29.1	399	181.06	22.63	8170
C0-4	25.1	381	155.85	19.48	10410
C0-5	31.6	382	168.29	21.04	10993
C0-6	18.7	288	259.47	32.43	9380
C0-7	27.3	368	212.76	26.59	6552
C0-8	18.6	420	238.86	29.86	13270
C0-9	18.3	290	271.35	33.52	10053
			Mean	27.08	9727
			CoV	0.19	0.19

3.2.4 Discussion of the tests results

It is important to remember that the values exposed in the bibliography, namely, LNEC (1997), were obtained from two sets of specimens with non structural dimensions ($4 \times 10 \times 200\text{cm}^3$ and $5 \times 15 \times 300\text{cm}^3$), each set composed of pieces from different regions trying to represent the national population of this wood specie. Over the tests results obtained in the two samples, the adjustment factors suggested by EN 384 (2004) for the sample size, timber size and test length were applied. Those values have been adopted by the Portuguese Nationally Determined Parameters of Eurocode 5 (NP ENV 1995-1-1, 1998). To compare the test results obtained in this work with the ones reported in LNEC (1997) it is also necessary to apply the adjustment factors suggested by EN 384 (2004) for the timber size and the moisture content. The adjustment factor for the number of samples and their size was not used in the consequence of the number of tests performed. Comparing the wood characterization tests results obtained with the values reported by LNEC (1997), for *Pinus pinaster*, Ait. of quality class E, (Table 3.5) it can be concluded that: (1) the tests results obtained for the bending and compression parallel to the grain strengths (f_m, and $f_{c,0}$) above the values suggested in all cases; (2) all tests results of the compression perpendicular to the grain strength ($f_{c,90}$) were lower than the value suggested; (3) the test result of the modulus of elasticity

in bending, mean and characteristic values, are very similar to the reported in bibliography.

Table 3.5: Comparison between the mechanical properties for *Pinus Pinaster*, Ait. quality class E obtained in the test results and reported by LNEC (1997).

Source	E_{m} (MPa)	$E_{0,05}$ (MPa)	f_{m} (MPa)	$f_{\mathrm{c},0}$ (MPa)	$f_{\mathrm{c},90}$ (MPa)
LNEC (1997)	12000	8000	18	18	6.9
Test results	11156	7992	25	20	4.0

The analysis of the tests results obtained must be done carefully. The size of the sample is very small (considering the objective is to characterize the mechanical properties of the Maritime pine timber) and the moisture content presents significant variability. As a natural material, wood presents significant variability in the physic and mechanical properties highly depending of faults and moisture content. Moreover, it is recognized that significant variation of the mechanical properties of exists as function of the tree class quality and location of the specimens on the stem (Machado and Cruz, 2005).

3.2.5 test setup and instrumentation

The arrangement allows independent control of two hydraulic jacks (Figure 3.4). One jack, aligned with the rafter, induced constant compression throughout the test. The other, a double-acting jack, positioned above the center of the joint, applied a transversal force, with a programmed load cycle, and generated a moment at the joint. Force (F) versus displacement (d) curves were measured. The two jacks have a maximum loading capacity of 50 kN and 100 kN and a maximum stroke of 160 mm and 50 mm, respectively. Type and location of instrumental channels, including load cells and (LVDT), are shown in Figure 3.4.

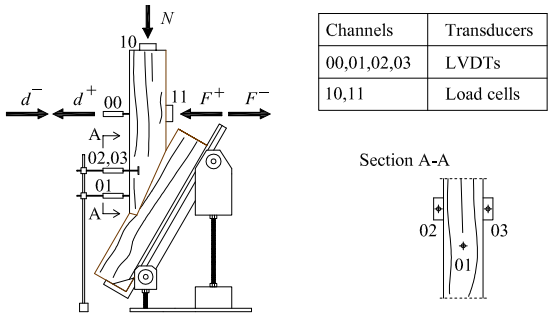
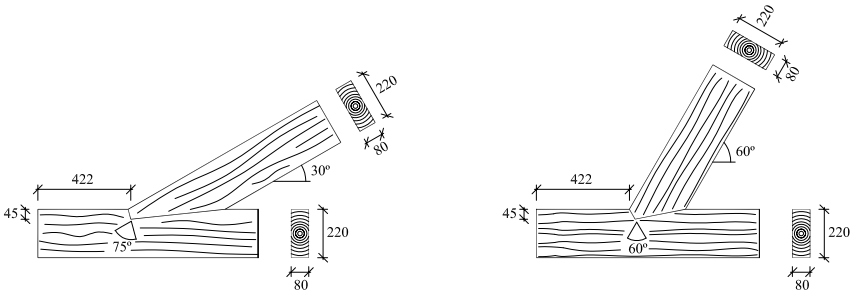


Figure 3.4: Testing apparatus and instrumentation layout.

Tests were performed under displacement control for the typical birdsmouth joint skew angle of 30° and 60°. For all the specimens, the cross sections of the elements were $80 \times 220\text{mm}^2$, the step depth was 45 mm and the notch length was 422 mm as represented in Figure 3.5.



(a) 30° skew angle (b) 60° skew angle

Figure 3.5: Connections geometry (mm).

The first step of the loading procedures in both the monotonic and cyclic tests was the application of an axial compression force on the rafter. The axial force, simulating the effect of the dead load presented in the structure, was kept constant during the test. In the subsequent loading steps, a transversal force (F), acts perpendicular to the rafter axis. When the skew angle increases, it is defined as the positive direction and when the skew angle decreases, it is defined as the negative direction. Monotonic tests were performed to determine the elastic behaviour, in particular, the apparent elastic limit displacement d_e^+ and d_e^-. Under displacement control at channel 00, a maximum displacement value of 50 mm, was imposed under a movement rate of 0.028 mm/s and 0.18 mm/s in the case of connections with a skew angle of 30° and 60°, respectively.

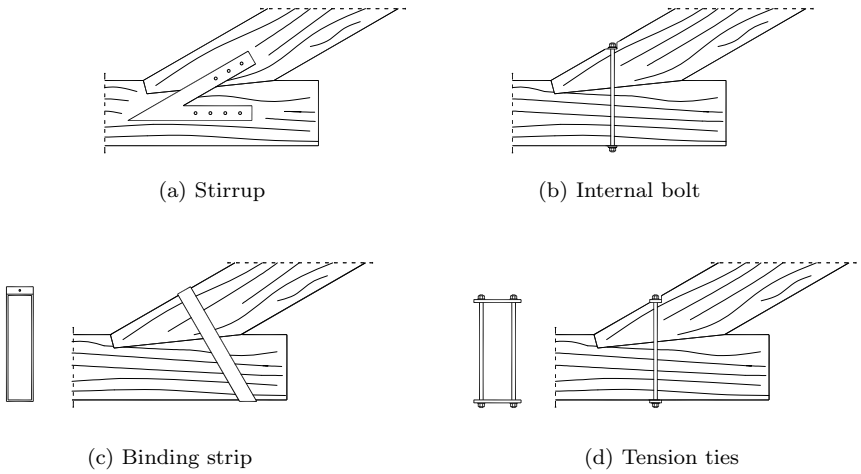
3.3 Cyclic test procedure

Full-scale connections, similar to the specimens of monotonic loading, were tested with a quasi static cyclic loading. In particular, the test program included one cycle in the range $[0.25d_e^+; 0.25d_e^-]$; one cycle in the range $[0.50d_e^+; 0.50d_e^-]$; three cycles in the range $[0.75d_e^+; 0.75d_e^-]$; three cycles in the range $[nd_e^+; nd_e^-]$ until joints failure. The values used for the elastic limit displacements, for both positive (d_e^+) and negative (d_e^-) directions, are based on results obtained in the monotonic tests. However, some difference exists between the two phases of the experimental set (30° and 60° skew angle connections, respectively). While in the first case, asymmetric values were adopted for the apparent elastic limit displacements d_e and n assumes 0, 1, 2, 3, 4, 5,.... In the second, a mean value for the d_e was adopted, obtained from the mean value in each direction, and n assumes 1, 2, 4, 6, ... The first sequence is in accordance with Dolan (1994)

and the second agrees with EN 12512 (2001). The first phase of this experimental campaign is based in previous works (Candelpergher (1999) and Parisi and Piazza (2000)) and with the evolution of the work, some improvements were implemented.

3.4 Strengthening techniques studied

Metal connectors have been applied occasionally in timber joints for centuries. However, this practice became common only in the 19th century, when the development of industrial production methods made bolts, rivets, and other metal elements easily available. Metal devices were intended to counteract out-of-plane actions, which could not be resisted by the assemblage itself. Nowadays, strengthening also concerns the behaviour of the friction-based connection in its own plane, and is intended to avoid the detachment of the connected members. Particularly in seismic areas, strengthening can prevent loss of capacity and possible separation of friction surfaces due to the decrease of compression forces, and, under cyclic loading, the application of strengthening solutions can maintain a stable structural behaviour (Parisi and Piazza, 2000). The four basic types of intervention considered in this study are modern implementations of traditional strengthening techniques: the stirrups, the internal bolt, the binding strip and the tension ties (Figure 3.6).



(a) Stirrup (b) Internal bolt

(c) Binding strip (d) Tension ties

Figure 3.6: Traditional strengtheneing techniques evaluated.

Metal stirrups placed in pairs at two opposite sides of the joint were very popular in the past and are still considered adequate and frequently adopted. The effect of the large increase of in-plane stiffness connection is particularly important and should be investigated. In this study, each stirrup was composed of two steel plates welded in a V-shape. Each prong was 50 mm wide and 5

mm thick. They were parallel to the rafter or to the tie beam, and bolted to it with seven bolts of 10 mm diameter. The use of a steel rod, with 12 mm diameter, was also considered. The rod was fixed by a nut at both ends and secured by using a special rectangular-shape washer ($70 \times 30\text{mm}^2$ and 5 mm thick). The rod was located at the mid-joint and normal to the axis of the tie beam. A suitable seat area was formed in the rafter for accommodating it, which allows perfect contact between surfaces. Metal binding strips, considered obsolete today, were very frequently adopted in the 19th century roof structures, particularly to strengthen the rafter and tie beam connection in configurations that had skew angles typically of 30°, see Branco et al. (2005b). Two updated versions of this layout were considered: a) the joint was bound with a hollow steel ribbon, 50 mm wide and 5 mm thick, located at mid-joint, normal to the tie beam (BSi); and b) the joint was bound with two steel plates located in the bottom surface of the tie beam and upper surface of the rafter, with the dimensions of $40 \times 159\text{mm}^2$ and 10 mm thick, tightened through two rods of 12 mm (TTi). The rods, having a nut at both ends, located at midjoint, normal to the tie beam, enable full control in the tightening force during the strengthening lifetime. The first version, called rigid binding strip, was only used for 30° skew angle case.

3.5 Analysis and discussion of the tests results

The first set of connections tested was composed by three unstrengthened joints with a skew angle of 30° (U3-1.4-1,2 and 3). A permanent compression force of 25 kN (corresponding to 1.4 MPa compression stress) was applied to the rafter throughout the vertical jack, and the second jack imposed a monotonic transversal force (perpendicular to rafter axis). The test results illustrate perfect elasto plastic behaviour for the three tests (Figure 3.7). The behaviour is perfectly elastic until the elastic limit displacement ($\approx$ 8mm) is reached, thus the behaviour became non-linear but only within a small range. Subsequently, a quasi-perfect plastic behaviour appears. This pseudo-plastic phase, starting at a 10 mm displacement, remains practically constant until the maximum displacement (50 mm), presenting a small decrease of the resistance after 25 mm displacement. The subsequent sets of tests aim to evaluate the influence of the compression stress level applied to the rafter. While the first set was analysed under a compression level of 25 kN, corresponding to a compression stress of 1.4 MPa, representing the dead load applied on the roof structure, later, a compression force of 44 kN, corresponding to a stress level of 2.5 MPa, was used. The stress level adopted in these tests was defined for the serviceability limits states defined according to standards for common Portuguese timber roof structures (Branco et al., 2005b). Comparing the force-displacement of the two different compression level considered, apart of an increased in the maximum force also a higher stiffness is achieved with the increase of the compression level (Figure 3.7). With the increment of the rafter compression stress, the stiffness more than duplicate, the maximum force reached is 61.3% higher but

the elastic displacement limit decreases 34.2%. However, the development of the force-displacement curves remains similar.

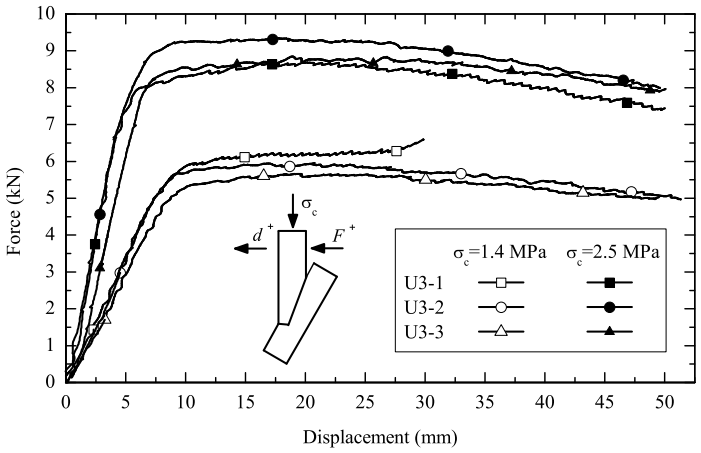
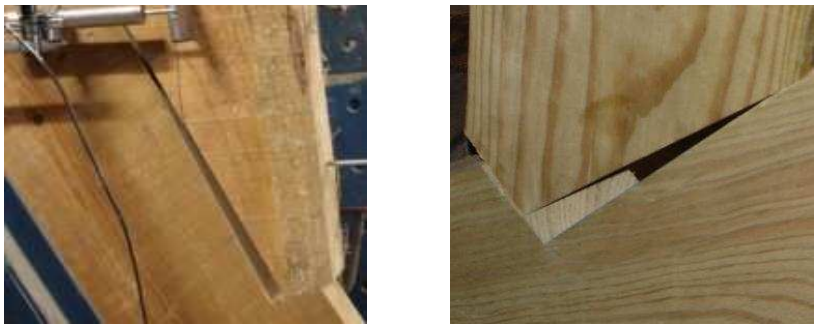


Figure 3.7: Force-displacement curves of unstrengthened connections with 30° skew angle for monotonic loading in positive direction and different rafter compression stress.

A more brittle behaviour and excessively depending of the friction conditions was detected when the skew angle is reduced. The curves presented in Figure 3.8 show a perfectly elastic behaviour just at the maximum force, after which a slip, followed by a loss of friction, induces a rapid decrease of the resistance. When the new stable position of the joint is reached, the brittle behaviour is replaced by a pseudo-plastic phase. This ductile behaviour is due to the local compression of wood. Finally, a total loss of friction occurs with the failure of the connection.



(a) 30° skew angle (b) 60° skew angle

Figure 3.8: Slip mechanism observed when decreasing the skew angle (negative direction).

Comparing the force-displacement curves obtained for the two different rafter compression stress considered, under the same transverse loading history (negative field), only an increase in the maximum force and corresponding elastic limit displacement can be pointed out (Figure 3.9). The same brittle behaviour after the elastic displacement limit is observed. The development of the force-displacement curves, in particular their stiffness characteristics, remains constants.

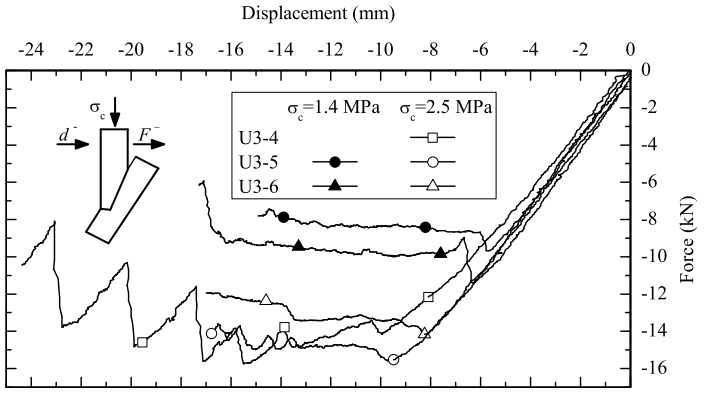


Figure 3.9: Force-displacement curves of unstrengthened connections with 30° skew angle for monotonic loading in negative direction and different rafter compression stress.

Comparing the force-displacement curves obtained for both rafter compression stress levels, under monotonic loading in positive and negative directions (Figure 3.10) important conclusions can be pointed out. First, the behaviour is quite asymmetric. The elastic-plastic behaviour presented in the positive direction becames brittle and more depending of the friction conditions in the negative direction. This difference is a consequence of the distinct mechanism developed, in particular, the ductile behaviour of wood under compression, contrary to the fragile behaviour characteristic of the friction conditions that stipule the behaviour in the negative loading direction. No failure is reached in the positive loading direction while in the negative one, an early failure happen near the 15-20 mm of displacement. For a rafter compression stress of 1.4 MPa, the stiffness and the maximum force obtained for the positive loading direction represents 50% of the ones measured in the negative field (Table 3.6). However, the behaviour in the positive loading direction is more ductile, allows higher displacements and elastic limits. In the case of a rafter compression stress equal to 2.5 MPa, the stiffness is very similar but the maximum force is higher in the negative loading direction.

Stiffness was computed using three different methodologies: (1) force displacement linear regression (the square of the correlation coefficient should be

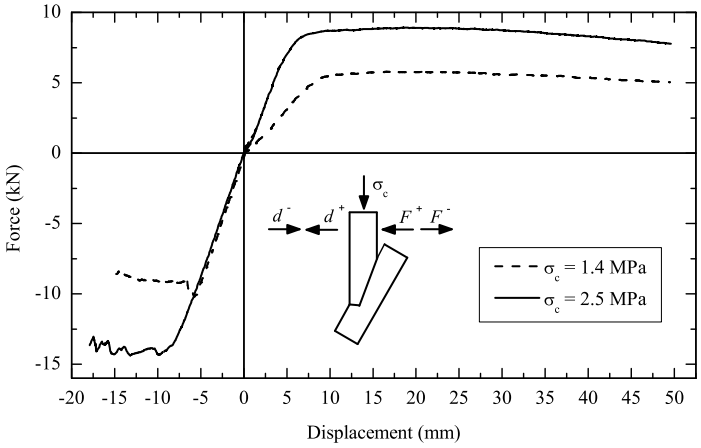


Figure 3.10: Force-displacement curves of unstrengthened connections with 30° skew angle for monotonic tests under different rafter compression stress.

Table 3.6: Effect of the rafter compression levels in the response of unstrengthened connection with 30° skew angle under monotonic loading.

Skew angle	σ_c (MPa)	d_e (mm)	F_{max} (kN)	Stiffness (kN/mm)×10^3		
				Regression	F_e/d_e	$F_e^{50\%}/d_e^{50\%}$
30°	1.4	8.31	6.72	674	634	647
		-5.76	-10.75	1771	1785	1958
	2.5	5.47	10.84	1569	1389	1408
		-8.13	-15.32	1705	1661	1758

greater than 0.99); (2) division of the force (F_e) by the displacement (d_e) measured in the elastic limit and (3) division of the force ($F_e^{50\%}$) by the displacement ($d_e^{50\%}$) gauged when the displacement is half of the elastic limit value. In the case of the skew angle equal to 60°, some differences in the monotonic tests results under the two distinct rafter's compression stress levels have to be pointed out (Figure 3.11). Despite the asymmetric behaviour between the negative and positive loading direction is still present, the difference decreases. With 60° skew angle, the same elasto-plastic behaviour is obtained in the positive loading direction, the brittle nature of resistant mechanism in the negative loading direction is reduced. This reduction is explained by the change in the step angle. In consequence of the increase in the compression component in the grain direction, caused by the reduction of the step angle, the resistant mechanism in the negative loading direction, in the case of 60° skew angle connections, becomes less friction based. The mean values for the maximum force

($F_{\max}$) and the elastic displacement (d_e) in both fields are different, but the stiffness is very similar (Table 3.7). The elastic stiffness of the connection is independent of the transverse loading direction and does not change with the rafter compression stress. The maximum force and the elastic displacements values increase with the compression stress in the rafter.

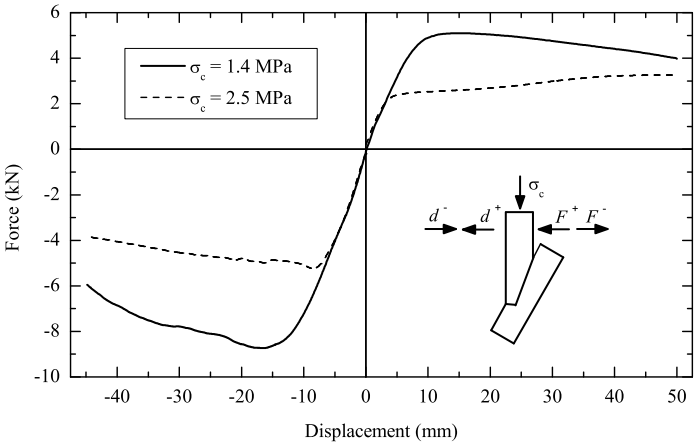


Figure 3.11: Force-displacement curves of unstrengthened connections with 60° skew angle for monotonic tests under different rafter compression stress.

Table 3.7: Effect of the rafter compression levels in the response of unstrengthened connection with 60° skew angle under monotonic loading.

Skew angle	σ_c (MPa)	d_e (mm)	$F_{\max}$ (kN)	Stiffness (kN/mm)×10^3		
				Regression	F_e/d_e	$F_e^{50\%}/d_e^{50\%}$
60°	1.4	2.98	3.31	621	668	882
		-5.32	-4.18	780	780	900
	2.5	7.47	5.12	597	586	680
		-11.18	-9.02	692	715	779

Both effects of rafter compression stress and skew angle, in the behaviour of unstrengthened connection under monotonic loading are compared in Figure 3.12. While the effect of the first variable has been already discussed, the change in the skew angle value result in: a) bigger the skew angle, less is the connection resistance and the elastic stiffness; b) smaller the skew angle, more brittle and friction based is the resistant mechanism in the negative loading direction; and c) bigger the skew angle, less is the difference between the elastic stiffness of both loading directions.

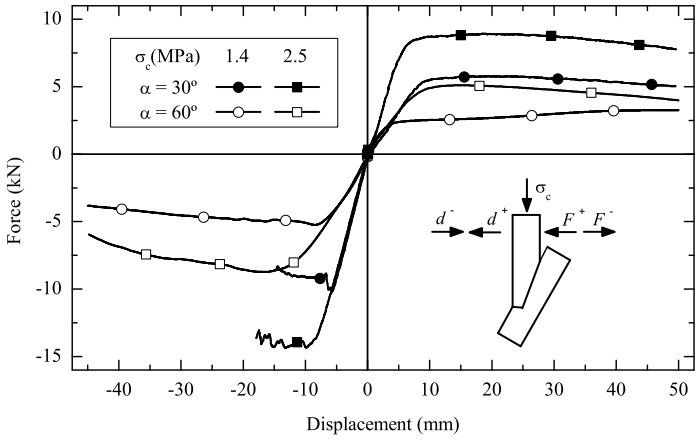


Figure 3.12: Force-displacement curves of unstrengthened connections with 30º and 60º skew angle for monotonic tests under different rafter compression stress.

The asymmetric behaviour observed under monotonic loading for unstrengthened connections with 30º and 60º skew angle, as result of the different resistant mechanism in each direction, has consequences in the behaviour under cyclic loading. The obtained response is asymmetric (Figure 3.13). Energy dissipation occurs only in the negative direction. However, the force-displacement curves show a non-linear development in both directions. This energy dissipation is mainly produced by the sliding of the rafter when pulled into the negative direction. Increasing the rafter compression stress, the force-displacement curves shape remain similar, presenting an increment in the maximum force values. With the rafter compression stress, the energy dissipation and the equivalent viscous damping ratio (V_{eq}) grow from 2.45% to 3.96% and from 23.40% to 36.00%, respectively (see Table 3.8). Nevertheless, the higher increase is due to the skew angle enlarge from 30º to 60º. The main difference between the rafter compression stress applied was that, for 1.4 MPa, no failure was reached, while, with 2.5 MPa, all three specimens presented damage (Figure 3.14).

3.5.1 Efficiency evaluation of the strengthening techniques

Four strengthening schemes, representing modern implementations of traditional techniques using metal elements, have been studied. Three of them, stirrup, bolt and binding strip were analysed for two values of the skew angle, 30º and 60º, while the forth, the rigid binding strip, was only evaluate in the case of a 30º skew angle. This last technique was abandoned because of the difficulties that it practical implementation and use revealed. All strengthen-

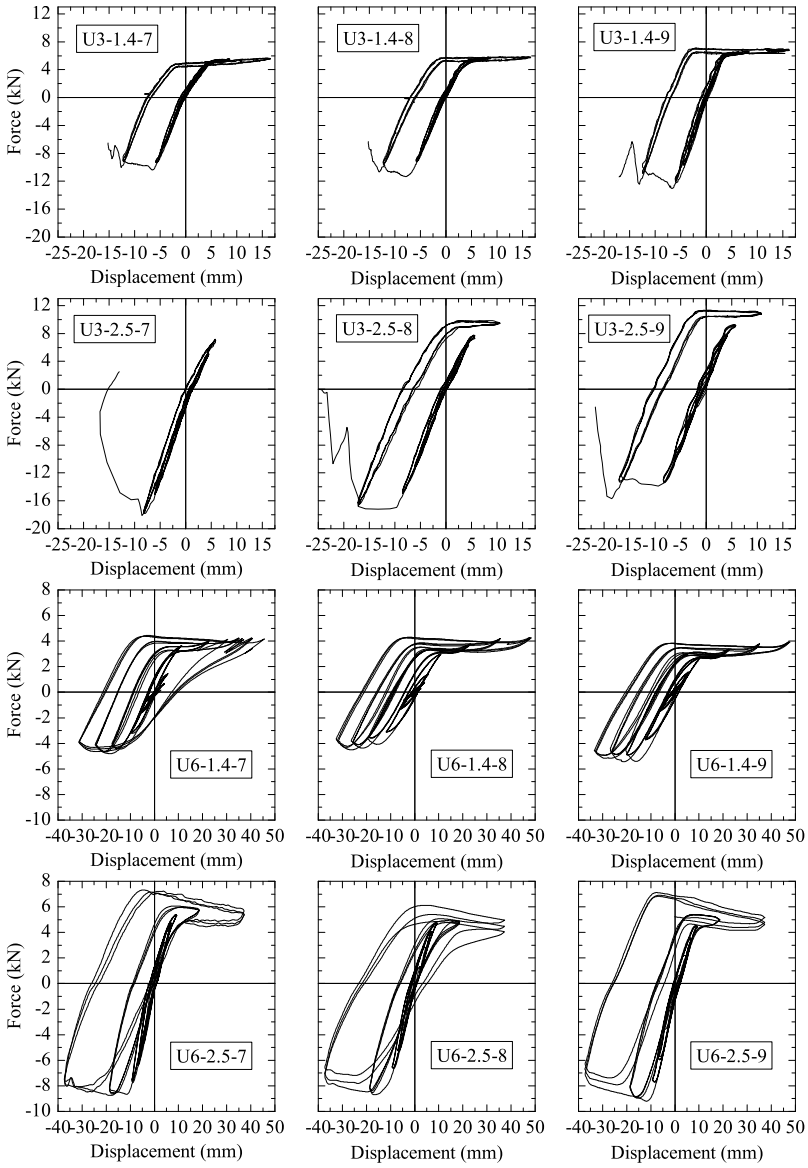


Figure 3.13: Force-displacement curves of unstrengthened connections with 30° and 60° skew angle under ciclic loading for different rafter compression stress.

Table 3.8: Effect of the rafter compression stress in the response of unstrengthened connection under monotonic loading.

Skew angle	σ_c (MPa)	d^+_{max} (mm)	d^-_{max} (mm)	F^+_{max} (kN)	F^-_{max} (kN)	Dissipated Energy (kJ)	V_{eq} (%)
30°	1.4	16.49	-15.83	6.20	-11.57	230	2.45
	2.5	9.15	-21.17	9.45	-17.00	380	3.96
60°	1.4	33.36	-33.36	4.06	-5.27	809	23.4
	2.5	37.30	-37.30	6.87	-8.99	1503	36.0



(a) Compression damage in U3-2.5-7 (b) Shear failure in U3-2.5-9

Figure 3.14: Damages observed in the connections with a skew angle of 30° in the cyclic tests for 2.5 MPa compression stress.

ing techniques have been evaluated under monotonic and cyclic loading for a constant rafter compression stress of 1.4 MPa. Tests under monotonic loading aim at definying the cyclic test procedure to be use for each strengthening techniques but gave also important indications on the improvement, in terms of ductility and resistance, provided by the strengthening. Monotonic tests results are also of paramount importance in the definition of synthetic laws representing the semi-rigid behaviour of the connections evaluated.

3.5.1.1 Stirrup

The experimental force-displacement curves obtained for the connections strengthened with stirrups under monotonic loading for 30° and 60° skew angles are shown in Figure 3.15.

Small differences are observed in the strengthened connections behaviour

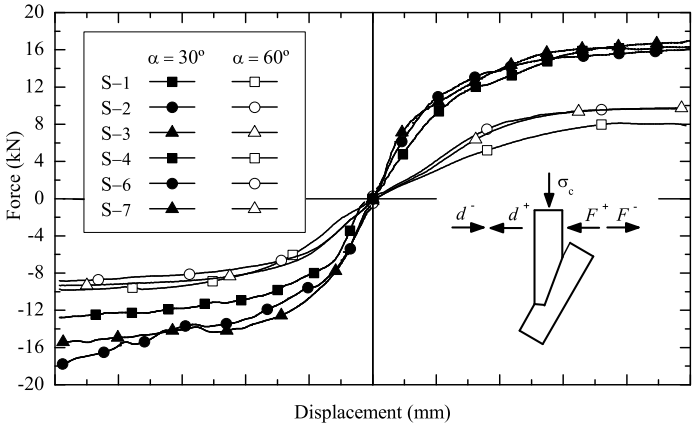


Figure 3.15: Force-displacement curves of stirrup strengthened connections with 30º and 60º skew angles under monotonic loading.

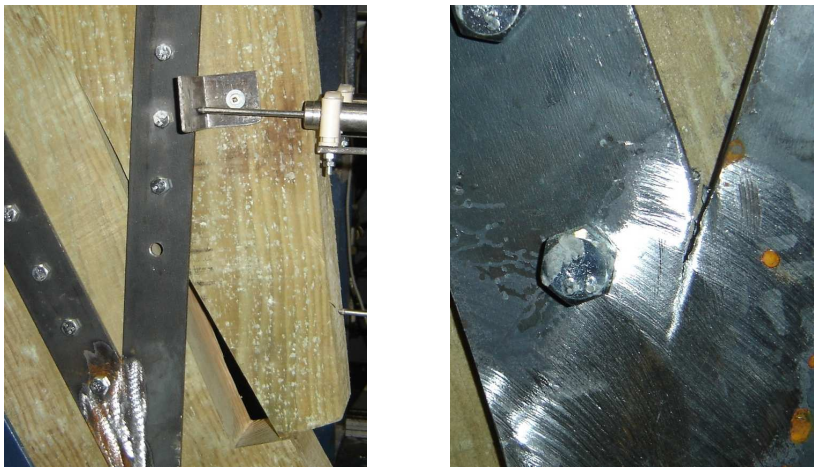
with the direction of the monotonic loading. The more important difference detected is the variation of the stiffness with the direction of loading in the case of 30º skew angle. The skew angle is associated with: a) the resistance and the stiffness decrease with the increase of the skew angle and, b)increase in the apparent elastic displacement limit, reached in the positive direction, with the enlargement of the skew angle from 30º to 60º. The maximum force value increases oven the entire test, which indicates that maybe, if the tests were extended, the maximum force value could increase. Table 3.9 summarised the monotonic tests results obtained for strengthened connections with stirrups.

Table 3.9: Monotonic tests results of strengthened connections with stirrups.

Skew angle	σ_c (MPa)	d_e (mm)	F_{max} (kN)	Stiffness (kN/mm)$\times 10^3$		
				Regression	F_e/d_e	$F_e^{50\%}/d_e^{50\%}$
30º	1.4	5.62	16.48	1517	1312	1239
		-5.79	-15.34	1428	1257	1310
60º	1.4	18.71	9.23	377	360	356
		-8.51	-9.38	526	546	580

At the end of the tests diferrent damages were detected (sse Figure 3.16). In the negative direction, no damage is observed with exception of the local compression in the posterior part of the notch, while, in positive direction, the most common damage is the failure of the stirrup itself (through its metal part).

Based on the monotonic tests results for the apparent elastic displacement



(a) Negative loading direction (b) Positive loading direction

Figure 3.16: Final position of the strengthened connections under monotonic loading (30º skew angle).

limit (d_e), the values of $d_e^+ = d_e^+ = 5.70$ mm and $d_e^+ = d_e^+ = 13.61$ mm were assumed for the 30º and 60º skew angle connections, respectively, for the imposed displacement time history used in the cyclic tests. A quasi-static history of loading and unloading was applied under a movement rate of 0.224 mm/s and 0.18mm/s in the case of 30º and 60º skew angle connections, respectively. The experimental force-displacement loops obtained, for the strengthened connections with stirrups tested under cyclic loading are presented in Figure 3.17.

The most important conclusion that can be drawn from the Figure 3.17 is the ability of these strengthened connections, under cyclic loading, to dissipate energy in both loading directions as show by the large loops. The maximum force values and displacement for both loading directions are quite similar (Table 3.10). As expected, and in agreement with the results obtained in the monotonic tests, higher the skew angle result in less energy dissipated and lower joint resistance. However, the equivalent viscous damping ration (V_{eq}) increase with the skew angle of the connections strengthened with stirrups. Table 3.10 summarised the cyclic tests results obtained for strengthened connections with stirrups.

3.5.1.2 Bolt

The experimental force-displacement curves obtained in the case of the connections strengthened with bolt, under monotonic loading for 30º and 60º skew angles, shows a full non-linear development with high ductility (Figure 3.18).

The three specimens considered for each variable shows very consistent results, only diverging in the maximum force value (F_{max}), in particular, in the case of 30º skew angle connections under monotonic positive loading. Higher

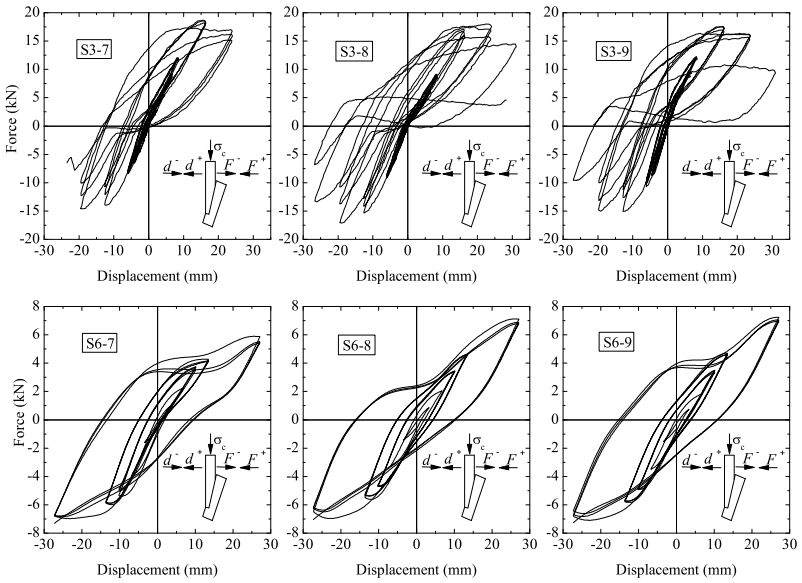


Figure 3.17: Force-displacement loops for stirrup strengthened connections with 30° and 60° skew angle under cyclic loading.

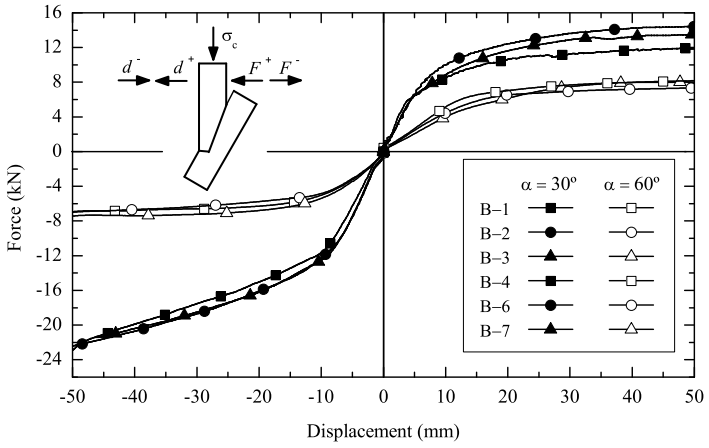


Figure 3.18: Force-displacement curves of bolt strengthened connections with 30° and 60° skew angles under monotonic loading.

Table 3.10: Cyclic tests results of strengthened connections with stirrups.

Skew angle	σ_c (MPa)	d^+_{max} (mm)	d^-_{max} (mm)	F^+_{max} (kN)	F^-_{max} (kN)	Dissipated Energy (kJ)	V_{eq} (%)
30°	1.4	28.68	-21.75	18.09	-15.60	1859	15
60°		27.16	-27.28	7.09	-7.21	1080	36

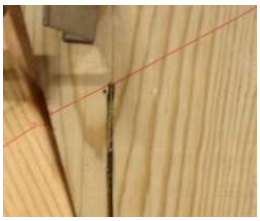
is the skew angle, smaller is the resistance and the stiffness achieved by the strengthened connection. In the case of the skew angle equal to 60°, the direction of the loading do not seems to have influence in the connection resistance while affects the stiffness and the apparent elastic displacement limit. Despite the asymmetry observed in the values of the apparent displacement limit and in the maximum force reached, with a 30° skew angle, the stiffness do not depends of the loading direction. Table 3.11 summarised the monotonic tests results obtained for strengthened connections with bolts.

Table 3.11: Monotonic tests results of strengthened connection with bolts.

Skew angle	σ_c (MPa)	d_e (mm)	F_{max} (kN)	Stiffness (kN/mm)$\times 10^3$		
				Regression	F_e/d_e	$F_e^{50\%}/d_e^{50\%}$
30°	1.4	4.94	13.83	1468	1381	1459
		-7.829	-22.41	1488	1387	1409
60°	1.4	10.92	7.85	442	446	465
		-5.22	-7.08	623	657	838

The ductility provided by the strengthening is optimized when the bolt is aligned with the force caused by the external load applied. The best results are achieved for 30° skew angle under monotonic loading in the negative direction (closing the skew angle), because corresponds to the case of higher tension in the bolt. Higher tension in the bolt, higher the resistance and more ductility is obtained. When opening the skew angle, monotonic loading in the positive direction, the bolt is tensioned but is also subjected to bending, in particular in the case of 30° skew angle (Figure 3.19).

In the other direction, negative direction, apart the action of the bolt, primarily subjected to tension and after under bending, with the increment of the imposed displacement another resistant mechanism is revealed: the local compression perpendicular to the grain in the tie beam element (Figure 3.20). As observed in the unstrengthened connections, but now extended due to the strengthening effects, a local compression of wood is detected in the back of the connection. This local effect is responsible for a plastic phase in the force-displacement response of these connections.



(a) Yielding of the bolt



(b) Gap between the two elements



(c) Bending of the washer

Figure 3.19: Damages observed in the 30° skew angle strengthened connections with bolt under monotonic loading in the positive direction.



(a) Bending of the bolt



(b) Local compression perpendicular to the grain

Figure 3.20: Damages observed in the 30° skew angle strengthened connections with bolt under monotonic loading in the negative direction.

The apparent elastic displacement limit values of $d_e^+ = 5$mm and $d_e^- = -8.5$mm and $d_e^+ = d_e^- = 8.15$mm were assumed for the 30° and 60° skew angle connections, respectively, for the imposed displacement time history that represents the cyclic tests. A quasi-static history of loading and unloading was applied under a velocity of 0.224 mm/s and 0.18 mm/s in the case of 30° and 60° skew angle connections, respectively. The experimental force-displacement loops obtained, for the strengthened connections with bolts tested under cyclic loading are presented in Figure 3.21. The force-displacement loops obtained for the strengthened connections with bolt under the cyclic loading tests, are asymmetric, in particular in the case of 30° skew angle connections. The force and displacement values are higher for the negative loading direction and the main dissipation of energy appends there. Increasing the skew angle from 30° to 60° the resistance of the strengthened connections is reduced. With a 30° skew angle and under monotonic loading in the positive direction a plastic phase is observed, preceded by a small elastic branch, as consequence of the bending of the bolt. In all other cases, no significant bending of the bolt seems to happen. The pinching effect observed in the force-displacement loops is quite higher in the case of the 30° skew angle connection. Higher the skew angle, smaller resistance is obtained and less energy is dissipated. However,

with an increase of the skew angle from 30° to 60°, a significant improvement is achieved in the equivalent viscous damping ration (Table 3.12).

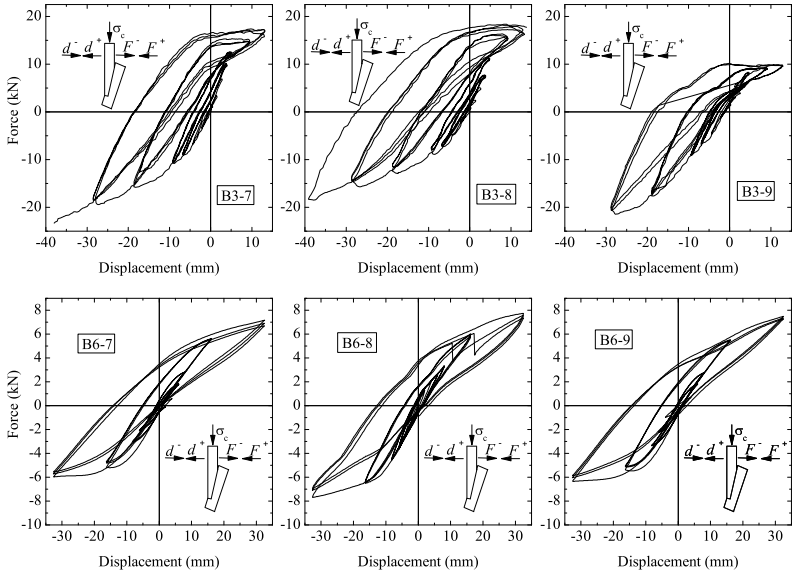


Figure 3.21: Force-displacement loops for bolt strengthened connections with 30° and 60° skew angle under cyclic loading.

Table 3.12: Cyclic tests results of strengthened connection with bolts.

Skew angle	σ_c (MPa)	d^+_{max} (mm)	d^-_{max} (mm)	F^+_{max} (kN)	F^-_{max} (kN)	Dissipated Energy (kJ)	V_{eq} (%)
30°	1.4	13.30	-35.30	15.29	-21.80	1877	11
60°		32.55	-32.67	7.36	-6.72	762	24

3.5.1.3 Binding strip

The binding strip was analysed only in the case of 30° skew angle, and corresponds to a first phase of the experimental campaign carried out. The experimental results shows that this strengthening technique is able to improve the connections behaviour, in terms of resistance, ductility and dissipation of energy, however it implementation, especially *in situ*, is extremely difficult. The rigid hollow steel ribbon that materializes this binding strip is only suitable for new applications. Although this limitation, the experimental results

obtained can be of practical interest. Figure 3.22 shows the experimental force-displacement curves obtained in the case of the connections strengthened with rigid binding strip, under monotonic loading for 30° skew angle.

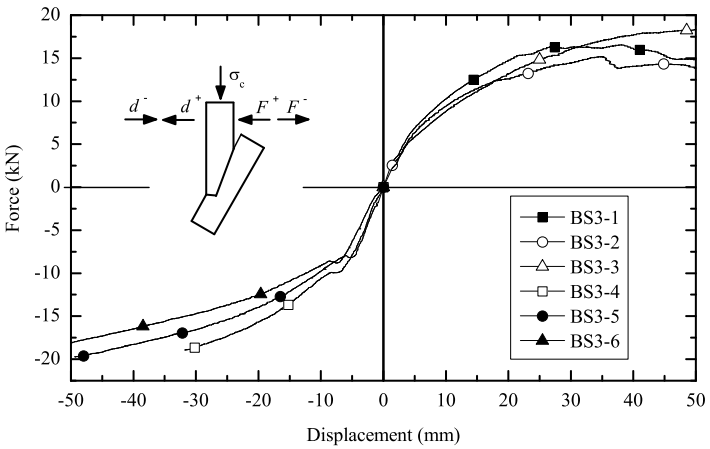


Figure 3.22: Force-displacement curves for 30° skew angle strengthened connections with binding strip under monotonic loading.

The experimental force-displacement curves obtained showed a full non-linear evolution, however, specimens BS3-1, BS3-2 and BS3-4 revealed a limitation on the ductility. The elastic phase of the force-displacement curves is small (the average apparent elastic displacements limits are 4.37 mm and −6.33 mm). In the negative loading direction, firstly, when the binding strip is tightly fit to the connection all materials behave linear elastic. In a second phase, the elastic part is followed by formation of a plastic hinge in the contact rafter/tie beam (see Figure 3.22). In this phase, a minor decrease of the force is observed corresponding to the beginning of the plastification of wood. After that, in a third phase, a constant hardening process is revealed. A high ductility is characteristic of this phase in consequence of the plastification process of wood and tension of the binding strip. The resistance of the strengthened connections is considerable ($\approx$ 19kN) and seems to be independent of the monotonic loading direction. Changing the loading direction the stiffness presents an insignificant variation. Table 3.13 presents the main results obtained from the monotonic tests on strengthened connections with binding strip.

The strengthened connections with binding strip are strong, in terms of resistance, but the damages induced in the timber elements during the tests are important (figure 3.23). The tie effect provided by the binding strip is so high that, under monotonic loading in the positive direction, the bottom part of the rafter does not move and all imposed displacement history is suffered by the top part. In consequence, major bending stresses are induced in the rafter. In the other loading direction, negative or decreasing the skew angle,

Table 3.13: Monotonic tests results of strengthened connection with binding strip.

Specimen	σ_c (MPa)	d_e (mm)	F_{max} (kN)	Stiffness (kN/mm)$\times 10^3$		
				Regression	F_e/d_e	$F_e^{50\%}/d_e^{50\%}$
BS3-1		4.00	17.01	1629	1489	1608
BS3-2	1.4	4.80	15.82	1430	1306	1367
BS3-3		4.30	18.81	1357	1252	1384
	Mean	4.37	17.21	1472	1349	1453
	CoV	9.25	8.75	9.56	9.21	9.26
BS3-4		-7.00	19.10	1583	1452	1634
BS3-5	1.4	-5.00	-20.00	1809	1796	1778
BS3-6		7.00	-18.81	1428	1239	1194
	Mean	-6.33	-19.30	1607	1496	1535
	CoV	18.23	3.21	11.93	18.79	19.82

the damages are essentially located in the tie beam member, where in the back of the connection, local compression perpendicular to the grain of the timber is observed.



Figure 3.23: Damage observed in the 30º skew angle strengthened connections with binding strip under monotonic loading in positive direction.

A quasi-static history of loading and unloading was applied under a movement rate of 0.224 mm/s using the apparent elastic displacement limit values of $d_{max}^{+} = 4.5$ mm and $d_{max}^{-} = 7$ mm obtained in the monotonic tests. The

experimental force-displacement loops obtained, for the strengthened connections with binding strip tested under cyclic loading are presented in Figure 3.24.

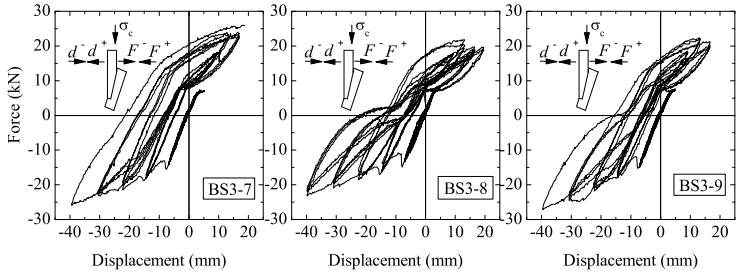


Figure 3.24: Force-displacement loops for 30º skew angle strengthened connections with binding strip under cyclic loading.

In agreement with the monotonic tests, the loops obtained in the cyclic tests are asymmetric. If, under negative loading direction the force-displacement curves are linear elastic, more depending of the friction conditions, when subjected to positive loading direction, the curves force-displacement presents a non-linear development. After firsts cycles with no dissipation of energy, large loops are exhibits for the negative loading direction while the ones obtained in the positive loading direction are thin. Therefore, it can be concluded that dissipation of energy only occurs in the negative field. However, the dissipation of energy is considerable (see Table 3.14). the maximum load values achieved in each loading direction are quite the same and the value calculate for the equivalent viscous damping ration is very consistent (CoV = 0.07).

Table 3.14: Cyclic tests results of strengthened connection with binding strip.

Specimen	σ_c (MPa)	d^+_{max} (mm)	d^-_{max} (mm)	F^+_{max} (kN)	F^-_{max} (kN)	Dissipated Energy (kJ)	V_{eq} (%)
BS3-7		18.79	-39.43	25.97	-25.97	3335	6.75
BS3-8	1.4	19.64	-39.80	21.79	-23.28	2737	6.49
BS3-9		16.72	-39.67	22.39	-27.16	2550	7.40
	Mean	18.38	-39.63	23.38	-25.47	2874	6.88
	CoV	0.08	0.00	0.10	0.08	0.14	0.07

Under cyclic loading, the failure appends with local damages in the step edge and through shear stresses revealed in front of the step (see Figure 3.25).



(a) Local damage of the step edge (b) Shear failure in front of the step

Figure 3.25: Damages observed in the 30° skew angle strengthened connections with binding strip under cyclic loading.

3.5.1.4 Tension ties

The experimental force-displacement curves obtained in the case of the connections strengthened with tension ties, under monotonic loading for 30° and 60° skew angles, shows a full non-linear development with high ductility (see Figure 3.26).

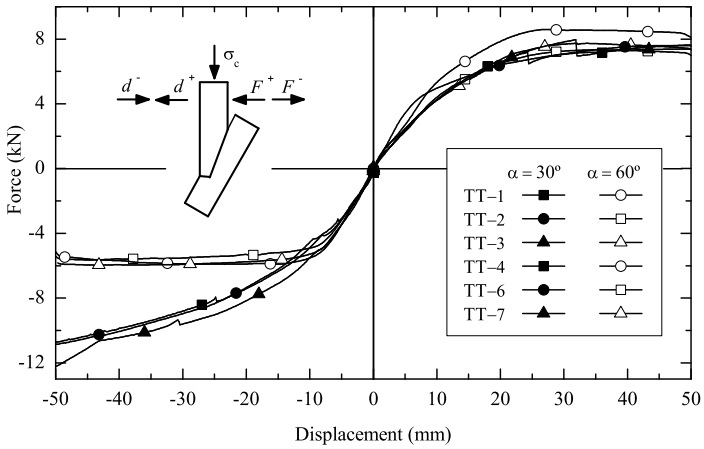


Figure 3.26: Force-displacement curves of tension ties strengthened connections with 30° and 60° skew angles under monotonic loading.

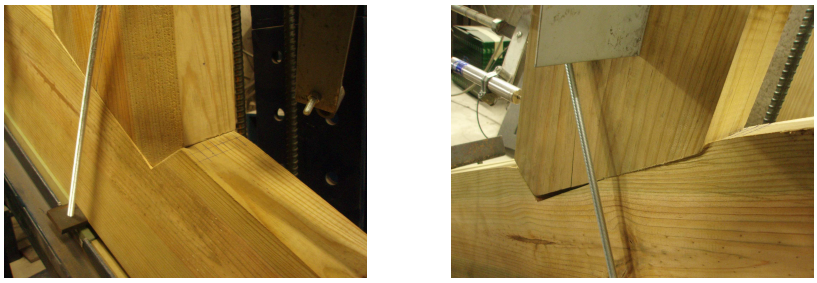
All results are very consistent and the response is poorly affected by the skew angle value and by the monotonic loading direction. Resistance, stiffness and the development of the force-displacmerent curves are quite constant. Only

when the skew angle is 30° and the strengthened connections are subjected to monotonic loading in the negative direction, the results obtained exhibits some variation. In this loading direction, in the case of a 60° skew angle, a significant plastic phase is observed in the force-displacement experimental curves obtained. Table 3.15 summarised the main results of the monotonic tests of strengthened connections with tension ties were this observations can be measure.

Table 3.15: Monotonic tests results of strengthened connection with tension ties.

Skew angle	σ_c (MPa)	d_e (mm)	F_{max} (kN)	Stiffness (kN/mm)$\times 10^3$		
				Regression	F_e/d_e	$F_e^{50\%}/d_e^{50\%}$
30°	1.4	4.91	7.65	556	555	570
		-4.91	-11.26	610	651	749
60°	1.4	9.72	7.91	461	471	495
		-6.71	-6.08	639	664	710

Only the 60° skew angle strengthened connections with tension ties showed visible damages. Those local damages are different for each monotonic loading direction (see Figure 3.27). When opening the skew angle (positive direction) local compression of the front of the knot is observed. In the other direction, negative or decreasing the skew angle, local compression perpendicular to the grain is detected in the back of the connection.



(a) Positive loading direction (b) Negative loading direction

Figure 3.27: Damages observed in the 60° skew angle strengthened connections with tension ties under monotonic loading.

From the monotonic tests results, apparent elastic displacement limit values equal to $d_e^+ = d_e^- = 4.90$ mm and $d_e^+ = d_e^- = 8.20$ mm were assumed for the 30° and 60° skew angle connections, respectively. Those values were used in the imposed displacement time history assumed for the cyclic tests. A quasi-static history of loading and unloading was applied under a velocity of 0.18 mm/s.

The experimental force-displacement loops obtained for the strengthened connections with tension ties tested under cyclic loading are presented in Figure 3.28.

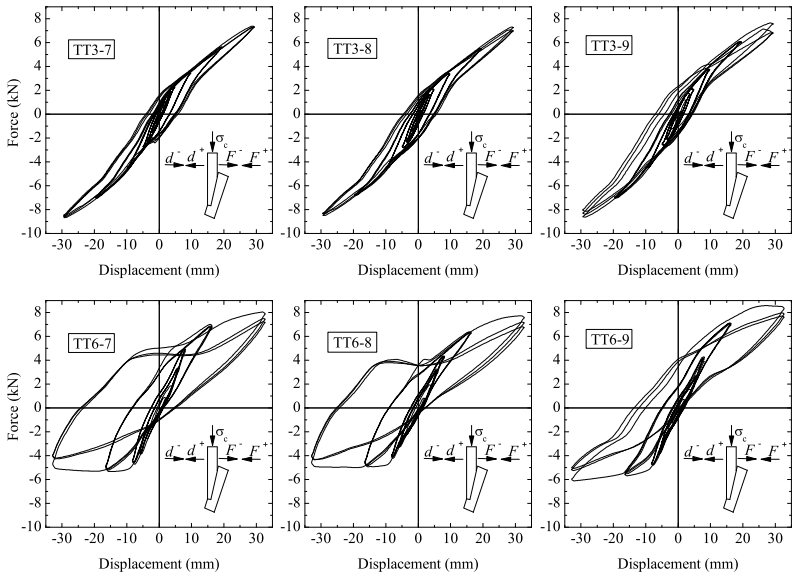


Figure 3.28: Force-displacement loops for tension ties strengthened connections with 30º and 60º skew angle under cyclic loading.

Despite the asymmetry exhibited by the monotonic tests results, the 30º skew angle strengthened connections presents loops quite symmetric. However, in this case, the maximum force achieved in the negative direction is slightly higher (15.7%). In contrary, the cyclic tests results of 60º skew angle strengthened connections are quite asymmetric. The loops development is different for the negative and the positive loading direction. In the negative loading direction, a plastic behaviour is observed which results in a reduction in the connections resistance, in comparison with the positive loading direction. The maximum load values achieved are quite constant and with the increase of the skew angle from 30º to 60º, the capability to dissipated energy is improved with clear consequences in the increase of the equivalent viscous damping ration (Table 3.16).

3.5.1.5 Strengthening conclusions and comparisons

Comparing the experimental force-displacement curves, obtained for the unstrengthened and strengthened connections (Figures 3.29 and 3.30) it is recognize that all the strengthening schemes improve the behaviour of the originals connections. In the case of connections with 30º skew angle (see Figure 3.29),

Table 3.16: Cyclic tests results of strengthened connection with tension ties.

Skew angle	σ_c (MPa)	d^+_{max} (mm)	d^-_{max} (mm)	F^+_{max} (kN)	F^-_{max} (kN)	Dissipated Energy (kJ)	V_{eq} (%)
30°	1.4	29.41	-29.55	7.53	-8.71	554	13
60°		32.80	-32.96	8.13	-5.50	990	38

the strengthening techniques analysed increases the stiffness, in particular, in the positive loading direction and the maximum resistance for both directions.

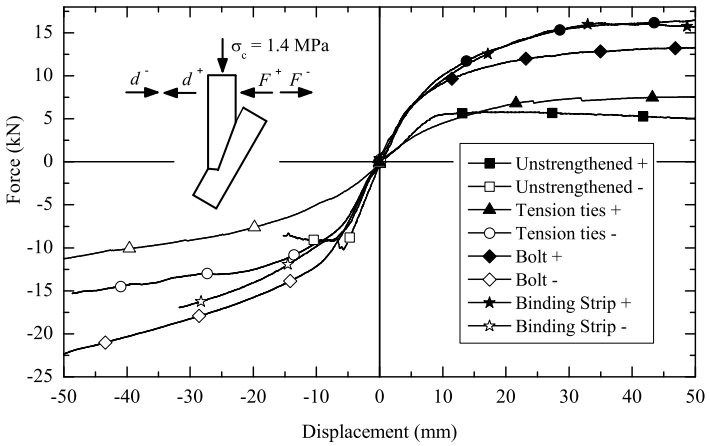


Figure 3.29: Force-displacement curves for unstrengthened and strengthened connections with 30° skew angle under monotonic loading.

The elasto-plastic behaviour with limited ductility evidenced by the unstrengthened connections under negative loading direction is substituted by full non linear curves exhibiting high ductility in the strengthened connections. Comparing the strengthening techniques evaluated, the less efficient (maximum force and stiffness), is the tension ties. Connections strengthened with stirrups and binding strip attained the same range of maximum force, however, this later scheme has a lower ductility capacity. In particular, the maximum resistance for the strengthened connections with stirrups and internal bolt is achieved near the end of the test. However, in the strengthened connections with binding strip, when the tests were interrupted, the force value was already decreased. Therefore, between the internal bolt and the binding strip, the first one is more efficient in terms of ductility capacity with the goal to assure a better seismic behaviour of the connection. The effect of the strengthening schemes in the negative loading directions of the monotonic tests is obvious: the increase of the maximum force and of the ductility capacity. The bene-

fits to the stiffness are not significant (the stiffness exhibit by the tension ties technique is even minor). However, the brittle behaviour exhibited by unstrengthened connections disappears in all strengthened specimens. Therefore, the main profit of adding a metal device to the joints is the improvement of ductility with clear advantages in their seismic behaviour. Only the binding strip showed limitations in terms of maximum displacement. Extending the comparison in the case of connections with 60º skew angle, the main conclusions are kept (see Figure 3.30). The more evident benefit, which is normally the main goal of a strengthening intervention, is the improvement of the connection ductility. In particular under monotonic loading in the negative direction, the original behaviour of the unstrengthened connections, characterize by having limit ductility, is substituted, when strengthened, by a full non-linear behaviour with considerable ductility. The strengthening techniques evaluated do not cause changes in the stiffness but results in an increase of the maximum force achieved in the tests in both directions, in particular, under monotonic loading in positive direction. Between the strengthening techniques studied, the differences in the force-displacement curves are only visible when under monotonic loading in the negative direction. In this case, stirrup is the more efficient (maximum load achieved), while the response of the tension ties and the bolt are quite similar.

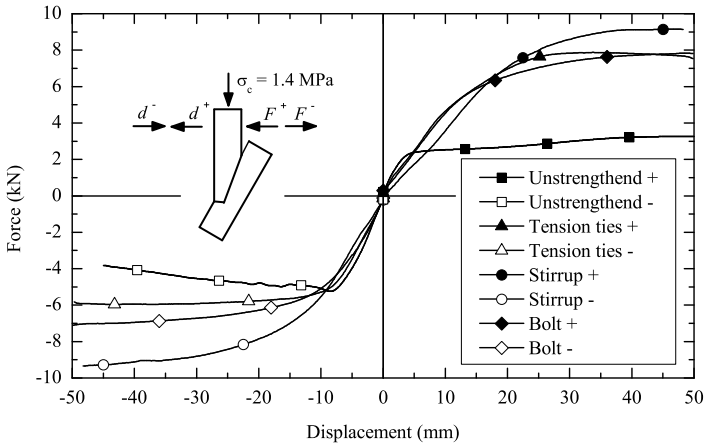


Figure 3.30: Force-displacement curves for unstrengthened and strengthened connections with 60º skew angle under monotonic loading.

The improvements in the connections behaviour under monotonic loading, provided by the strengthening techniques evaluated are highlight by the response under cyclic loading (Figure 3.31 and 3.32).

Without any strengthening device, the connection is not able to prevent the failure causes by load reversals (detachment of the connected elements) even when the rafter compression stress is augmented (from 1.4 MPa to 2.5 MPa).

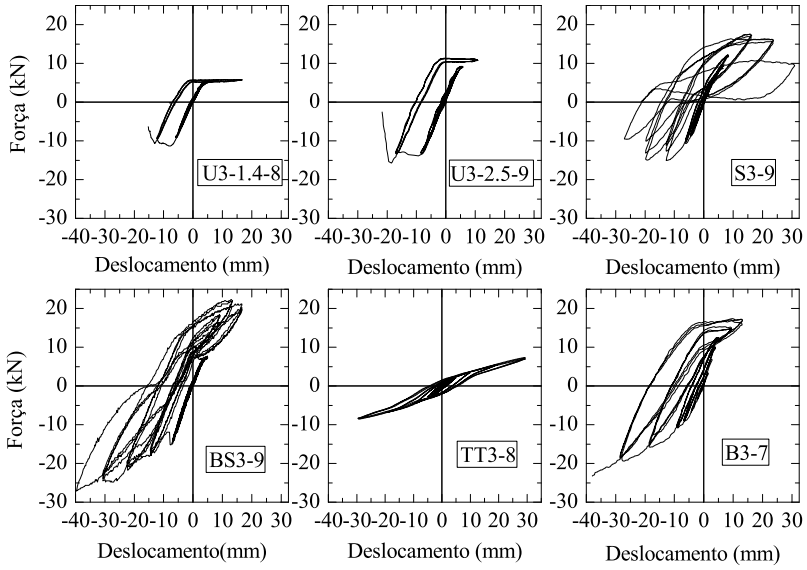


Figure 3.31: Force-displacement loops for unstrengthened and strengthened connections with 30° skew angle under cyclic loading.

The unstrengthened connections showed a very limited capability to dissipate energy. All strengthening techniques adopted were efficient in the improvement of the hysteretic behaviour of the connections. Hysteretic equivalent viscous damping ratios (V_{eq}) evaluated from tests results are considerable (Table 3.17). The best results under cyclic loading are achieved when the stirrup, bolt and tension ties techniques are used. The binding strip provide the strongest connections but the equivalent damping ratio is nearly half of the values presented by the others strengthened connections.

Table 3.17: Cyclic tests results of 30° skew angle connections.

Connection	d^+_{max} (mm)	d^-_{max} (mm)	F^+_{max} (kN)	F^-_{max} (kN)	Dissipated Energy (kJ)	V_{eq} (%)
Unstrengthened	16.49	-15.83	6.20	-11.57	230	2.45
Tension ties	4.91	-4.91	7.65	-11.26	554	12.83
Bolt	13.30	-35.30	15.29	-21.08	1877	11.28
Stirrup	28.68	-21.75	18.09	-15.60	1859	14.57
Binding strip	18.38	-39.63	23.38	-25.47	2874	6.85

In the case of 60° skew angle, the strengthening techniques evaluated provide a force-displacement behaviour more stable (see Figure 3.32). More cycles

are achieved, the pinching effect of the unstrengthened connections is reduced and a more symmetric response is obtained.

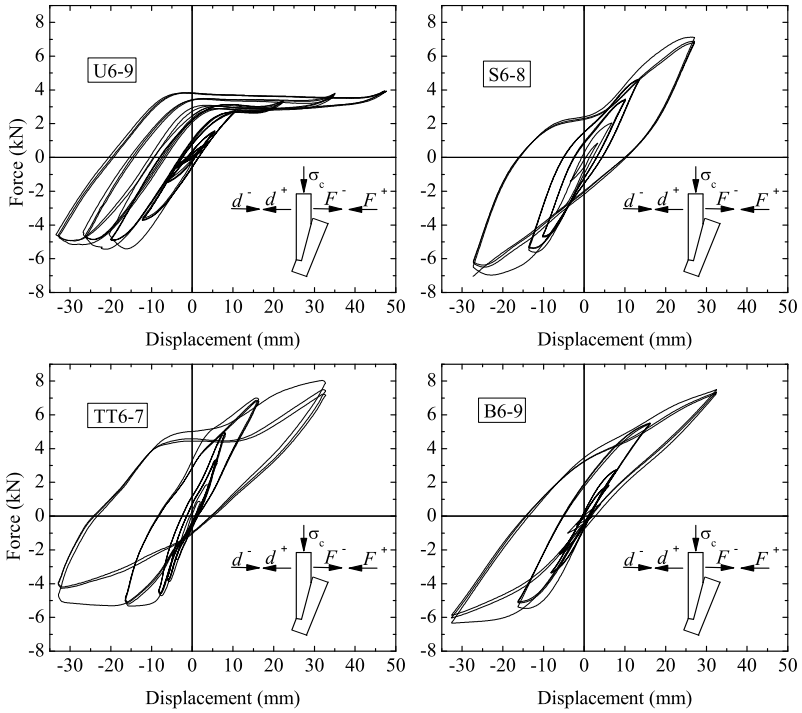


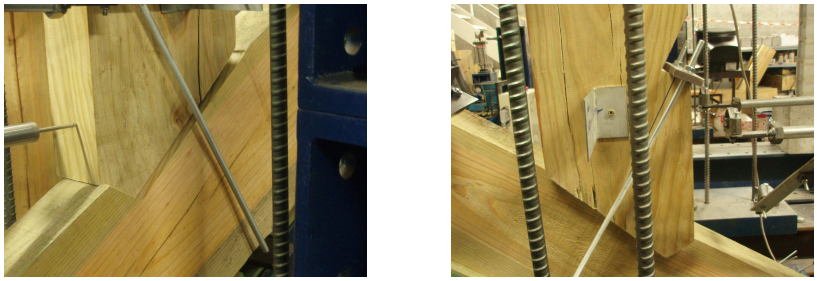
Figure 3.32: Force-displacement loops for unstrengthened and strengthened connections with 60º skew angle under cyclic loading.

It is important to point out that the unstrengthened connections under cyclic loading, because of high step angle, are able to retrieve the slip of the rafter compared to the step, during the impose history. In consequence, an extra amount of energy, which in practice does not occur, were dissipated (Table 3.18).

The strengthening techniques evaluated in the 60º skew angle connections case, when compared with the unstrengthened connections, results in an increase of the connections resistance, energy dissipation and equivalent viscous damping. The results achieved by the connections strengthened with tension ties are influenced by the out-of-plane movements observed during the tests. In fact, the poor capability to prevent out-of-plane movements by the tension ties techniques is a serious disadvantage when compared with the others strengthening techniques (Figure 3.33).

Table 3.18: Cyclic tests results of 60º skew angle connections.

Connection	d^+_{max} (mm)	d^-_{max} (mm)	F^+_{max} (kN)	F^-_{max} (kN)	Dissipated Energy (kJ)	V_{eq} (%)
Unstrengthened	33.36	-33.36	4.06	-5.27	809	14.23
Tension ties	32.80	-32.96	8.13	-5.50	990	37.82
Bolt	32.55	-32.67	7.36	-6.72	762	24.38
Stirrup	27.16	-27.28	7.09	-7.21	1080	35.77



(a) Positive loading direction (b) Cyclic test

Figure 3.33: Out-of-plane movements detected in the 60º skew angle connections strengthened with binding strip.

3.6 Conclusions

Traditional timber connections, even without any strengthening device, usually have a significant moment-resisting capacity. Therefore, they cannot be represented by common constraint models, like perfect hinges, but should be considered semi-rigid and friction based. The test results show that this capacity is function of the compression stress applied in the rafter and skew angle. Moreover, it is clear that the heigth of the rafter, the friction angle (Parisi and Piazza, 2000), the existence of mortise and tenon and the moisture content (Palma and Cruz, 2007) are also important. The experimental analysis has been of fundamental importance in order to understand the real behaviour, by pointing out some important aspects like force transmission mechanisms, failure modes and guidance for appropriate strengthening solutions. Strengthening, usually performed by insertion of metal devices, is indispensable for ensuring adequate joint response, in particular, for seismic loading, or in other adverse and unpredictable loading conditions. All strengthening techniques analysed results in a significant increase of the equivalent viscous damping ratio, higher resistance and significant improvement of the ductility. The energy dissipation became significant as more stables cycles are achieved. Between the strengthening techniques evaluated, the insertion of one bolt across the joint axis and

metal stirrups positioned at the two sides of the joint, bolted to the timber elements, have given more favourable results.

Chapter 4

Numerical modelling of traditional timber connections

The finite element method (FEM) has become the prevalent technique used for analysing physical phenomena in the field of structural, solid and fluid mechanics as well as for the solution of filed problems. Also in the case of wood, FEM as proved to be a suitable tool to study the material, and their mechanical properties, and to evaluate the mechanical performance of its connections. Here, FEM is adopted to simulated the structural behaviour of unstrengthened traditional timber connections. Numerical analysis is not thought as a substitute of the full-scale tests - their results are complementary.

4.1 Numerical modelling

The tests results on full-scale specimens became the fundamental reference for the subsequent step of the research: finite element modelling of unstrengthened connections. Bi-dimensional models were set up using the commercial package Abaqus (2007). The geometry and loading of the connections permits the assumption of a state of plane stress for the model. Details of the finite element model concerning the material model, the geometric constraints and the load path are reported in the following sections. The constant reference to experimental tests allowed the calibration first and the validation of numerical results afterwards.

4.1.1 Material model

Timber is anisotropic, but may be satisfactorily represented as orthotropic (Bodig and Jayne, 1982) in the system of so-called anatomic cylindrical coordinates corresponding to the longitudinal, L, radial, R, and transversal, T, directions of the tree trunk. When the material is extracted from the outer region, curvature may be neglected and the coordinate system may be approximately considered orthogonal. A complete knowledge of orthotropic behavior

in a material requires values of three Youngs moduli, E, three shear moduli, G, and six Poissons ratios, ν. If symmetry is considered, only nine independent parameters need be defined. For softwood, the following approximate values are acceptable:

$$E_{\mathrm{L}} : E_{\mathrm{R}} : E_{\mathrm{T}} \approx 20 : 1.6 : 1 \tag{4.1}$$

$$G_{\mathrm{LR}} : G_{\mathrm{LT}} : G_{\mathrm{RT}} \approx 10 : 9.4 : 1 \tag{4.2}$$

$$E_{\mathrm{L}} : G_{\mathrm{LT}} \approx 14 : 1 \tag{4.3}$$

A simpler, axisymmetric model with $E_{\mathrm{R}} = Y_{\mathrm{T}}$ and $G_{\mathrm{LR}} = G_{\mathrm{LT}}$ may be reasonably adopted and has been used here. The corresponding elastic moduli are E_0 in the direction along the fiber, and E_{90} orthogonal to it, plus a shear modulus, G, and a Poissons ratio, ν.

Compression in the direction normal to the fiber easily brings the material beyond the elastic limit (Kollmann and Cote, 1984); for this reason, a Hill-type plasticity rule has been adopted (eqn 4.4), considering the limit strengths in the fiber direction, $\bar{\sigma}_{11} = f_{\mathrm{c},0}$, and in the normal direction, $\bar{\sigma}_{22} = 0.7 f_{\mathrm{c},90}$, and a shear strength, $\bar{\tau}_{12} = f_{\mathrm{v}}$.

$$F\sigma_{22}^2 + G\sigma_{11}^2 + H\left(\sigma_{11} - \sigma_{22}\right)^2 + 2N\tau_{12}^2 = 1 \tag{4.4}$$

where:

$$F = \frac{\bar{\sigma}_0^2}{2}\left(\frac{1}{\bar{\sigma}_{22}^2} + \frac{1}{\bar{\sigma}_{33}^2} - \frac{1}{\bar{\sigma}_{11}^2}\right) \tag{4.5}$$

$$G = \frac{\bar{\sigma}_0^2}{2}\left(\frac{1}{\bar{\sigma}_{33}^2} + \frac{1}{\bar{\sigma}_{11}^2} - \frac{1}{\bar{\sigma}_{22}^2}\right) \tag{4.6}$$

$$H = \frac{\bar{\sigma}_0^2}{2}\left(\frac{1}{\bar{\sigma}_{11}^2} + \frac{1}{\bar{\sigma}_{22}^2} - \frac{1}{\bar{\sigma}_{33}^2}\right) \tag{4.7}$$

$$N = \frac{3}{2}\left(\frac{\tau_0}{\bar{\tau}_{12}}\right)^2 \tag{4.8}$$

The plastic behaviour of wood is directly given by the experimental curve $\sigma - \epsilon$ of compression perpendicular to the grain (Edlund, 1995). The law adopted in the numerical modelling depends of the compression strength and modulus of elasticity in the direction normal to the grain, $f_{\mathrm{c},90}$ and E_{90}, respectively (see Figure 4.1).

Table 4.1 shows the material properties adopted in the numerical model. The values adopted for the shear properties were obtained using the relations proposed by EN 338 (2003) while the others properties values were taken from the material characterization previously reported. Commonly, for wood, a value of 0.3 is assumed for the Poisson coefficient.

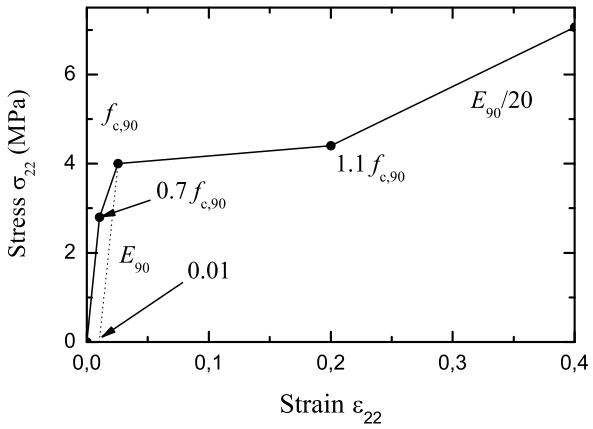


Figure 4.1: $\sigma - \epsilon$ law for compression ortogonal to the grain assumed in the model.

Table 4.1: Material properties adopted in the numerical model.

E_1 (MPa)	E_2 (MPa)	υ_{12}	G_{12} (MPa)	ρ (kg/m^3)	$f_{c,0}$ (MPa)	$f_{c,90}$ (MPa)	f_v (MPa)
7992	266	0.3	500	460	20	4	2.63

4.1.2 Geometric constraints, mesh and loading

Figure 4.2 shows the test set-up, including loading, boundary conditions and material axes. The tie beam of the joint assembly is constrained by eliminating all displacement at the base and left-side border. The rafter is in contact with the tie beam at the notch and has not been otherwise restrained. The loading reproduce exactly the experimental campaign: a first loading step, consisting of an axial compression at the free end of the rafter engaged the contact surfaces at the joint. Subsenquently, a transverse displacement was applied, with a constant movement rate, at the appropriate height on the rafter (see Figure 4.2). It is noted that the self-weight of the wood elements is considered in the analyses.

The adopted finite element mesh used quadrilateral plane 8-node elements (named by the software package as CPS8R) considering a strain thickness of 80 mm (Figure 4.3a). The key element of the finite element model (FEM) used is the interaction between the two wood elements (rafter-tie beam). The overall response of the joint is highly dependent of the behaviour adopted for the interaction. The interaction was modelled assuming a surface-to-surface contact. For that, the notch surface of the tie beam was considered as mas-

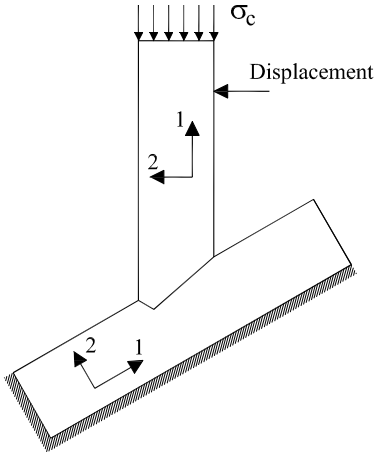


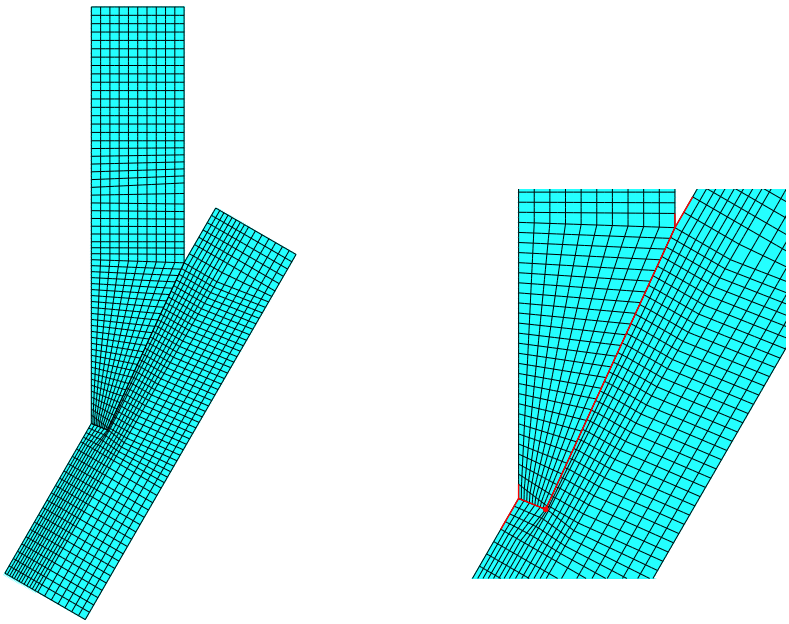
Figure 4.2: Boundary conditions and material axes adopted.

ter surface and the notch surface of the rafter as the slave. For the sliding formulation, *finite sliding* formulation (Oden and Pires, 1983), based on the node-to-surface discretization method was taken on. Due to the rotational movement applied to the connections, the contact surfaces must be extended to outside the limits of the original contact surface (see Figure 4.3b). Friction, along with tangential constraints or relative displacements between contact surfaces, was implemented with reference to Coulomb's friction model after an appropriate choice of friction coefficients. By default, a value of 0.2 was used for the friction developed in the interaction however, a sensitivity study, which the results are presented in next sections, was performed to evaluate the influence of this parameter in the joint behaviour.

4.2 Numerical *versus* experimental results

A first set of numerical analysis was performed on FEM of the specimens used in the experimental work. Tests results were used to calibrated the numerical models for 30° and 60° skew angles. Results are expressed in terms of force-displacement curves, evaluated at the same location and under the same load history as the tests. Figures 4.4 and 4.5 compares behaviour curves obtained with the numerical model calibrated for the case of 30° and 60° skew angles and for both compression level in the rafter (σ_c=1.4MPa and σ_c=2.5MPa) with the tests results.

In general, the numerical analysis seems to supply satisfactory information about the joint behaviour. Despite some difference, numerical models show to be adequately fitted to the experimental results. The accuracy of the models increase significantly under negative rotation. In this situation, the mechanism of reaction is soon concentrated in a highly compressed zone. The joint

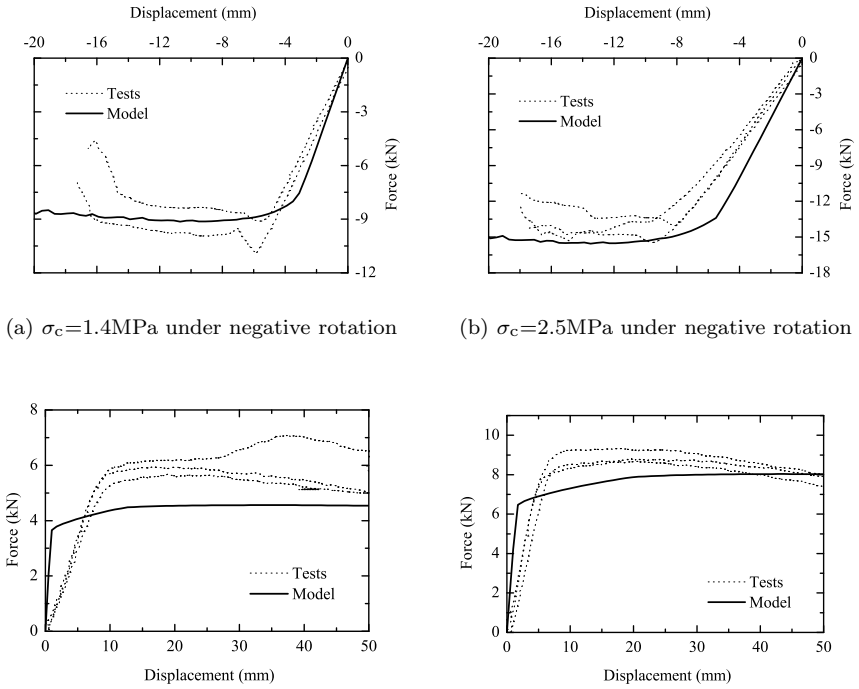


(a) Mesh (b) Contact surfaces

Figure 4.3: Finite element mesh adopted and definition of the contact surfaces.

behaviour depends of friction, as described below. Friction acts in the front notch surface, with a real contribution to the reaction mechanism and in the larger surface of the notch, with involvement in the transmission mechanism of the axial load only. In negative direction, the model is not capable to reach the same yield point, in particular, in terms of force, however, the post-elastic behaviour showed by numerical results is more stable. The elastic stiffness of the negative rotation show a good agreement considering the heterogeneity obtained in the tests performed, in particular, under 2.5MPa compression level of the rafter.

The numeric model show to be less effective comparing to the tests results obtained for positive rotation. Nevertheless, it is important to point out that the tests results for both skew angles values analysed presented significant variations when submmitted to positive rotation. As expected, the results from the numerical model for positive rotation show a higher stiffness than the experimental results due to the regularity in the representation of the facing surfaces, which contrasts the reality of hand-sawn indentations. The reaction mechanism is located in a decreasing portion of the front notch surface. The rotation progressly separated the surfaces in the front notch and the connection rapidly moves toward its ultimate behaviour mode. Ultimately, only a small contact area remains at the slant. The joint behaviour under positive rotation is



(a) σ_c=1.4MPa under negative rotation

(b) σ_c=2.5MPa under negative rotation

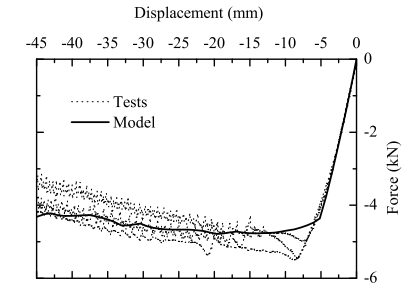
(c) σ_c = 1.4MPa under positive rotation

(d) σ_c = 2.5MPa under positive rotation

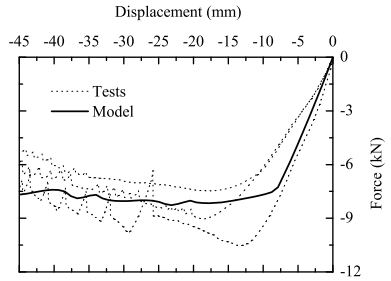
Figure 4.4: Comparison between experimental and numerical force-displacement curves (30° skew angle).

highly dependent of the notch geometry. A perfect definition of the geometry of the notch, controlled by the cutting process, is needed. During the calibration process of the numerical model, it was found that the necessary quality in the geometry definition was not ensured by the carpentry which supplied the specimens. In fact, to fit the numerical model to the experimental results in the case of 60° skew angle connections, a deviation of 3 mm was assumed for front notch surface cutting process (see Figure 4.6).

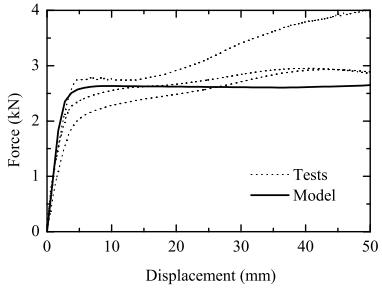
The carpentry which supplied the specimens do not have CAD-CAM systems and all cutting process, although been performed by machines, is human controlled. A deviation of 3 mm can represent the thickness of the cutting disk itself. This small deviation, which can easly happen if high quality standards are not implemented in carpentry during the cutting fase, represents a significant decrease in the rotational capacity of the connections (see Figure 4.6). The resistance capacity is affected due to the resistant mechanism change. In particular under positive rotation, the center point of the rotation moves from the upper edge of the front notch surface to the lower one (see Figure 4.7).



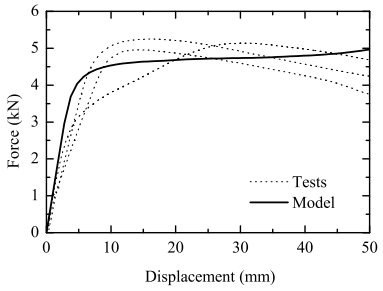
(a) σ_c=1.4MPa under negative rotation



(b) σ_c=2.5MPa under negative rotation



(c) σ_c = 1.4MPa under positive rotation



(d) σ_c = 2.5MPa under positive rotation

Figure 4.5: Comparison between experimental and numerical force-displacement curves (60^o skew angle).

4.3 Sensitivity study

Experimental results are not always possible to obtained as tests are expensive and time consuming. Therefore, numerical simulations are normally used to extend the study to others parameters as material properties, geometry, load, etc. Parametric studies can be easily carried out and the sensitivity of the response can be assessed with significant benefits for the understanding of the structural response. The results of the sensitivity study carried out are reported in the following sections.

4.3.1 Friction coefficient

Many factors influence the coefficient of friction, μ, between timber surfaces: the degree of roughness due to polishing or lack of it, the fiber directions, age, temperature and moisture content (McKenzie and Karpovic, 1968). Therefore, its value may differ during the time use of the structure. Despite its importance in some particular applications, like the case under investigation, friction as not been adequatly studied. The friction coefficient is not a well determine value,

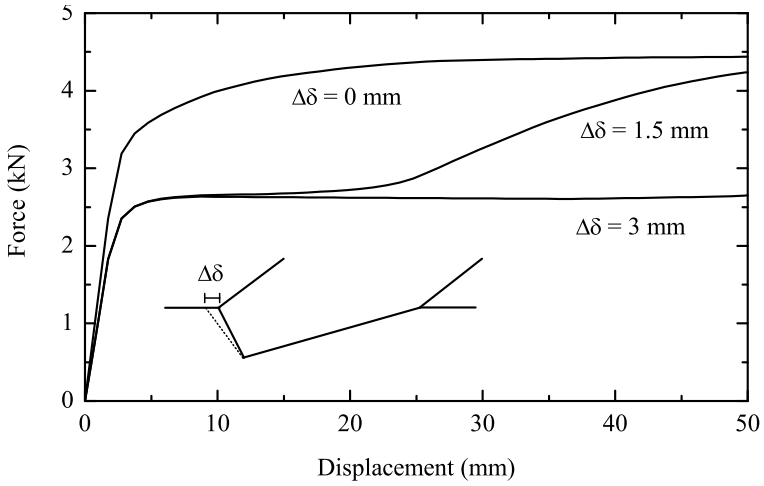
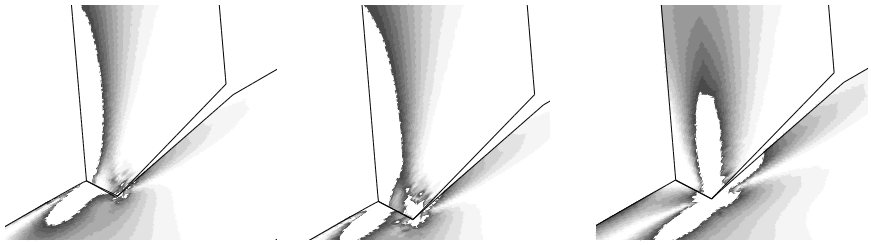


Figure 4.6: Front notch geometric deviation effect in the force-displacement numerical curve for 60º skew angle under positive rotation.

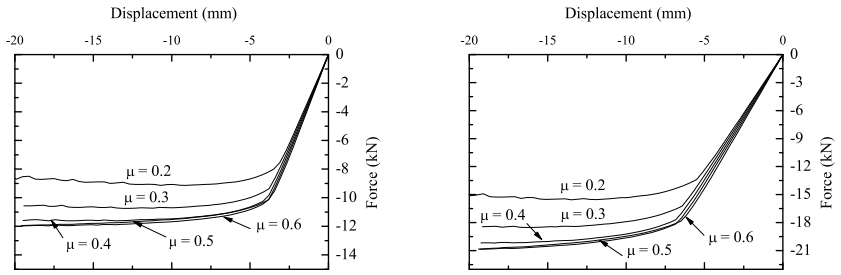


(a) $\Delta\delta = 0$ mm (b) $\Delta\delta = 1.5$ mm (c) $\Delta\delta = 3$ mm

Figure 4.7: Front notch geometric deviation effect in the resistant mechanism for 60º skew angle under positive rotation.

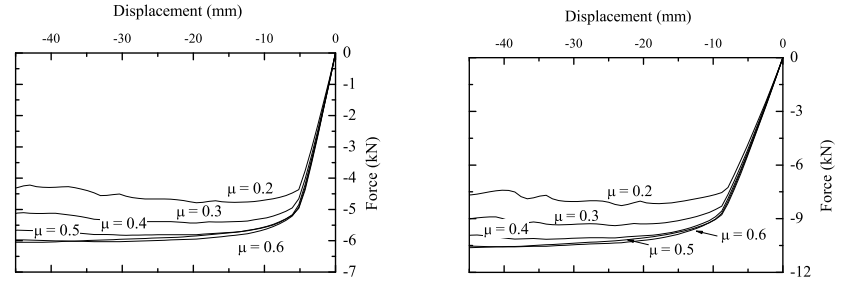
and it is normal to assume a possible range of values. For the case of the traditional timber connections, made from new timber elements, a reference value of $\mu = 0.2$ has been used in all numerical analysis. However, an upper limit of 0.60 may be reasonable when a partial penetration of compressed fibers occurs (Parisi and Piazza, 2000). Intermediate values have also been analysed, resulting in the force-displacement curves shown in Figures 4.8 and 4.9.

The results show that the conenctions analysed are not affected by the friction coefficient, present in the interface between both connected surfaces, under positive rotation. However, and, as indicative of the frictional mechanism of the connection in this direction, friction as significant effect on the response of the connections when submmited to positive rotation. Numerical results shows that stiffness as slight dependency of friction but the resistant capacity



(a) σ_c=1.4MPa (b) σ_c=2.5MPa

Figure 4.8: Friction coefficient effects on the numerical force-displacement curves under negative rotation (30º skew angle).



(a) σ_c=1.4MPa (b) σ_c=2.5MPa

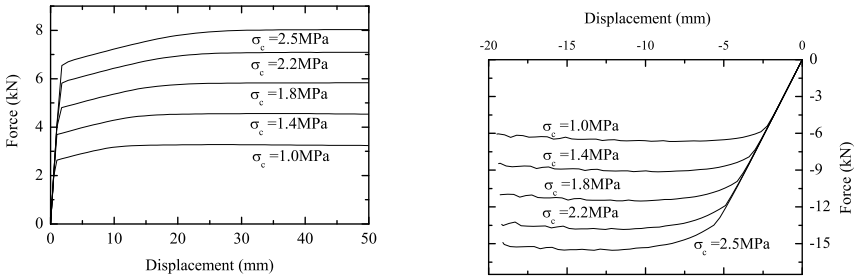
Figure 4.9: Friction coefficient effects on the numerical force-displacement curves under negative rotation (60º skew angle).

is considerably affected by the friction coefficient. This influence decreases over a friction coefficient of 0.5.

4.3.2 Compression level on the rafter

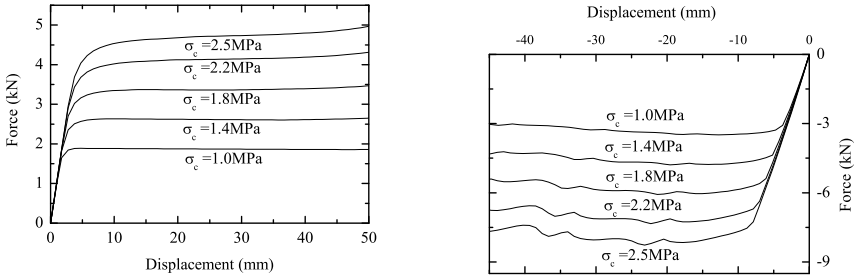
The response of traditional timber joints is directly dependent of the rafter compression level. In fact, one characterising aspect of the friction connections under study is that the yield point, the post elastic behaviour and the ultimate resistance are directly related to the level of compression in the rafter. This influence has particular significance when variations of the axial forces of truss elements may occur, induced by asymmetric loads, as snow and wind, and seismic forces. It is then important to study the effect of the axial compression level of the rafter in the response of the connections analysed. Figures 4.10 and 4.11 shows the numerical results obtained for the case of 30º and 60º skew angle unstrengthened connections for both rotation directions and, for the different compression level on the rafter adopted.

As expected, the axial compression level on the rafter as direct effect in



(a) Positive rotation (b) Negative rotation

Figure 4.10: Effect of the rafter's compression level on the numerical force-displacement curves (30° skew angle).



(a) Positive rotation (b) Negative rotation

Figure 4.11: Effect of the rafter's compression level on the numerical force-displacement curves (60° skew angle).

the joint behaviour under analysis. The numerical results obtained showed to have linear dependency of that parameter in term of resistant capacity while no variations was detected on the stiffness properties.

4.3.3 Skew angle

The tests results on full-scale connections presented previously, in agreement with Candelpergher (1999) and Palma and Cruz (2007), show that the structural behaviour of the unstrenghened traditional timber connections is function of the connections's skew angle. In the previous geometric surveys undertaken in Portugal and Italy, the range of 20° - 65° has been identified as possible values for the skew angle presented by traditional connections of timber structures of both countries. In the experimental campaign performed, the values of 30° and 60° skew angle were studied as consequence of their frequency. The decision to duplicate the study on the behaviour of unstrengthened conenctions

and the effectiveness of different strengthening techniques, taking into account two skew angle values, despite been recognize its crucial importance, represents a significant augment in the costs (time and financial) associate to the research performed. Therefore, and, because its effect is of great importance in the connections behaviour, the numeric analysis was extended to the case of a 45º skew angle. For the geometry definition, the same assumptions made for the others two skew angle (α) were kept. The depth of the notch is 45 mm and the angle on the front notch surface obey the practical rule ($\alpha/2$). Figure 4.12 shows the geometry assumed for the connections with 45º skew angle.

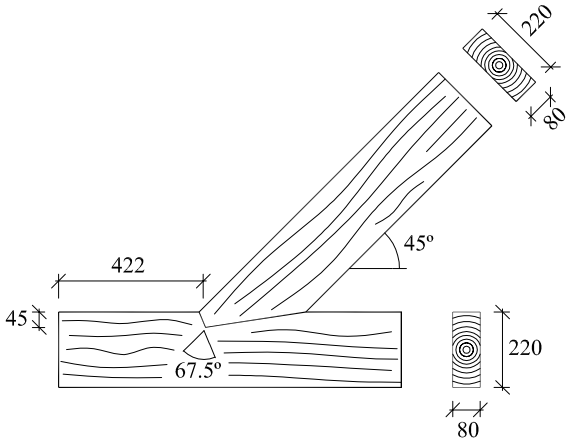
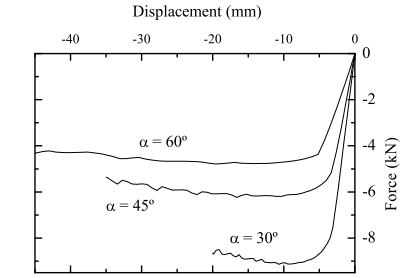


Figure 4.12: Geometry of the 45º skew angle connection (mm).

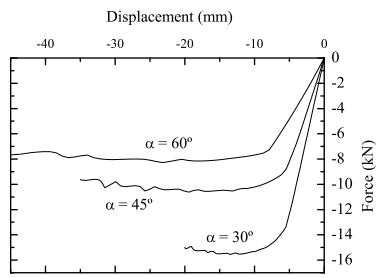
Figure 4.13 point out the effects of the skew angle in the connections behaviour. With the skew angle, the rotational resistant capacity of the connections decreases. In fact, the lower values for the force-displacement curves are obtained in the case of 60º skew angle case. The variation cannot be quantified by a linear law, as Figure 4.13 proves, but, the behaviour of the 45º skew angle connection is intermediate to the 30º and 60º skew angle cases, being supperior and inferior limits, respectively. The elastic stiffness is affected by the skew angle value, in particular for negative rotation and increases with the axial compression level of the rafter. The post-elastic stiffness is less sensitive to the skew angle. However, it seems that increasing the skew angle of the connections the ductility of the connections is improved. For negative rotation, the most important effect of the skew angle is the ultimate displacement achieved. Higher the skew angle upper is the displacement achieved by the numerical model

4.3.4 Notch depth

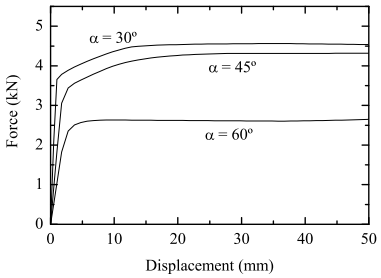
One of the most common font of variability identified during the geometric surveys is the notch depth of traditional timber connections. Even in the same



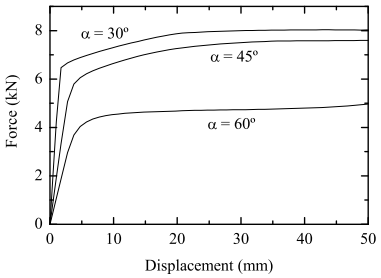
(a) σ_c=1.4MPa under negative rotation



(b) σ_c=2.5MPa under negative rotation



(c) σ_c = 1.4MPa under positive rotation



(d) σ_c = 2.5MPa under positive rotation

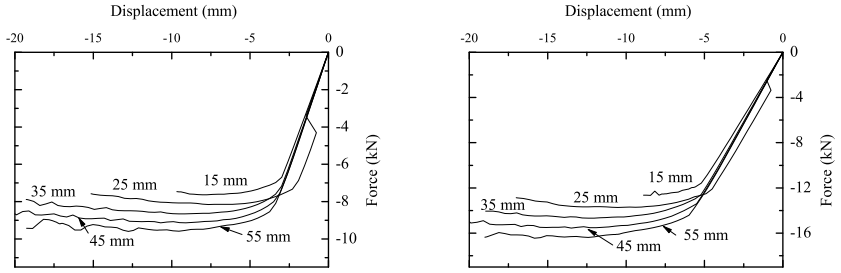
Figure 4.13: Effect of the skew angle on the numerical force-displacement curves.

structure, it is normal to find different notch depth values for the different connections. In the best examples, the notch depth is function of the loads transmitted through the connection. However, this simple rule is not verified in all structures surveyed. Despite is importance in the rotational capacity of the connections, this geometric parameter is of crucial significance for the shear resistance of the joint.

With the aim to assess its importance in the rotational behaviour, different values of the notch depth were adopted during the numeric simulations. Besides the depth value used in the experimental campaign, value found with the aim to prevent possible shear failures, the values of 15 mm, 25 mm, 35 mm and 55 mm were analysed. Figures 4.14 and 4.15 shows the numerical force-displacement curves obtained. Firstly, the effect of the notch depth is asymmetric. While for negative rotation the notch depth shows influence in the case of 30º skew angle connection, in the other direction, a slight effect is reported. Only a variation of the yield point is showed by the numeric results for positive rotation. For this skew angle value and negative direction, the rotational capacity and the ultimate displacement augments with the notch depth while no significant variation is detected in the stiffness. This behaviour and dependency is confirmed by tests results on full-scale connections presenting a

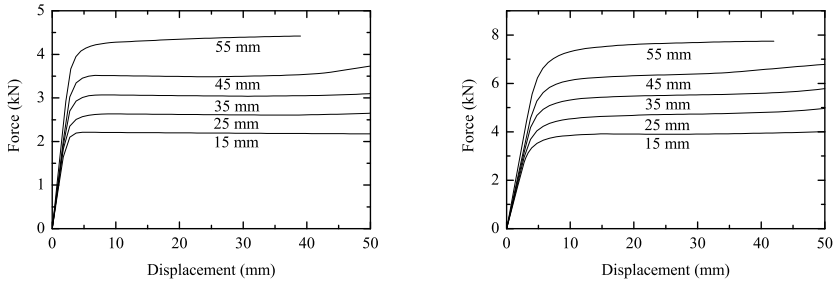
notch depth of 35 mm and 45 mm (see Palma and Cruz (2007)).

For the 60º skew angle connections, the effect of the notch depth is similar but, for opposite rotation directions. This diference is due to the deviation (3 mm) considered in the front notch surface cutting process. In consequence, the importance of the notch surface in the resistant mechanism under negativce rotation decreases. By contrary, as the rotation point is located in the lower notch edge, under positive rotation, the increase of the notch depth represents and augment of the resistant mechanism (lever arm). For that reason, the influence of the notch depth in this particular case, is similar to the effect of the axial compression level on the rafter. This observation is interesting and have particular practical interested based on the fact that the small geometry deviation assumed, is valid.



(a) σ_c=1.4MPa under negative rotation (b) σ_c=2.5MPa under negative rotation

Figure 4.14: Effect of the notch depth on the numerical force-displacement curves (30º skew angle).

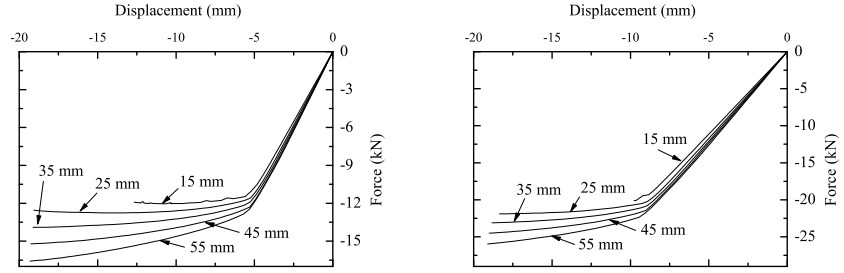


(a) σ_c = 1.4MPa under positive rotation (b) σ_c = 2.5MPa under positive rotation

Figure 4.15: Effect of the notch depth on the numerical force-displacement curves (60º skew angle).

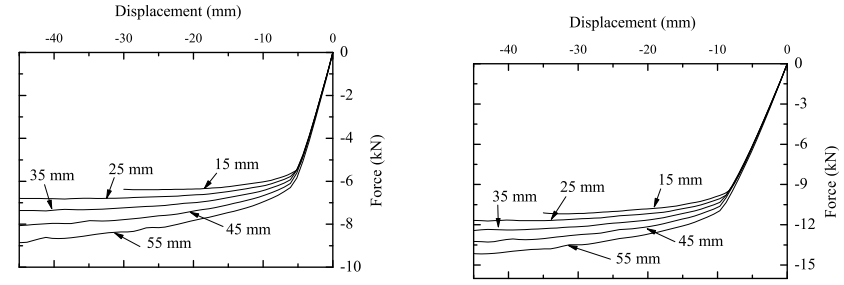
4.3.5 Angle of the notch

One significant font of uncertainities in the definition of traditional timber connections is the geometry of the notch. Besides the notch depth, the angle of the front notch surface is also of great importance. In the ideal geometry, the front notch surface have an angle of $\alpha/2$, with α equal the skew angle of the connection. However, this rule is not always followed. For practical reasons, in terms of aiding the cuttings, sometimes necessary to operate in place, it is usual to found front notch surfaces ortogonals to the longitudinal axes of the tie beam. This possibility was analysed through the numerical analysis.



(a) σ_c=1.4MPa (b) σ_c=2.5MPa

Figure 4.16: Effect of the notch angle on the numerical force-displacement curves under negative rotation (30º skew angle).



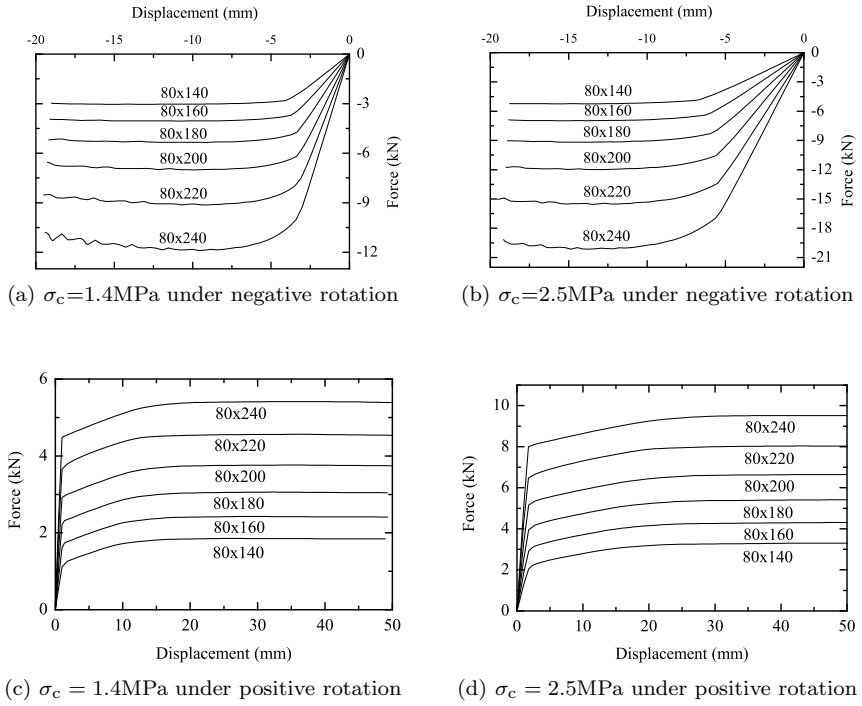
(a) σ_c=1.4MPa (b) σ_c=2.5MPa

Figure 4.17: Effect of the notch angle on the numerical force-displacement curves under negative rotation (60º skew angle).

4.3.6 Height of the rafter

The extensive experimental campaign performed, considering two values for the skew angle, and the parametric studies accomplished throught the numeric analysis, allows to extend the application of the research carried out to almost all possible step joints geometries. In a timber truss structure, besides the

different skew angle existing, the cross sections of the connected elements can presented significant deviations. Normally, the width is constant but the struts, for example, are slender than the tie beam and the rafter. Therefore, it is important to assess the influence of the rafter dimensions, in particular, its height, in the structural response of the connections that have been studied. Because the full-scale specimens tested presented all the same cross section for the rafter and tie beam, this sensitivity study was achieved using finite element simulations. According to the results of the numerical analysis, Figures 4.18 and 4.19, and in agreement with Parisi and Piazza (2000), the rafter cross section, in this case, the rafter height, is a primary factor in the connection strength and deformability. For the same axial compression stress on the rafter, the total axial force in the joints increases with the rafter height.



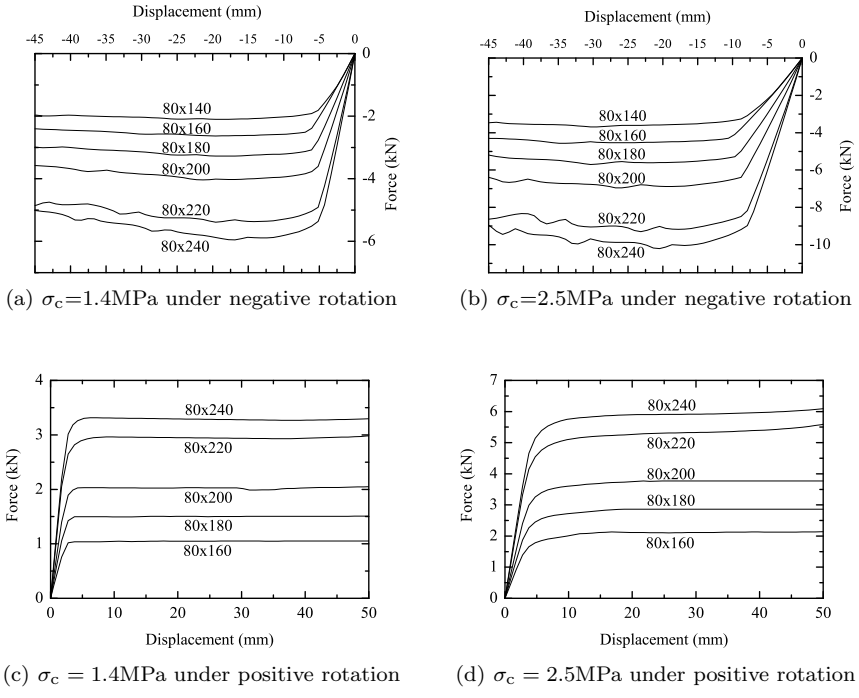
(a) σ_c=1.4MPa under negative rotation (b) σ_c=2.5MPa under negative rotation

(c) σ_c = 1.4MPa under positive rotation (d) σ_c = 2.5MPa under positive rotation

Figure 4.18: Effect of the rafter height's on the numerical force-displacement curves (30^o skew angle).

4.4 Effects of the wood specie

Maritime pine (*Pinus pinaster*, Ait) is the most common wood species in the Portuguese timber structures. However, others species, in particular, Eucalyptus (*Eucalyptus globulus*, Labill.) and Chestnut (*Castanea sativa*, Mill.) can



(a) σ_c=1.4MPa under negative rotation

(b) σ_c=2.5MPa under negative rotation

(c) σ_c = 1.4MPa under positive rotation

(d) σ_c = 2.5MPa under positive rotation

Figure 4.19: Effect of the rafter height's on the numerical force-displacement curves (60º skew angle).

be found. For the extensive experimental campaign performed, the Maritime pine wood was used and the material properties are expected to have minor influence in the structural response of the joint analysed. The material properties used in the finite element model for the maritime pine were obtained from the material characterization tests performed. With the aim to analysed the two others wood species (Eucalyptus and Chestnut) material properties found in UNE 56546 (2007) and Feio (2005), respectively, was assumed. Table 4.2 shows the material properties adopted in the numerical model for this sensitivity study.

As expected, the wood species, or, by others words, the class resistance, has a minor influence in the joint response (see Figure 4.20). This influence increases with the compression stress level in the rafter and for negative rotation. A small variation on the elastic stiffnes was achieved on the numerical results for the different wood species considered. Only the yield point, transition between the elastic and post-elastic phases, seems to be dependent of the wood species. Because both wood species analysed in the parametric study are from higher strength classes, an slight increase in the mechanical performance of the joint is obtained, comparing with the numerical results achieved with Maritime Pine wood. As conclusion, the wood species has shown minor effect

Table 4.2: Material properties adopted in the numerical model.

Wood	E_1 (MPa)	E_2 (MPa)	υ_{12}	G_{12} (MPa)	ρ (kg/m^3)
Maritime Pine	7992	266	0.3	500	460
Eucalyptus	9400	750	0.3	700	672
Chestnut	8800	800	0.3	530	516
	$f_{c,0}$ (MPa)	$f_{c,90}$ (MPa)	f_v (MPa)		
Maritime Pine	20	4	2.63		
Eucalyptus	26	8.8	3.8		
Chestnut	47.6	7.74	3.8		

on the inquired behaviour because the variations reported are equivalent to those in the material properties.

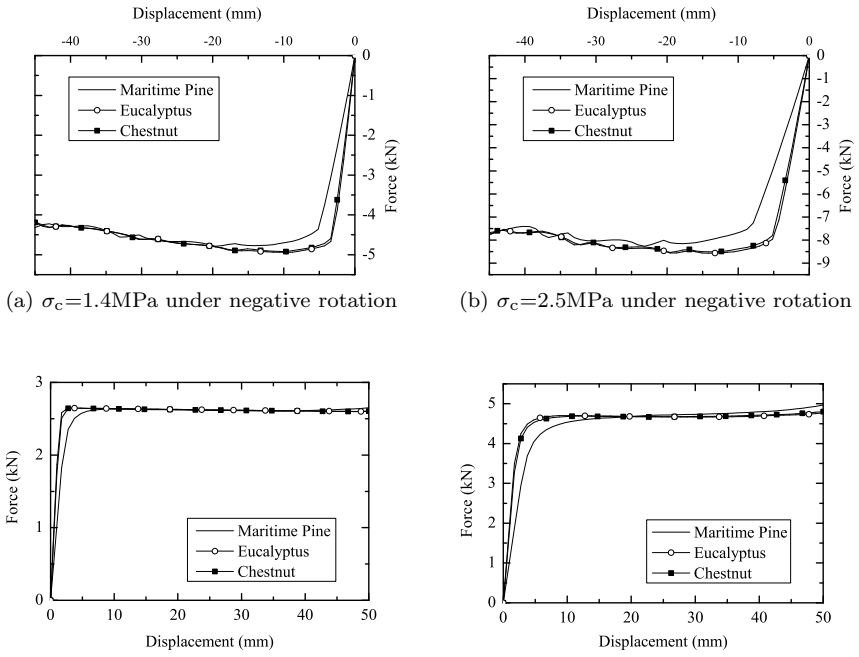
4.5 Conclusions

Numerical analysis have confirmed the tests results: traditional timber connections have a not symmetric semi-rigid friction based behaviour. The rotational response and capacity is function of the joint geometry and parameters as friction and axial compression level of the rafter are of primary importance. The sensitivity study have shown that different parameters have distinct influence in the connections behaviour and, this influence depends, not only of the rotational direction, but also, of the skew angle. However, it is important to point out that deformation properties (stiffness) are less depending of the parameters analyzed. During the analysis of the numerical resuls achieved the main conclusion have been point out, which can be summarized:

- the friction coefficient has influence in the connection response only under negative rotation. The stiffness as slight dependency while the resistance can be significantly affected. This influence decreases over a friction value of 0.5;

- the axial compression stress of the rafter has primary importance in the connection behaviour. The connections stiffness is not affected but a higher axial compression stress of the rafters corresponds to a high resistance. The influence seems to be linear and is not affected by the rotational direction;

- connection behaviour is function of the skew angle. The rotational capacity and stiffness of the connection decreases with the skew angle. This dependency is not linear and, in the particular case of connections re-



(a) σ_c=1.4MPa under negative rotation (b) σ_c=2.5MPa under negative rotation

(c) σ_c = 1.4MPa under positive rotation (d) σ_c = 2.5MPa under positive rotation

Figure 4.20: Material properties effects on the numerical force-displacement curves (60º skew angle).

sponse under negative rotation, the skew angle increase results in a more fragil behaviour;

- in a correct joint geometry definition, the notch depth as influence only in the response under negative rotation. If the connection geometry has a bad definition, as example, a slight deviation of 3 mm is consider in the cutting process of the notch, the influence of the notch depth moves to the positive rotation. In both cases, the notch depth has influence only in the resistant capacity;

- the geometry of the rafter, in particular, the heigth of rafter cross-section, as a significant influence in the connection behaviour. Higher cross-section correponds to resistance and stiffness rising, however, stiffness shows to be less affected under positive rotation;

- wood species shows to have a minor influence in the connection behaviour.

Chapter 5

Semi-rigid modelling of traditional timber connections

5.1 Introduction

The behaviour of timber structures is generally controlled by the properties of the connections within the structure especially, when loaded under non-symmetric conditions and by extreme events. In these situations, the connections are loaded well beyond their pseudo-elastic limit (Collins and Kasal, 2001). In order to better predict and understand the behaviour of timber structures, analytical models of connections are crucial. Numerous models of connections exist, both phenomenological and mechanics based. However, little attention has been devoted to traditional timber joints. Despite been historically considered to have a good seismic performance, few studies have covered the response of traditional timber construction and, in particular, the behaviour of their connections. The development of behavioural models for traditonal timber joints, to be used for the investigation of structural dynamic response is needed (Parisi and Piazza, 1998). This researh necessity is not claimed only by Earthquake Engineering. In the case of existing structures to be rehabilitated, a realistic interpretation of the global structural behaviour is a primary need. In some typical structural configurations of timber constructions, the commonly used hinge models are inadequate; because in real structures, where joints have moment resisting capability, the equilibrium conditions may not be reached analytically. The semi-rigid modelling of timber connections, using nonlinear moment-rotation laws and hysteretic rules, intends to represent the behaviour of timber structures with a comparable level of detail for all the structural components. In particular, with these models, the seismic design acknowledges and exploits the dissipation capabilities of their hysteretic behaviour.

5.2 Models behaviour of semi-rigid traditional timber connections

Different hysteretic models for timber structures have been developed. Kivell et al. (1981) derived a hysteretic model for moment resisting nailed timber joints. Sakamoto and Ohashi (1986), Stewart (1987) and Dolan (1989) each developed hysteretic models to describe the cyclic behaviour of timber frame walls with nailed connections between the framing and the sheathing. Ceccotti and Vignoli (1990) modelled the pinching hysteretic for moment resisting semi-rigid timber joints made from glulam and drift pins. Prion and Foschi (1994) proposed a hysteresis model for dowel type fasteners.

There is a wide variety of available hysteresis models in general structural dynamics literature. Together with those that have been proposed for timber joints and structural systems, there seems to be no shortage of hysteretic models that can be used in dynamic analysis of timber structures. However, the same is not valid for historical timber constructions. Monotonic tests with the aim to assess the rotational properties of traditional timber connections, are available (Shanks and Walker (2005), Shang (2005) and Palma and Cruz (2007)) but, cyclic tests are rare. Drdácký et al. (1994) performed cyclic tests on full-scale specimens made of timber with several hundred years and on authentic historical joints taken from a reconstructed structure. Based on the tests results, a component method for historical timber joints was developed. Parisi and Piazza (1999) interpreted and modelled the experimental cyclic behaviour of a full-scale traditional timber connection strenghtened with one bolt. Moreover, the correponding finite element implementation has supplied a nonlinear rotational spring element, by which some timber roof examples have been studied under seismic excitation (see Fumanelli (2001)). In this chapter, the tests performed on original and strenghened traditional timber connections are numerically modelled using a nonlinear spring element available in a commercial Finit Element Method package.

5.3 Numerical modelling

5.3.1 Definition of the model parameters

When modelling experimental test results with a synthetic law, different levels of approximation may be adopted for the first loading curve and for the cyclic case. The former describes completely the joint behaviour for structures under monotonic loading. The adoption of a hyperbola permits to describe quite precisely the transition between the elastic and the post-elastic branches, but a bilinear approximation may also be generally satisfactory. In order to define it, the characteristic intersection points between branches must be derived from the experimental moment-rotation curves, $M-\phi$. To this purpose, the following parameters have special importance (see Figure 5.1):

- the initial tangent stiffness, k_0^+ (positive means rotation forcing the skew

angle to increase) or k_0^- (and negative means rotation forcing the skew angle to decrease);

- the maximum moment and maximum rotation at first loading, determined on the curve of monotonic behaviour, $M - \phi$, for positive or for negative rotation $(M_u^+, M_u^-, \phi_u^+, \phi_u^-)$;

- the moment and rotation values corresponding to the yielding (transition between the elastic and post-elastic behaviour), M_y^+, M_y^-, ϕ_y^+, ϕ_y^-; Indications for assessing their values and those of the parameters in the following when the post-elastic behaviour field can be easily identified or when the mechanical behaviour of the joint exhibits a continuous change of curvature are given in EN 12512 (2001). However, using these methods, the synthetic law can present different amounts of energy dissipation when comparing with the experimental curves. In this work, the method applied supports the bilinear approximation which minimize the difference to the energy dissipated during the tests;

- the elastic stiffness, k_e^+ or k_e^-, given by the elastic branch (first segment) of the bilinear curve;

- the post-elastic stiffness, k_p^+ or k_p^-, given by the post-elastic branch of the bilinear curve.

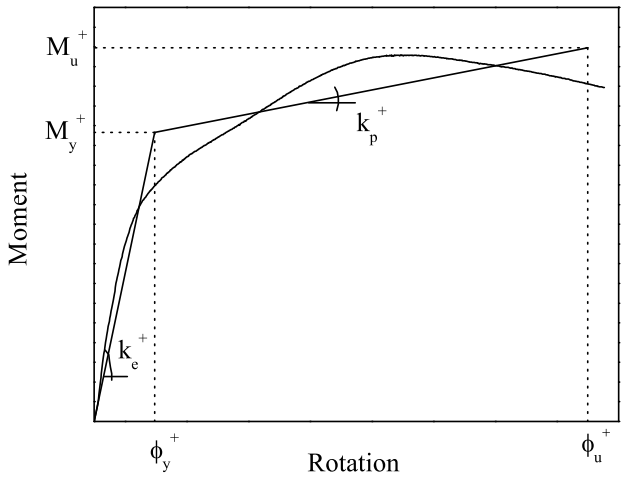


Figure 5.1: Model parameters of the experimental $M - \phi$ first loading curve (positive rotation).

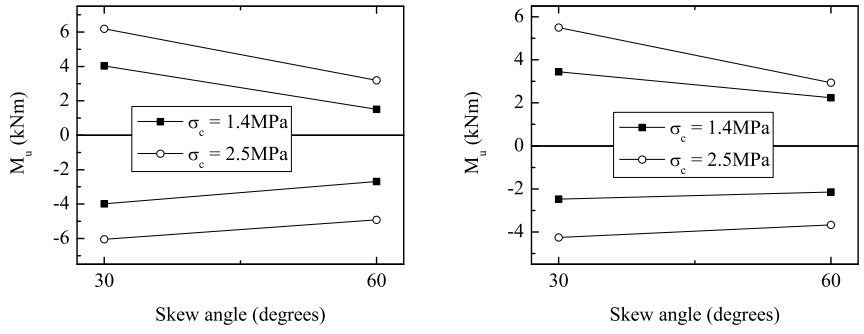
These first parameters are common to a monotonic and a cyclic model; the latter requires defining additional values, as follows:

- the secant stiffness at complete unloading, after an excursion in the non elastic field, k_u^+, for the positive, and k_u^-, for the negative quadrant;
- the average residual stiffness passing from the positive to the negative moment, or vice-versa, after an excursion in the non elastic field; it is generally reasonable to assume a single, average value, k_r, instead of the two values k_r^+ and k_r^-

.

5.3.2 Assessment and discussion of the model parameters

One characterising aspect of the friction connections under study is that the ultimate and yield moments, M_u and M_y, are directly related to the level of compression in the rafter (Figure 5.2). In seismic conditions, significant variations of axial forces in these elements may be expected to occur during the strong motion phase already at medium intensities. Consequently, the relationship between the axial compression level and the limit moments needs to be expressed and included in the synthetic model. The test results also shows that the connections skew angle influence is reflected in the first loading curve. Moreover, the numerical analysis results, see Chapter 4, allow to conclude that others geometric properties, as notch depth and rafter height's, have also influence in the first loading curve.



(a) Yielding Moment (b) Ultimate Moment

Figure 5.2: Yielding and ultimate moments dependency reported by tests results on unstrengthened connections.

The coordinates of the transition point (M_y^+, M_y^+/k_e^+) or ($M_y^-, M_y^-/k_e^-$) are dependent of the rotation direction, positive or negative, corresponding to opening and closing the skew angle, respectively. The most sensible parameter is the yield moment (M_y). Under positive rotation, the elastic stiffness is quite constant with exception of U6-2.5 tests. Disregarding this case, the ratio between the elastic stiffness in both rotation direction vary from 0.95 to 1.43. The post elastic stiffness is quite constant, and with exception of U6-1.4 tests the

negative value proves the limited ductility showed by the tests on unstrengthened connections performed. Figure 5.3 presents the comparison between the bilinear curves fitted to the experimental $M - \phi$ curves obtained in the tests of unstrenghened connections, for 30º and 60º skew angles and 1.4 MPa and 2.5 MPa axial compression stress of the rafter.

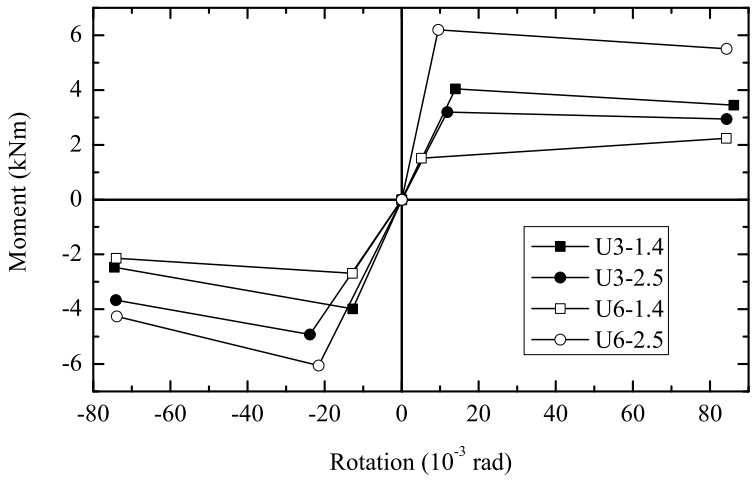


Figure 5.3: Comparison of the $M - \phi$ bilinear curves fitted to tests results on unstrengthened connections.

As reported in previous Chapter, strengthening modified drastically the behaviour of the connections and this variation is function, obviously, of the technique used. The strengthening technique influence depends of the skew angle and of the rotation direction. Despite the effect of the strengthening direction relatively to the contact surface was not studied during the experimental work, this parameter should have influence in the effectiveness of the strengthening technique. Otherwise, the results of the strengthened connections were not function of the connection skew angle. The test results shows that some stregnthening techniques results in a increase of the connection resistance, in particular, for the 30º skew angle connections. However, all strengthened connections tested presented a considerable improvement in the ductility. In fact, while the unstrengthened connections had negative values for the post-elastic stiffness (k_p), as consequence of their limited ductility, every strengthened connections presented positive values for that stiffness, with direct consequences in the enhancement of the ductility of those connections. Tables 5.1 and 5.2 summarizes the different parameters of the $M - \phi$ experimental curves obtained in the experimental work performed, for negative and positive rotation, respectively.

Table 5.1: Parameters of the $M-\phi$ experimental curves obtained for negative rotation.

α (°)	σ_c (MPa)	M_y^- (kNm)	M_u^- (10^{-3} rad)	ϕ_y^- (kNm)	ϕ_u^- (10^{-3} rad)	k_e^- (kN/m)	k_p^- (kN/m)
Unstrengthened							
30	1.4	3.99	12.71	2.47	74.56	313.55	-24.61
	2.5	6.05	21.57	4.26	73.88	283.20	-34.36
60	1.4	2.69	12.79	2.14	74.05	210.54	-8.90
	2.5	4.92	23.84	3.67	74.16	215.35	-25.15
Bolt							
30	1.4	4.68	19.23	7.34	73.92	224.84	46.42
60		2.58	21.49	2.99	73.78	119.87	7.93
Binding strip							
30	1.4	3.57	14.46	7.31	79.80	252.29	5.71
Tension Ties							
30	1.4	3.67	23.24	5.65	74.05	159.01	38.96
60		2.60	17.40	2.79	73.83	149.69	3.37
Stirrup							
30	1.4	7.18	11.85	11.07	74.24	611.17	61.11
60		3.60	29.85	4.17	73.74	123.62	12.95

5.3.3 Synthetic characterization

5.3.3.1 Monotonic tests

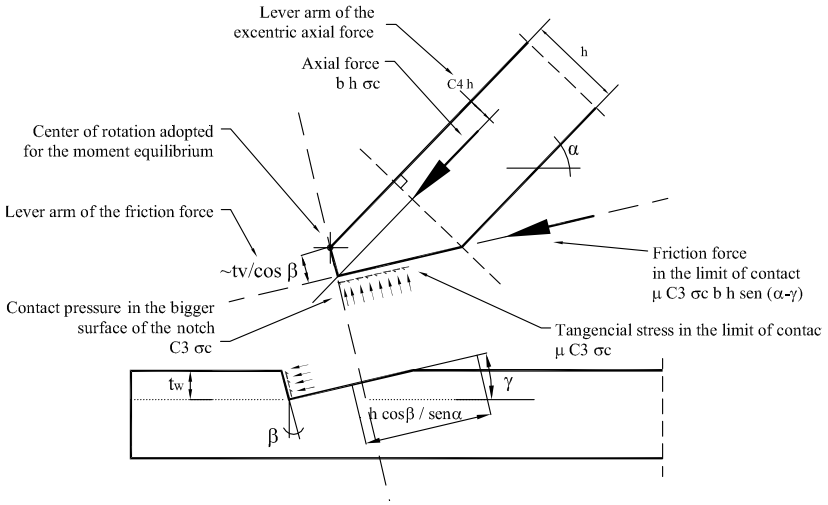
The extensive experimental campaign performed and the numerical analysis undertaken maked possible to calibrate some simple physical models (Candelpergher (1999) and Parisi and Piazza (2000)) helpfull in reinterpreting the load bearing mechanisms, as shown in the following. Moreover, they can be used to predict the behaviour of others connections, with different geometries and/or load conditions. The models are based on the hypothesis of a simplified joint behaviour. They allow the direct estimation of all parameters necessary to characterize the so-called *first-load curves*, i.e., the quasi-static response. The effectiveness of such models, however, is directly related to the correctness of the assumptions made on the connection behaviour. As a result, they lead to a very essential insight, highlighting the most relevant aspects and parameters: the elastic and post-elastic rotational stiffness remains basically constant, regardless of the axial compression, while the threshold corresponding to the transition from elastic to post-elastic response clearly depends upon axial compression in a nearly linear way. The Parisi and Piazza (2000) work complets the model proposed by Candelpergher (1999) adding the possibility to predict the ultimate moments values. Because the behaviour of the joint is asymmetric

Table 5.2: Parameters of the $M-\phi$ experimental curves obtained for positive rotation.

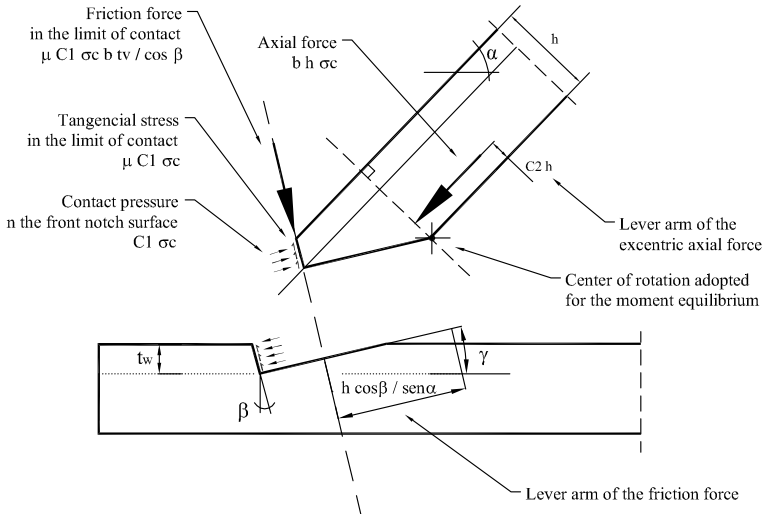
α (°)	σ_c (MPa)	M_y^+ (kNm)	M_u^+ (10^{-3} rad)	ϕ_y^+ (kNm)	ϕ_u^+ (10^{-3} rad)	k_e^+ (kN/m)	k_p^+ (kN/m)
Unstrengthened							
30	1.4	4.04	13.93	3.15	86.14	298.79	-8.15
	2.5	6.19	9.47	5.29	84.32	661.34	-9.29
60	1.4	1.51	5.13	2.24	84.18	301.03	9.11
	2.5	3.19	11.87	2.94	84.29	276.40	-3.76
Bolt							
30	1.4	7.34	13.91	9.46	79.91	536.80	32.43
60		3.65	15.00	5.11	83.32	249.20	21.02
Binding strip							
30	1.4	10.35	25.44	10.69	77.90	411.75	5.42
Tension Ties							
30	1.4	5.85	15.12	8.27	83.48	411.02	34.80
60		4.35	28.38	4.79	82.48	153.99	8.22
Stirrup							
30	1.4	8.44	16.31	12.41	79.21	529.97	62.85
60		4.72	25.89	5.98	82.50	183.14	22.62

with respect to rotation, two interpretative models, one for each direction, are needed. Figure 5.4 shows the load bearing mechanism assumed at the positive and negative elastic limit (where positive means rotation forcing the skew angle to increase).

In the case of positive rotation, it is assumed that the achievement of the limit conditions corresponds to the incipient development of a rigid rotation of the rafter about the left end of the notch in the tie beam. With respect to this point, rotational equilibrium is imposed. Such equilibrium is sought considering the ideal lower portion of the rafter, from the front side of the notch surfaces to the first full size rafter section, where the rotation center is also placed. The force that, due to friction, is developed along the larger surface of the notch contributes, in this simplified scheme, to the transmission of the axial load only. The contribution of friction to the rotational resistance is, in practice, fully ascribed to the front smaller surface of the notch: in this region a stress gradient can be observed. Numerical models provide full support to this interpretation and have been referenced in order to assess the values of coefficient C_1, which accounts for the rate of the total axial load passing through the concerned surface. The eccentricity of the axial load in the rafter is accounted when evaluating the contribution to the rotational resistance given by the axial force, through coefficient C_2 shown in Figure 5.4. Those two



(a) Positive rotation



(b) Negative rotation

Figure 5.4: Synthetic model of the resisting mechanism at elastic proportionality limit (Candelpergher, 1999).

coefficients have been suggested by Candelpergher (1999) and, based on the observations made during the experimental and numerical analysis, different values have been calibrated for the tests conditions adopted in this work (see Table 5.3).

Further contribution to the moment-rotation resistance of the joint eventually depends upon the presence of metal reinforcement. The steel element

Table 5.3: Coefficients C_1 and C_2.

Font	Skew angle	C_1	C_2
Candelpergher (1999)	30	0.70	0.40
	60	0.60	0.25
Tests	30	0.70	0.55
	60	0.70	0.45
Numerical analysis	30	0.70	0.55
	45	0.70	0.35
	60	0.70	0.45

is subjected to axial and bending stresses, which contribution to the resistant mechanism depends of the connections skew angle and of the rotation direction. Higher contribution of the steel element is achieved when its axial stresses are increase. The test results shows that, for all strengthening techniques the M_y^+ value is increase while, for the opposite rotation direction (M_y^-), only the technique based on stirrups and the bolt for the 30° skew angle connections the same improvement is obtained. In fact, even with a smaller value, the biggest is 10.5%, the others techniques under negative rotation has no signifficant effect in the M_y^- experimental value. The starting of the axial stresses in the metal reinforcement depends of how the joints is tie before the test. If the joint is tie enough, tension in metal element appears even for a small rotation. Otherwise, its contribution to the joint resistance can be evaluated as the corresponding elastic limit bending moment steel element taken alone, thus at first yield in the outer fibers. Then, only in the post-elastic phase and after significant joint rotations, the tension in the metal element becomes relevant. At that stage, the reinforcement prevents the complete disconnection by pressing the wood fibers. However, further analysis are needed to be possible to include these parameters in a simplify model. According to the mechanism assumed in Figure **??**, for the case of unstrengthened connections, it is then possible to derive the following expression for the negative moment value for the elastic proportionality limit:

$$M_y^- = N \left[C_1 \cdot \frac{t_v \cdot \mu}{\sin \alpha} + C_2 \cdot h \right] \tag{5.1}$$

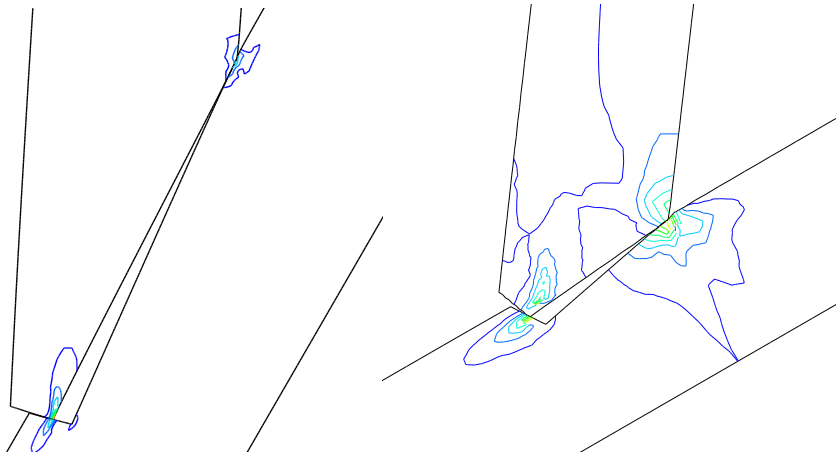
The binomial formulation of eqn 5.1 helps a clear understanding of the two contributions just mentioned. The linear dependence from axial load is moreover evident: its contribution to resistance is indeed formulated as the product of the rafter force N times an appropriate lever arm. Such lever arm, in particular, allows for:

- friction in the front notch (through coefficient C_1), and is therefore function of the friction coefficient μ, notch depth and skew angle;

- moment due eccentric axial load in the rafter (through coefficient C_2).

Estimating the rotational stiffness is then possible, once determined an appropriate value of limit moment using eqn 5.1, provided a corresponding value of the relative rotation between tie beam and rafter can be assessed. However, it is more appropriate to use experimental values when they exist.

Figure 5.5, traced from numerical results, shows the position of the two contact surfaces at the ultimate state (just prior to loss of equilibrium). Two small contact zones where the reaction develops are visible. One is at the lower surface of the notch and the other is at the right end of the notch side in the tie beam. Assuming that a reaction arises in both locations, the resultant must counterbalance the axial force N. The resultant will act with the same intensity and opposite in direction to N, but will act at some distance from the line of action of the axial force.



(a) 30° skew angle (b) 60° skew angle

Figure 5.5: Relative negative rotation of elements at ultimate state under 2.5 MPa axial compression of the rafter.

With reference to Figure 5.6, and considering a state of limit equilibrium before final sliding takes place, the line of action of the reaction R_1 at the slant base will be rotated with respect to the normal to the slant to an angle less than or equal to the friction angle, α_u. The reaction R_2 at the right notch edge in the tie beam will act again at an angle α_u to the normal to that surface. The resultant, will be parallel to N and will act on a line passing from the point of intersection of the former two reaction lines. The distance from this intersection to the line of action of N is the lever arm of the couple that offsets the resultant and the axial force, b_l. In an ultimate equilibrium state, this couple represents the ultimate moment that the connection may resist. With reference to Figure 5.6, $M_u^- = N \times b_l$, where b_l is the lever arm. The derivation

of an expression for b_l is presented by Parisi and Piazza (2000). For a given value of the connection angle α, the distance b_l depends on the inclination of the reaction lines and, consequently, is a function of the geometric parameters of the connection, i.e., rafter angle and height, notch angle and friction angle.

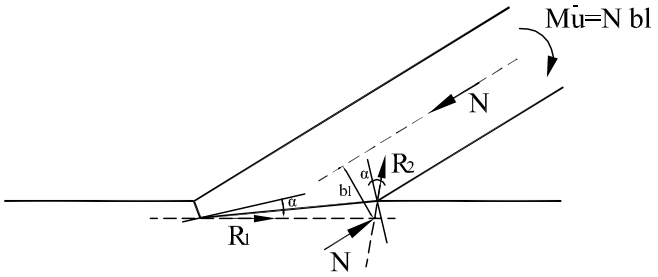


Figure 5.6: Ultimate equilibrium for negative rotation.

Under a positive rotation, increasing the skew angle, it is assumed that the centre of this rotation is located in the upper edge of the front notch. The front surface of the notch does not contribute to the resistant mechanism because the resultant friction force acts on a line passing to that point. However, this part of the notch (front) is important, transmitting the axial force N from the rafter to the tie beam. During the opening of the skew angle, the rear surfaces of the notches become separate and the stress concentration in the notch front increase significantly. Therefore, it is important to divide the friction effects: the friction that contributes to the resistant mechanism corresponds to the bigger notch surface. The numeric analysis has showed a progress unloading of the notch surface with the rotation enlargement. The proposed model takes this observation in care through coefficient C_3: the contact stresses are uniformly distributed along the bigger surface of the notch with a value depending of the rafter compression pondered through C_3. Contrarily to negative rotation, the main resistant mechanism results from the eccentric axial force of the rafter. The eccentricity of the axial force resultant is more significant as consequence of the rear notch surfaces separation that leads to a stress concentration into the front notch. This eccentricity is measured through coefficient C_4 showed in Figure 5.4a. Based on those assumptions, the positive moment value for the elastic proportionality limit can be expressed as:

$$M_y^+ = N\left[C_3 \cdot t_v \cdot \mu \frac{\sin\alpha - \gamma}{\cos\beta} + C_4 \cdot h\right] \tag{5.2}$$

The equation is similar to the one derived for the negative rotation case. In fact, there is a constant term due to the steel reinforcement and, the linear dependency of the axial force is evident. The imaginary arm based on which the resistant mechanism proportional to the rafter's axial force is quantified, is again used to measure friction term and the axial force eccentricity in the notch

front. The difference is that, now, as consequence of the friction be located in the bigger surface of the notch, is depending of the slope γ (eqn 5.3).

$$\gamma = \tan^{-1}\left[\frac{t_v}{\frac{h}{\sin\alpha} - t_v \tan\beta}\right] \tag{5.3}$$

Table 5.4 shows the C_3 and C_4 coefficients suggested by Candelpergher (1999) and the ones calibrated based on the observations made during the experimental (Chapter 3) and numerical analysis (Chapter 4).

Table 5.4: Coefficients C_3 and C_4.

Font	Skew angle	C_3	C_4
Candelpergher (1999)	30	0.10	0.15
	60	0.40	0.20
Tests	30	0.30	0.70
	60	0.30	0.30
Numerical Analysis	30	0.15	0.50
	45	0.30	0.40
	60	0.15	0.30

In comparison with the negative rotation cases, the resultant of the axial force in the rafter, measured through coefficient C_4, presents higher values for the eccentricity and the front notch behaviour become more important, as indicated by coefficient C_3. This last coefficient gives the real distribution of the contact stresses along the bigger notch surface, measuring the portion of the axial force is transferred by friction from the rafter to the tie beam: is then possible to conclude that most of the axial force is transmitted by the front notch and only 30% use the bigger notch surface. When a positive rotation opens the skew angle, the notchs surfaces at the inner side of the joint separate, while compression in the rafter still keeps a decreasing portion of the head zone surfaces in contact (Figure 5.7). A reaction parallel to the axial force in the rafter, N, may be developed, because friction allows a force component parallel to the slant. This component points downward, as required for equilibrium. A corresponding downward displacement occurs during testing once friction is overcome. Further rotation progressively separates the surfaces in the head zone and the connection rapidly moves toward its ultimate behaviour mode.

Ultimately, only a small contact area remains at the upper extreme of the slant. In this process, the reaction that equilibrates the axial force in the rafter moves upward, increasing the lever arm. The upper limit is obtained if this reaction, which must be colinear with the axial force, is assumed at the upper extreme (Figure 5.8), with a lever arm of half the height of the rafter. With reference to Figure 5.8, the ultimate positive moment may be simply evaluated as $M_u^+ = N \times h/2$. The direction of the resultant which must be



(a) 30° skew angle (b) 60° skew angle

Figure 5.7: Relative positive rotation of elements at ultimate state.

the same as that of N is not, in general, orthogonal to the slanted surface; the necessary transverse component with regard to the slant is allowed by friction (and other local effects). The mechanism indicates that the ultimate negative moment is highly dependent on the level of axial compression and on the height of the rafter. The friction value is not critical, as long as a suitable transverse component of reaction is available. This also may be evident from Chapter 4, where the behaviour curves for different levels of friction and a same connection are compared. This also justifies assigning a low level of influence to other parameters.

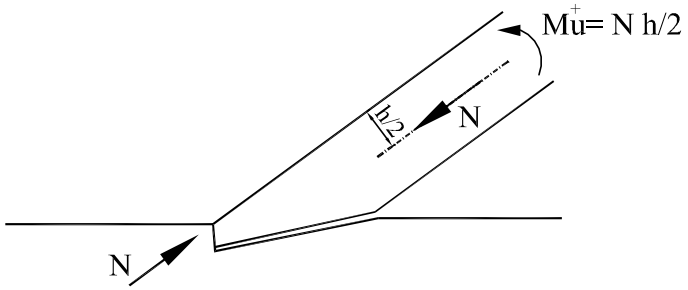


Figure 5.8: Ultimate equilibrium for positive rotation.

5.3.3.2 Cyclic tests

It is possible to follow the evolution of the behaviour of a connection under cyclic loading and to define the individual branches composing the correspond-

ing linearised $M - \phi$ curve. In addition to the first loading considered in the previously described formulation, rules for unloading and reloading must be supplied. In a complete formulation, also unloading into the basic curve from the elastic stage or from limited post-elastic excursion must be allowed. Parisi and Piazza (1998) proposed a simplified model for cyclic test based on a linearised $M - \phi$ curve (see Figure 5.9). This model allows fitting the behaviour characteristics of strengthened or unstrengthened step joints: namely, different stiffness in loading and unloading, non symmetric behaviour for positive and negative rotations, and moments at the elastic and ultimate limit as functions of the current level of axial compression.

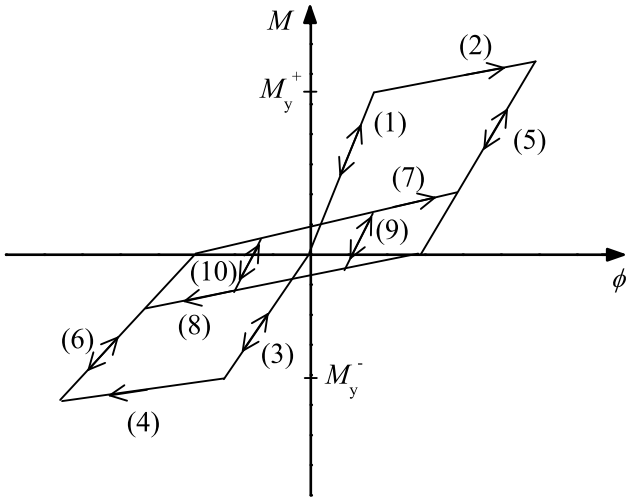


Figure 5.9: Non linear rotational spring element proposed by Parisi and Piazza (1998).

However, in this work a different approach was followed. Based on the linearised $M - \phi$ curve for the first loading, i.e., the curve corresponding to monotonic tests, universal hysteretic rules were used to model the joint behaviour under cyclic loading. The purpose was to use a commercial finite element method package. Therefore, the definition of specific hysteretic rules for each type of connection experimentally evaluated was substituted by the adjustment of universal hysteretic rules, present in almost commercial programs, using the $M - \phi$ curves calibrated based on the monotonic tests performed. In particular, the finite element method (FEM) package used in this work, SAP2000 (2007), presents a nonlinear spring element (NLink element) which may exhibit nonlinear behaviour. Each element is assumed to be composed of six separate "springs", one for each of six deformational degrees-of-freedom (axial, shear, torsion, and pure bending). NLink elements may exhibit up to three different types of behaviour: linear, nonlinear, and frequency-dependent, according to the types of properties assigned to that element and the type of

analysis being performed. Among the several types of nonlinear behaviour that can be modelled with this element, the following features have been used:

- Multi-linear uniaxial elasticity;
- Multi-linear uniaxial plasticity with three types of hysteretic behaviour: Kinematic, Takeda, and Pivot.

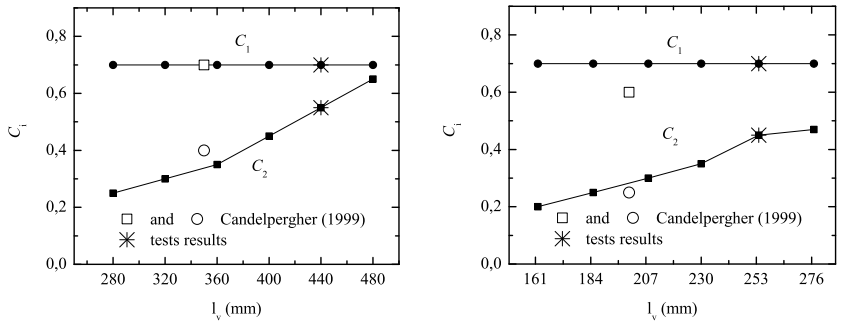
For each non linear type of NLink Property, you may specify six uncoupled linear effective-stiffness coefficients, one for each of the internal springs, that will be used for all nonlinear analyses, and for linear analyses that continue from nonlinear analyses.

5.3.4 Effectiveness of the physical models

Based on a simplified joint behaviour, the physical models proposed by Candelpergher (1999) and completed with Parisi and Piazza (2000) works, represents and attempt to assess the semi-rigid behaviour of traditional timber connections. By identifying the load bearing mechanism it is then possible to predict the key parameters of the monotonic response of the connections. However, the models need to be calibrated and validate for different geometries and load conditions. The calibration of the models for the elastic proportional limit to the tests results achieved in this work has been already reported. Values for the constants C_1, C_2, C_3 and C_4 based on the test results and from the numerical analysis were presented and compared with the ones suggested by Candelpergher (1999). A more detail analysis of the models shows that the constant values proposed for the case of negative rotation (C_1 and C_2) are function of the l_v (length of notch) value. Normally, the notch length is function of the rafter height. Figure 5.10 shows the dependency reported by the numerical analysis of those constants from the geometry of the notch. This dependency explains the different constants values here obtained comparely to Candelpergher (1999) works in the case of 30º skew angle. In the case of 60º skew angle, it is important to point out that the efficiency of the physical model is affected by the deviation in the notch cutting considered in the FEM model (see Chapter 4).

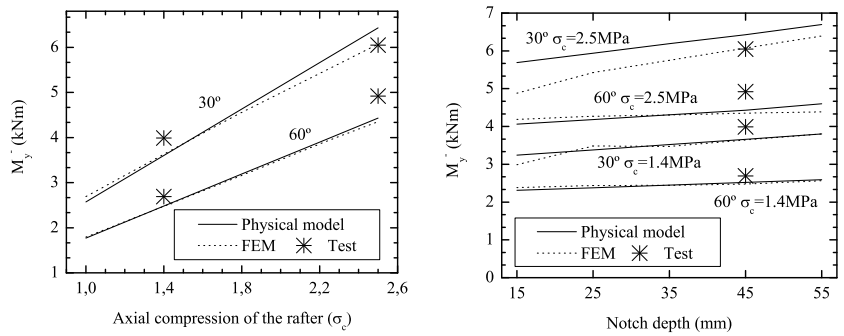
The model proposed for the elastic proportional limit under negative rotation is sensible to: a) skew angle, b) axial compression of the rafter (σ_c) and c) notch depth (t_v). This dependence is confirmed by the numeric results (see Figure 5.11). FEM results (see Chapter 4) also shows that the negative moment value for the elastic proportionality limit is function of the rafter height's (h). The model is sensible to this parameter since C_1 and C_2 are dependent of the notch length.

For the case of positive rotation, the same effectiveness study of the physical model cannot be performed. In fact, it is for the positive moment value for the elastic proportionality limit that the FEM results are most diverging from the test results (see Table 5.5).



(a) 30° skew angle (b) 60° skew angle

Figure 5.10: C_1 and C_2 dependency from l_{v} value.



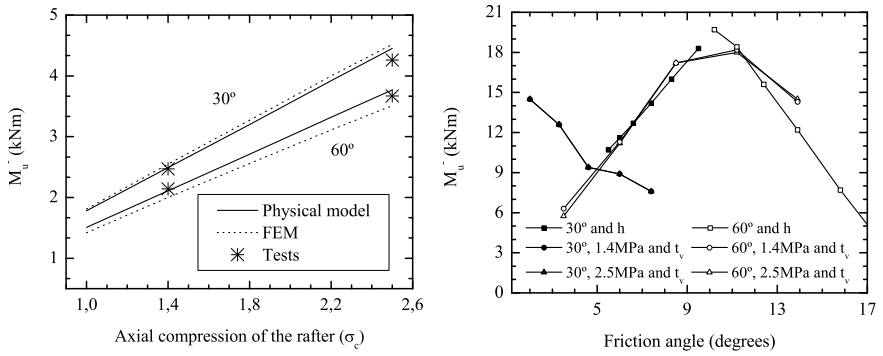
(a) Skew angle and σ_{c} (b) Skew angle and t_{v}

Figure 5.11: Effectiveness of the M_y^- prediction.

Table 5.5: Effectiveness of the FEM results. Error in (%) of the FEM prediction in comparison with the test result.

Skew angle	σ_c	M_u^-	M_y^-	M_y^+	M_u^+
30	1.4	-3.2	9.0	29.8	-0.3
	2.5	-6.1	-0.3	22.1	-6.8
60	1.4	7.0	7.8	-4.0	29.5
	2.5	4.4	11.6	16.3	-1.4

The models presented by Parisi and Piazza (2000) for the ultimate moment values have been also analysed. The model for the ultimate negative moment, M_u^-, fits adequately the tests results and the FEM used to perform the parametric study about the effect of the axial compression of the rafter. The equilibrium point depends of the axial compression of the rafter (see Figure 5.12a) and of the geometry of connections. However, the key geometrical element is the friction angle (see Figure 5.12b). The parametric studies performed based on the FEM shows that the notch depth, the heigh of the rafter and the skew angle effects in the M_u^- value can be reduced to the variation of the friction angle.



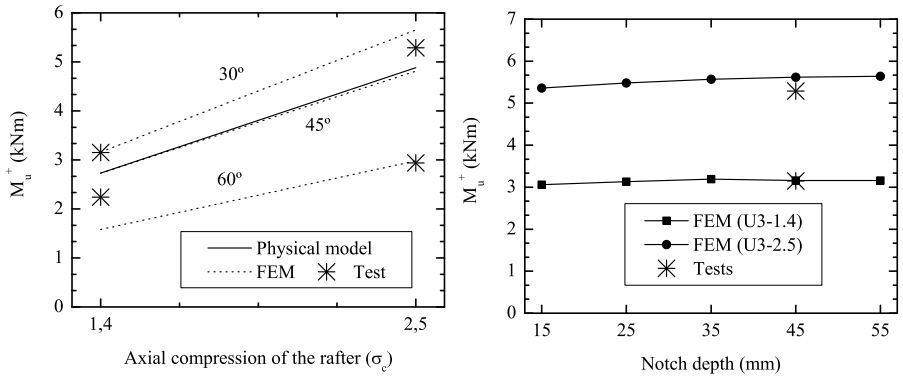
(a) Skew angle and σ_c (b) Friction angle

Figure 5.12: M_u^- dependency.

In terms of the ultimate positive moment value, M_u^+, the FEM results fits the values obtained in the tests however, the same is not valid for the physical model values. The last, suggested by Parisi and Piazza (2000) is function of the axial compression of the rafter and rafter height's. The test results confirm this dependency but, are also function of the connection skew angle (see Figure 5.13a). The same conclusion is achieved by the Candelpergher (1999) work. The numerical analysis performed using the FEM allows to confirm that M_u^+ does not vary woth the notch depth value (see Figure 5.13b).

5.4 Application to the full-scale tests results

Here, the cyclic full-scale tests performed and reported in Chapter 3 are modelled using semi-rigid models. The commercial finite element method package SAP2000 (2007) is used to modelled the tests results through a nonlinear spring element. The behaviour of this nonlinear element is calibrated based on the response of the similar and precedent monotonic tests, using for that the so-called first loading curve. The hysterectic behaviour is simulated using the common nonlinear behaviours suply by the program.



(a) Skew angle and σ_c (b) Notch depth

Figure 5.13: M_u^+ dependency.

5.4.1 FEM model

The test geometry and loading have been modelled using a simple model composed by beam elements with elastic behaviour while the semi-rigid behaviour is introduced through NLink elements, assuming anyway a linear behaviour of the material. Figure 5.14 shows the FEM model adopted where is possible to identify the beam elements, the restraints and the NLink element.

Figure 5.14: FEM model adopted to modelled the cyclic tests.

Besides the nonlinear properties to be assigned to the NLink element, it is important to define the axial stiffness of the joints. The axial stiffness (k_{ax}) depends from the lumber mechanical properties, the geometric proportions of the connected elements and the connection angle (skew angle):

$$k_{\mathrm{ax}} = \frac{E_\alpha \cdot S}{L} \tag{5.4}$$

where, applying the Hankinson Equation 5.5:

$$E_\alpha = \frac{E_0}{\cos^2 \alpha + \frac{E_0}{E_{90}} \sin^2 \alpha} \tag{5.5}$$

represents the wood elastic modulus in the direction forming an angle α with the fiber. E_0 and E_{90} are the elastic modulus in the direction along the fibers and orthogonal, respectively.

$$S = \frac{A_{rafter}}{\sin \alpha} \tag{5.6}$$

represents the nominal notch area, where stress was assumed to be transmitted. A_{rafter} is the cross-section of the rafter.

$$L = \frac{h}{2 \sin \alpha} \tag{5.7}$$

represents the nominal notch length, where compression deformation occurred. h is the height of the tie beam.

5.4.2 unstrengthened connections

In a first step, cyclic tests have been modelled using the models parameters obtained from their first loading curve (corresponding to first cycle of the first amplitude). Later, the effectiveness of the numerical modelling using the synthetic characterization above formulated, has been evaluated.

5.4.3 strengthened connections

5.5 Conclusions

The derived models are proposed as tools, which are handful and immediately employable for practical design and analysis. At the same time, they lead to a significant improvement of the quality of global structural analyses of traditional timber trusses, since they allow the transition from classical schemes (with hinged or fixed joints) to more sophisticated ones with semi-rigid joints.

Chapter 6

Laboratory tests on full-scale timber trusses

6.1 Introduction

Visual inspections are the basis of any analysis of traditional timber structure. They enable detection of external wood decay, as well as, of visible mechanical damages. Moreover inspections can be used to characterize past or current dangerous climate condition, as evidenced by moisture stains on exposed surfaces. In current practice, visual inspection is coupled with non-destructive tests (NDT) (Piazza and Del Senno, 2001) in order to provide information pertaining to the properties, performance, or condition of the material and of the structure. Visual inspection is also a prerequisite to *in-situ* visual strength grading. Visual grading is based on the premise that mechanical properties of lumber differ from mechanical properties of clear wood due to several growth characteristics, which can be identified and evaluated visually. Visual strength grading procedures use empirical relationships, based on laboratory mechanical tests and statistical relationships, to assign lumber members to an established strength class by measuring some visual features, such as growth characteristics, surface decay and geometrical features. Non-destructive evaluation (NDE) is the science of identifying the physical and mechanical properties of a piece of material without altering its end use capabilities and then using this information to make decisions regarding appropriate applications (Pellerin and Ross, 2002). NDE can be classified in two distinct groups: Global Test Methods (GTM) and Local Test Methods (LTM) (Bertolini et al. (1998) Ceraldi et al. (2001)). The former includes, among others, the application of the ultrasonic and vibration methods. The latter includes the Resistograph® (Rinn, 1992) and the Pilodyn® (Görlacher, 1987), which plays usually a major role in the support of visual inspection of wooden elements and, consequently, structures. GTM represent techniques difficult to implement *in-situ*, more appropriate to laboratory facilities. Their advantage is the global evaluation of the material that they allow, overlapping small local defects which could reduce the me-

chanical evaluation of the entire piece. Usual applications of LTM are related to the prediction of the element residual section by analyzing abnormal density variations in the element generally associated with mass loss, resulting from biological degradation (Machado and Cruz, 1997). If some precautions are not taken into account, LTM may represent only the evaluation of a small part of the material. This kind of techniques, requires a considerable number of test results to be representing of the entire piece. Fortunately, usually, those non-destructive tests are easy to handle.

6.2 Trusses evaluated

The two full-scale timber trusses studied in this work were recovered from a construction located in Caldonazzo Lake. The date of the construction is not well known but it is supposed that the timber trusses have more than seventy years. Still in place, the trusses were marked and every member was named to enable the dismantling and transportation phases in safety, preventing eventual errors in the assembling process in laboratory. The trusses were stored four years in the laboratory. Figure 6.1 shows the geometry of the trusses evaluated and the rule adopted for the numbering of the timber elements.

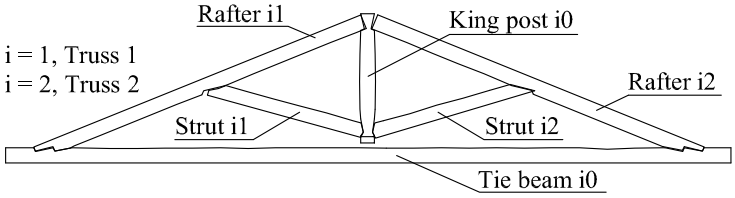


Figure 6.1: Scheme of the two king-post trusses evaluated with the rule adopted for numbering the timber elements.

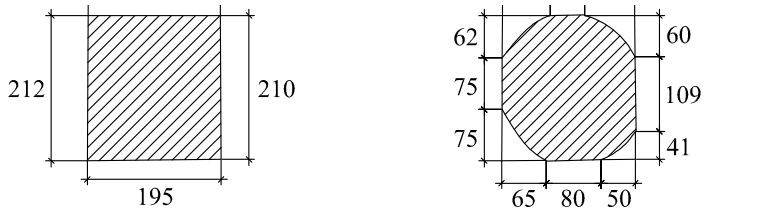
6.3 Non-destructive evaluation of the trusses

Using test methods from both NDE groups, the trusses were submitted to an accurate geometric and mechanical evaluation. After a detailed visual inspection the timber elements were visual graded. The geometric properties were recorded and references cross sections were defined. Pilodyn®, Resistograph®, hardness test, as LTM, and Sylvatest®, as GTM, were used to evaluate the biological and mechanical condition of the timber elements. The moisture content was measured and the density of each timber element was quantified.

6.3.1 Geometric assessment

Traditional timber members are characterized by presenting highly irregular geometries. Cut directly from the trees, the changes in the trunk cross-section

are reported along their length. Because all trusses elements are made by one single timber piece, it is usual to verify significant variability in the cross-section area of the elements, in particular in those longer like the tie beams. To have an adequate report of all those variabilities of the trusses geometry, a geometric assessment was performed. Every 40 cm, each element was marked, named and the cross section measured. Those cross-sections were used also in the non-destructive tests conducted and reported in following items. Figure 6.2 presents the cross section A of the tie-beam of the *Truss* 1, as example of the difference that can be obtained if an inadequate measurement of the cross-section is done.



Area = 409.3 cm^2
Principal moment I = 15188 cm^4
Principal moment J = 12837 cm^4

Area = 349.3 cm^2
Principal moment I = 10673 cm^4
Principal moment J = 8898 cm^4

Figure 6.2: Comparison between the geometric properties of the cross-sections: a) supposing rectangular and b) with detailed measurements (dimensions in millimeters).

6.3.2 Moisture content

Moisture content of wood is defined as the weight of water in wood expressed as a fraction, usually a percentage, of the weight of oven-dry wood. Weight, shrinkage, strength, and other properties depend upon the moisture content of wood. The moisture content determination, for each timber element, was based of three readings using a thermo hygrograph following the measuring scheme of UNI 11035-1 (2003). No significant variations between all moisture content values were detected, Table 6.1. All members of *Truss* 1 present an average value of the moisture content between 11.3% and 12.5% while for *Truss* 2, all members present an average value for the moisture content in the range 12.1% - 12.7%. In terms of service class, according to Eurocode 5, even if some members present moisture content values higher than 12%, it is possible to classify the timber elements as class 1.

6.3.3 Density evaluation

The density of wood is on the one hand an extremely variable property, but on the other, a very important one since the mechanical performance of wood is closely related to it. The density of wood is a measure of the amount of cell-wall

Table 6.1: Moisture content values measured in each element of both trusses.

Element	*Truss* 1	*Truss* 2
King-post	11.7	12.7
Tie-beam	12.2	12.4
Strut 1	11.5	12.2
Strut 2	11.3	12.3
Rafter 1	12.5	12.8
Rafter 2	11.9	12.1

material relative to the size of the cell cavities. Consequently, density is related first to the relative proportions of the different types of cells present, and second to the absolute wall thickness of any one type of cell. Density is certainly one of the two most important parameters determining the mechanical performance of wood (Dinwoodie, 1989). Density can be calculated by:

$$\rho = \frac{m}{Vapp} \tag{6.1}$$

where m is the mass of wood (kg) and V_{app} is the apparent volume of wood (m^3).

The volume obtained from the geometric assessment was considered equal to the apparent volume of wood (V_{app}) because, no significant cavities caused by deterioration or/and shrinkage were detected, the process used to measure the volume was significantly accurate, and the moisture content present by all elements is very near of the reference value (12%).

For the wood specie used, *Picea Abies* Karst., a density value of 415 kg/m^3 was expected, according to UNI 11035-2 (2003), value not far from the range values measured for timber trusses elements (384 kg/m^3 - 479 kg/m^3), see Table 6.2.

6.3.4 Visual grading

The grading criteria according to the European (EN 518 (1997)) and the Italian national standards (UNI 11035-1 (2003) and UNI 11035-2 (2003)) have been applied. UNI 11035-1 (2003) defines terminology and measurement of features for the visual strength grading of Italian structural timbers. Hence, it defines reference moisture content, direct or indirect evaluation of the density, the latter performed by measuring the number of growth rings contained in a reference line, limits to defects reducing the strength (knots, slope of grain, checks, splits, shakes), limits to geometrical features representing growth defects (wane and warp) and decay. The second part of the code, UNI 11035-2 (2003), contains visual strength grading rules and characteristic values for Italian structural

Table 6.2: Density values for each element of the two trusses studied.

Element	Volume (m^3)	Mass (kg)	Moisture (%)	Density (kg/m^3)
King-post 10	0.0712	32	11.7	450
Tie-beam 10	0.4207	201	12.2	478
Strut 11	0.1009	43	11.5	432
Strut 12	0.0951	39	11.3	410
Rafter 11	0.2014	94	12.5	467
Rafter 12	0.1736	79	11.9	460
King-post 20	0.0700	32	12.7	457
Tie-beam 20	0.4280	185	12.4	432
Strut 21	0.0730	28	12.2	384
Strut 22	0.1001	45	12.3	450
Rafter 21	0.1922	92	12.8	479
Rafter 22	0.1836	82	12.1	447
		Average	12.1	446
		CoV(%)	6	4

timber population. Grading rules are specified for different Italian timbers that are identified by coupling species and provenance. Timbers are assigned to strength classes by measuring the visual features specified in the first part of the code. Finally, strength values are referred to strength classes for each timber group. The species of the two king-post trusses analysed is Spruce (*Picea Abies* Karst.), from North Italy, accordingly, grading criteria referred to the group 'softwood 1' in UNI 11035-1 (2003) § 5.3 have been adopted. Unlike an on-site inspection, in the laboratory it was possible to examine all the faces and ends of the elements. Each element face and each face portion (approx. 40 cm wide) has been numbered by mean of a section. Hence, all the defects, present on each face, were localized, measured and mapped. According to UNI 11035 (2003), single knots were measured considering the ratio A of the minimal diameter to the width of the element face, while knots clusters were evaluated through the ratio A_g of the sum of the minimal diameters of all the knots, in a 150 mm range, to the width of the element face. General slope of grain was detected by means of a scribe, or when present, by measuring shrinkage splits on the longitudinal faces. Table 6.3 presents the visual grading results for both trusses timber elements.

Table 6.3: Results of the visual strength grading according to UNI 11035 (2003).

Element	Strength Class	$E_{0,\text{mean}}$ (MPa)
King post 10	S1	12000
King post 20	S1	12000
Tie beam 10	S2	10500
Tie beam 20	S1	12000
Strut 11	S1	12000
Strut 21	S2	10500
Strut 12	S2	10500
Strut 22	S3	9500
Rafter 11	S2	10500
Rafter 21	S1	12000
Rafter 12	S1	12000
Rafter 22	S1	12000

6.3.5 Non-destructive tests

6.3.5.1 Hardness test

Hardness is generally defined as resistance to indentation. Actually, wood hardness involves compression, shear strength and fracture toughness. Wood hardness is positively correlated to density, and as a consequence to the material strength properties. Moreover hardness is in inverse proportion to the moisture content. In the performed tests, hardness has been estimated by measuring the load force R required to embed 5 mm a 10 mm diameter steel hemispherical bit (Turrini and Piazza, 1983). The test area must be clear, that is without visible defects. The value of R was obtained by averaging the test results made in the four longitudinal faces of the element, in numbered sections every 80 cm wide. Each test consisted in five measures taken in each tested area. The result of each test was obtained by averaging the three middle values among the five measures. It means that, for each considered section: 9 for the tie beam, 5 for the rafters and 2 for the struts and king post; twenty tests were done (four per surface) making a total of 1000 hardness tests performed. The correlation between R and elastic modulus in longitudinal tension E_0 is expressed by the experimental equation:

$$E_0 = \delta \cdot 350 \cdot R^2 \tag{6.2}$$

where δ indicates a reduction factor, $0.5 \leq \delta \leq 0.8$, that depends on the defectiveness of the element

Because the 6.2 is experimentally founded, its reliability depends on the

limits of the experimentation itself: namely on the species of the tested samples that are Silver fir (*Abies Alba*) and Larch (*Larix decidua*), on load force R (700 $\div$ 3000 N) and moisture content in the range 12% - 14%. Due to the large amount of hardness tests performed and since mechanical determination of the elastic modulus of some elements (tie beams and rafters) is available, it was possible to calibrate the equation for the case o Spruce (*Picea Abies* Karst.). In the case here presented, the value of $\delta = 0.6$ was founded. After the calibration of the δ value, it was possible to calculate the elastic modulus of all the elements belonging to the two king-post trusses. The elasticity modulus of each element, estimated by means of the hardness test, is reported in Table 6.4.

Table 6.4: Elastic modulus estimated by means of the Turrini-Piazza hardness test.

Element $Truss$ 1	$E_{0,\text{mean}}$ (MPa)	Element $Truss$ 2	$E_{0,\text{mean}}$ (MPa)
King post 10	10991	King post 20	12316
Tie beam 10	13202	Tie beam 20	12183
Strut 11	9572	Strut 21	10312
Strut 12	8447	Strut 22	12156
Rafter 11	11646	Rafter 21	13443
Rafter 12	10605	Rafter 12	12640

6.3.5.2 Pilodyn®

The Pilodyn® method uses a steel pin of a fixed diameter driven into the material by a dynamic force. The depth of penetration is correlated with material density. Görlacher (1987) developed relationships between the depth of penetration of a standard pin and the density of the wood. The correlation coefficient varied from 0.74 to 0.92, depending on the number of measurements and species. The empirical relationships are obviously affected by moisture content. For all elements that compose both trusses, in each section used for the geometric assessment, the penetration depth obtained trough the Pilodyn® in the 4 faces was measured, in a total of 548 tests. Table 6.5, presents the mean values of the depth penetration measured for each element of both trusses.

A linear correlation between density and depth penetration seems adequate to represent the test results, however the lower coefficient of determination $R^2 = 0.50$ (Figure 6.3).

6.3.5.3 Resistograph®

The use of a small-diameter needle-like drill was introduced by Rinn (1992). The cutting resistance of a needle is recorded as a function of depth as the needle penetrates the timber. The resulting profile can be used to determine the

Table 6.5: Depth penetration mean values measured with the Pilodyn®.

Element	Number tests	Moisture (%)	Density (kg/m^3)	Depth penetration (mm)	
				Mean	Range
King post 10	20	11.7	450	16.25	7-21
Tie beam 10	104	12.2	478	10.41	5-17
Strut 11	24	11.5	432	19.63	10-29
Strut 12	24	11.3	410	20.42	11-31
Rafter 11	52	12.5	467	12.38	6-17
Rafter 12	48	11.9	460	11.98	7-17
King post 20	20	12.7	457	13.10	6-19
Tie beam 20	104	12.4	432	15.68	8-23
Strut 21	24	12.2	384	21.42	16-27
Strut 22	24	12.3	450	10.75	7-15
Rafter 21	52	12.8	479	11.54	4-17
Rafter 22	52	12.1	447	13.62	10-18

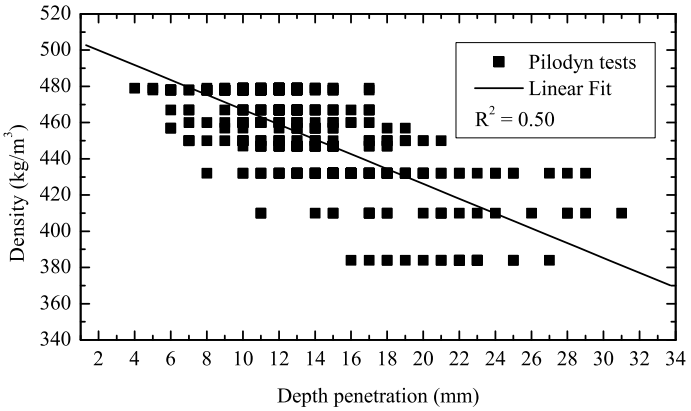


Figure 6.3: Correlation between depth penetration obtained with Pilodyn® and density

location and extent of voids and variation in material density. This technique is highly effective for quantifying the extent of deterioration in timbers. Some researchers have tried to use the results of the resistograph® as prediction of the mechanical properties. For example, Feio (2005) compared the resistance drilling achieved with resistograph® directly with destructive tests. For that, he used the Resistance Measure (RM), given by the quotient between the integral of the area of the resistograph® chart and the depth penetration of the nail in the specimen, equation 6.3.

$$RM = \frac{\int_0^{depth} Area}{depth} \tag{6.3}$$

Feio (2005) showed that the correlation between the RM value and measured density is $R^2 = 0.71$ for new timber and $R^2 = 0.68$ for old timber. RM had a correlation to modulus of elasticity of $R^2 = 0.60$ for new timber, and $R^2 = 0.64$ for old timber. Correlation of RM to longitudinal compressive strength was shown to be $R^2 = 0.59$ and $R^2 = 0.64$ for new and old timber respectively.

However, the use of the RM value to estimate mechanical properties is questionable (Lear, 2005). The area of a resistance-drilling plot can be affected by multiple parameters including drill bit sharpness and general equipment use such as drill orientation. On a single member, changes in the orientation of the drill with respect to growth rings will change the calculated RM value with each drilling. Nevertheless, resistance drilling can be used to estimate mechanical properties of members based on the quantification of deterioration and basing calculations on the remaining sound material and information on clear strength that can be estimated with other non- and semi-destructive testing. In this work, resistograph® was used mainly with the purpose to detect deterioration and to evaluate the voids existing inside the timber members. The main objective of using this technique was not to predict mechanical properties but to complete the information given by the others non-destructive tests realized. In particular, the evaluation of the deterioration level and the voids existing inside the members, and for that, not visible, were the main purpose of the use of resistograph® in the two trusses analysed. In each element of the two trusses, a small number of sections were selected, in which two resistograph® charts were collected (one in direction perpendicular to the other). Forty one and thirty six tests were performed in *Trusses* 1 and 2, respectively, however, no suistanable correlation between the RM and density was founded.

6.3.5.4 Sylvatest®

The ultrasound device Silvatest® allows sending and receiving a longitudinal ultrasound wave using two piezoelectric probes. It measures the duration of the stress wave course in the tested sample, with regard to its moisture content and temperature, which are also controlled. Since there is a one-to-one relation between this speed and the mechanical and physical properties of timber (elasticity modulus and density), the instrument displays directly the measured mechanical quality after taking the influence of humidity and temperature of the timber into consideration. The results are given in the form of quality classes or by mechanical values, indicating an evaluation of the elastic modulus and the allowable bending strength of the element (Sylvatest, 1991). Two measurement methods are available: the direct method, where the transmission

of the wave is done along the fibres and the indirect method, through transmission across the fibres. The first method was used for all elements, whiles the direct method was not applied for both tie-beams because, the Sylvatest® equipment used do not allow measurement lengths above 10 meters. To assess the influence of the test method on the results, both methods were applied whenever possible. Each single measured value represents the third reading value, to avoid bigger variability in the test results. As pointed out above, after the entry of the distance between the two ultrasonic sensors (*Length*), the Sylvatest® instrument shows the time spent by the ultrasonic wave ($Time$), the measured mechanical quality is displayed ($Class$) and mechanical values for the elastic modulus in bending (E_b) and the allowable bending strength (F_b) are proposed. In table 6.6, the tests results of the Sylvatest® for the one rafter of the *Truss* 2 (Rafter 22), considering both measurement methods, are reported.

Table 6.6: Sylvatest® results for the element Rafter 22.

Method	Surface	Length (mm)	Time (μs)	Class	E_b (MPa)	F_b (MPa)
Direct		5.1	824	0	15600	30
B-F	Base	1.6	268	0	14800	26
H-L	Base	1.6	269	0	14600	24
B-L	Base	4.0	778	H	—	—
B-F	Left	1.6	265	0	15400	30
H-L	Left	1.6	267	0	15000	26
B-L	Base	4.0	959	H	—	—

Different measurement method and probes position led to different Sylvatest® results. Even using the indirect method in two different longitudinal faces, between the same sections, inconsistency in the results is obtained. This discrepancy is more evident in the allowable bending strength (F_b), less important for the elastic modulus in bending (E_b) and disappears for the measured mechanical quality class. In consequence, it was decided that, whenever the results of the Sylvatest® are compared with the others results achieved in the non-destructive evaluation performed, the values obtained by the direct method are assumed. By the way, the speed of ultrasound waves is "physically" directly correlated only with material density and material modulus of elasticity. Table 6.7 shows the Sylvatest® results obtained using the direct method, when possible, for all elements that composed the two trusses.

Table 6.7: Sylvatest® results using the direct method.

Element	Moisture (%)	Length (m)	Time (μs)	Class	E_b (MPa)	F_b (MPa)
King post 10	11.7	1.88	329	0	13200	18
Tie beam 10	12.2	10.33	—	—	—	—
Strut 11	11.5	2.23	400	1	12200	12
Strut 12	11.3	2.23	393	1	12800	16
Rafter 11	12.5	5.10	850	0	15400	28
Rafter 12	11.9	4.85	869	1	12200	12
King post 20	12.7	1.87	315	0	14600	24
Tie beam 20	12.4	10.50	—	—	—	—
Strut 21	12.2	2.32	400	0	13600	20
Strut 22	12.3	2.42	459	3	—	—
Rafter 21	12.8	5.10	864	0	14400	28
Rafter 22	12.1	5.11	824	0	15600	30

6.3.5.5 Mechanical evaluation of the modulus of elasticity in bending

The stiffness of the timber elements of the trusses, which is normally expressed as MoE (Modulus of Elasticity) was determined by means of bending tests. MoE for timber contains not only information about the clear wood strength properties, but also to a large extent about defects affecting the stiffness. Therefore, results of bending tests have been used in this research to assess the reliability of visual grading and NDT results. Static bending tests were conducted in accordance with the four-point loading method, with reference to EN 408 (2003). The evaluation of the modulus of elasticity in bending is based on the deformations measured at the centre of a central gauge length of 5 times the depth of the section. This deformation shall be taken as the average of measurements on both faces at the neutral axis. The local modulus of elasticity in bending ($E_{m,l}$), that should be assumed as the MoE, is obtained from the follow equation:

$$E_{m,l} = \frac{a l_1^2 \Delta F}{16 I \Delta w} \tag{6.4}$$

where ΔF is an increment of load on the straight-line portion of the load deformation curve (N), Δw is the increment of correspondent deformation (mm), a is the distance between one loading point and the nearest support (mm), l_1 is the gauge length (mm) and I is the second moment of area (mm^4).

Because of the large span needed for the correct execution of the bending tests (18 times the depth), only the rafters and the tie beams were tested.

Results of the four-point bending tests are reported in table 6.8.

Table 6.8: Elastic modulus obtained by means of four-point bending tests.

Element (*Truss* 1)	$E_{\mathrm{m,l}}$ (MPa)	Element (*Truss* 2)	$E_{\mathrm{m,l}}$ (MPa)
Tie beam 10	12980	Tie beam 20	12929
Rafter 11	11149	Rafter 21	12646
Rafter 12	11367	Rafter 22	12863

6.3.6 Analysis and discussion of NDE

During the visual inspection, significant variation in cross-section geometric properties was found. Indeed, as all elements of the trusses are composed of one single timber piece, important deviations are expected, as consequences of the changes in the cross-section of the trunk. Using UNI 11035-1 (2003) and UNI 11035-2 (2003) it was possible to visually grade the strength of the timber elements. In particular, a strength class was assigned and a mean value for the modulus of elasticity (MoE) was suggested. Three values for MoE were found: 12000 MPa, 10500 MPa and 9500 MPa corresponding to strength class $S1$, $S2$ and $S3$, respectively. For visual grading, it was necessary to record the moisture content and to calculate density. No significant variations between moisture content values were detected. All members of $Truss$ 1 present an average value of the moisture content between 11.3% and 12.5% while for $Truss$ 2, all members present an average value for the moisture content in the range 12.1% - 12.7%. A density range of 384 kg/m^3 to 479 kg/m^3 was obtained for the timber trusses elements in accordance with the reference value suggested by UNI 11035-2 (2003) for *PiceaAbies* Karst. (415 kg/m^3). The hardness test developed by Turrini and Piazza (1983) permits the correlation between the load force (R) required to embed a steel bit into the wood with MoE. However, a reduction factor depending of the defectiveness of the element is needed. This reduction factor was calibrated (a value of 0.6 was found) using 760 hardness tests results and the MoE values obtained with the mechanical evaluation of the tie beams and the rafters of both trusses. Despite the considerable quantity of values used, the correlation found between the load force (R) and the density (ρ) is poor ($R^2 = 0.35$). Others researchers, Feio (2005) and Lear (2005), have tried to correlate the Resistance Measure (RM), obtained with the Resistograph® test, with density. The same attempt was made but the correlation obtained is very poor ($R^2 = 0.02$). The difficulties involved in this kind of test were already pointed out. The area of a resistance drilling plot can be affected by multiple parameters including drill bit sharpness and general equipment use such as drill orientation. These uncertainties are amplified in the case of old timber elements, with splits and slope of grain caused by mois-

ture content variation and shrinkage. These defects have a significant impact in the area of the resistance drilling plot used to calculate RM. As conclusion, and assuming the mechanical evaluation of the MoE as reference, correlation between the results of the non-destructive tests and MoE obtained through mechanical evaluation are low for Turrini-Piazza hardness test, as shown in Figure 6.4.

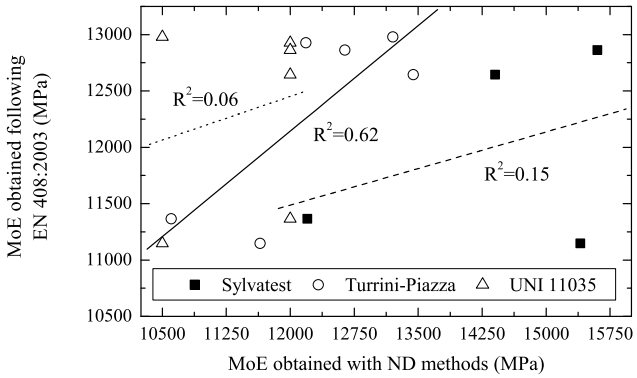


Figure 6.4: Correlation between MoE given by non-destructive methods and MoE found through the direct mechanical evaluation according EN408(2003).

A very poor correlation ($R^2 = 0.06$) was established between the MoE given by the visual grading and the mechanical evaluation. A correlation presenting $R^2 = 0.15$ was defined between the Sylvatest® results for the MoE and the values found through the mechanical evaluation. An interesting correlation, $R^2 = 0.62$, was obtained between the Turrini-Piazza hardness test, Turrini and Piazza (1983), and the mechanical evaluation, in terms of MoE prediction. Sandoz et al. (2000) state that nondestructive testing by means of ultrasound overestimates mechanical properties in 25%. Moreover, old wood has generally higher mechanical properties in comparison to recent plantation growth trees. Difference between old and new wood properties results in different velocity due to different wood density (Ehlbeck and Gorlacher, 1990). Görlacher (1991) investigated the correlation between modulus of elasticity and strength of old wood and he found that correlation coefficients are approximately the same for old and new wood. However, Kasal and Anthony (2004) found only a weak correlation between ultrasound pulse velocity methods and ancient wood member density.

6.4 Load-carrying tests

The load-carrying tests were performed in the Materials and Structural Testing Laboratory of the University of Trento, Italy. Before assembling both trusses, an extend evaluation of each truss member was conducted as previously reported. The trusses were subjected to cyclic tests, under symmetric and non-

symmetric loading for two levels of loads corresponding to the Serviceability and Ultimate Limit States. Considering their behaviour under this series of tests, the trusses were strengthened. Later, the same sequence of tests was carried out over the strengthened trusses. If, after that, the failure of the truss was not been achieved, a final test under growing loading is perform. In the following, the main conclusions of the tests results are presented.

6.4.1 Test setup, instrumentation and procedure

The timber trusses were tested under cyclic loading subjected to two point loads, each one directly applied over the strut-rafter joint. Symmetric and non-symmetric tests were performed using two values of load, corresponding to Service and Ultimate Limit states (SLS and ULS, respectively). The loads considered include self-weight of the original timber roof and the snow load corresponding to the location of the trusses, Caldonazzo Lake (500 m of altitude). Before the load-carrying tests, and after the reconstruction of the disassembled trusses, trusses were subjected to a series of loading and unloading tests aiming at adjusting all trusses elements together reducing to the minimum the free movements between them. The first step of the load-carrying tests was the application of the load corresponding to the self-weight of the timber roof (covering material and structure and purlins). After that, the remaining load corresponding to each loading case was divided in four steps. Therefore, the load target was reached after 4 cycles of loading and unloading keeping constant the minimum load applied corresponding to the self-weight. In each test carried out, three cycles were performed (Figure 6.5). The non-symmetric tests results from the asymmetric value of the snow load that should be considered in accordance with D.M. 14/9 (2005).

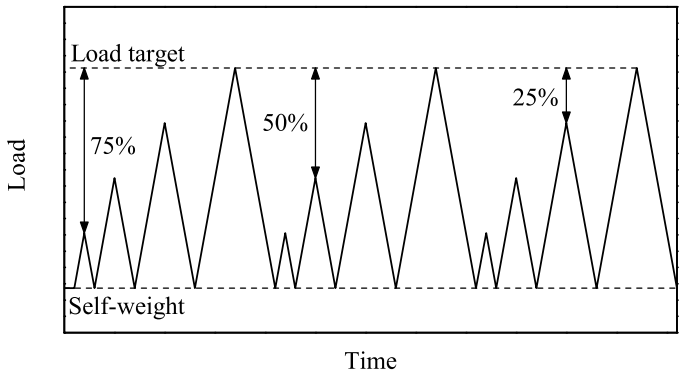


Figure 6.5: Load procedure applied in the load-carrying tests.

During the tests the main global displacement of the trusses, the relative displacement between the king post and the tie beam and the rotation of each joint were measured, using for that fourteen transducers. Two manual hy-

draulic jacks, supported by a steel frame fixed to the reaction slab of the laboratory, were used for applying the loads. Two supports restraining the vertical displacement and right support restrained also the horizontal movement were placed at each end of the truss. Figure 6.6 shows a general overview of the test setup and measurement layout used in the tests and Table (6.9) summarized the load-carrying tests performed in both trusses.

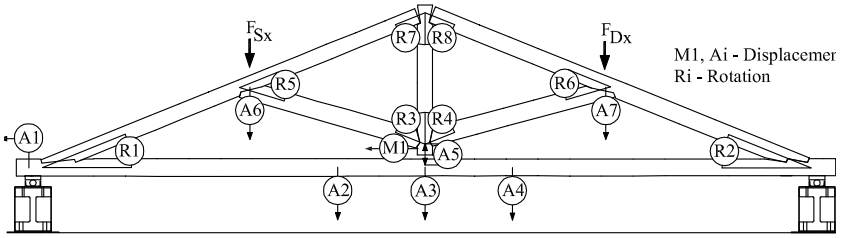


Figure 6.6: Instrumentation layout.

Table 6.9: Load-carying tests performed.

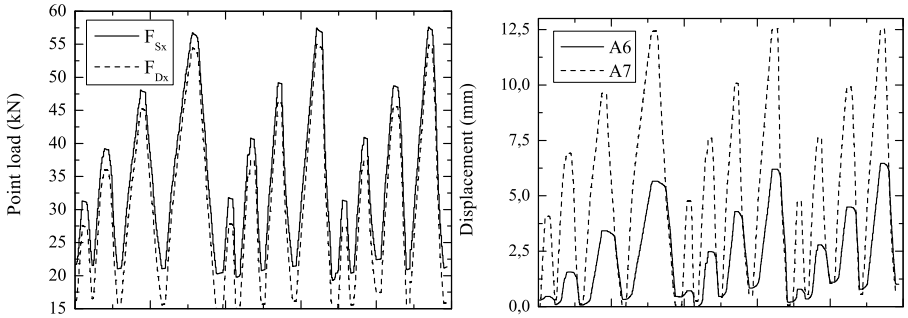
Test	*Truss* 1		*Truss* 2	
	F_{Sx} (kN)	F_{Dx} (kN)	F_{Sx} (kN)	F_{Dx} (kN)
S-U-S	57.6	55.0	40.5	46.2
S-U-Dx	25.7	47.9	34.2	53.7
S-U-Sx	58.4	30.9	61.9	34.9
U-U-S	65.8	68.7	82.2	84.6
U-U-Dx	n.p.	n.p.	44.4	82.9
U-U-Sx	n.p.	n.p.	82.8	44.9
S-S-S	65.8	68.7	61.0	63.7
S-S-Dx	22.1	44.3	31.7	59.1
S-S-Sx	45.4	27.4	61.9	30.9
U-S-S	74.5	69.0	85.8	85.7
U-S-Dx	n.p.	n.p.	41.8	83.6
U-S-Sx	n.p.	n.p.	84.2	44.2
Failure	54.6	55.2	108.1	107.5

n.p. - test not performed

6.4.2 Evaluation of the trusses behaviour

The response of both trusses under the different type of tests performed is highly dependent on the variability, previously detected and reported, along the

truss members in terms of cross sections area and principal moments. Moreover, it is recognized the difficulty associated with tests over existing structures, in which the members can present residual deformations and signs of degradation and/or the connections are not well tight. The tests results shows that even under symmetric loading conditions, the behaviour of both trusses is non-symmetric. This conclusion is more evident in the response of $Truss$ 1 under symmetric loading corresponding to SLS (Figure 6.7).



(a) Point loads (b) Global displacement

Figure 6.7: Asymmetric behaviour of $Truss$ 1 under symmetric loading condition (S-U-S).

The connection between the king post and the tie beam, made by a steel rod of 20 mm diameter fixed in the king post, aligned in the longitudinal direction, passing through the tie beam and having in the extremity one nut fastening the two elements, performs adequately. A increase of the relative displacement between those two elements is avoided and a negative displacement(king post approaching) is allowed (Figure 6.8).

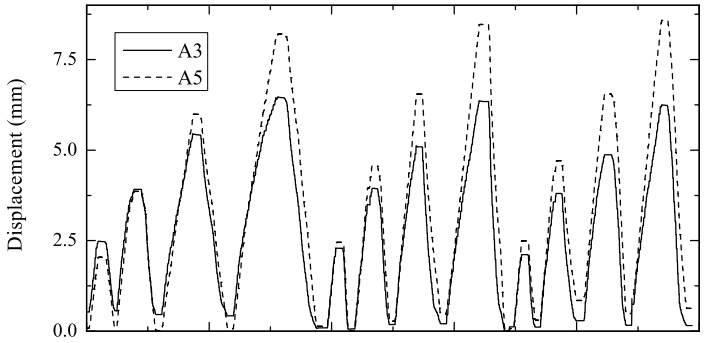


Figure 6.8: Behaviour of the connection between the king post and the tie beam under symmetric loading conditions.

As consequences of the trusses deformations under the vertical loads ap-

plied, horizontal displacements of the non-restrained support in the horizontal direction were recorded (Figure 6.9).

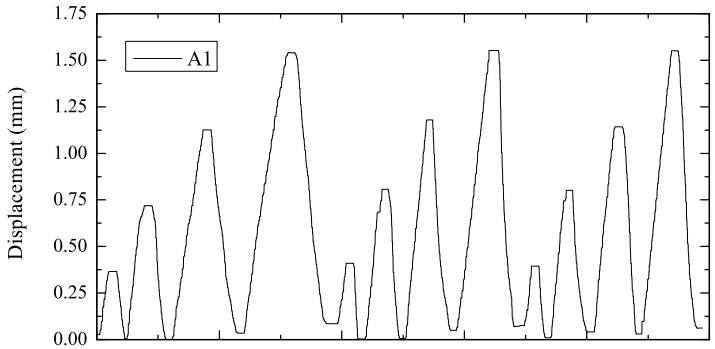
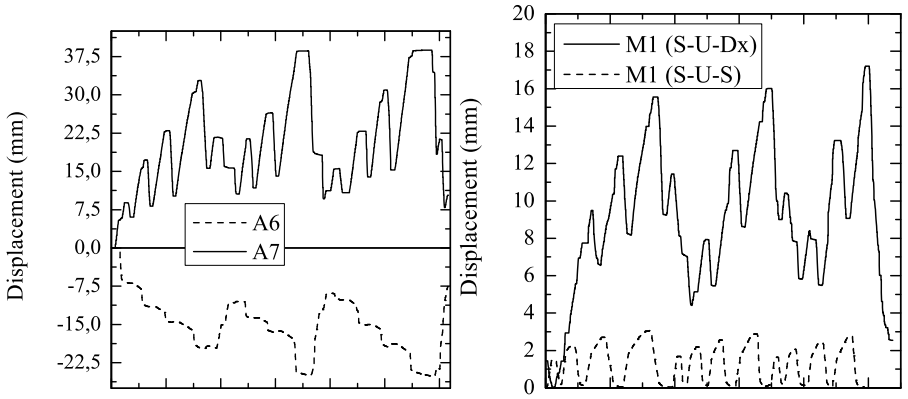


Figure 6.9: Horizontal displacement recorded in the support under symmetric loading.

Under non-symmetric loading conditions, the asymmetric trusses behaviour, already pointed out, is emphasised. Channels $A6$ and $A7$ shows non-symmetric displacement and the horizontal movement in the bottom of the king post, recorded by channel $M1$, is largely higher than under symmetric loading, Figure 6.10.



(a) Global displacement (b) M1 displacement

Figure 6.10: Asymmetric behaviour emphasised under non-symmetric loading of $Truss$ 1 during S-U-Dx test.

This asymmetric behaviour of the trusses introduces bending stress in the rafters and tie beam. Due to the rotational stiffness of the king post-tie beam connection, the asymmetric response of the overall truss induces distortion in

the tie beam (Figure 6.11). This distortion induces important bending stresses in the bolt of this connection (Figure 6.11).

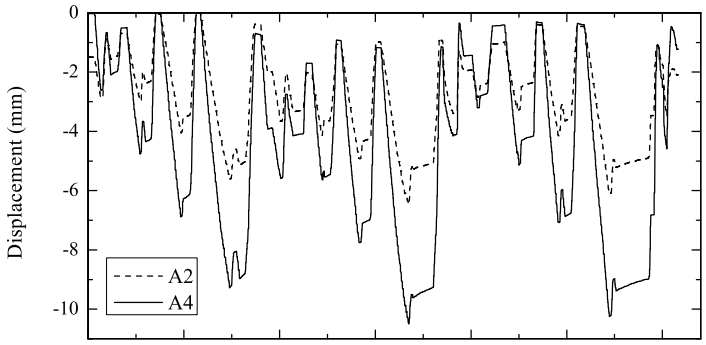


Figure 6.11: Distortion of the tie beam under non-symmetric loading of $Truss$ 1 during S-U-Sx test.

The connection between the king post and the tie beam presents rotational stiffness in both the plane of the truss and the plane perpendicular to the truss. Therefore, this connections prevent also the out-of-plane movement improving consequently the stability of the substructure composed by the rafters, the king post and the struts (Figure 6.12).



(a) In the plane truss (b) In the normal plane of the truss

Figure 6.12: Bending of the steel rod inserted in the tie connection.

As expected, under non-symmetric loading the relative displacement between the king post and the tie beam, measured in the connection between both elements, is nearly zero. In addition, the horizontal movement recorded

in the non-restrain supports is reduced. For the case of the Ultimate Limit State (ULS) different behaviour were observed for both tested trusses. While *Truss* 2, was able to sustain all tests (symmetric and two non-symmetric), in *Truss* 1 only the first cycle of the symmetric tests was finished. When the maximum load corresponding to this limit state was reached, considerable out-of-plane movements were visible (Figure 6.13). To prevent the global failure of the truss it was decided to stop the tests and to strength *Truss* 1 before proceeding with the experimental program.



Figure 6.13: Out-of-plane movement observed in the *Truss* 1 (unstrengthened) under ULS at the end of 1st cycle.

In the case of *Truss* 2, the tests undertaken for SLS were repeated for the load level corresponding to the ULS. The main conclusion about the overall behaviour of the truss pointed out for the SLS can be extended to ULS. Therefore, it can be concluded that, apart from the instability observed in the case of *Truss* 1, the trusses safety under ULS was verified. No local collapse or failure in the timber members occurred. It is important to point out that the bracing forces transmitted by the purlins and the covering structure, boundaries conditions existing *in-situ*, should prevent the instability observed in the case of *Truss* 1 load-carrying tests.

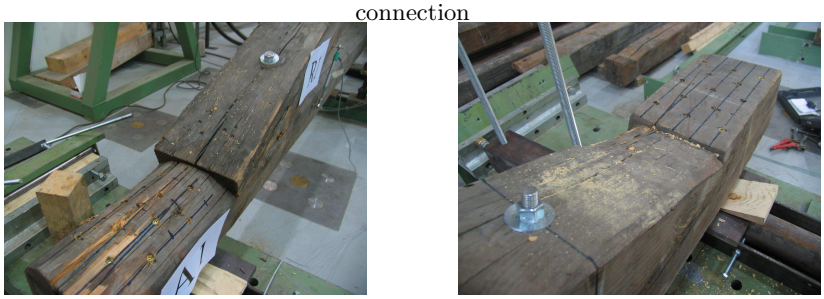
6.4.3 Strengthening

In the next load-carrying tests phase, the trusses were strengthened, based in the response obtained in first tests, and the strengthening effectiveness was assessed through the same test history. Strengthening aimed at improving the overall behaviour of each truss preventing local failures which could hamper the complete test history defined. Strengthening of *Truss* 1 aimed essentially at repairing the out-of-plane movement observed and to preventing this instability,

allowing tests corresponding to the ULS. The out-of-plane deformations were removed and a UPN profile was bolted to the king post. The objective was to prevent the out-of-plane movements, increasing the stiffness of the connection in this direction, keeping the tie beam suspended to the king-post (Figure 6.14). The timber elements did not presented any local failure or damage however, the connections between the rafters and the tie-beam were weakened. In particular, the left connection, over the support with horizontal displacement, the depth of the step was insufficient and the timber beyond the step showed some fissured. Therefore, it was decided to strength this part of the tie beam (beyond the step) with screws (12 screws M6-200) in order to increase its shear resistance. Moreover, using the pre-existing holes, an internal bolt of 20 mm diameter was introduced at midjoint, normal to the rafter in each rafter/tie beam connection (Figure 6.14). Similar bolts existed in those connections before the dismantling of the trusses.



(a) UPN profile preventing the out plane movements in the king post-tie beam connection



(b) Screws and internal bolt to strength the tie beam-rafter connections

Figure 6.14: Strengthening of *Truss* 1.

In the case of *Truss* 2, only the connections between the rafters and the tie

beam were strengthened. The stiffness of the king post/tie beam connections demonstrated to be adequate to prevent the instability of the truss. Rather, the timber beyond the step demonstrated some signs of deterioration and the depth of the steps in the rafters/tie beam connections appeared insufficient. The same strengthening technique used in *Truss* 1 was applied: one internal bolt tightening the connection and screws beyond the step to improve the shear resistance. However, and as an improvement based in the failure modes observed in *Truss* 1 tests, a binding strip was used to confine the timber in the notch front (Figure 6.15).

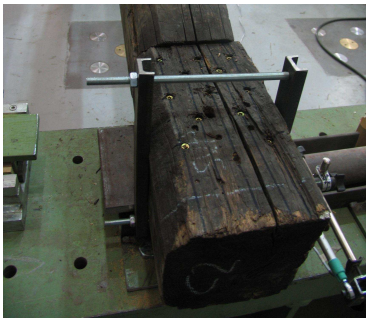


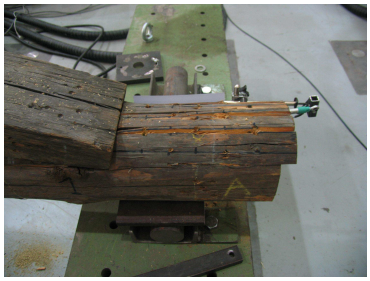
Figure 6.15: Strengthening of *Truss* 2. Screws and binding strip applied in the beyond part of the step in the rafter/tie beam connection.

6.4.4 Efficiency evaluation of the strengthening

The series of tests corresponding to the SLS were repeated after the trusses strengthening. The main objective was to analyse the influence of the stiffness of the tie beam-rafter connection, in the overall behaviour of the truss, in particular, under non-symmetric loads. Nevertheless, the main goal of the strengthening was to increase the truss load capacity: to make *Truss* 1 able to perform all load procedures corresponding to ULS and to assess the failure load of *Truss* 2.

The load capacity of *Truss* 1 was improved by the strengthening but, only the symmetric test corresponding to the ULS was accomplished. At the end of this test, the local damages in the tie beam-rafter connections hamper the execution of the non-symmetric tests. In consequence, it was decided to proceed with a symmetric load test until failure. It is important to point out that the ultimate load achieved in the failure test is lower than the load level attained in the precedent ULS test. Despite the strengthening measures undertaken to improve it, the failure was caused by lack of shear resistance of the tie beam in front of the notch. Theoretically, the screws should increase the shear resistance but, because of the fissure already existing before the screws placing, the timber part in front of the notch the step did not work as a rigid body. The screws expanded the fissures and the rigid body became separate in small pieces

(Figure 6.16a). Moreover, the failure of this connection was cause by a previous shear failure of the rear step (Figure 6.16b). With the horizontal movement of the rafter in the connection tie beam-rafter, the joint king post-struts was dismantled (Figure 6.17a) and important bending stresses are introduced in the internal bolt (Figure 6.17b).



(a) Shear failure in the notch front



(b) Failure of the rear step



(c) Disassemble of king post-struts joint

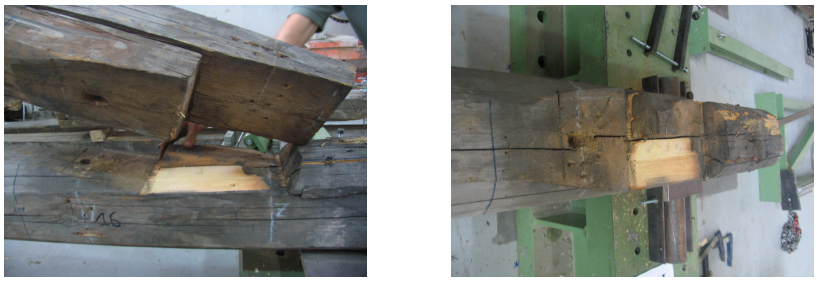


(d) Bending of the internal bolt

Figure 6.16: Failure damages of *Truss* 1.

In the case of *Truss* 2, it is difficult to conclude if the strengthening was efficient in the improvement of truss load capacity as no failure was obtained in the previous tests performed in unstrengthened conditions. The strengthened truss was subjected to the entire test history (SLS and ULS, under symmetric and non-symmetric loads). After that, a load procedure until failure was followed. This procedure is similar to the previous but now, the load increment did not stop at the value of 80 kN (maximum load corresponding to ULS). The maximum load value achieved in the failure tests was 100 kN. Again, the failure of the truss was obtained by shear failure in the timber in front of the notch in the connection tie beam-rafter. First, the shear failure of the rear step happened and then the shear failure of the timber in the front part of the notch took place (Figure 6.17).

It was the geometry of the tie beam-rafter connections that defined the failure. The failure happened in the double step connection in which the rear step presented a bad geometry (connection in the right side). This step must be deeper than the frontal. If not, the surface resisting to shear stress is insuf-



(a) (b)

Figure 6.17: Shear failure of the tie beam-rafter connection for *Truss* 2.

ficient. The double step connections of the right side (over the fixed supports) failed in consequence of a first shear failure in the rear step. Once the posterior step fails, the stresses concentrated in the frontal step and the failure is reached (Figure 6.18).



(a) Failed (right side) (b) Safe (left side)

Figure 6.18: Double step connections between the rafters and the tie beam of *Truss* 2.

6.4.5 Strengthening influence

Strengthening aimed at correcting local failures and improving the load-capacity of the trusses. However, strengthening had influence in the overall behaviour of the trusses during the tests. A detail analysis of the tests results obtained in terms of joints rotations and displacements measured in the most relevant points during the tests performed (Table 6.10 in the case of *Truss* 2) shows that:

- Strengthening reduced the distortion of the trusses, observed even under symmetric loading and measured by the horizontal movement of the bottom of the king post (LVDT called M1);

- Strengthening was able to reduce the deformation of the trusses by increasing the axial stiffness of the rafter-tie beam connections and by allowing the moment-rotation behaviour of these joints minimising pinching;

- Strengthening reduced the joints rotations, not by a significant increase in the stiffness value but, essentially, reducing the pinching effect observed in the unstrengthened conditions. In particular, in the first load cycle, the connections of the unstrengthened trusses presented significant pinching (Figure 6.19);

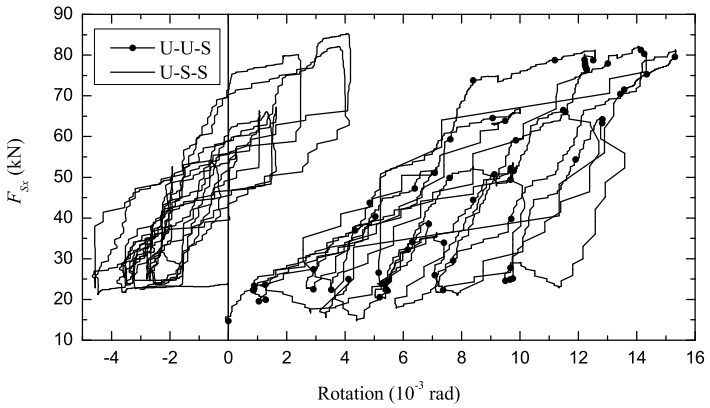


Figure 6.19: Moment-rotation response of the left rafter-tie beam connection of *Truss* 2 under unstrenghthened and strengthened conditions.

- In some cases, unstrengthened connections shows non-linear behaviour with an elasto-plastic phase in the moment-rotation (M-R) curves. By contrary, strengthened connections exhibits a full elastic M-R behaviour;

- In *Truss* 1, the strengthening of the left tie beam-rafter connection became efficient only during the 2nd and 3rd load cycle as result of the gap inside the pre-existing hole used to insert the bolt. The opposite connection, strengthened with the same technique but using a new hole, was efficient since the beginning of the tests (Figure 6.20);

- In *Truss* 2, rotation measured in the left tie beam-rafter connections was always higger than the ones registered in the similar connections located in the opposite side of the truss. Note that the right connection failed in the ultimate tests. The rotation capacity of this connection was reduced in consequence of the movement introduce by the shear failure in the front part of the notch which caused the failure of the truss;

- In *Truss* 2, strengthening results in displacements variation, in comparison with the unstrengthened conditions, not significant, mainly below 20% and with highers values in the SLS case, with the exception of the

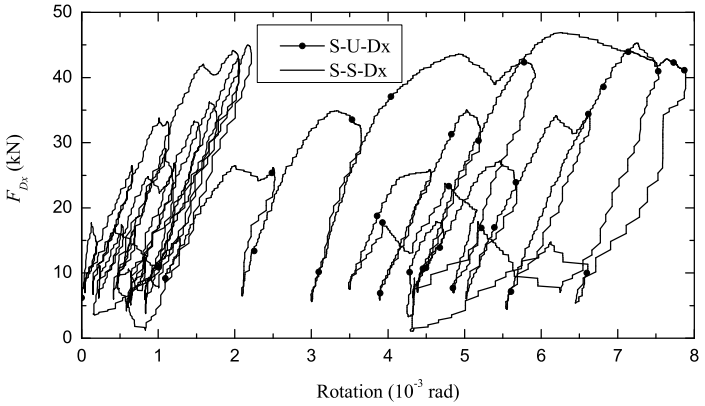


Figure 6.20: Moment-rotation response of the left rafter-tie beam connection of $Truss$ 1 under unstrenghthened and strengthened conditions.

horizontal movement of the king post bottom (recorded by M1) which, in some load cases, presented a reduction of 73%;

- In the case of $Truss$ 2, under non-symmetric loading conditions and for the ULS load level, the effect of the strengthening in the vertical displacement recorded is very limited.

Table 6.10: Maximum displacement recorded by the instrumentation setup during the load-carrying tests on *Truss 2*.

Order	Test	F_{Sx} (kN)	F_{Dx} (kN)	M1 (mm)	A1 (mm)	A2 (mm)	A3 (mm)	A4 (mm)	A5 (mm)	A6 (mm)	A7 (mm)
1st	S-U-S	39.8	43.2	3.4	1.9	7.0	6.6	6.6	6.8	12.8	13.1
2nd	S-U-Dx	30.2	53.7	12.1	2.4	5.4	7.2	9.6	8.0	10.3	25.7
3rd	S-U-Sx	60.7	24.8	10.7	1.2	7.7	6.4	4.9	6.2	30.5	18.1
4th	U-U-S	82.2	83.3	8.1	3.3	13.3	13.1	12.1	13.1	21.2	20.0
5th	U-U-Dx	39.3	81.8	15.9	3.0	6.4	8.8	11.7	9.2	18.3	38.9
6th	U-U-Sx	82.0	43.5	12.7	2.1	11.9	9.5	7.0	14.6	46.8	24.3
7th	S-S-S	58.9	63.4	3.5	2.6	10.3	11.0	11.1	8.9	11.0	20.5
8th	S-S-Dx	28.8	59.1	9.4	2.1	4.4	6.1	8.4	6.1	15.4	26.8
9th	S-S-Sx	61.9	28.0	18.5	1.2	9.5	6.6	4.7	7.2	34.4	22.0
10th	U-S-S	84.9	85.6	2.3	3.3	10.9	10.4	9.9	11.0	19.0	19.2
11th	U-S-Dx	39.8	81.5	10.4	3.2	6.6	9.2	11.7	9.4	18.9	33.0
12th	U-S-Sx	81.3	42.7	7.9	1.8	13.6	10.3	7.3	14.3	44.1	23.8

6.4.6 Numerical analysis

The structural analysis program SAP2000 (2007) was used to model the trusses under conditions similar to the experimental tests described above. It has been developed a model involving variable dimensions beam elements, and semi-rigid joints between the different elements, assuming a linear behaviour of the material.

6.4.6.1 Material model

Timber is assumed as an orthotropic material in the system so-called anatomic cylindrical coordinates corresponding to the longitudinal, L, radial, R, and transversal, T, directions of the tree trunk. Cylindrical coordinates may be approximated as orthogonal, for the material extracted from the outer region of the trunk. The elastic modulus, for an asymmetric model, are E_0 in the direction along the fibers, and E_{90} orthogonal to it, plus a shear modulus, G, and a Poisson's ratio, ν. The elastic modulus was obtained from the previous non-destructive evaluation performed, a value of 0.3 was adopted for the Poisson's ratio and the others two properties were calculated adopting the relations proposed by EN 338 (2003):

$$G = \frac{E_0}{16} \tag{6.5}$$

$$E_{90} = \frac{E_0}{30} \tag{6.6}$$

6.4.6.2 Geometric and mechanical models

The geometry and loading of the truss is compatible with the assumption of a state of plane stress for the model. The truss is analyzed as a frame structure, composed by several frame elements of two nodes, representing the geometric properties variability of each timber member of the truss. An elastic behaviour is assumed for the elements while a semi-rigid behaviour of the connections is introduced in the model with the Nonlinear link elements (Nlink).

6.4.6.3 Loads

During the tests, two types of loads were applied in the structure. Uniformly distributed loads representing the self-weight of the truss member and joint loads applied during the different load procedures of the tests performed.

6.4.6.4 Semi-rigid modelling of connections

Traditional timber connections transmit forces by contact and friction. The semi-rigid behaviour of the joints must be accounted for to accurately model the behaviour of the joints and the truss. In order to properly describe this behaviour, the stiffness of each Nlink must be defined, according to the different

geometric and mechanical features of the elements at each joint. To assign the axial and rotational stiffness at the connection, expressions and results of Chapter 5 are accounted. At the tie connection (between the king post and the tie beam) wood was compressed along the fibers by the bolt and across them by the washer, eventually giving rise to plastic embedding. The axial stiffness of the joint ($k_{ax,t}$) has been formulated taking into account the axial stiffness of the steel rod (eqn. 6.7) and the stiffness of the wood in contact with the steel washer for stresses orthogonal to the fiber (eqn. 6.8):

$$k_{ax,1} = \frac{E_s \cdot A_{rod}}{l_{rod}} \tag{6.7}$$

$$k_{ax,2} = \frac{E_{90} \cdot A_{washer}}{h_{tiebeam}/2} \tag{6.8}$$

where E_s is modulus of elasticity of steel, A_{rod} and l_{rod} is the cross-section and the length of the steel rod, respectively, E_{90} is the elastic modulus of wood in the orthogonal direction of fibers, A_{washer} is the contact area of wood with the washer and tie beam is the height of the tie beam.

Rotational and shear stiffness of the same joint can be easily evaluated on the basis of a computational length, obtained considering the part of the rod inserted in the wood equivalent to three times its diameter, as suggested by Piazza et al. (2005).

6.4.6.5 Numerical versus experimental results

Numerical modelling and experimental results have been compared in the case of the load-carrying tests performed on *Truss* 2 under the load procedures corresponding to ULS (Table 6.11). First, the numerical model has been implemented without considering the real behaviour of the truss observed in the performed tests. Then, the model was verified and calibrate based in the tests results. Finally, a sensitivity study was performed with the aim to assess the influence of the geometric and stiffness properties assumed for the timber elements and connections, respectively, on the numerical analysis results. The numeric model has been very helpful to understand the behaviour of the truss under each load-carrying test and to confirm observations taken during the experimental campaign. Moreover, it was possible to confirm the importance of the local damage oberved during the tests, in the response of the system in the following tests.

Firstly, the model was calibrated using the results of the U-U-S test. As consequence, the axial stiffness of the struts-rafters connections have been reduced. Otherwise, using the reference values, errors of 35% and 29% were obtained for LVDTs A6 and A7, respectively, between the numeric model and the test. This stiffness reduction is a result of the gaps existing in those connections. Using the reference values, the asymmetric truss behaviour observed, difference between the displacement measured by A6 and A7, is drastically

changed (A7 register the higher displacement in oppostion to the test where was this LVDT that measured the smaller value). The rotational and shear stiffness evaluated on basis on the computational length of the Nlink used to modelled the tie connection revealed to be adequate. Nevertheless, and as it will be pointed out further, the importance of this connection under symmetric loading condition is limited.

Despite those corrections, the calibrate model was incapable to reproduce the following non-symmetric tests. Under non-symmetric loading conditions the behaviour of the steel rod used in the tie connection became relevant. This element, after been inserted during the reconstruction of the truss, presented a null capacity of moment-rotation (in the plane of the structure) during the non-symmetric tests modelled. The previous tests, symmetric (SLS and ULS) and non-symmetric tests (SLS), have produced the necessary local embedment of wood for that. This local damage of the steel rood had also consequences in the shear stiffness of this connection. If, for the non-symmetric tests with the higher load in the left pitch (Sx), the embedmment of the steel rod in the wood represents a shear stiffness of 4000 kN/m, under opposite non-symmetric loading conditions, tests Dx, this connections do not shows shear stiffness. The local embedment of wood caused by the symmetric and Sx tests create the enough gap to avoid any shear stiffness in the connection when subjected to Dx tests.

The internal adjustment between the different timber members of the truss that occurred during the course of the test program, reduced the gaps existing in the connections. As result, the axial stiffness of the rafter-strut connections increase considerably, reaching the reference values. On the other end, the rafter connections with the king post and the tie beam of the less loaded pitch reduced it axial stiffness and, more important, the shear stiffness was drastically reduced. This effect was expected as no additional elements (strengthening) were adopted to induce the contact between the connected elements. In unstrengthened conditions, traditional timber connections are not able to perform under load reverse conditions. Those observations are valid for both non-symmetric tests performed in unstrengthened conditions and under ULS.

The strengthening of the truss, materialized with one bolt in each rafter-tie beam connection plus the shear reinforcement of the notch front, stabilized the truss behaviour. The strengthening reduced in particular the truss distortion, observed even under symmetric loading and measured by the horizontal movement of the bottom of the king post (LVDT M1). The presence of the bolt increases significantly the axial and shear stiffness of rafter-tie beam connections, improves the contact between the connected elements and allows full development of their moment-rotation capacity. Due to the local damages imposed by precedent load-carrying tests (enlargement the hole around the steel rod), after strengthening, the tie connection presents shear and bending stiffness equal to zero with a rigid behaviour in axial direction.

Table 6.11: Maximum displacement recorded by the instrumentation setup during the load-carrying tests on *Truss 2*.

Order	Test		M1 (mm)	A1 (mm)	A2 (mm)	A3 (mm)	A4 (mm)	A5 (mm)	A6 (mm)	A7 (mm)
4th	U-U-S	Test	8.1	3.3	13.3	13.1	12.1	13.1	21.2	20.0
		Model	7.6	3.5	13.2	12.7	13.1	12.3	20.7	19.9
		Error [%]	5.2	-6.7	1.0	2.8	-8.2	6.0	2.4	0.4
5th	U-U-Dx	Test	15.9	3.0	6.4	8.8	11.7	9.2	-18.3	38.9
		Model	18.0	2.8	6.9	8.2	10.5	10.0	-15.8	35.6
		Error [%]	-13.5	6.6	-8.0	7.0	10.3	-9.4	13.4	8.4
6th	U-U-Sx	Test	-12.7	2.1	11.9	9.5	7.0	14.6	46.8	-24.3
		Model	-13.6	2.3	11.1	9.4	7.3	13.1	42.7	-21.5
		Error [%]	-7.3	-12.4	6.8	1.3	-4.2	10.5	8.9	11.6
10th	U-S-S	Test	2.3	3.3	10.9	10.4	9.9	11.0	19.0	19.2
		Model	2.2	3.5	10.4	10.2	9.6	10.5	17.9	19.0
		Error [%]	5.5	-7.6	5.0	2.5	2.9	4.9	5.9	1.2
11th	U-S-Dx	Test	10.4	3.2	6.6	9.2	11.7	9.4	-18.9	33.0
		Model	11.3	3.1	7.1	8.7	11.3	9.9	17.7	31.6
		Error [%]	-8.6	3.2	-7.5	5.3	2.8	-5.7	6.5	4.5
12th	U-S-Sx	Test	-7.9	1.8	13.6	10.3	7.3	14.3	44.1	-23.8
		Model	-8.2	1.9	13.2	10.2	7.3	14.3	44.1	-23.1
		Error [%]	-3.8	-7.4	2.9	0.8	-3.7	-7.4	2.3	2.7

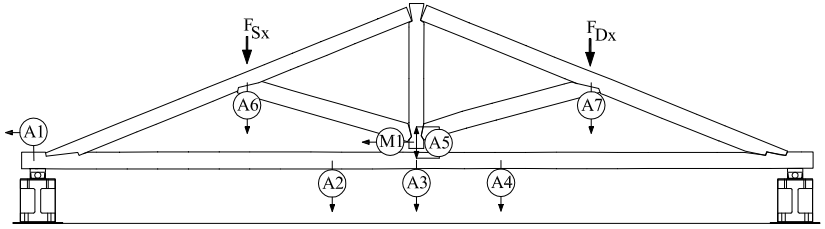


Table 6.12 presents the non-linear behaviour adopted for each Nlink in the numerical model. The theoretic stiffness values used as references are also reported.

Finally, a sensitivity study on the influence of some key parameters in the performance of the numeric model was performed. Based on the results obtained it is possible to conclude:

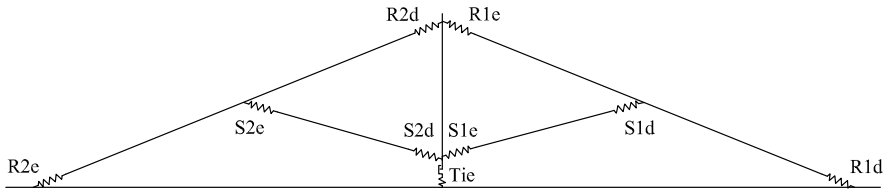
- The consideration of variable cross sections for the timber elements has no significant importance, except near the connections;
- The axial stiffness assumed for each connection is crucial;
- The behaviour of the tie beam-king post connections is very important for the overall behaviour of the truss evaluated, in particular, under non-symmetric loading and unstrengthened conditions;
- Without any strengthening some connections, in particular those that under non-symmetric loading present reverse loads, show a significant reduction of the shear stiffness and a low moment rotation capacity;
- Strengthening improves the global behaviour of the truss, decreasing the deformations, reducing the distortion of the system and making possible the moment-rotation capacity of the connections to develop.

6.4.7 Conclusions

The load-carrying tests of both trusses were preceded by an extensive ND evaluation of the timber elements. Weak correlations between the ND tests performed and destructive tests were obtained. Even in laboratory conditions, when evaluating old timber elements with real dimensions (and not using manufactured specimens) ND evaluation is a very hard task that should be based on wider range of ND tests available. The detailed geometric assessment performed has revealed to be of crucial importance, not only in the interpretation of the ND evaluation but especially in the the analysis of the load-carrying tests observations and results. Load-carrying tests confirm the need to strength connections. Strengthening improves the resistance of the trusses and, in particular, their overall behaviour under non-symmetric loading conditions. The connections between the tie beam and the rafters and the tie connection that suspend the tie beam to the king post are the most important. The first are the most loaded and the last has particular importance when the truss is subjected to distortion, caused specially by non-symmetric loads. The geometry of the connections is shown to have significant influence in the behaviour of the connection and, consequently, in the truss behaviour. The numerical analysis of the load-carrying tests performed on *Truss* 2 adopted the models suggested on Chapter 5 for the semi-rigid behaviour of traditional timber connections. The calibration process undertaken permitted to assess the effectiveness of the models proposed for traditional timber connections, on the structural analisys of full-scale timber trusses.

Table 6.12: Nlinks stiffness values used on numeric analysis of the load-carrying tests on *Truss 2*.

Test	Nlink							
	R1e	R1d	R2e	R2d	S1e	S1d	S2e	S2d
	Stiffnesss theoretical values							
Axial (kN/m)	403618	788889	846051	177485	121043	359403	409521	196793
Shear (kN/m)	∞	∞	∞	∞	∞	∞	∞	∞
Rotational (kNm/m)	700	1500	1500	700	700	1500	1500	700
	Adopted values							
	Axial Stiffness (kN/m)							
U-U-S	$*$	$*$	$*$	$*$	$*$	15952	20940	$*$
U-U-Dx	$*$	$*$	$*$	$*$	∞	$*$	$*$	∞
U-U-Sx	$*$	$*$	$*$	$*$	∞	$*$	$*$	∞
U-S-S	$*$	∞	∞	$*$	$*$	20952	20940	$*$
U-S-Dx	$*$	∞	∞	$*$	∞	$*$	$*$	∞
U-S-Sx	$*$	∞	∞	$*$	∞	$*$	$*$	∞
	Shear Stiffness (kN/m)							
U-U-S	$*$	$*$	$*$	$*$	$*$	$*$	$*$	$*$
U-U-Dx	$*$	$*$	0	0	$*$	$*$	0	$*$
U-U-Sx	$*$	4000	0	0	$*$	$*$	0	$*$
U-S-S	$*$	∞	∞	$*$	$*$	$*$	$*$	$*$
U-S-Dx	$*$	∞	∞	0	$*$	$*$	0	$*$
U-S-Sx	$*$	∞	∞	0	$*$	$*$	0	$*$
	Rotational Stiffness (kNm/m)							
U-U-S	$*$	$*$	$*$	$*$	$*$	$*$	$*$	$*$
U-U-Dx	0	$*$	$*$	0	0	0	0	0
U-U-Sx	0	$*$	$*$	0	0	0	0	0
U-S-S	$*$	$*$	$*$	$*$	$*$	$*$	$*$	$*$
U-S-Dx	$*$	$*$	$*$	$*$	$*$	$*$	$*$	$*$
U-S-Sx	$*$	$*$	$*$	$*$	$*$	$*$	$*$	$*$



$*$ equal to the theoretical value

Chapter 7

Field load tests on full-scale timber trusses

7.1 Abstract

In-situ cyclic tests on an existing traditional timber truss were performed. The main goal of the tests was to evaluate the overall behaviour of the timber truss under symmetric and non-symmetric loading. Moreover, the influence of the location of point loads application, without and with eccentricity relatively to joints, was assessed. The carrying tests were preceded by a visual and non-destructive inspection aiming to collect geometric data and to assess the decay level. The field tests results of a queen-post truss are presented and analyzed. A numerical model was developed to reproduce the test results.

7.2 Introduction

The lack of practical, but realistic, numerical models for the simulation of the behaviour of joints in traditional timber structures normally leads to the replacement of old roof structures, instead of their retrofitting to satisfy safety and serviceability requirements present in recent Codes and Recommendations. Moreover, the misunderstanding of the global behavior of traditional timber roof structures can result in unacceptable stress distribution in the members, as a result of inappropriate joints strengthening, in terms of stiffness and/or strength (Parisi and Piazza, 2000). To overcome this need, laboratory tests on scaled or full-scale specimens of members, connections and trusses can be done. However, only with field-tests the behaviour in real conditions can be evaluated. Field tests on traditional timber trusses are not common. Researchers (Del Senno and Piazza (2003), Piazza et al. (2005) and Branco et al. (2008a)) have preferred to transport the full-scale specimens to laboratory. In-situ working conditions are a barrier and the setup implementation (measurement system and load application) is often difficult. The work presents the field test results of a timber queen-post truss under symmetric and non-

symmetric loading. The influence of the number of point loads was studied. The truss has been characterized with regard to geometry, material properties, material decay using non-destructive tests methods. A numerical analysis has been developed to reproduce the test results.

7.3 Preliminary tests

Three trusses have been evaluated through field load tests: Adico princess-post truss, Luanda princess-post truss and Adico queen-post truss. However, only the last example was able to produce acceptable results. In the precedent tests, the low level of load applied and the less accurate measurement system used avoid to turn out reliable results. The Adico princess-post truss belongs to the roof structure of one zone of the Adico industry, located at Avanca (55 km South from Oporto). The roof, covered with ceramic tiles, have a free span of 12.7 m with a slope of 26º. The timber members made of Maritime pine (*Pinus pinaster*, Ait.) presented cross-sections of 95×150 mm^2 for the posts, 95×180 mm^2 for the struts and rafters and 95×220 mm^2 for the tie beam and king post (Figure 7.1). In the tests, water containers were used as loads, applied in the joints below the purlins and the ridge (5 point loads) and eight dial gauges were used to record the most relevant displacement. Symmetric and non-symmetric tests were performed applying a total load of 5 kN. The load applied in the tests has revealed to be insufficient to obtained reliable measurement using the dial gauges.



Figure 7.1: Adico princess-post truss.

The second truss evaluated belongs to the roof structure of the Central Post Office in Luanda (Angola). The truss made of Iroko (*Milicia excelsea*) had a free span of 14.75 m and a typical princess-post truss configuration. All timber members have a width of 100 mm while the height vary from 200 mm in the case of the posts and struts, 250 mm for the rafters and king post and 280

mm for the tie beam. The timber members are in good conditions and the connections presents deep steps and metal devices (Figure 7.2).



Figure 7.2: Luanda princess-post truss configuration and connection detail.

Cement bags, over wood pallets suspended in the truss by steel cables were used as point loads. The point loads applied in the joints below the purlins and the ridge (5 point loads) reached a total load level of 10 kN. Displacements of the most important joints were measured using rulers and tapes. The tests were performed by the workers responsible for the building rehabilitation following the test procedure send from Portugal by the author of this work. Again, in consequence of the low stresses applied in the truss and the minor reliability of the measurement system available, the tests results obtained show an unreliable behaviour of the truss evaluated.

7.4 Adico queen-post truss

The queen-post timber truss evaluated belongs to the roof structure of an old warehouse of Adico industry, located at Avanca (55 km South from Oporto). The exact date of the construction is not known but the industry exists since 1920 and some plans of the village from 1942 already show the warehouse. Trusses are the main elements of the roof structure, covered with ceramic tiles, 27^{o} slopes and rafters spaced 50 cm over the purlins and the ridge. The free span of the trusses is 11.8 m and the average distance between their centres is 3.5 m. The geometry of the truss is particular: the configuration is typical of a king-post truss, but queen posts were added connecting the joint strut-rafter to the tie beam. This is not the traditional queen-post truss geometry, in which the king post is substituted by a straining beam connecting horizontally (in the superior part) the two queen-posts, those located below the higher purlin, and the struts connecting the bottom part of the queen-posts to the lower purlins. Clearly, it is an example of a timber truss with an incorrect configuration for the span of the roof. The correct queen-post truss geometry should have been used or two extra posts (princess posts) should have been located below the lower

purlin. Point loads out of the joints, causing bending moments in the rafters, are the most common error detected in the preliminary survey performed in previous steps of the research program, see Branco et al. (2006). The truss is made of maritime pine (*Pinus pinaster*, Ait.). The timber members of the truss are slender, as characteristic of traditional Portuguese roofs structures, with cross-sections varying from 80×145 mm^2 for the struts to 80×220 mm^2 for the tie beam. The tie beam is suspended to the posts by iron straps nailed into the posts. Between the tie beam and the king post there is a gap of 5 cm while queen posts are in contact with the tie beam. Connections between the others timber members are made by single step joints, in some cases nailed, and the queen posts-rafters connections have a heel strap nailed (25 mm wide and 5 mm tick), Figure 7.3.

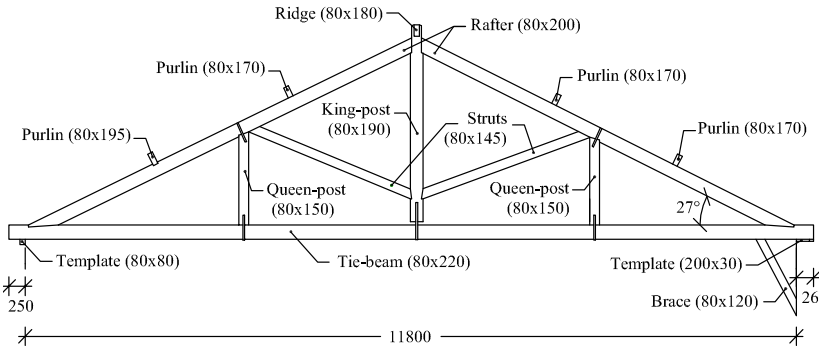


Figure 7.3: Truss geometry (mm).

Despite the apparent good condition of the timber members of the truss, the visual inspection revealed insects attack in the tie beam, queen posts and struts. In these timber members, emergence holes over the surface of sapwood are visible however, without signs of active infestation, Figure 7.4.



Figure 7.4: Emergence holes over the surface of sapwood.

To evaluate the extension of decay in the timber truss, Figure 7.5, Pilodyn® and Resistograph® non-destructive tests were performed. The Pilodyn 6J was used with the aim to assess the surface hardness through the depth penetration of the pin steel (2.5 mm) measured in each test performed. Resistograph permits to plot profiles (drill resistance versus penetration depth) that can be used to determine the location and extent of voids, allowing the calculation of the residual cross section, since decayed wood presents lower penetration resistance, see Figure 7.6, and variation in material density.

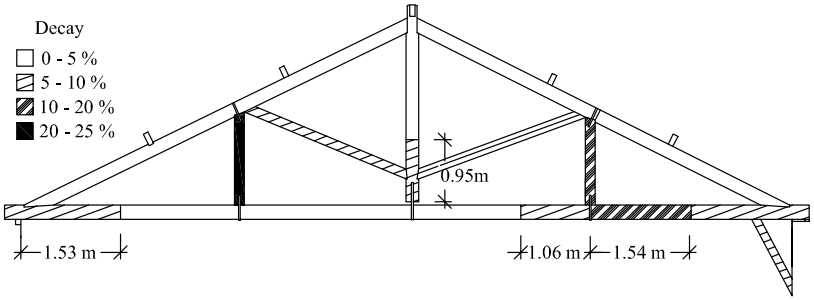


Figure 7.5: Map of the decay extension in the truss.

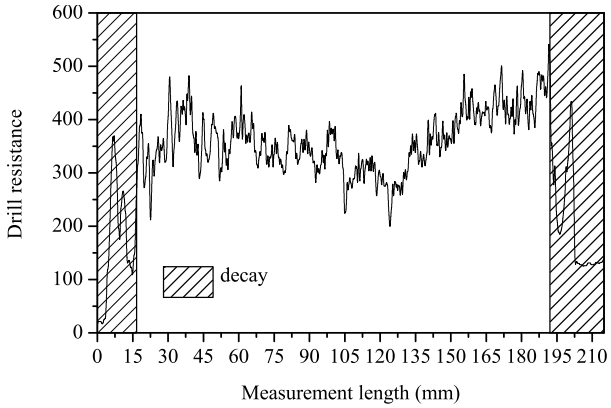


Figure 7.6: Calculation of the cross-section reduction based in a Resistograph test profile.

7.5 Test setup, instrumentation and procedure

The main goal of the tests was to evaluate the overall behaviour of the timber truss selected under symmetric and non-symmetric loading. Moreover, as

consequence of the roof structure definiton, the influence of the point loads location, without and with eccentricity relatively to joints, was assessed. Therefore, firstly, points loads were applied in the joints (F_1, F_2 and F_3) and, in a second step, loads were applied over the purlins and ridge (F_1, F_4, F_5, F_6 and F_7). Loading and unloading were recorded and an attempt to measure the creep of the structure under symmetric loading was made. The behavior of the truss under non-symmetric loading was evaluated, in the first scheme, only by one test and in the second with two tests (one in each pitch side). Table 7.1 resumes the tests performed.

Wood pallets suspended in the truss by four steel cables (ϕ 6 mm) supported the 35 kg cement bags used as loads. Each loading and unloading procedure was divided in steps of 175 kg (5 bags). A total load of 2625 kg (3×875 kg) and 2975 kg (5×595 kg) was used in the first (three point loads) and second (five point loads) schemes, respectively. The difference in the maximum load value applied between both schemes, 350 kg, is due to the difficulty to increase the number of bags over the pallets in the first case. To record the deformation of the truss during the tests, eight LVDTs (Linear Variable Differential Transformer) and six dial gauges (DG) were used. LVDTs were responsible for measuring the global displacement (LVDTs 1 to 3), the behavior of the king post-tie beam connection (LVDT-5) and the displacement below the purlins (LVDTs 4 to 8) also used to calculate the rotational behavior of the joints rafter-tie beam and rafter-strut. The values of the LVDTs during the tests were acquired by a Data Acquisition System, with 8 channels, using LabVIEW (2007) software package. Dial gauges measured the opening of the queen post-tie beam connections (DG 3 and 4), the horizontal displacement of the rafter in the rafter-tie beam connections (DG 5 and 6) and two additional points to calculate the rotation of rafter-tie beam connections (DG 1 and 2). Figure 7.7 shows the instrumentation used in the tests performed.

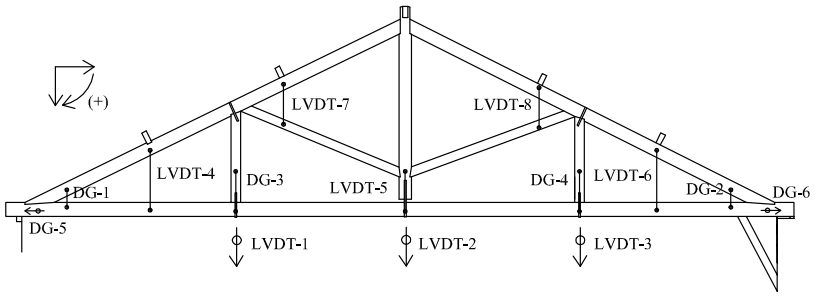
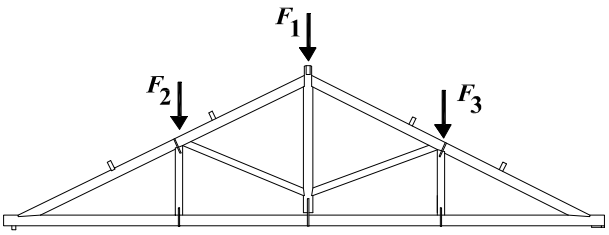


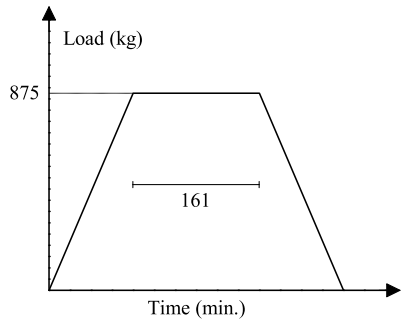
Figure 7.7: Instrumentation of the tests. Eight LVDTs and six DGs.

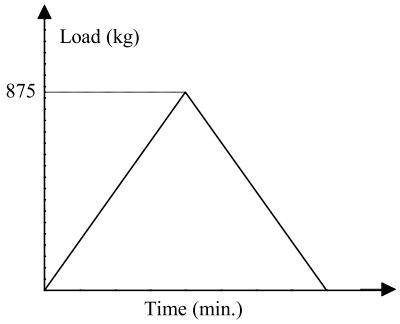
In every loading and unloading step the displacement values of the LVDTs were recorded; however, in the case of the dial gauges, only some steps were acquired, as results of the little variation verified.

Table 7.1: Summary of the tests performed.

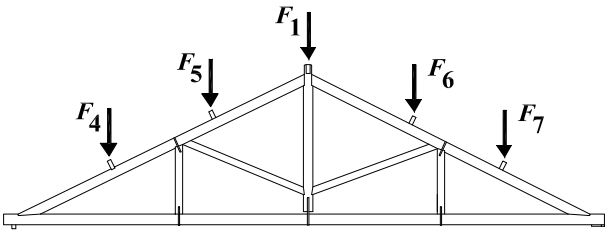


Procedure

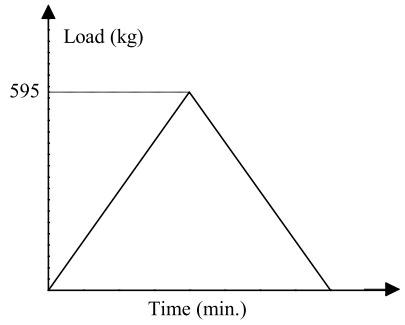


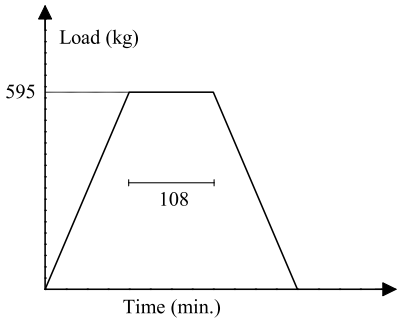


Test	Point loads	Test	Point loads
3FC	F_1, F_2 and F_3	3FN	F_3



Procedure





Test	Point loads	Test	Point loads
5FS	F_1, F_4, F_5, F_6 and F_7	5FC	F_1, F_4, F_5, F_6 and F_7
5FN1	F_6 and F_7		
5FN2	F_4 and F_5		

7.6 Analysis of the test results

The behaviour of the traditional timber trusses even under symmetric loading is non-symmetric. The response of traditional timber trusses is highly depending on the variability of the timber member cross-sections, material properties, connections, supports and loading conditions. When using a natural and anisotropic material like wood, it was impossible for carpenters, sometimes in extremely difficult working conditions, to avoid that variability during construction. Moreover, in the case of old constructions, due to decay processes and lack of maintenance, this heterogeneity is emphasized. The field test results confirm that the truss under investigation presents a non-symmetric behavior even when subjected to symmetric loading conditions (Figure 7.8).

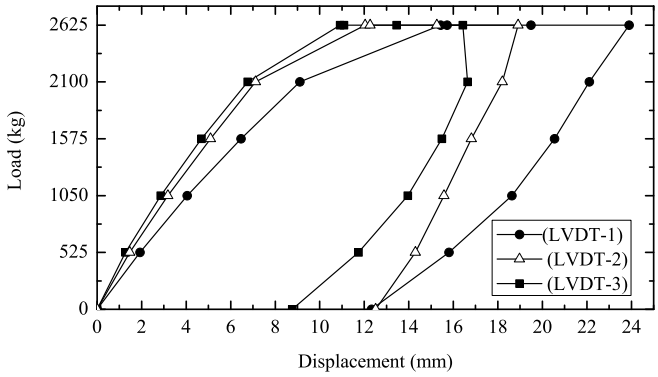


Figure 7.8: Displacement recorded by LVDTs 1, 2 and 3 during 3F-C test.

The difference observed between the displacement-load curves of LVDT's 1, 2 and 3 can represent the influence of the decay observed in the left queen-post. The constant load rate applied during 161 minutes (see Table 1) results in a deformation increment of the truss (creep). The truss presents important plastic deformations (average value of 57%) after the complete unloading. The king post-tie beam connection works effectively, i.e. the tie beam is suspended to the king post (see Figure 7.9).

The heel strap is able to suspend the tie beam, reducing therefore the deformation of this element (see LVDT-2 in Figure 7.8), and presents also creep, however, less than the one presented by the wood members. The connections between the queen posts and the tie beams, where a heel strap suspended the tie beam, show different behaviours (Figure 7.10). Just the left connections, measured by DG-3, in the second series of tests (5F, 5 point loads), behave properly - the tie beam is suspended to the queen post. In the first series of tests, both connections present residual deformations. Therefore, it can be concluded that, before the tests, those connections were dismantled. The first series of tests were sufficient for the left connections to recover, while the gap

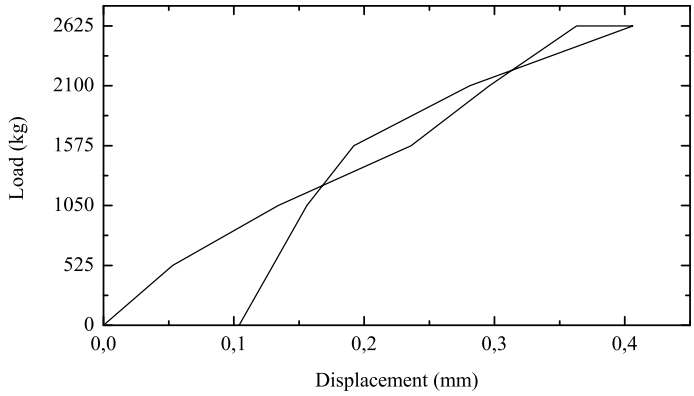


Figure 7.9: Behaviour of the king post-tie beam connection during 3F-C test.

between both connected elements existing in the right connection was never recovered.

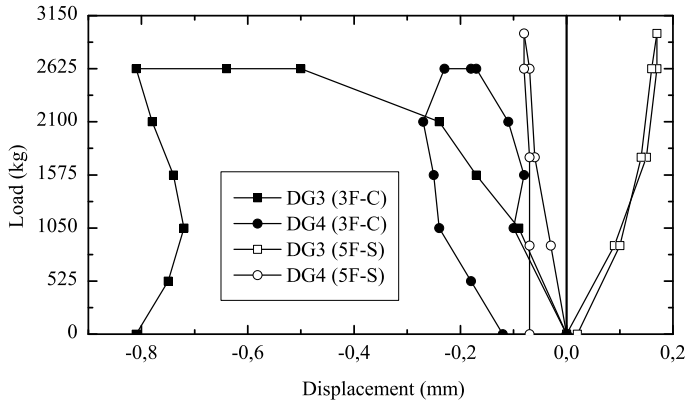
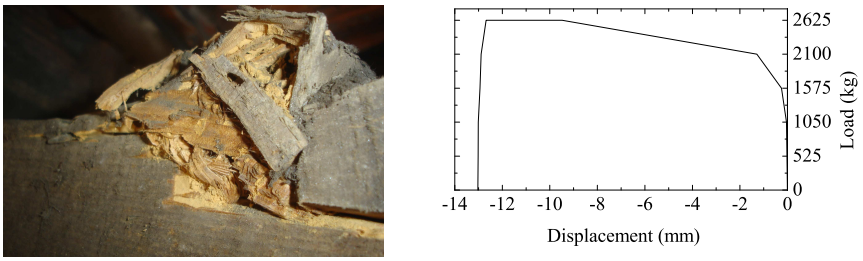


Figure 7.10: Behaviour of the connections between the queen posts and the tie beams during 3F-C and 5F-S tests. Negative values are recorded when the two elements are approaching.

During the 3F-C test, significant damage was detected on the left rafter-tie beam connection, over the DG-5 (Figure 7.11a). Damage started for a point load level of 700 kg and with 850 kg the measurement of the DG-5 only became stable after 30 minutes. At the end of the loading period, the maximum relative horizontal displacement between the rafter and the tie beam (measured by DG-5) was reached and no recover was observed during and after the unloading procedure (Figure 7.11b).

Under non-symmetric loading, as the one imposed during the test 3F-N,



(a) Damage (b) Load-displacement curve of DG-5

Figure 7.11: Behaviour of the left rafter-tie beam connection during 3F-C test.

distortion of the truss is observed, in particular, in the tie beam, as shown in Figure 7.12. Non-symmetric behaviour is acquired by LVDT-1 and 3 with lower values in the first LVDT as consequence of the bigger stiffness (compression of the left queen-post). Dividing the total amount of load applied by more point loads in the second tests series, from 3 to 5, the same general conclusions about the asymmetric behaviour of the truss, even when subjected to symmetric loading, can be drawn. The main difference between the tests under 3 and 5 point loads is, in the second case, the introduction of significant bending stresses in the rafters.

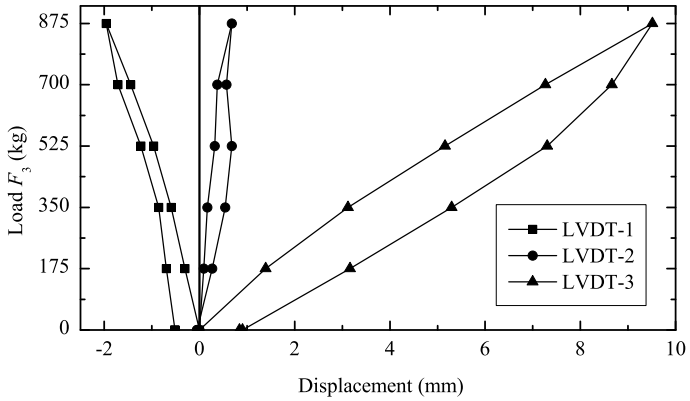


Figure 7.12: Displacement recorded by LVDTs 1, 2 and 3 during 3F-N test.

As a consequence, greater values of rotation in the connections are obtained (Figure 7.13) while the global displacements are lower (Figure 7.14), when compared with the 3 point loads case. In the first case the system is more rigid.

Applying the loads with eccentricity relatively to joints, the main stresses are found in the rafters, caused by bending, and greater rotations of the rafter-struts and rafter-tie beam are obtained. When the point loads are applied

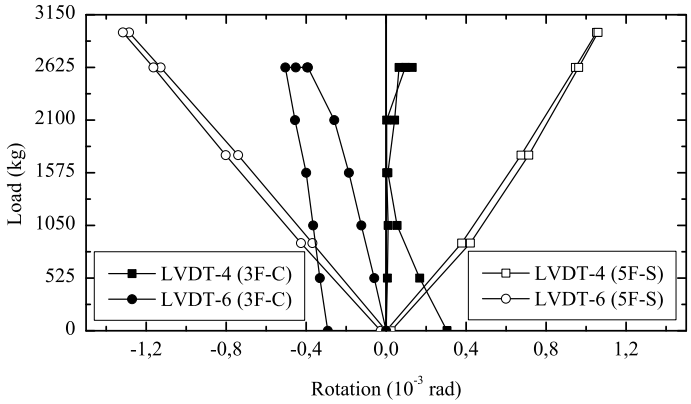


Figure 7.13: Comparison between rotations calculated based on values recorded by LVDTs 4 and 6 during 3F-C and 5F-S tests.

directly in the joints, the main stresses are observed in queen posts (compression), pushing the tie beam down. As a consequence, LVDTs 1, 2 and 3 show higher values of displacement (see Figure 7.14). In addition, the creep behaviour observed in the case of three point loads (3F-C) is significantly greater but, in this case, the influence of the damages observed in the rafter-tie beam connection must be taken into account.

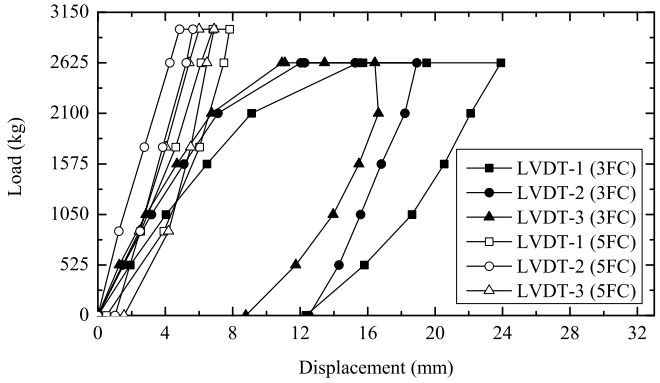


Figure 7.14: Comparison between the displacements recorded by LVDTs 1, 2 and 3 during 3F-C and 5F-C tests.

7.7 Numerical Analysis

The structural analysis program SAP2000 (2007) has been used to model the field tests carried out. The model developed follow the assumptions made in the previous model of Chapter 6 tests. Linear beams elements, with the material properties suggested by LNEC (1997) for the Maritime pine wood, connected through semi-rigid joints, modelled using nonlinear link elements (Nlinks), were used. The Nlinks elements, used in all connections between timber elements of the truss, placed in the end of the connected elements with a negligible length, are characterized by one axial stiffness (see eqn 5.4) and the rotational stiffness defined by means of a $M-\phi$ law proposed in Chapter 5. It is also important to point out that the conclusion of the diagnosis phase carried out were introduce in the model, in particular, the cross-section have been reduced according to the map of decay (see Figure 7.5).

7.8 Numerical *versus* tests results

Numerical modelling and experimental results have been compared. First, *Step* 0, the numerical model has been implemented without considering the real behaviour of the truss observed in the performed tests. Then, *Step* 1, the model was verified and calibrate based in the tests results. Symmetric tests were used essentially to calibrated the axial stiffness of the connections while rotational stiffness have been adjusted with asymmetric tests results. In the following the main conclusions of the model effciency are discussed and presented.

7.8.1 Symmetric tests

Using the calculate axial stiffness at the connections, *Step* 0, the computed values for the global displacements (LVDT 1 to 3) represents only 33% of the test results obtained for the first test (3F-C). The main reason for this difference is the fact that all connections, in particular the ones between the posts and the tie beam, showed significant gaps between the metal devices and the joint itself. Moreover, the deterioration and loss of strength of the steel elements are not considered in the calculated stiffness values. The gaps between the metal devices and the joints are confirmed by the tests results (see Figures 7.9 and 7.10). It is also important to point out that the plastic deformation measured in the global displacement after the 3F-C test represents 52%, 66% and 53% of the maximum displacement, respectively for LVDT 1, 2 and 3. In the case of the relative displacements measured in the tie beam-posts connections, the residual values represents 57%, 100% and 52% of the maximum displacement recorded at LVDT-5, DG-3 and DG-4, respectively. Therefore, the stiffness values calibrated for the first tests performed, 3F-C, should be only account as informative because they report the influence of the original gaps existing between the metal devices and the joints. It is important to note that during the first test, 3F-C, a significant damage of the left rafter-tie beam

connections was detected (Figure 7.11) which influences directly the global displacements values. However, the calibrated model was able to reproduce the non-symmetric response of the truss even under symmetric loading conditions applied during the 3F-C test (Figure 7.15).

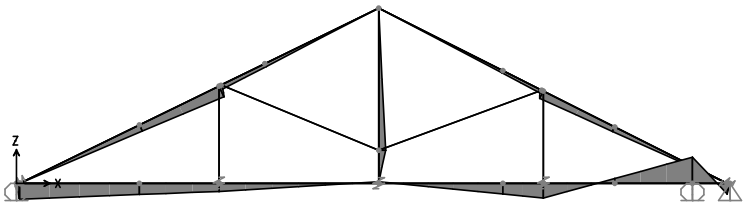


Figure 7.15: Bending moment on the truss in the 3F-C test.

Table 7.2 gives a comparison between experimental and numerical results for both symmetric tests performed with regard to the displacements in the relevant joints of the truss. The values reported in Table 7.2 are the maximum displacement of the symmetric tests performed.

Table 7.2 show a good fit between the values worked out by means of the numerical model and the experimental results, with exception of the LVDT-2 and 3 values, all errors reported by the numerical model are under 10%. Experimental results for the global vertical displacement of the truss under the king post are clearly increase by the numerical model. This inconsistency can be explained by the faulty connections between the king post and the tie beam. The heel strap must introduce a "frictional stiffness" which reduces the mid-span deformations of the tie beam when the truss is loaded. Ideally, in the tie beam-post connections it shall be used a heel strap, nailed only in the post, suspending the tie beam with a connection without bending stiffness.

The calibration process of the numeric model shows that during the experimental campaign a stiffness updating of the connections occurs (Table 7.3). This conclusion, confirmed by the test results (see Figure 7.14), is due essentially to the fact of the connections were originally dismantled (significant gaps existed between the metal devices and the joints). When using the numeric models calibrated for the case of symmetric tests under non-symmetric loading conditions, a significant discrepancy is obtained between the numeric and experimental results. In particular, the global displacement, LVDT-1, 2 and 3, and the connections between the tie beam and the posts, recorded by DG-3, DG-4 and LVDT-5 are sensible to the connections rotational stiffness.

7.8.2 Asymmetric tests

Calibrated the axial stiffness of the connections based on the test results achieved through the symmetric tests, the asymmetric tests were used to evaluated the influence of the rotational connection's stiffness in the overall behaviour of the truss during the tests performed. In this process the chronology

Table 7.2: Comparison between numerical values (Num.) and tests results (Exp.). Error express in (%).

Test 3F-C								
Global displacement (mm)								
LVDT-1			LVDT-2			LVDT-3		
Exp.	Num.	Error	Exp.	Num.	Error	Exp.	Num.	Error
15.40	15.25	0.9	12.00	13.71	14.3	10.90	9.64	11.6
Relative displacement (mm) - tie beam-posts connections								
DG-3			LVDT-5			DG-4		
Exp.	Num.	Error	Exp.	Num.	Error	Exp.	Num.	Error
-0.64	-0.69	2.8	0.36	0.35	2.8	-0.18	-0.17	7.4
Relative displacement (mm) - rafters-tie beam connections								
DG-5			DG-6					
Exp.	Num.	Error	Exp.	Num.	Error			
-0.25	-0.26	4.6	0.18	0.19	6.7			
Test 5F-S								
Global displacement (mm)								
LVDT-1			LVDT-2			LVDT-3		
Exp.	Num.	Error	Exp.	Num.	Error	Exp.	Num.	Error
7.53	7.98	6.0	4.48	4.94	10.3	5.30	5.40	2.0
Relative displacement (mm) - tie beam-posts connections								
DG-3			LVDT-5			DG-4		
Exp.	Num.	Error	Exp.	Num.	Error	Exp.	Num.	Error
-0.17	-0.18	7.6	0.14	0.14	2.9	0.07	0.07	4.3
Relative displacement (mm) - rafters-tie beam connections								
DG-5			DG-6					
Exp.	Num.	Error	Exp.	Num.	Error			
-0.28	-0.30	7.1	0.11	0.10	7.0			

Table 7.3: Axial stiffness values (kN/m) used in the numerical model.

Test	DG-5	DG-6	DG-3	DG-4	LVDT-5
3F-C	3900	10000	4000	3400	12000
5F-S	292108	250169	4000	7000	30000

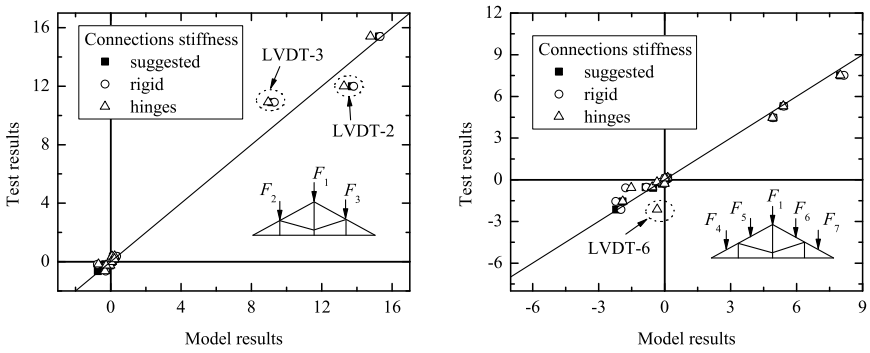
of the tests was considered, assuming the axial stiffness values as the ones calibrated in the previous symmetric test model. Therefore, in the model concerning the 3F-N test, the axial stiffness assumed for the connections were derived from 3F-C test and, the values assumed in the models of 5F-N1 and 5F-N2 tests, were based on the axial stiffness values calibrated through 5F-S test model. However, during the calibration process of the model, it was necessary to update the axial stiffness of some connections of the 3F-S test model. That fact allows to concluded that, after 3F-C test, the response of the connections were still unstable, still depending of the gaps existing between the connected surfaces, like the calibration process of the axial stiffness of the connections have shown (see Table 7.3). During the test history performed, the gaps of the connections were reduzed and the stiffness of the connections increased. Table 7.4 shows the axial stiffness values updated during the calibration process of the 3F-N test model.

Table 7.4: Axial stiffness values (kN/m) used in the numerical model of 3F-N test.

Test	DG-5	DG-6	DG-3	DG-4	LVDT-5
3F-N	292108	17000	4000	7000	16000

In the numeric model of the tests performed the rotational stiffness properties assumed were directly derived from the work presented in previous Chapter. Bilinear $M - \phi$ laws were assumed for the Nlinks elements responsible to modelled the semi-rigid behaviour of the connections. The model results were compared with the tests results and a sensitivity study of the connections rotational stiffenss value was performed. Therefore, beyond the suggested values, the two extremes rotational stiffness models, rigid joints and perfect hinges, were studied. As expected, the connections rotational stiffness can be important under non-symmetric loading conditions and negligible for symmetric loading conditions. The numeric results (Figure 7.16) shows that the influence of the rotational stiffness assumed for the connections under symmetric loading conditions (3F-C and 5F-S tests) is trivial. The rotational stiffness assumed for the connections can change the deformation of the truss but, those variations are not important. The same is not true for tests under non-symmetric loading conditions. Figure 7.17 shows that the rotational stiffness assumed for the connections as direct consequences in the truss behaviour under asymmetric tests.

The connections rotational stiffness importance in the truss behaviour raise with the truss distortion introduced through the tests. In the case of 5F-N1 and 5F-N2 tests, the truss distortion caused by the tests increases and the response of the truss becames more dependent to the rotational stiffness propoerties adopted for the connections. In particular the global displacement of the truss, measured by LVDT's 1, 2 and 3, are sensible of the connections rotational



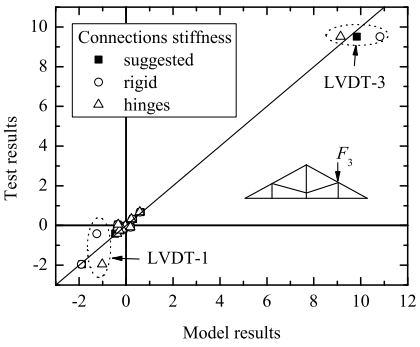
(a) 3F-C (b) 5F-S

Figure 7.16: Rotational stiffness of connections influence in the model results in comparison with test results under symmetric loading.

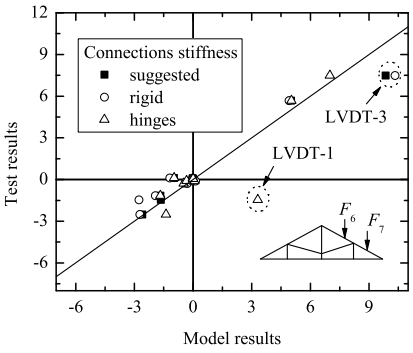
stiffness. The variations reported by the numeric models are not only in the displacement value measured but, as in the case of LVDT-1 during the 5F-N1 tests considering rigid connections, in the signal. In this particular case, while the test result for the LVDT-1 is -1.452 mm (the minus sign corresponds to a lift of the point) the model with rigid joints presented a +3.317 mm displacement for the same point. This modification in the deformation of the truss as natural consequences in the stresses distribution. However, this change in the stresses distribution is not important in terms of maximum value.

7.9 Conclusions

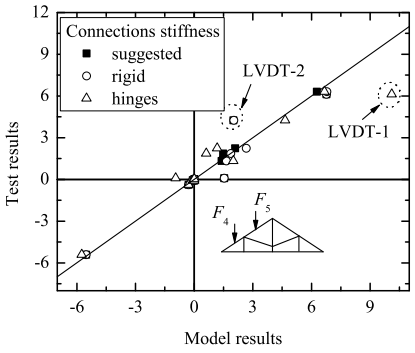
The work results highlight the importance of the *in-situ* experimentation, to assess the global behaviour of traditional timber trusses, identify the critical areas, to plan the upgrade interventions and to quantify their effects. Experimentation gave an insight of the truss behaviour hardly reachable otherwise. The effects of the incorrect truss configuration for the roof span, the faulty connections geometry and the existing gaps in the joints in the overall behavior of the truss tested were assessed. The numeric model implemented through a general purpose and very simple finite element code SAP2000 (2007) has proved to be an effective and accurate method of modelling timber truss behaviour, on condition that a semi-rigid behaviour of the traditional connections is assumed. The comparison between the tests results and the ones achieved by the numerical models shows that the rotational stiffness assumed for the connections has particular importance for the truss behaviour in terms of deformations under non-symmetric loading conditions, and the magnitude raise with the distortion introduced into the truss.



(a) 3F-N



(b) 5F-N1



(c) 5F-N2

Figure 7.17: Rotational stiffness of connections influence in the model results in comparison with test results under non-symmetric loading.

Chapter 8

Conclusions and Recommendations

8.1 Conclusions

The thesis aimed to assess the influence of the joint stiffness in the monotonic and cyclic behaviour of traditional timber trusses identifying and evaluating different strengthening techniques with metal devices. The work is based on three important experimental campaigns. First, an extensive experimental evaluation of the monotonic and cyclic behaviour of traditional timber connections, through full-sacle specimens was performed. Strengthened specimens with traditional metal strengthening techniques have been also evaluated. Then, in Italy, two dismantled King-post trusses were evaluated. After an accurate geometric and mechanical evaluation of the timber members, the truss were assembled and tested through cyclic tests under symmetric and non-symmetric loadging conditions. In a second phase, trusses were strengthened with techniques early studied. Finally, a timber truss example was tested in real conditions, *i.e, in situ*, through cyclic tests under symmetric and non-symmetric loading conditions and considering, or not, eccentricity of the point loads with respect to the truss joints. The results of the first tests allowed to calibrate semi-rigid behavioural models for the connections. The effectiveness of those models was then evaluated by comparing the results worked out by the numerical analysis and the ones reported during the tests.

After a short introduction, a chapter presents the results of a preliminary survey intending to describe must common geometries, materials and on site pathologies. Following a brief historic resume The overall structural behaviour of traditional Portuguese timber trusses is analysed and special attention is paid to structural connections and construction errors effects. The conclusion of this chapter were fundamental for the further work, specially, identiying the parameters to study and helping in the definition of the connections geometries and strengthening techniques to be assess. The structural study conclusions reinforce the necessity of the thesis goals.

In Chapter 3 a series of monotonic and cyclic tests on unstrengthened specimens were performed in order to characterize the original behaviour of connections representative of traditional timber trusses. Subsequently, connections strengthened with metal devices were tested under monotonic and cyclic loading. Tests on assembled connections were preceded by accurate material characterization, in terms of the mechanical properties of the timber elements used for all full-scale models. The tests results have confirmed similar works (Candelpergher (1999) and Palma and Cruz (2007)) conclusions:

- Traditional timber connections, even without any strengthening device, usually have a significant moment-resisting capacity;
- The moment-resisting capacity is function of the compression stress applied in the rafter and skew angle. Moreover, it is clear that the heigth of the rafter, the friction angle, the existence of mortise and tenon and the moisture content (Palma and Cruz, 2007) are also important;
- Strengthening, usually performed by insertion of metal devices, is indispensable for ensuring adequate joint response, in particular, for seismic loading, or in other adverse and unpredictable loading conditions;
- All strengthening techniques analysed results in a significant increase of the equivalent viscous damping ratio, higher resistance and significant improvement of the ductility. The energy dissipation became significant as more stables cycles are achieved;
- Between the strengthening techniques evaluated, the insertion of one bolt across the joint axis and metal stirrups positioned at the two sides of the joint, bolted to the timber elements, have given more favourable results.

Because it is impossible to evaluate all main parameters affecting the mechanical behaviour of traditional timber connection through tests, a parametric study, based on FEM results, was performed in Chapter 4. Unstrengthened connections test results were used to calibrate the model and then parametric studies were developed aiming to analyse parameters like coefficient of friction, skew angle, notch depth, rafter heigh and axial compression of the rafter. Numerical analysis have confirmed previous conclusions (Parisi and Piazza (2000) and Palma and Cruz (2007)). The rotational response and capacity is function of the joint geometry and parameters as friction and axial compression level of the rafter are of primary importance. The sensitivity study have shown that different parameters have distinct influence in the connections behaviour and, this influence depends, not only of the rotational direction, but also, of the skew angle. However, it is important to point out that deformation properties (stiffness) are less depending of the parameters analyzed. Briefly, it is possible to concluded that:

- The friction coefficient has influence in the connection response only under negative rotation;

- The connections stiffness is not affected but to a higher axial compression stress of the rafters corresponds a high resistance;
- The rotational capacity and stiffness of the connection decreases with the skew angle. This dependency is not linear and, in the particular case of connections response under negative rotation, the skew angle increase results in a more fragil behaviour;
- in a correct joint geometry definition, the notch depth as influence only in the response under negative rotation. If the connection geometry has a bad definition, as example, a slight deviation of 3 mm is consider in the cutting process of the notch, the influence of the notch depth moves to the positive rotation.
- The notch depth has influence only in the resistant capacity;
- Higher cross-section correponds to resistance and stiffness rising, however, stiffness shows to be less affected under positive rotation;
- Wood species, or in others words, the timber resistant class, shows to have a minor influence in the connection behaviour.

Based on the tests results and the parametric studies conclusions, semi-rigid models were adapted. Existing models where analysed, discussed and callibrated. After, the tests results on full-scale connections were reproduce in a numerical analysis considering those semi-rigid models. For that, synthetic Moment - Rotation curves, defined based in the monotonic tests results, were introduced in the SAP2000 (2007) commercial software. Using this software and the synthetic curves, cyclic tests of unstrengthened and strengthened connections were reproduced. The main achiving of that chapter is the possibility to use a commercial software to model the semi-rigid behaviour of traditional timber connections. Based on few parameters, that can be predict without test results, it is possible to reproduce the behaviour of unstrengthened and strengthened traditional timber connections under cyclic tests.

Chapter 6 presents the first step aiming to evaluate the importance of the semi-rigid modelling of traditional timber connections. Addition, the numerical analysis performed after the tests aloows to assess the effectiveness of the semi-rigid models suggested. Two dismantled Italian King-post timber trusses were tested under symmetric and non-symmetric cyclic loads. For the correct interpretation of the tests results, an accurate geometric and mechanical evaluation of the timber elements of the trusses was performed, based in grading results with data gathered from non-destructive tests (NDT), including mechanical evaluation of the modulus of elasticity in bending (MoE). The non-destructive evaluation pointed out some difficulties and limitations of using NDT in real structures, even if in laboratory facilities, and not over manufactured specimens. The NDT have reported a low effectiveness when applied in old timber elements. The significant variation in cross-section geometric properties and

the consequences of aging, shrinkage and degradation represents significant drawbacks in the application of those NDT.

The trusses were reassembled in laboratory and submitted to a series of symmetric and non-symmetric tests, according to the Limit States. Despite been similar, the behaviour under tests of both trusses was diverging. The global behaviour was asymmetric even under symmetric loading conditions, in both trusses, and, the overall response was function of local failures. The strengthening performed aimet at correcting local failures and improving the load capacity of the trusses. However, strengthening had influence in the overall behaviour of the trusses when the tests were repeated.

The load-carrying tests performed on both trusses allowed to confirm force mechanisms and local behaviours pointed out in the structural analysis performed in chapter 2.

In chapter 7, as final conclusion of the work, the behaviour of traditional timber trusses in real conditions is evaluated. The field tests confirmed the complexity behind the structural analysis of old timber trusses. Firstly, the safety level and load-carrying capacity of those structures are normally underestimated. Only after some attempts, and using a load level significantly higher than the predicted, the load tests were able to introduce the right level of deformations. Then the tests point out that the lack of maintenance is the most important enemy of the safety of those structures. Connections untied and degradation, in particular, in the rafter-tie beam connections and near of the supports, are the main responsible for significant decreases in the safety level of traditional timber trusses.

The numerical analysis performed allows concluding the importance of the use of semi-rigid models for the connections and the effectiveness of the models proposed in chapter 5.

8.2 Recommendations

This thesis is a result of an international research program envolving University of Minho (Portugal), University of Trento (Italy) and the Timber Structures Division of National Laboratory for Civil Engineering (Portugal). The work as been carried out in both Universities while others important parameters in the timber connections behaviour have been analyzed in the National Laboratory. The effect of aging, the presence of tenon and mortise and the effect of the moisture content are some examples of variables that have been studied in the Timber Structures Division of National Laboratory for Civil Engineering. Therefore, even the thesis results represents a step forward in the structural analysis of traditional timber trusses, the final conclusions and recommendations of the research program must be considered.

The work present in this thesis is a small contribution for the structural analysis of traditional timber connections and trusses. Further research is necessary to improve the effectiveness of the models behaviour proposed for traditional timber connections. Others geometries, in particular the double

step joint, and the effect of the presence of tenon and mortise must be analysed. The results of the complementary numerical analysis, using FEM, of the strengthened connections should be included in the semi-rigid models proposed.

However, the importance of the joint behaviour in the overall response of roof structures, the connection between the truss and the supports must be investigated. Specially, under seismic loading, the misunderstood of the connection truss-support behaviour can lead to improper conclusions.

Traditional timber trusses should be carefully analyzed, with the same level of detail that structures of others materials are studied. Because of their significance and constant presence in construction the importance of their correct modelling should not be neglected, with the risk that, with the underestimation of the resistance of those structures, in few years, they will disappear.

Bibliography

Abaqus (2007). *Abaqus/CAE User's manual. Version 6.7.* ABAQUS, Inc.

Alvarez, R., Martitegui, F., and Calleja, J. (1996). *Estructuras de madera - Diseño y cálculo.* Alvarez, R.A. and Martitegui, F.A.

Appleton, J. (2003). *Reabilitação de edifícios antigos. Patologias e tecnologias da intervenção.* Orion, Lisboa, Portugal.

Barbisan, U. and Laner, F. (2000). *Capriate e tetti in legno - progetto e recupero.* FrancoAngeli, Milan, Italy.

Bertolini, C., Brunetti, M., Cavallaro, P., and Macchioni, N. (1998). A non destructive diagnostic method on ancient timber structures: some practical application examples. In *Proceedings of the 5th World Conference on Timber Engineering*, volume 1, pages 456–465, Montreux, Switzerland.

Bodig, J. and Jayne, B. (1982). *Mechanics of wood and wood composites.* Van Nostrand, New York, USA.

Branco, J., Cruz, P., and Piazza, M. (2008a). Diagnosis and analysis of two king-post trusses. In *SAHC 2008: Structural Analysis of Historical Constructions*, Bath, UK, (Accepted).

Branco, J., Cruz, P., Piazza, M., and Varum, H. (2005a). Experimental analysis of birdsmouth joints. Technical Report E-11/05, Guimarães, Portugal.

Branco, J., Cruz, P., Piazza, M., and Varum, H. (2006). Behaviour of traditional portuguese timber roof structures. In *Proceedings of World Conference on Timber Engineering WCTE 2006*, Portland, USA.

Branco, J., Cruz, P., Varum, H., and Piazza, M. (2005b). Portuguese traditional timber trusses. static and dynamic behaviour. Technical Report E-19/05, Guimarães, Portugal.

Branco, J., Santos, A., and Cruz, P. (2008b). Traditional timber trusses: evolution, behaviour and strengthening with composites. *Revista Portuguesa de Engenharia de Estruturas.* Accepted.

Bulleit, W., Sandberg, B., Drewek, M., and O'Bryant, T. (1999). Behaviour and modelling of wood-pegged timber frames. *J.Struct. Engrg.*, 125(1):3–9.

Candelpergher, L. (1999). Sperimentazione, modellazione numerica e caratterizzazione sintetica del comportamento di collegamenti lignei tradizionali con elementi metallici. Master's thesis, Università Degli Studi di Trento.

Ceccotti, A. and Vignoli, A. (1990). Engineered timber structures: An evaluation of their seismic behaviour. In *Proceedings of the 1990 International Timber Engineering Conference*, pages 946–953, Tokyo, Japan.

Ceraldi, C., Mormone, V., and Ermolli, E. (2001). Resistographic inspection of ancient timber structures for the evaluation of mechanical characteristics. *Materials and Structures, RILEM*, 34:59–64.

CNR-DT 206 (2006). *Istruzioni per il progetto, l'esecuzione ed il controlo delle strutture di legno*. Decreto ministeriale, del ministero infrastrutture e trasporti, published on official gazettente nazionale italiano di unificazione.

Collins, M. and Kasal, B. (2001). Modelling of nonlinear hysterectic connections. In *PRO 22 - Proceedings of the International RILEM Symposium Joints in Timber Structures*, pages 543–549, Stuttgart, Germany.

Costa, F. (1955). *Enciclopédia Prática da Construção Civil*. Depositária Portugália Editora, Lisboa, Portugal.

C.T.E. (2006). *Documento Básico SE-M. Seguridad estructural - Estructuras de madera*. Acódigo técnico de la edificación, ministerio de vivienda.

Del Senno, M. and Piazza, M. (2003). Behaviour and rehabilitation of queen post timber trusses. a case study. In *Proceedings of the STREMAH 2003 Sixth International Conference Structural Studies, Repairs and Maintenance of Heritage Architecture VIII*, Halkidiki, Greece.

DIN 1052 (2004). *Entwurf, Berechnung und Bemessung von Holzbauwerk*. Allgemeine bemessungsregeln und bemessungsregeln für den hochbau.

Dinwoodie, J. (1989). *Wood: Nature's cellular polimeric fibre-composite*. The Institute of Materials, London, UK.

D.M. 14/9 (2005). *Norme tecniche per le costruzioni*. Decreto ministeriale, del ministero infrastrutture e trasporti, published on official gazettente nazionale italiano di unificazione.

Dolan, J. (1989). *The dynamic response of timber shear walls*. PhD thesis, University of British Columbia.

Dolan, J. (1994). Timber structures in seismic regions. *Materials and Structures*, 27(167):157–184.

Drdácký, M. F., Wald, F., and Mares, J. (1994). Modelling of real historic timber joints. In *Proceedings of the STREMAH 99 Sixth International Conference Structural Studies of Historical Buildings*, pages 169–178, Dresden, Germany.

Edlund, B. (1995). Tension and compression. In *Timber Engineering STEP 1*. Centrum Hout.

Ehlbeck, J. and Gorlacher, R. (1990). Zur problematik bei der beurteilung der tragfahigkeit von altem konstruktionsholz. *Bauen mit Holz*, 2(90):117–120.

EN 12512 (2001). *Timber structures - Test methods - Cyclic testing of joints made with mechanical fasteners*. European Committee for Standardization.

EN 338 (2003). *Structural timber - Strength classes*. European Committee for Standardization.

EN 384 (2004). *Structural timber - Determination of characteristics values of mechanical properties and density*. European Committee for Standardization.

EN 408 (2003). *Timber structures. Structural timber and glued laminated timber. Determination of some physical and mechanical properties*. European Committee for Standardization.

EN 518 (1997). *Structural timber. Grading. Requirements for visual strength grading standards*. European Committee for Standardization.

Eurocode 5 (2004). *EN 1995-1-1: Design of timber structures - Part 1-1: General - Common rules and rules for buildings*. European Committee for Standardization.

Eurocode 8 (2004). *EN 1998-1: Design of structures for earthquake resistance - Part 1: General rules, seismic actions and rules for buildings*. European Committee for Standardization.

Feio, A. (2005). *Inspection and Diagnosis of Historical Timber Structures: NDT Correlations and Structural Behaviour*. PhD thesis, University of Minho.

Fumanelli, M. (2001). Analisi teorico sperimentale del comportamento sismico di coperture lignee tradizionali. Master's thesis, Università Degli Studi di Trento.

Giordano, G. (1999). *Tecnica delle construzioni in legno*. Ulrico Hoepli, Milan, Italy.

Görlacher, R. (1991). Untersuchung von altem konstruktionsholz: Bestimmung des elastizitatsmodulus. *Bauen mit Holz*, 8(91):582–586.

Görlacher, V. (1987). Zerstörungsfreie prüfung von holz: ein in situ verfahren zur bestimmung der rohdichte. *Holz als Roh- und Werkstoff*, 45(7):273–278.

Götz, K.-H., Hoor, D., Möhler, K., and Natterer, J. (1993). *Construire en Bois - Choisir, concevoir, réaliser*. Presses Polytechniques et Universitaires Romandes, Lausanne, Switzerland.

Kasal, B. and Anthony, R. (2004). Advances in in situ evaluation of timber structures. *Progress in Structural Engineering and Materials*, 6(2):94–103.

King, W., Yen, R., and Yen, A. (1996). Joint characteristics of traditional chinese wooden frames. *Engrg. Struct.*, 18(8):635–644.

Kivell, B. T., Moss, P. J., and Carr, A. J. (1981). Hysteretic modelling of moment resisting nailed timber joints. *Bull. New Zeal. Nat. Soc. Earthquake Engineering*, 14(4):233–245.

Kollmann, F. and Cote, W. (1984). Principles of wood science and technology. *Springer*, pages 336–341.

LabVIEW (2007). *LabVIEW User's manual. Version 8.2*. National Instruments.

Larsen, H. and Jensen, J. (2000). Influence of semi-rigidity of joints on the behaviour of timber structures. *Prog. Struct. Engng Mater.*, 2:2767–2778.

Lear, G. (2005). Improving the assessment of in situ timber members with the use of non-destructive and semi-destructive testing techniques. Master's thesis, North Carolina State University.

LNEC (1997). *Madeira para construção - Pinho bravo para estruturas*. Ficha m2.

Machado, J. and Cruz, H. (1997). Avaliação do estado de conservação de estruturas de madeira. determinação do perfil densidade por métodos não destrutivos. *Revista Portuguesa de Engenharia de Estruturas*, 42:15–18.

Machado, J. and Cruz, H. (2005). Within stem variation of maritime pine timber mechanical properties. *Holz als Roh- und Werkstoff*, 63:154–159.

McKenzie, W. and Karpovic, H. (1968). The frictional behaviour of wood. *Wood Science and Technology*, 2:139–152.

NP 4305 (1995). *Structural matime pine sawn timber - Visual grading*. Instituto Português da Qualidade.

NP ENV 1995-1-1 (1998). *Eurocódigo 5 - Projecto de estruturas de Madeira. Parte 1-1: Regras gerais e regras para edifícios*. Instituto Português da Qualidade.

Oden, J. and Pires, E. (1983). Nonlocal and nonlinear friction laws and variational principles for contact problems in elasticity. *Journal of Apllied Mechanics*, 50:67–73.

Ordinanza 3431 (2005). *Primi elementi in materia di criteri generali per la classificazione sismica del territorio nazionale e di normative tecniche per le construzioni in zona sismica*. Ordinanza del presidente del consiglio dei ministri.

Palladio, A. (1945). *I quatro libri dell'architettura. In Venetia: Apresso Dominico de Franceschi*. Ulrico Hoepli, Milan, Italy.

Palma, P. and Cruz, H. (2007). Mechanical behaviour of traditional timber carpentry joints in service conditions - results of monotonic tests. In *From material to Structure - Mechanical behaviour and failures of the timber structures XVI International Symposium*, Venice, Italy. ICOMOS IWC.

Parisi, M. and Piazza, M. (1998). Seismic behaviour and modelling of traditional timber roof structures. In *Proceedings of the 11th European Conference on Earthquake Engineering*, Paris, France.

Parisi, M. and Piazza, M. (1999). Dynamic modeling of friction joints in traditional timber structures. In *Proceedings of the Eurodyn'99 Conference*, Prague, Czech Republic.

Parisi, M. and Piazza, M. (2000). Mechanics of plain and retrofitted traditional timber connections. *Journal of Structural Engineering*, 126(12):1395–1403.

Pellerin, R. and Ross, R. (2002). *Nondestructive evaluation of wood*. Forest Products Society.

Pfeil, W. and Pfeil, M. (2003). *Estruturas de madeira*. LTC.

Piazza, M. and Del Senno, M. (2001). Proposals and criteria for the preliminary evaluation, the design and the execution of works on ancient load bearing timber structures. In *Wooden Handwork/Wooden Carpentry: European Restoration Sites*, pages 263–277, Paris, France. Elsevier.

Piazza, M., Riggio, M., and Brentari, G. (2005). Strengthening and control methods for old timber trusses: the queen-post truss of the trento theatre. In *Structural Analysis of Historical Constructions*, pages 957–976, Padova, Italy. A.A. Balkema.

Prion, H. and Foschi, R. (1994). Cyclic behaviour of dowel type connections. In *Proceedings of the Pacific Timber Engineering Conference PTEC'94*, pages 19–25, Gold Coast, Australia.

Rinn, F. (1992). Chancen und grenzen bei der untersuchung von konstruktionshölzern mit der bohrwiderstandsmethode. *Bauen mit Holz*, 9:745–748.

Sakamoto, I. and Ohashi, Y. (1986). Relationship between lateral strength and story drift of wooden dwellings. In *Proceedings of the 7th Japan Earthquake Engineering Symposium*, pages 1819–1824, Tokyo, Japan.

Sandoz, J., Benoit, Y., and Demay, L. (2000). Wood testing using acousto-ultrasonic. In *Proceedings of the 6th World Conference on Timber Engineering*, British Columbia, Canada.

SAP2000 (2007). *SAP2000 - Linear and nonlinear static and dynamic analysis and design of three-dimensional structures. User's Manual. Version 10.* Computers and Structures, Inc., Berkeley, USA.

Seo, J.-M., Choi, I.-K., and Lee, J.-R. (1999). Static and cyclic behaviour of wooden frames with tenon joints under lateral load. *J. Strut. Eng.*, 125(3):344–349.

Serlio, S. (1584). *II sette libri dell'architettura. Venezia.* Re-printed Forni Editions, Bologna, Italy.

Shang, W.-S. (2005). *On rotational performance of traditional Chuan-Dou timber joints in Taiwan.* PhD thesis, National Cheng Kung University.

Shanks, J. and Walker, P. (2005). Experimental performance of mortice and tenon connections in green oak. *The structural Engineer*, pages 30–45.

SIA 265 (2003). *Constructions en Bois.* Swiss society of engineers and architects (sia) norm.

Stewart, W. G. (1987). *The seismic design of plywood sheathed shear walls.* PhD thesis, University of Canterbury.

Sylvatest (1991). *Sylvates user's manual.* Cableries and Trefileries de Cossonay SA, Switzerland.

Tampone, G. (1996). *Il restauro delle strutture di legno.* Ulrico Hoepli, Milan, Italy.

Turrini, G. and Piazza, M. (1983). Il recupero dei solai in legno. esperienze e realizzazioni. *Recuperare*, 7.

UNE 56546 (2007). *Visual grading for structural sawn timber. Hardwood timber.*

UNI 11035-1 (2003). *Structural timber - Visual strength grading for Italian structural timbers: terminology and measurement of features.* Ente nazionale italiano di unificazione.

UNI 11035-2 (2003). *Structural timber - Visual strength grading rules and characteristics values for Italian structural timber population.* Ente nazionale italiano di unificazione.

Uzielli, L. (2004). *Il manuale del Legno Strutturale, Vol IV - Interventi sulle strutture.* Mancosu, Rome, Italy.

Appendix A

Examples of Portuguese traditional timber trusses

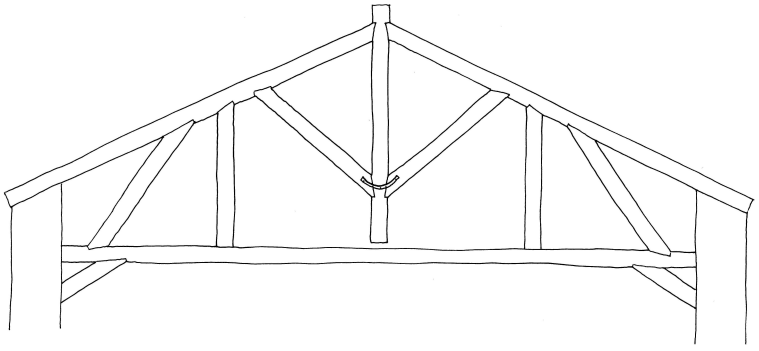


Figure A.1: City hall, Pátio do Salema (Évora).

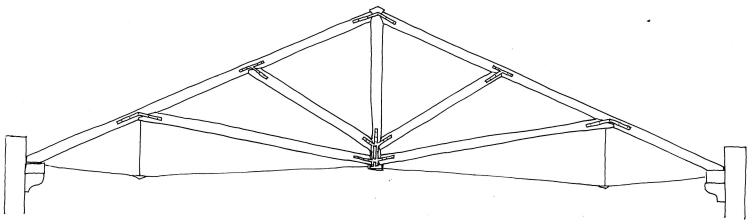


Figure A.2: University of Évora, Verney College (Évora).

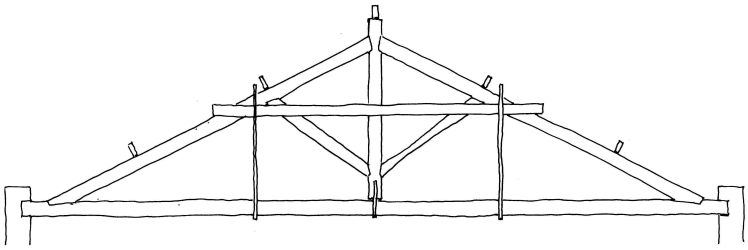


Figure A.3: Galp garage, main truss (Guimarães).

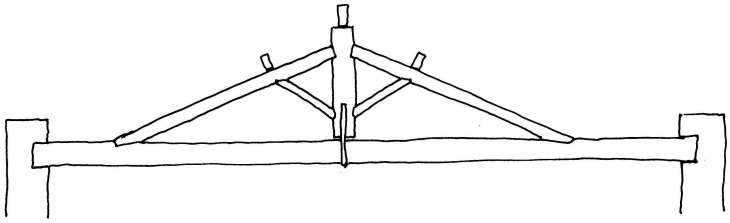


Figure A.4: Galp garage, secondary truss (Guimarães).

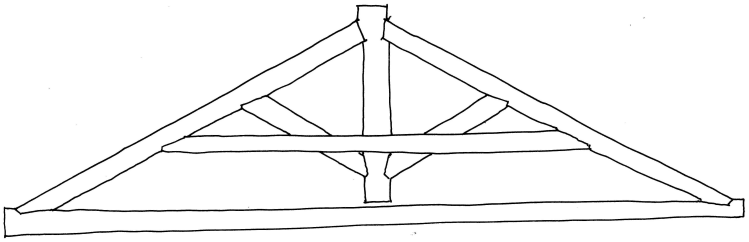


Figure A.5: Rodrigues de Freitas High school, building A (Porto).

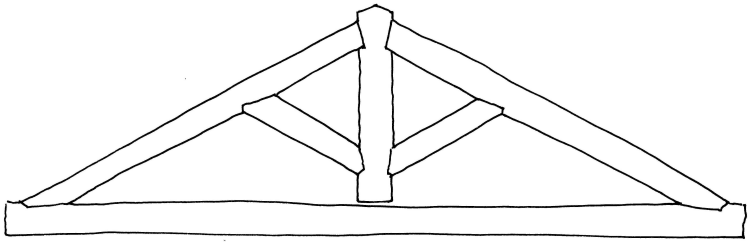


Figure A.6: Rodrigues de Freitas High school, building B (Porto).

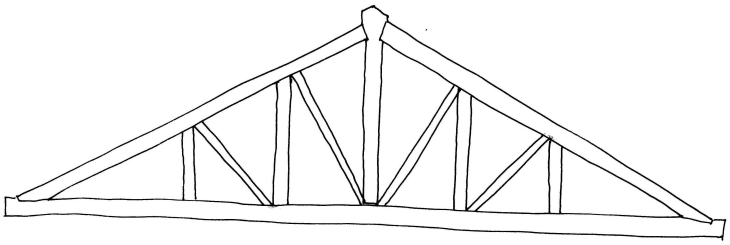


Figure A.7: Rodrigues de Freitas High school, building C (Porto).

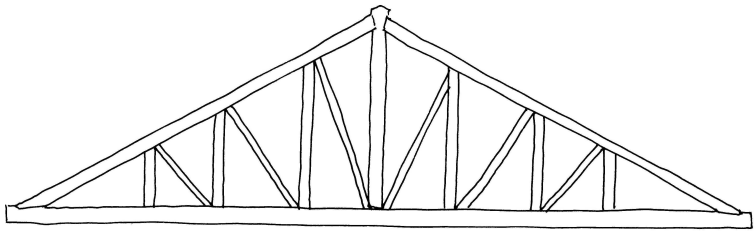


Figure A.8: Rodrigues de Freitas High school, building D (Porto).

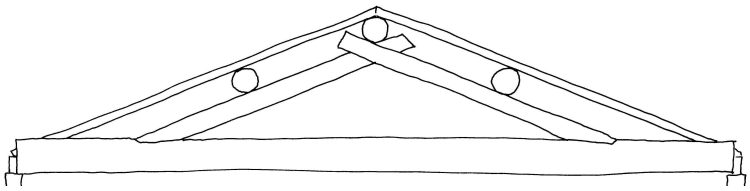


Figure A.9: St. Domingos building (Porto).

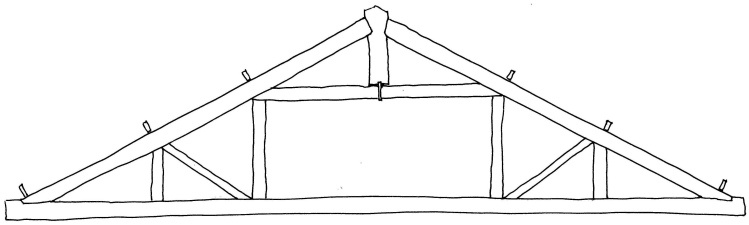


Figure A.10: Sá de Miranda High school, main building (Braga).

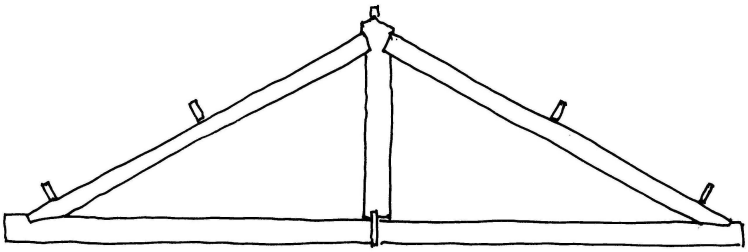


Figure A.11: Sá de Miranda High school, secondary building (Braga).

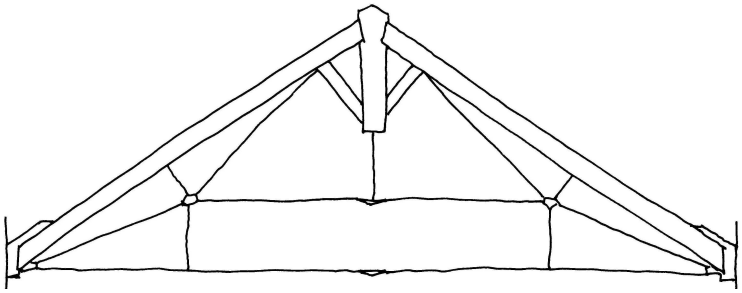


Figure A.12: Sá de Miranda High school, gymnasium (Braga).

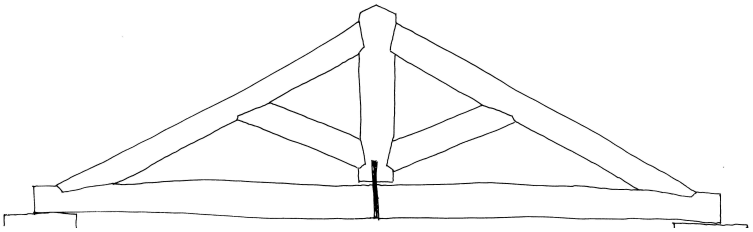


Figure A.13: Jacques Delors rail-station (Mirandela).

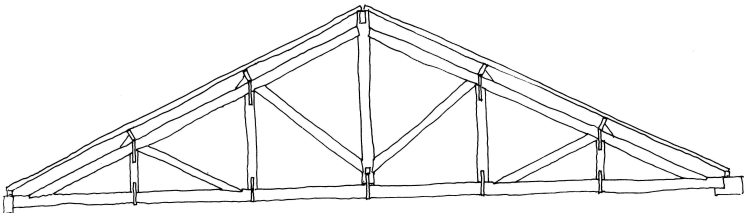


Figure A.14: Adico Industries (Avanca).

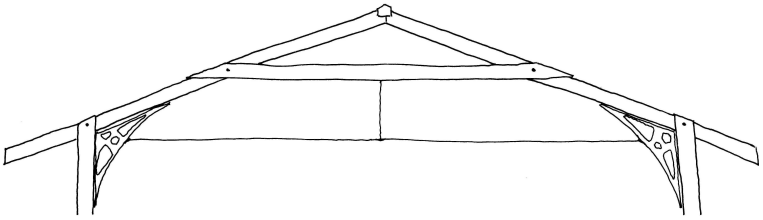


Figure A.15: Refer warehouse (Ovar).

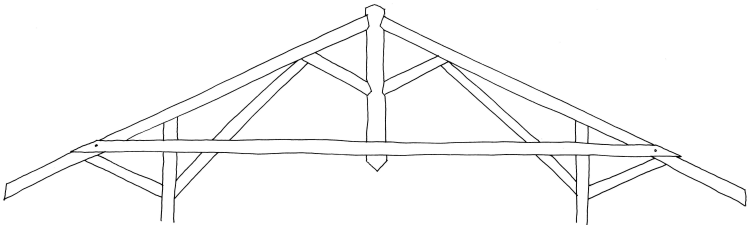


Figure A.16: Refer warehouse (Régua).

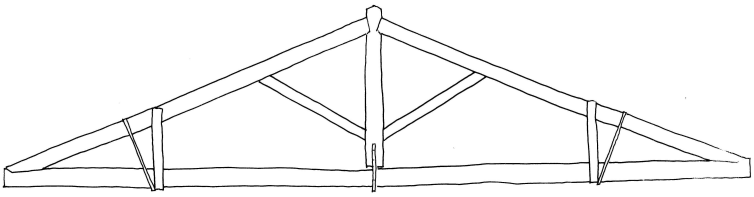


Figure A.17: Teixeira sawmill (S. João da Madeira).

Appendix B

Full-scale connections tests results

In this Appendix more detailed tests results are reported.

B.1 Unstrengthened connections

The first test (U3-1.4-1) was interrupted when the displacement reached 30 mm in consequence of the anomaly detected in the jack responsible for the transverse force: the correct movement of the jack head was block by an imprecise position of the safety system. As result, an increase of the force was detected. Apart of this situation, a pleasant homogeneity is reveal by the force-displacement experimental curves (Figure B.1). A perfect elastic plastic development is follow by the three curves.

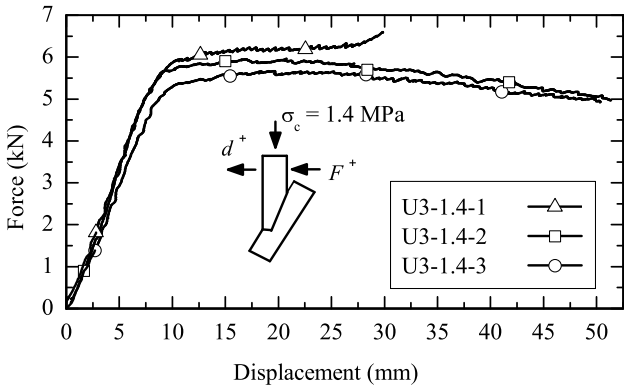


Figure B.1: Force-displacement curves of unstrengthened connections with 30° skew angle for monotonic loading in positive direction under 1.4MPa rafter compression stress.

Table B.1: Tests results of unstrengthened connections with 30° skew angle for monotonic loading in positive direction under 1.4MPa rafter compression stress.

Specimen	σ_c (MPa)	d_e^+ (mm)	F_{max} (kN)	Stiffness (kN/mm)$\times 10^3$		
				Regression	F_e/d_e	$F_e^{50\%}/d_e^{50\%}$
U3-1.4-1		8.33	-	698	659	627
U3-1.4-2	1.4	8.60	7.16	682	645	719
U3-1.4-3		8.00	6.27	641	598	596
	Mean	8.31	6.72	674	634	647
	CoV	3.62	9.37	4.35	5.10	9.86

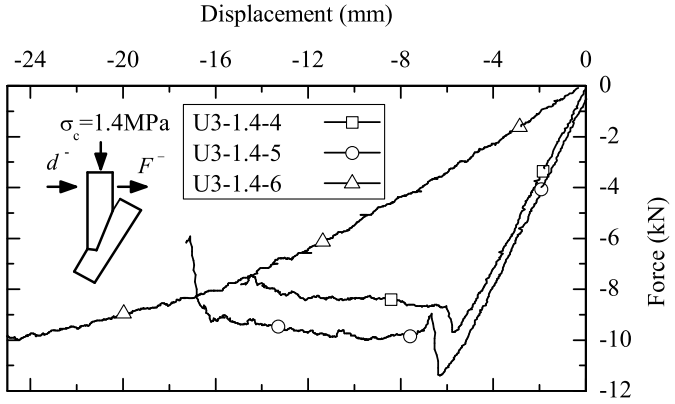


Figure B.2: Force-displacement curves of unstrengthened connections with 30° skew angle for monotonic loading in negative direction under 1.4MPa rafter compression stress.

The first test result (U3-1.4-4) should not be considered. The lack of stiffness revealed during this test by the test setup compromise the results achieved. The others two connections were tested only after the correct stiffening of test setup.

B.2 Strengthened connections

Table B.2: Tests results of unstrengthened connections with 30° skew angle for monotonic loading in negative direction under 1.4MPa rafter compression stress.

Specimen	σ_c (MPa)	d_e^- (mm)	F_{max} (kN)	Stiffness (kN/mm)×10^3		
				Regression	F_e/d_e	$F_e^{50\%}/d_e^{50\%}$
U3-1.4-4		-	-	-	-	-
U3-1.4-5	1.4	-5.59	-9.85	1729	1708	1811
U3-1.4-6		-5.93	-11.64	1812	1862	2104
	Mean	-5.76	-10.75	1771	1785	1958
	CoV	4.17	11.78	3.32	6.10	10.58

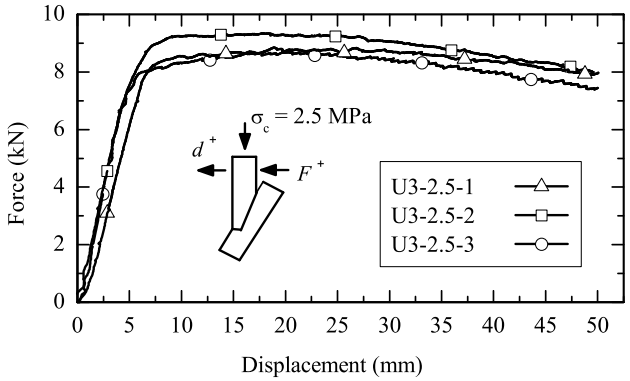


Figure B.3: Force-displacement curves of unstrengthened connections with 30° skew angle for monotonic loading in positive direction under 2.5MPa rafter compression stress.

Table B.3: Tests results of unstrengthened connections with 30° skew angle for monotonic loading in positive direction under 2.5MPa rafter compression stress.

Specimen	σ_c (MPa)	d_e^- (mm)	F_{max} (kN)	Stiffness (kN/mm)×10^3		
				Regression	F_e/d_e	$F_e^{50\%}/d_e^{50\%}$
U3-2.5-1		4.70	9.55	1717	1489	1523
U3-2.5-2	2.5	5.30	11.64	1571	1467	1583
U3-2.5-3		6.41	11.34	1420	1211	1119
	Mean	5.47	10.84	1569	1389	1408
	CoV	1586	10.42	9.47	11.13	17.92

Table B.4: Tests results of unstrengthened connections with 30° skew angle for monotonic loading in negative direction under 2.5MPa rafter compression stress.

Specimen	σ_c (MPa)	d_e^- (mm)	F_{max} (kN)	Stiffness (kN/mm)$\times 10^3$		
				Regression	F_e/d_e	$F_e^{50\%}/d_e^{50\%}$
U3-2.5-4		-7.90	-15.82	1601	1511	1651
U3-2.5-5	2.5	-8.50	-15.82	1796	1719	1764
U3-2.5-6		-8.00	-14.37	1719	1754	1860
	Mean	-8.13	-15.32	1705	1661	1758
	CoV	3.95	5.61	5.76	7.91	5.95

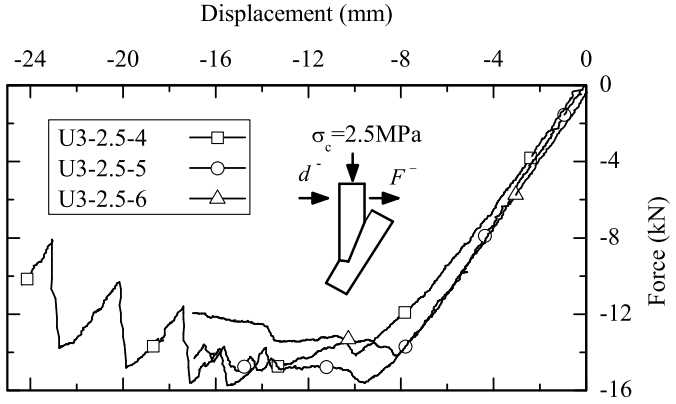


Figure B.4: Force-displacement curves of unstrengthened connections with 30° skew angle for monotonic loading in negative direction under 2.5MPa rafter compression stress.

Table B.5: Tests results of unstrengthened connections with 60° skew angle for monotonic loading in positive direction under 1.4MPa rafter compression stress.

Specimen	σ_c (MPa)	d_e^- (mm)	F_{max} (kN)	Stiffness (kN/mm)$\times 10^3$		
				Regression	F_e/d_e	$F_e^{50\%}/d_e^{50\%}$
U6-1.4-1		3.09	2.93	539	542	651
U6-1.4-2	1.4	2.75	2.96	632	713	935
U6-1.4-3		3.11	4.03	692	749	881
	Mean	2.98	3.31	621	668	822
	CoV	0.07	0.19	0.12	0.17	0.18

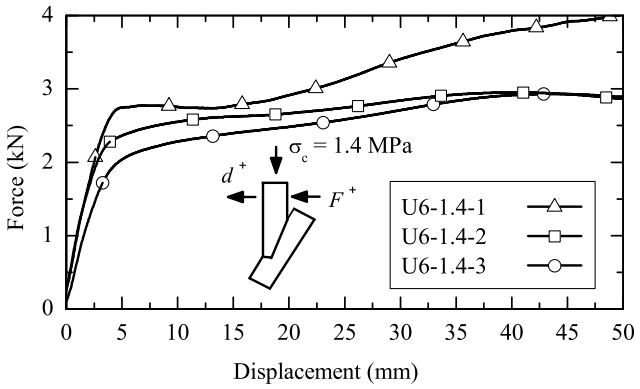


Figure B.5: Force-displacement curves of unstrengthened connections with 60° skew angle for monotonic loading in positive direction under 1.4MPa rafter compression stress.

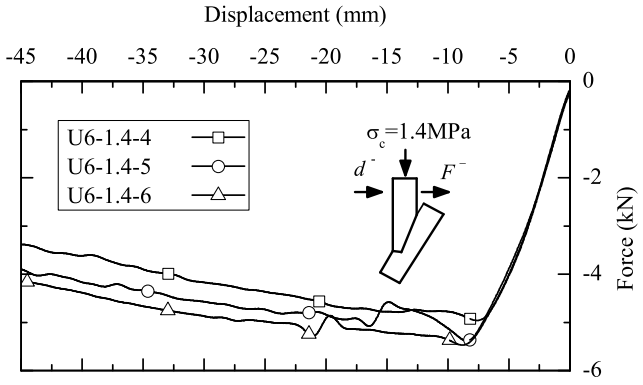


Figure B.6: Force-displacement curves of unstrengthened connections with 60° skew angle for monotonic loading in negative direction under 1.4MPa rafter compression stress.

Table B.6: Tests results of unstrengthened connections with 60° skew angle for monotonic loading in negative direction under 1.4MPa rafter compression stress.

Specimen	σ_c (MPa)	d_e^- (mm)	F_{max} (kN)	Stiffness (kN/mm)×10^3		
				Regression	F_e/d_e	$F_e^{50\%}/d_e^{50\%}$
U6-1.4-4		-5.40	-4.99	790	789	910
U6-1.4-5	1.4	-5.40	-5.47	747	764	891
U6-1.4-6		-5.27	-5.51	802	788	898
	Mean	-5.32	-4.18	780	780	900
	CoV	0.05	0.02	0.04	0.02	0.01

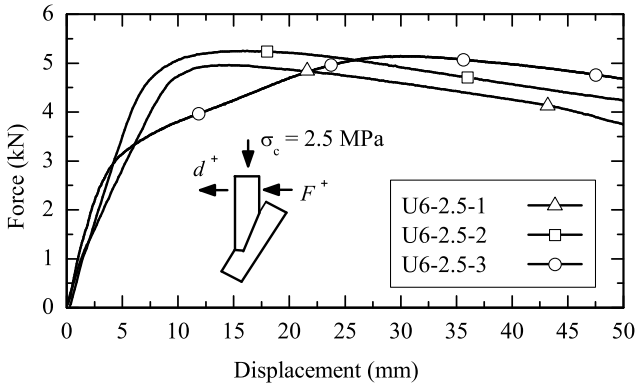


Figure B.7: Force-displacement curves of unstrengthened connections with 60° skew angle for monotonic loading in positive direction under 2.5MPa rafter compression stress.

Table B.7: Tests results of unstrengthened connections with 60° skew angle for monotonic loading in positive direction under 2.5MPa rafter compression stress.

Specimen	σ_c (MPa)	d_e^- (mm)	F_{max} (kN)	Stiffness (kN/mm)×10^3		
				Regression	F_e/d_e	$F_e^{50\%}/d_e^{50\%}$
U6-2.5-1		2.78*	5.14	880*	844*	1038*
U6-2.5-2	2.5	7.02	5.25	690	646	757
U6-2.5-3		7.92	4.96	503	525	603
	Mean	7.47	5.12	597	586	680
	CoV	0.06	0.032	0.22	0.15	0.16

* value not used for the statistics

Table B.8: Tests results of unstrengthened connections with 60° skew angle for monotonic loading in negative direction under 2.5MPa rafter compression stress.

Specimen	σ_c (MPa)	d_e^- (mm)	F_{max} (kN)	Stiffness (kN/mm)$\times 10^3$		
				Regression	F_e/d_e	$F_e^{50\%}/d_e^{50\%}$
U6-2.5-4	2.5	-9.62	-10.54	914	956	1072
U6-2.5-5		-13.31	-9.03	564	579	631
U6-2.5-6		-10.61	-7.48	598	608	634
	Mean	-11.18	-9.02	692	715	779
	CoV	0.17	0.17	0.28	0.29	0.33

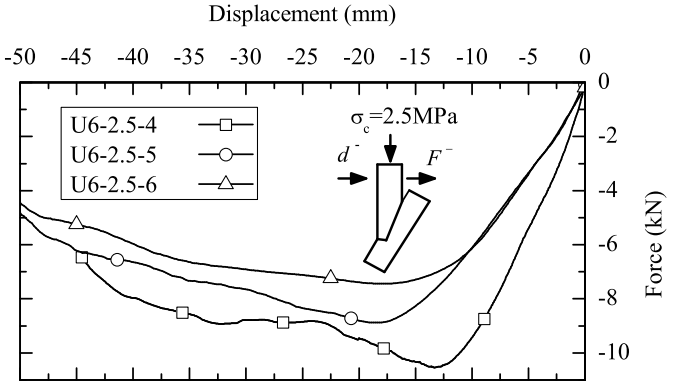


Figure B.8: Force-displacement curves of unstrengthened connections with 60° skew angle for monotonic loading in negative direction under 2.5MPa rafter compression stress.

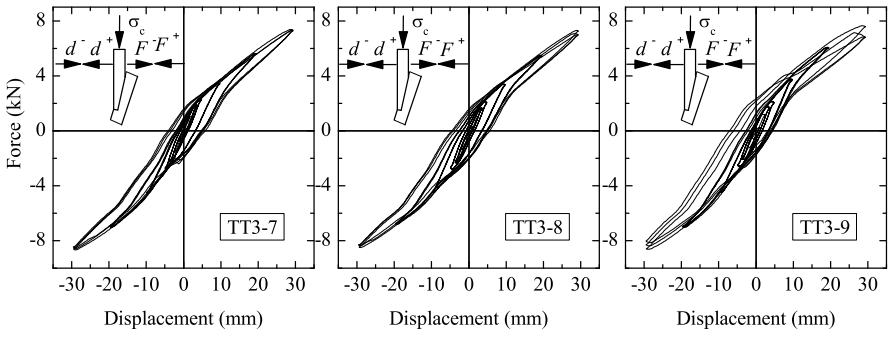


Figure B.9: Force-displacement loops of 30° skew angle strengthened connections with tension ties under cyclic loading.

Table B.9: Cyclic tests results of 30° skew angle strengthened connections with tension ties.

Specimen	σ_c (MPa)	d^+_{max} (mm)	d^-_{max} (mm)	F^+_{max} (kN)	F^-_{max} (kN)	Dissipated Energy (kJ)	V_{eq} (%)
BS3-7		29.41	-29.55	7.46	-8.78	520	11.56
BS3-8	1.4	29.41	-29.55	7.39	-8.60	553	11.95
BS3-9		29.41	-29.54	7.75	-8.76	588	14.98
	Mean	29.41	-29.55	7.53	-8.71	554	12.83
	CoV	0.00	0.00	0.03	0.01	0.06	0.15

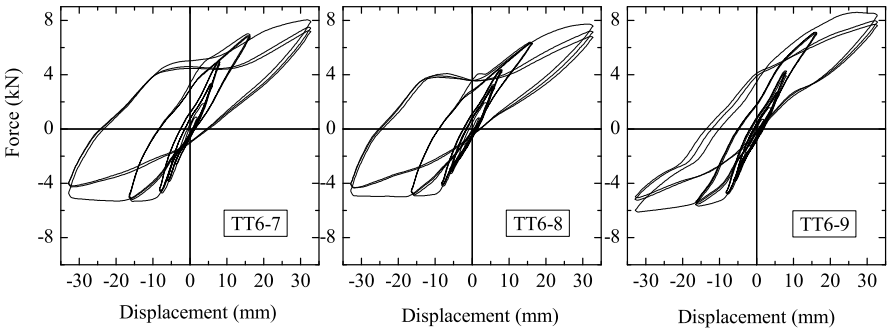


Figure B.10: Force-displacement loops of 60° skew angle strengthened connections with tension ties under cyclic loading.

Appendix C

ABAQUS/Standard input file

```
*Heading
** Job name: Ligacao30 Model name: Ligacao30
*Preprint, echo=NO, model=NO, history=NO, contact=NO
**
** PARTS
**
*Part, name=Linha-30
*End Part
**
*Part, name=Perna-30
*End Part
**
**
** ASSEMBLY
**
*Assembly, name=Assembly
**
*Instance, name=Linha-30-1, part=Linha-30
*Node
1, 0.0284455363, 0.399269134
2, -0.010525601, 0.421769142
3, -0.190525606, 0.109999999
(...)
3493, 0.308712661, 0.851372659
3494, 0.288995773, 0.83388871
3495, 0.297329098, 0.848322451
*Element, type=CPS8R
1, 1, 23, 321, 72, 1197, 1198, 1199, 1200
2, 23, 24, 322, 321, 1201, 1202, 1203, 1198
3, 24, 25, 323, 322, 1204, 1205, 1206, 1202
(...)
```

```
1102, 265, 1195, 268, 21, 3490, 3494, 2903, 2658
1103, 1195, 1196, 269, 268, 3492, 3495, 2895, 3494
1104, 1196, 270, 9, 269, 3493, 2916, 2886, 3495
*Nset, nset=Linha, generate
1, 3495, 1
*Elset, elset=Linha, generate
1, 1104, 1
*Nset, nset=Encastramento
13, 14, 18, 19, 142, 143, 144, 145, 146, 147, 148, 149, 150, 151, 152, 153
154, 155, 156, 157, 158, 178, 179, 180, 181, 276, 277, 278, 279, 280, 281, 282
283, 284, 285, 286, 287, 288, 289, 290, 291, 292, 293, 294, 295, 296, 297, 298
299, 300, 301, 302, 303, 304, 305, 306, 307, 308, 309, 310, 311, 312, 313, 314
315, 316, 317, 318, 319, 320, 1954, 1971, 1983, 1995, 2007, 2019, 2031, 2043,
2055, 2067
2079, 2091, 2103, 2115, 2127, 2139, 2151, 2163, 2304, 2307, 2309, 2311, 2313,
2937, 2950, 2963
2976, 2988, 3000, 3012, 3024, 3036, 3048, 3060, 3072, 3084, 3096, 3108, 3120,
3132, 3144, 3156
3168, 3180, 3192, 3204, 3216, 3228, 3240, 3252, 3264, 3276, 3288, 3300, 3312,
3324, 3336, 3348
3360, 3372, 3384, 3396, 3408, 3420, 3432, 3444, 3456, 3468, 3479
*Elset, elset=Encastramento
354, 360, 366, 372, 378, 384, 390, 396, 402, 408, 414, 420, 426, 432, 438, 444
450, 456, 522, 523, 524, 525, 526, 820, 826, 832, 838, 844, 850, 856, 862, 868
874, 880, 886, 892, 898, 904, 910, 916, 922, 928, 934, 940, 946, 952, 958, 964
970, 976, 982, 988, 994, 1000, 1006, 1012, 1018, 1024, 1030, 1036, 1042, 1048,
1054, 1060
1066, 1072, 1078, 1084, 1090
*Elset, elset=M-Linha-S3, internal, generate
325, 333, 1
*Elset, elset=M-Linha-S4, internal, generate
289, 325, 9
*Elset, elset=M-Linha-S1, internal, generate
527, 564, 1
*Elset, elset=M-Linha-S2, internal, generate
796, 804, 4
*Surface, type=ELEMENT, name=M-Linha
M-Linha-S3, S3
M-Linha-S4, S4
M-Linha-S2, S2
M-Linha-S1, S1
*Orientation, name=Ori-1
1., 0., 0., 0., 1., 0.
3, 60.
** Section: Madeira
*Solid Section, elset=Linha, orientation=Ori-1, material=Madeira
```

```
0.08,
*End Instance
**
*Instance, name=Perna-30-1, part=Perna-30
*Node
1, 0.0144744003, 1.14956713
2, 0.234474406, 1.14956713
3, 0.234474406, 1.4530127
(...)
1757, 0.185585514, 1.14120817
1758, 0.21002996, 1.14122105
1759, 0.234474406, 1.1412338
*Element, type=CPS8R
1, 1, 15, 155, 58, 611, 612, 613, 614
2, 15, 16, 156, 155, 615, 616, 617, 612
3, 16, 17, 157, 156, 618, 619, 620, 616
(...)
538, 608, 609, 21, 20, 1745, 1757, 630, 1756
539, 609, 610, 22, 21, 1747, 1758, 633, 1757
540, 610, 140, 2, 22, 1749, 1759, 636, 1758
*Nset, nset=Perna, generate
1, 1759, 1
*Elset, elset=Perna, generate
1, 540, 1
*Nset, nset=Ponto
13,
*Elset, elset=S-Perna-S2, internal, generate
387, 405, 9
*Elset, elset=S-Perna-S3, internal, generate
397, 405, 1
*Elset, elset=S-Perna-S4, internal, generate
136, 397, 9
*Surface, type=ELEMENT, name=S-Perna
S-Perna-S2, S2
S-Perna-S3, S3
S-Perna-S4, S4
*Elset, elset=ForcaAxial-S3, internal, generate
127, 135, 1
*Surface, type=ELEMENT, name=ForcaAxial
ForcaAxial-S3, S3
*Orientation, name=Ori-1
1., 0., 0., 0., 1., 0.
3, 90.
** Section: Madeira
*Solid Section, elset=Perna, orientation=Ori-1, material=Madeira
0.08,
```

```
*End Instance
**
*End Assembly
**
** MATERIALS
**
*Material, name=Madeira
*Elastic, type=LAMINA
7.992e+09, 2.66e+08, 0.3, 5e+08, 5e+07, 5e+07
*Fail Stress
1.5e+07, -2e+07, 600000., -4e+06, 2.63e+06, 0., 2.63e+06
*Plastic
4e+06, 0.
5.7e+06, 0.0093804
6.27e+06, 0.199319
9.83e+06, 0.389318
*Potential
4.5e+06, 1e+06, 1e+06, 1.3793e+06, 1.3793e+06, 1.3793e+06
**
** INTERACTION PROPERTIES
**
*Surface Interaction, name=Atrito
0.08,
*Friction, slip tolerance=0.005
0.2,
**
** BOUNDARY CONDITIONS
**
** Name: Encastramento Type: Symmetry/Antisymmetry/Encastre
*Boundary
Linha-30-1.Encastramento, ENCASTRE
**
** INTERACTIONS
**
** Interaction: Atrito
*Contact Pair, interaction=Atrito, smooth=0.1
Perna-30-1.S-Perna, Linha-30-1.M-Linha
** ----------------------------------------------------------------
**
** STEP: Forca
**
*Step, name=Forca, nlgeom=YES
Esforço Axial
*Static
0.05, 1., 1e-05, 0.1
**
```

```
** LOADS
**
** Name: ForcaVertical Type: Pressure
*Dsload
Perna-30-1.ForcaAxial, P, 1.4e+06
**
** OUTPUT REQUESTS
**
*Restart, write, frequency=0
**
** FIELD OUTPUT: F-Output-1
**
*Output, field, variable=PRESELECT
**
** HISTORY OUTPUT: Ponto
**
*Output, history
*Node Output, nset=Perna-30-1.Ponto
RF1, U1
*End Step
** ----------------------------------------------------------------
**
** STEP: Deslocamento
**
*Step, name=Deslocamento, nlgeom=YES, inc=1000
*Static
0.01, 1., 1e-06, 0.02
**
** BOUNDARY CONDITIONS
**
** Name: Deslocamento Type: Displacement/Rotation
*Boundary
Perna-30-1.Ponto, 1, 1, -0.0493405
**
** OUTPUT REQUESTS
**
*Restart, write, frequency=0
**
** FIELD OUTPUT: F-Output-1
**
*Output, field, variable=PRESELECT
**
** HISTORY OUTPUT: Ponto
**
*Output, history
*Node Output, nset=Perna-30-1.Ponto
```

```
RF1, U1
*End Step
```

Appendix D

Parameters of the $M - \phi$ experimental curves

Table D.1: Parameters of the $M-\phi$ experimental curves obtained on unstrengthened connections under negative rotation.

α (°)	σ_c (MPa)	M_y^- (kNm)		M_u^- (10^{-3} rad)		ϕ_y^- (kNm)		ϕ_u^- (10^{-3} rad)		k_e^- (kN/m)		k_p^- (kN/m)	
30	1.4	3.67	3.99	12.38	12.71	2.41	2.47	72.63	74.56	296.84	313.55	-21.02	-24.61
		4.31		13.04		2.52		76.48		330.25		-28.20	
	2.5	6.22	6.05	24.78	21.57	3.97	4.26	74.6	73.88	251.14	283.20	-45.22	-34.36
		6.22		21.11		5.07		73.26		294.8		-22.05	
		5.71		18.81		3.74		73.79		303.67		-35.80	
60	1.4	2.60	2.69	11.99	12.79	1.93	2.14	74.62	74.05	217.11	210.54	-10.8	-8.90
		2.66		12.89		2.19		73.76		206.47		-7.83	
		2.81		13.49		2.32		73.78		208.04		-8.08	
	2.5	5.58	4.92	18.91	23.84	4.26	3.67	75.27	74.16	295.31	215.35	-23.51	-25.15
		4.94		28.82		3.58		73.26		172.22		-30.66	
		4.25		23.80		3.18		73.96		178.52		-21.28	

Table D.2: Parameters of the $M-\phi$ experimental curves obtained on strengthened connections under negative rotation.

α (°)	σ_c (MPa)	M_y^- (kNm)		M_u^- (10^{-3} rad)		ϕ_y^- (kNm)		ϕ_u^- (10^{-3} rad)		k_e^- (kN/m)		k_p^- (kN/m)	
Bolt													
		3.83		11.75		7.48		75.00		229.35		53.53	
30	1.4	5.38	4.68	22.54	19.23	7.39	7.34	73.00	73.92	238.54	224.84	39.98	46.42
		4.84		23.41		7.14		73.77		206.64		45.75	
		2.60		21.91		2.95		73.78		118.75		6.72	
60	1.4	2.31	2.58	19.43	21.49	2.86	2.99	73.77	73.78	119.01	119.87	10.04	7.93
		2.82		23.12		3.17		73.78		121.84		7.04	
Binding strip													
		3.94		15.13		8.21		79.79		260.35		6.61	
30	1.4	3.27	3.57	11.27	14.46	7.35	7.31	79.97	79.80	290.35	252.29	5.93	5.71
		3.50		16.97		6.38		79.64		206.17		4.59	
Tension ties													
		3.80		21.19		5.95		75.034		179.42		39.87	
30	1.4	3.51	3.67	22.47	23.24	5.44	5.65	73.11	74.05	155.96	159.01	38.20	38.96
		3.69		26.05		5.55		73.99		141.66		38.81	
		2.38		17.19		2.64		74.99		138.18		4.59	
60	1.4	2.79	2.60	18.90	17.40	2.71	2.79	73.01	73.83	147.66	149.69	-1.49	3.37
		2.63		16.10		3.03		73.48		163.24		6.99	
Stirrup													
		6.22		9.70		9.46		73.77		641.27		50.56	
30	1.4	6.77	7.18	10.92	11.85	12.84	11.07	77.50	74.24	619.96	611.17	91.19	61.11
		8.55		14.94		10.90		71.44		572.27		41.58	
		4.00		38.66		4.44		74.78		103.39		12.12	
60	1.4	3.19	3.60	23.78	29.85	3.89	4.17	73.00	73.74	134.06	123.62	14.24	12.95
		3.62		27.11		4.20		73.44		133.43		12.48	

Table D.3: Parameters of the $M-\phi$ experimental curves obtained on unstrengthened connections under positive rotation.

α (°)	σ_c (MPa)	M_y^+ (kNm)		M_u^+ (10^{-3} rad)		ϕ_y^+ (kNm)		ϕ_u^+ (10^{-3} rad)		k_e^+ (kN/m)		k_p^+ (kN/m)	
30	1.4	4.16	4.04	13.44	13.92	3.14	3.15	84.34	86.14	309.26	298.79	-9.14	-8.15
		3.92		14.41		3.17		87.94		272.03		-7.17	
	2.5	5.96	6.19	8.37	9.47	5.33	5.29	83.54	84.32	711.56	661.34	-8.33	-9.29
		6.55		9.18		5.62		81.40		713.55		-12.92	
		6.07		10.86		5.56		88.03		558.91		-6.62	
60	1.4	1.38	1.51	6.13	5.13	1.98	2.24	80.00	84.18	224.68	301.03	8.16	9.11
		1.56		4.73		1.97		83.00		330.41		5.26	
		1.58		4.53		2.76		89.54		348.02		13.91	
	2.5	2.60	3.19	8.96	11.87	3.58	2.94	79.98	84.29	301.33	276.40	12.38	-3.76
		3.58		12.27		2.81		83.11		291.47		-10.86	
		3.40		14.38		2.44		90.00		236.39		-12.79	

Table D.4: Parameters of the $M-\phi$ experimental curves obtained on strengthened connections under positive rotation.

α (°)	σ_c (MPa)	M_y^+ (kNm)		M_u^+ (10^{-3} rad)		ϕ_y^+ (kNm)		ϕ_u^+ (10^{-3} rad)		k_e^+ (kN/m)		k_p^+ (kN/m)	
Bolt													
		6.24		10.69		8.81		76.87		586.09		38.76	
30	1.4	7.97	7.34	14.35	13.91	10.10	9.46	74.73	79.91	555.36	536.80	35.22	32.43
		7.82		16.68		9.49		88.12		468.95		13.32	
		3.95		12.38		5.24		79.71		318.68		19.24	
60	1.4	3.69	3.65	16.36	15.00	4.63	5.11	82.70	83.82	225.55	249.20	14.22	21.02
		3.31		16.26		5.46		89.04		203.39		29.60	
Binding strip													
		10.99		24.50		10.02		98.11		448.63		-13.18	
30	1.4	9.75	10.35	23.78	25.44	8.79	10.69	98.09	77.90	418.66	411.75	-12.82	5.42
		10.32		28.047		13.25		37.49		367.97		42.25	
Tension ties													
		5.06		9.41		9.01		79.47		537.97		56.37	
30	1.4	6.52	5.85	19.06	15.12	7.62	8.27	82.26	83.48	342.32	411.02	17.34	34.80
		5.96		16.89		8.16		88.73		352.78		30.68	
		3.94		27.00		4.45		75.81		148.21		10.22	
60	1.4	4.82	4.35	27.21	28.38	5.20	4.79	82.50	82.48	177.11	153.99	6.94	8.22
		4.28		31.34		4.72		89.14		136.66		7.49	
Stirrup													
		8.79		16.06		11.66		76.01		547.37		47.92	
30	1.4	8.10	8.44	13.18	16.31	12.64	12.41	75.08	79.21	614.59	529.97	73.27	62.85
		8.43		19.70		12.93		86.56		427.95		67.37	
		3.96		26.13		5.40		75.81		151.42		29.03	
60	1.4	5.11	4.72	24.17	25.89	6.18	5.98	82.57	82.50	211.21	183.14	18.43	22.62
		5.11		27.36		6.37		89.14		187.00		20.38	